

Molecular Engineering Strategies for Expanding the Capabilities of Fluorescent Zinc(II)
Sensors

by

Carolyn C. Woodroffe
B. A. Chemistry and Integrated Science
Northwestern University, 1998

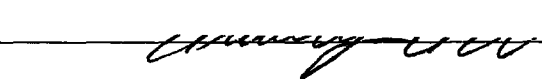
SUBMITTED TO THE DEPARTMENT OF CHEMISTRY IN PARTIAL
FULFILLMENT OF THE REQUIREMENTS FOR THE DEGREE OF

DOCTOR OF PHILOSOPHY IN ORGANIC CHEMISTRY
AT THE
MASSACHUSETTS INSTITUTE OF TECHNOLOGY


September 2004

© Massachusetts Institute of Technology, 2004
All rights reserved

Signature of Author: _____

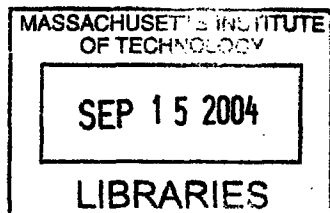

Department of Chemistry
August 17, 2004

Certified By: _____


Stephen J. Lippard
Arthur Amos Noyes Professor of Chemistry
Thesis Supervisor

Accepted by: _____


Robert W. Field
Chairman, Departmental Committee on Graduate Studies



ARCHIVES

This doctoral thesis has been examined by a committee of the Department of Chemistry as follows:

x - ———

Barbara Imperiali
Committee Chairman
Class of 1922 Professor of Chemistry and Professor of Biology

o o ||

Stephen J. Lippard
Arthur Amos Noyes Professor of Chemistry
Thesis Supervisor

^ ^

— —

Stephen L. Buchwald
Camille Dreyfus Professor of Chemistry

2011.05.10

Molecular Engineering Strategies for Expanding the Capabilities of Fluorescent Zinc(II) Sensors

By
Carolyn C. Woodroffe

Submitted to the Department of Chemistry on August 17, 2004, in partial fulfillment of the requirements for the Degree of Doctor of Philosophy

Abstract

Chapter 1. The Development and Use of Fluorescent Sensors in the Imaging of Physiological Zinc(II): A Review

This chapter presents an overview of fluorescent techniques used to image chelatable zinc(II) *in vivo*. Many intensity-based sensors take advantage of photoinduced electron transfer quenching pathways. Peptide- and protein-based sensors offer excellent selectivity but are poorly suited to intracellular applications. Recently, ratiometric sensors in which the zinc(II) binding event interrupts or alters conjugation within the fluorophore have been described.

Chapter 2. Carboxylate-Functionalized Zinpyr-1 Sensors: Synthesis, Characterization, and In Vivo Staining Patterns

A class of Zinpyr-1 sensors containing a carboxylic acid or ester at the 5- or 6-position of the fluorescein has been prepared. These sensors offer decreased background fluorescence and enhanced fluorescence response compared to the parent Zinpyr-1. The acid-functionalized sensors bear a negative charge at physiological pH, rendering them cell-impermeable. The esterified sensors are cell-permeable, but are hydrolyzed *in vivo* by intracellular esterases, affording a clear delineation of zinc(II)-containing damaged neurons in mechanically-injured or seizure-induced rats, rather than the punctate staining pattern obtained with Zinpyr-1.

Chapter 3. Esterase-Dependent Two-Fluorophore Ratiometric Sensing of Zinc(II)

This chapter describes a new approach to ratiometric sensing in which a zinc(II)-sensitive fluorescein fluorophore based on Zinpyr-1 is functionalized with a zinc(II)-insensitive coumarin fluorophore via a flexible ester linker. The flexible linker enables intramolecular quenching of the two fluorophores. Esterase hydrolysis of the linker affords the two fluorophores, such that excitation of the coumarin at 445 nm and measurement of the emission at 488 nm affords information of the amount of sensor present, while excitation of the fluorescein at 505 nm and measurement of the emission at 535 nm indicates the amount of sensor in the zinc(II)-bound form. This system has been characterized and applied to the study of exogenous zinc(II) fluxes in HeLa cells.

Chapter 4. Unimolecular Two-Fluorophore Ratiometric Zn²⁺ Sensing Systems

Dichlorofluorescein compounds covalently bound to zinc(II)-insensitive reporter fluorophores via a rigid cyclohexyl linker have been prepared and characterized. Based on favorable photophysical properties, a Zinpyr-1 species covalently bound to coumarin 343 has been prepared and shown to afford a ratiometric response to excess zinc(II).

Chapter 5. ZP1 Synthons for Functionalization of Biological Targets

Installation of a functional group prior to Mannich reaction is impractical in many cases. This chapter describes the preparation of reactive ZP1 synthons for direct functionalization of biological targets containing an amine or azide, and reports applications to the synthesis of ZP1 conjugates.

Appendix 1. Synthetic Approaches to Other Isomerically Pure Functionalizable Fluorophores

Crystallization approaches have been applied to separate fluorescein 5- and 6-sulfonic acid, and subsequent generation of the sulfonyl chlorides is discussed. A dibromofluoran approach to isomerically pure rhodamine carboxylates is based on a similar separation. Basic hydrolysis of the previously described 2',7'-dichlorofluorescein carboxylates generates carboxylate-substituted benzophenones suitable for acid-catalyzed condensation to afford an isomerically pure carboxy-substituted seminaphthofluorescein.

Appendix 2. Modulation of Zn²⁺ Affinity By Ligand Switching of ZP1

Analogues of Zinpyr-1 containing two or four carboxylates in place of the pyridyl ligands have been prepared, and their metal-dependent fluorescence response have been examined.

Thesis Supervisor: Stephen J. Lippard
Title: Arthur Amos Noyes Professor of Chemistry

Dedication

For Don: my inspiration, distraction, motivation and reward.

Acknowledgements

During the past five years, I have had the opportunity to interact with a staggering array of people. First and foremost, I thank my advisor, Steve Lippard, for giving me both the opportunity to join his laboratory and a great deal of scientific freedom, as well as for never accepting less than my best effort. He has also recruited many excellent scientists and wonderful people, with whom it has been a pleasure to work. The neurochemistry subgroup has included Shawn Burdette, who began the zinc(II) sensing project; Scott Hilderbrand, NO guru and soccer player extraordinaire; Ben Davis, always entertaining; and Matt Clark, whose excellent synthetic advice made my tenure here run much more smoothly. Liz Nolan has provided an ideal sounding board for problems and ideas, as well as good company, and Chris Chang brought new insight and new enthusiasm to the sensing project—especially in late-night discussions! For the past year or two, I have had the pleasure of interacting with the next generation of graduate students, Mi Hee Lim and Andy Tennyson, and I have seen for myself that the future of the subgroup is exceedingly bright. Finally, my UROP Annie Won has been very helpful, enthusiastic, and very patient with a project that seems to change constantly. I thank all of these people, and wish them the best in their continued research endeavours.

Other members of the group have also been integral to my work here. In particular, I thank Katie Barnes and Olga Burenkova for alternately helping and training me in tissue culture technique, and Katie and Caroline Saouma have kindly and constantly provided cells for my imaging studies. Yongwon Jung and Andy Tennyson have had helpful advice for HPLC use, and Leslie Murray is an apparently endless source of knowledge on the topic of aging PC computers, among other things. Emily Carson has

helped monitor my weight by ensuring that I don't have to eat all of my snacks by myself. Although the sheer number of group members with whom I have overlapped prevents me from naming them all here, I thank the Lippard Group in general for providing support, help, advice, and an excellent environment for research.

Alice Ting has graciously allowed the use of her microscope for quantitative imaging studies, and her graduate student Chi-Wang Lin has been extremely patient and knowledgeable in answering all of my questions about it. Chris Frederickson and Rafik Masalha (NeuroBioTex) were kind enough to test some of our sensors in vivo. Above all among our collaborators I must acknowledge Grant Walkup, whom I have never met, but whose simple and powerful application of the Mannich reaction has formed the basis of my work here, and whose freely shared expertise in the characterization of fluorescent zinc(II) binding systems has been integral to the work of the subgroup.

Outside of the scientific aspect, I acknowledge the MIT women's club hockey team for providing a much-needed outlet and distraction, and the Detroit Red Wings for playing fantastic hockey and for winning the ultimate prize in 2002. I thank my parents for their unwavering support and encouragement, and my brother Blake for his down-to-earth perspective on life. And finally, I thank Don Hitko, who has been supportive and encouraging in more ways than I can ever say.

Table of Contents

Abstract.....	3
Dedication.....	5
Acknowledgements.....	6
Table of Contents.....	8
List of Tables.....	14
List of Equations.....	15
List of Schemes.....	16
List of Figures.....	18

Chapter 1**The Development and Use of Fluorescent Sensors for Imaging Biological Zinc(II):**

A Review.....	20
Introduction to Physiological Zn ²⁺	21
Zn ²⁺ in the Brain.....	22
Obstacles in Imaging Zn ²⁺	23
Properties of an Ideal Biosensor.....	23
Small-Molecule Fluorescent Sensors with UV Excitation Wavelengths.....	24
Peptide- and Protein-Based Sensors.....	26
Small-Molecule Sensors with Visible Excitation.....	27
Ratiometric Small-Molecule Sensors.....	29

Concluding Remarks	31
References	32
Chapter 2	
Membrane-Permeable and Impermeable Sensors of the Zinpyr Family and Their Application to Imaging of Hippocampal Zinc in Vivo.....	50
Introduction	51
Experimental.....	53
Materials and Methods.....	53
Synthetic Procedures.....	53
Spectroscopic Measurements.....	58
Imaging.....	60
Results and Discussion	62
Synthesis.....	62
Photophysics and Thermodynamics.....	63
Biological Imaging Studies.....	65
Conclusions	67
Acknowledgements.....	67
References	68
Chapter 3	
A Two-Fluorophore Esterase-Based Ratiometric Sensing System for Intracellular Zinc(II).....	87
Introduction	88

Experimental.....	90
Materials and Methods.....	90
Synthetic Procedures.....	90
Spectroscopic Measurements.....	99
Imaging.....	101
Results and Discussion	102
Synthesis.....	102
Photophysics and Thermodynamics.....	104
Biological Imaging	107
Conclusions	108
Acknowledgements.....	109
References	109
Chapter 4	
Bisfluorophore Approaches to Ratiometric ZP1 Sensors.....	133
Introduction	134
Experimental.....	135
Materials and Methods.....	135
Synthetic Procedures.....	136
Spectroscopic Measurements.....	141
Results and Discussion	142
Experimental Design.....	142
Synthesis.....	144

Photophysical Characterization of the Two-Fluorophore Compounds	146
Two-Fluorophore-Based Ratiometric Zn ²⁺ Sensing.....	148
Conclusions	149
Acknowledgement.....	149
References	149
Chapter 5	
ZP1 Synthons for Direct Functionalization of Biological Targets	171
Introduction	172
Experimental.....	173
Materials and Methods.....	173
Synthetic Procedures.....	174
Results and Discussion	177
Synthesis.....	177
Choice of Biological Targets	179
Conclusions	180
Acknowledgement.....	180
References	181
Retrospective.....	185
Summary Table of Sensor Properties.....	187
Appendix 1	
Isomerically Specific Approaches to Other Substituted Fluorophores	188

Introduction	189
Experimental.....	190
Materials and Methods.....	190
Synthetic Procedures.....	190
Results and Discussion	200
Fluorescein Sulfonamides.....	200
Rhodamines and Rhodamine Carboxylates.....	201
Toward Isomerically Pure Asymmetric Fluorescein or Rhodafluor Carboxylates.	202
Conclusions	203
Acknowledgements.....	204
References	204
 Appendix 2	
Modulation of Zn²⁺ Affinity By Modification of ZP1.....	221
Introduction	222
Experimental.....	222
Materials and Methods.....	222
Synthetic Procedures	223
Spectroscopic Measurements.....	225
Results and Discussion	225
Synthesis.....	225
Photophysics and Thermodynamics.....	226

Conclusions	226
References	227
Appendix 3	
Selected Spectra	235
Chapter 2 Spectra.....	236
Chapter 3 Spectra.....	239
Chapter 4 Spectra.....	245
Chapter 5 Spectra.....	251
Appendix 1 Spectra.....	254
Appendix 2 Spectra.....	270
Biographical Note.....	272

List of Tables

Table 1.1 Thermodynamic and photophysical properties of small-molecule intensity-based Zn ²⁺ sensors	41
Table 1.2. Thermodynamic and photophysical properties of small-molecule ratiometric Zn ²⁺ sensors	42
Table 2.1. Photochemical constants of ZP1(5/6-CO ₂ R) in the presence and absence of Zn ²⁺	72
Table 3.1. Photochemical properties of CZ dyes and their expected cleavage fragments	112
Table 3.2. Michaelis-Menten constants for CZ dyes.....	113
Table 4.1. Photophysical characteristics of potential calibrating fluorophores	153
Table 4.2. Photophysical characteristics of bisfluorophore rigid linker compounds.....	154
Table 4.3. Photophysical characteristics of 11.....	155
Table A1.1. Crystallographic parameters.....	209
Table A1.2. Bond lengths and angles for 3a.	210
Table A1.3. Bond lengths and angles for 5a.	210
Table A2.1. Photophysical and thermodynamic constants.....	228

List of Equations

Fitting Equation for Fluorescence-Dependent pK_a Values.....	59
Fitting Equation for Fluorescence-Dependent Dissociation Constant.....	60
Marcus Theory of Electron Transfer Rate Equation.....	142
Förster Resonance Energy Transfer Rate Equation.....	142
Förster Radius.....	143
Dexter Energy Transfer Rate Equation.....	147

List of Schemes

Scheme 1.1. Synthesis of ZP2	43
Scheme 2.1. Synthesis of ZP1(5/6-CO ₂ R)	73
Scheme 2.2. Protonation equilibria of ZP1(6-CO ₂ R).....	74
Scheme 3.1. Proposed mechanism of ratiometric Zn ²⁺ sensing	114
Scheme 3.2. Synthesis of CZ1	115
Scheme 3.3. Intramolecular cyclization under Mitsunobu conditions.	116
Scheme 3.4. Synthesis of CZ2	117
Scheme 3.5. Synthesis of putative ZP1 metabolites.....	118
Scheme 3.6. Possible esterase digestion products of CZ2.....	119
Scheme 4.1. Synthesis of ZP1-cyclohexylamine.	156
Scheme 4.2. General synthetic approach	157
Scheme 5.1. Synthesis of ZP1 alkyne and subsequent click chemistry reaction.....	183
Scheme 5.2. Synthesis of ZP1-OSu and adducts	184
Scheme A1.1. Attempted synthesis of fluorescein-2',7'-disulfonate.	213
Scheme A1.2. Synthesis, separation and attempted activation of fluorescein-5(6)-sulfonic acid.	214
Scheme A1.3. Oxalyl chloride-mediated coupling of fluorescein sulfonic acid.	215
Scheme A1.4. Dibromofluoran route to rhodamine synthesis.....	216
Scheme A1.5. Separation of dibromofluoran carboxylates and conversion to rhodamines	217

Scheme A1.6. Synthesis and potential applications of carboxylate-substituted benzophenone synthon.....	218
Scheme A2.1. Synthesis of ZP1 analogues.....	229

List of Figures

Figure 1.1. Small-molecule intensity-based sensors with UV excitation wavelengths	44
Figure 1.2. The mechanistic basis of some common sensing mechanisms: A. ESIPT, ³⁷ B. PET	45
Figure 1.3. Small-molecule intensity-based sensors with visible excitation	46
Figure 1.4. Numbering and nomenclature of fluorescein and Zinpyr sensors.....	47
Figure 1.5. Ratiometric sensors with UV excitation wavelengths.....	48
Figure 1.6. Ratiometric sensors with visible excitation	49
Figure 2.1. Structural diagrams of ZP1 and ZP4.....	75
Figure 2.2. Photophysical and thermodynamic characterization of ZP1(6-CO ₂ R).....	77
Figure 2.3. Comparison of ZP1-CO ₂ Et and ZP1 staining.	79
Figure 2.4 (A-D). Imaging of ZP1(6-CO ₂ Et) (A, B, C, D) and ZP1 (E, F, G, H)-stained rat hippocampus.....	81
Figure 2.5. Detail of ZP1(6-CO ₂ Et) imaging of the CA3 region after pilocarpine-induced seizure.....	85
Figure 3.1. Time-dependent changes in absorption spectra for CZ1 over 6 h (A) and CZ2 over 3 h (B) on treatment with porcine liver esterase.....	121
Figure 3.2. Michaelis-Menten fit of CZ esterase hydrolysis rate.	123
Figure 3.3. Fluorescence response of esterase-treated CZ1 (A) and CZ2 (B).....	125
Figure 3.4. Time course of CZ staining in HCN-A94-02 cells.	127
Figure 3.5. Fluorescence ratio images of HeLa cells treated with CZ2 after addition of ZnCl ₂ and sodium pyruvate (A, 0 min; B, 8 min), and after subsequent treatment with TPEN (C, 8 min). D: DIC image.	129

Figure 3.6. Intensity ratios of ZP1 emission divided by coumarin emission as a function of time.....	131
Figure 4.1. Structures of naphthofluorescein, X-rhodamine, and coumarin 343.....	158
Figure 4.2. Schematics of expected fluorophore interaction	159
Figure 4.3. Dichlorofluorescein-cyclohexamide-linked reporter fluorophores	161
Figure 4.4. Proton NMR spectra of 7 and 8	162
Figure 4.5. Comparative emission spectra of 8 (1 μ M) in aqueous HEPES buffer (pH 7.5, red circles) and methanolic solution (blue squares).	163
Figure 4.6. AM1 optimized equilibrium geometries of 8 (A) and 9 (B).	165
Figure 4.7. Fluorescence response of 11 to excess $ZnCl_2$	167
Figure 4.8. Change in spectral overlap integral J of coumarin 343 emission with ZPA3 absorbance upon addition of Zn^{2+}	169
Figure A1.1. Crystal structure of fluorescein-6-sulfonic acid.	219
Figure A1.2. Crystal structure of fluorescein-6-sulfonamidopicoline.	220
Figure A2.1. Structures of ZP1 and analogues.....	230
Figure A2.2. pH Dependent fluorescence of 2 (red circles) and 3 (blue squares).	231
Figure A2.3. Change in fluorescence intensity of 3 (0.5 μ M, pH 10.5, KCl 100 mM) in the presence of 10 μ M concentrations of various divalent transition metals.	233

**Chapter 1 The Development and Use of Fluorescent Sensors for Imaging Biological
Zinc(II): A Review**

Introduction to Physiological Zn²⁺

Divalent zinc plays many important roles in biology.¹ Intracellularly, most Zn(II) is tightly bound by proteins, where it may serve catalytically as a redox-inactive Lewis acid or stabilize a folding motif. Well-known examples of Zn²⁺-binding proteins include zinc finger domains, superoxide dismutase, alcohol dehydrogenase, and serine proteases. A very effective system for buffering Zn²⁺ supplies in vivo has evolved, where only extreme conditions can significantly deplete or saturate Zn²⁺ stores.^{2,3} Prolonged dietary Zn²⁺ deficiency, particularly in prenatal stages, childhood and puberty, causes a multitude of problems, primarily associated with a failure of Zn²⁺-deprived cells to divide and differentiate.⁴

Because the ligand field stabilization energy for Zn(II) is zero, the ion is amenable to wide variation in ligand type and coordination number. Hard, soft and borderline ligands are accepted, and the number of ligating amino acid functional groups generally varies between three and six.⁵ Hard ligands are more favored in catalytic systems, whereas cysteines are more common in structural Zn²⁺-binding sites.¹ Coordinative unsaturation is common in cases where the ion is an integral part of the catalytic mechanism, so that the substrate may serve as the fourth, fifth, or sixth ligand. The cysteine-rich metallothioneins may bind up to seven atoms of Zn²⁺ per protein⁶ and are capable of metallating and thus activating apoenzymes in vitro.⁷ Under conditions of oxidative stress Zn²⁺ is released, presumably via oxidation⁸ or nitrosation of the thiol ligands. Such increases in intracellular Zn²⁺ are indicative of physiological stress because intracellular Zn²⁺ concentrations are closely controlled under typical conditions. The normal level of free or loosely bound Zn²⁺, also referred to as chelatable or

histochemically reactive Zn^{2+} , in the cytoplasm has been suggested to be subfemtomolar.⁹ Zn^{2+} fluxes within the cell are controlled in part by the zinc transporter proteins ZnT-1-7, which serve to expel Zn^{2+} ions through the plasma membrane or to sequester excess Zn^{2+} in endosomes or Golgi bodies.² Metallothioneins may also act as intracellular Zn^{2+} reservoirs.¹⁰ Careful regulation of Zn^{2+} trafficking is clearly essential, for extracellular concentrations of 30 μ M or higher are toxic to all cells.¹¹

Zn^{2+} in the Brain

There exists in the CA3 region of the hippocampus a direct contrast to this picture of tightly controlled low Zn^{2+} concentrations. Although the majority of brain Zn^{2+} is bound in proteins, presynaptic vesicles in the mossy fiber region of the hippocampus contain histochemically reactive Zn^{2+} in concentrations of approximately 300 μ M.¹² This pool has been estimated to comprise approximately 5% of total brain zinc.¹³ Zn^{2+} -containing presynaptic vesicles occur exclusively at glutamatergic synapses, although not all glutamatergic synapses contain zinc-enriched vesicles, and their contents are released in a calcium- and voltage-dependent fashion.¹⁴ Over 200 effects of Zn^{2+} on neuronal receptors have been demonstrated; however, it is not known which effects are physiologically relevant. In vivo experiments suggest that moderate concentrations of Zn^{2+} can modulate neurotoxic effects of ischemia or stroke,¹⁵ whereas higher concentrations exacerbate neurotoxicity.^{16,17} Zn^{2+} -containing synaptic vesicles are decorated with ZnT-3, a zinc transporter protein that has been identified by knockout experiments as essential for loading Zn^{2+} into the vesicles.¹⁸ Knockout mice lacking synaptic Zn^{2+} show few neurological symptoms, presumably owing to the brain's ability to adapt,^{19,20} but are more susceptible to kainic acid-induced seizures.²¹ Physiological

release of Zn^{2+} is also age-dependent, because release is not observed in newborn or juvenile mice or rats.

Obstacles in Imaging Zn^{2+}

A major reason that synaptic Zn^{2+} is so poorly understood is the difficulty of studying it experimentally. The filled-shell d^{10} configuration that makes Zn^{2+} biologically valuable as a redox-inactive Lewis acid simultaneously excludes the possibility of monitoring Zn^{2+} movement by EPR or by UV-active d-d transitions. The Zn^{2+} nucleus has poor sensitivity to NMR. Turnover of brain Zn^{2+} is very slow, rendering replacement with radioactive ^{57}Zn an ineffective strategy.¹² Histochemically reactive Zn^{2+} is a relatively small fraction of total brain Zn^{2+} ; thus any approach in which Zn^{2+} is studied must selectively image chelatable Zn^{2+} to avoid burying the signal of interest in the high background. Zinc(II) in the brain has traditionally been studied by fluorescent sensors or autometallographic techniques, methodologies that selectively image free or loosely bound Zn^{2+} . Because autometallography is irreversible and requires relatively harsh conditions, it is not compatible with the study of living tissue.²² Hence, fluorescent biosensors are the method of choice for dynamic studies of biological Zn^{2+} .

Properties of an Ideal Biosensor

The ideal properties of a fluorescent biosensor have been outlined by Kimura and Koike.²³ Briefly, a fluorescent sensor should be intensely fluorescent and afford a selective response to the desired analyte, particularly in the presence of other biological cations such as Na^+ , K^+ , Ca^{2+} , and Mg^{2+} . Excitation wavelengths should exceed 400 nm in order to avoid irradiating biological samples with damaging UV light, and emission wavelengths should exceed 500 nm to avoid the autofluorescence of native species in the

cell. The dissociation constant should approach the median concentration of analyte under study to provide meaningful information about the amount of analyte present. The mode of delivery to the target system must also be considered. Ideally, the sensor should be able to diffuse passively into the region of interest and become trapped there. This is most often accomplished by inclusion of esters in the sensor.²⁴⁻²⁶ The lipophilic ester may diffuse passively across the cell membrane, where it can be hydrolyzed by intracellular esterases present in the cytoplasm, affording a charged carboxylate that cannot diffuse out of the cell. Acetoxymethyl esters are often used in place of alkyl esters because they are more easily hydrolyzed.²⁷ The sensor should ideally afford two easily differentiable fluorescent signals in the presence and absence of analyte, enabling ratiometric measurement of the amount of free and bound sensor and allowing a more precise analysis of analyte concentration.

Small-Molecule Fluorescent Sensors with UV Excitation Wavelengths

Various approaches to fluorescent Zn^{2+} sensing have been reported. The first Zn^{2+} probe reported was TSQ (1),²⁸ which gave rise to other sensors including Zinquin (2)²⁴ and 2-Me-TSQ (3)²⁹ (Figure 1.1). These probes bind Zn^{2+} as a 2:1 ligand:metal complex with loss of the sulfonamide proton, and are intensity-based, with excitation around 350 nm and emission at 480 nm. The TSQ staining protocol is not compatible with living cells, so Zinquin, which contains an ethyl ester to increase solubility and intracellular retention, is widely used for imaging in live cells. The aqueous coordination chemistry of Zinquin has been examined in depth by Fahrni and O'Halloran.³⁰ However, the high-energy wavelengths required, the formation of non-stoichiometric complexes, and the extremely high affinity for Zn^{2+} leave significant room for improvement. Photophysical

and thermodynamic characteristics of these and other intensity-based sensors are listed in Table 1.1.

Sensing systems with azamacrocyclic-based Zn^{2+} -binding moieties and dansyl (**4**, **5**) or anthracyl (**6**) fluorophore reporter units have been reported by Kimura et al.³¹⁻³³ The dansyl sulfonamides **4** and **5** are deprotonated upon binding of Zn^{2+} , affording a slight blueshift of the absorption spectrum and an approximately five-fold increase in fluorescence. The anthracyl system **6** operates by a photoinduced electron transfer (PET) mechanism, in which the presence of a proximal amine lone pair provides a non-radiative relaxation pathway for the excited fluorophore. Coordination of Zn^{2+} or protons to this lone pair blocks the non-radiative relaxation pathway such that the excited fluorophore must emit a photon in order to relax back to the ground state. This system was based on a similar system, described by Czarnik et al.,³⁴ lacking the ethyl spacer between fluorophore and macrocycle, and is effective at high pH. A tricarboxycyclen macrocycle has been appended to a 6,7-dimethoxycoumarin fluorophore in **7**³⁵ and affords a similar effect, but displays slow binding kinetics. The time scale of fluorescence increase for sensors **4-6** was not discussed. A similar dimethoxycoumarin-based sensor with a dipicolylamine binding unit (**8**) affords faster binding kinetics and a significantly improved dynamic range.³⁶ Finally, Fahrni and coworkers have investigated the properties of 2'-hydroxyphenyl benzoxazole **9** and its derivatives as potential ratiometric sensors based on an excited-state intramolecular proton transfer (ESIPT) mechanism.³⁷ Alcoholic or unbuffered aqueous environments afford a wavelength shift; however, physiologically relevant conditions interfere with the ESIPT process and render a 50-fold increase in

fluorescence intensity with no change in wavelength. Schematic representations of the ESIPT and PET mechanisms are shown in Figure 1.2.

Peptide- and Protein-Based Sensors

This review is primarily concerned with cell-permeable small molecule sensors; however, no discussion of Zn^{2+} sensors would be complete without mention of peptide- and protein-based sensors. A set of peptide-based sensors have been described by Imperiali et al.^{38,39} These sensors incorporate Zn^{2+} -finger binding motifs, which are among the few sensing systems that are selective for Zn^{2+} over Cu^{2+} , and the affinity of the peptide can be tuned by alteration of the ligating amino acids. Initial studies focused on peptide folding nucleated by binding of the metal ion, and on the resulting changes in the environment of the fluorophore. An environment-sensitive fluorophore such as dansyl or coumarin affords a large fluorescence enhancement under these conditions. More recently, an unnatural amino acid containing a chelation-enhanced fluorescence (CHEF)-capable 8-hydroxyquinoline fluorophore⁴⁰ has been incorporated adjacent to a β -turn in short (6-8 residue) peptides with varying affinities for Zn^{2+} , affording sensors with a range of sensitivities.⁴¹ Godwin and Berg⁴² also reported a peptide-based sensor in which each end of the peptide is functionalized with a different fluorophore. On binding Zn^{2+} , the two fluorophores are brought close to each other and can undergo fluorescence resonance energy transfer (FRET), giving rise to an emission shift on excitation of the donor and thereby a ratiometric response to Zn^{2+} . These large, charged peptides are not membrane-permeable, and because the fluorophores are not naturally occurring amino acid residues, the peptides cannot be expressed intracellularly by genetic manipulation. All of these peptide-based sensors require microinjection for intracellular studies.

A system based on carbonic anhydrase has been developed by Thompson, Fierke et al.⁴³ This enzyme binds Zn^{2+} with picomolar affinity in a coordinatively unsaturated configuration. Addition of various sulfonamides to the holoenzyme results in binding of the sulfonamide to the open coordination site of the zinc ion,⁴⁴ with a concomitant change in fluorophore environment. The signal can be measured by fluorescence anisotropy techniques,⁴⁵ or the enzyme can be labeled with a second fluorophore capable of FRET with the sulfonamide to afford a ratiometric measurement of Zn^{2+} binding.⁴⁶ This system has been applied to the measurement of extracellular Zn^{2+} fluxes.⁴⁷

Small-Molecule Sensors with Visible Excitation

Various fluorescein-based sensors have been reported. Fluorescein offers advantages in imaging owing to its visible excitation and emission, low toxicity, and compatibility with the argon ion laser. Fluorine substitution of fluoresceins confers added photostability.⁴⁸ The FluoZin class of probes (**10-12**, Figure 1.3), developed and supplied by Molecular Probes, is based on a difluorofluorescein platform in which the 2-carboxylate may or may not be present. The dissociation constants of these probes range from 15 nM to 7.8 μ M.⁴⁹ Newport Green (**13**), another Molecular Probes product, incorporates a dipicolylamine binding unit in which the amine is covalently bound to the 5-position of the descarboxy difluorofluorescein platform, and binds Zn^{2+} with a dissociation constant of 40 μ M.⁵⁰ FluoZin-like probes based on a rhodamine fluorophore platform have also been described (**14, 15**). At least one member of this class localizes to the mitochondria in living cells.⁵¹

Nagano et al. have described the synthesis of ZnAF-1(F) (**16a, b**) and -2(F) (**17a, b**),^{52,53} in which the Zn^{2+} -binding unit is based on dipicolylamine, and ACF-1 (**18a**) and -

2 (**18b**)⁵⁴, which incorporate a cyclen binding unit. Both classes of sensors are based on aminofluorescein, operate via a PET mechanism, and afford up to a 69-fold enhancement in fluorescence. The ACF sensors, however, suffer from slow binding kinetics, requiring more than an hour for equilibration. All of the fluorescein-based sensors described by Molecular Probes and Nagano et al are relatively complicated structures that require multi-step syntheses, many of them with low overall yields. Structures of intensity-based sensors with visible excitation maxima are shown in Figure 1.3.

Zinpyr-1 (ZP1, **19a**, Figure 1.4) was designed and synthesized in one step from commercially available starting materials by the Tsien group at UCSD in 1998. Independently but in parallel, the Lippard group synthesized the closely related ZP2 (**19b**) via the more general, if circuitous, route shown in Scheme 1.1.^{55,56} These ZP1-type probes are PET-based and contain two dipicolylamine Zn^{2+} -binding sites with subnanomolar binding constants for the first binding event, and micromolar for the second. Only the first binding event causes an increase in fluorescence. Both sensors are extremely bright and membrane-permeable without modification. The sensors display significant background fluorescence, a property that may be related to the high pK_a values (8.4 and 9.4 for **19a** and **19b** respectively) of the benzylic amines responsible for the PET effect. Protonation of these amines occurs at physiological pH, blocking the PET relaxation pathway. COS-7 cells treated with ZP1 exhibit a punctate staining pattern that increases in intensity upon addition of zinc(II) and pyrithione. The sensor is colocalized with the Golgi apparatus. A class of sensors referred to as ZP4-type (**20a-e**), based on an asymmetric fluorescein platform that allows for functionalization with a single Zn^{2+} -binding site, was subsequently designed and synthesized.⁵⁷ An aniline nitrogen atom was

incorporated for PET quenching to reduce the pH sensitivity of the sensors. The ZP4-type sensors are not membrane permeable, and this property has been exploited in the selective imaging of injured neurons in rat hippocampal slices.⁵⁸

Recent efforts have focused on the examination of substituent effects. Substitution at the 2' and 7' positions of the fluorescein is necessary to restrict Mannich reactivity to the 4' and 5' positions. Examination of fluorine, chlorine, and bromine substituents at these and at the 4, 5, 6, and 7 positions of the fluorescein revealed that fluorine substituents at the 2' and 7' positions reduce background fluorescence and greatly enhance the dynamic range of the sensor ZP3 (**19c**) compared to ZP1 (**19a**).⁵⁹ The numbering scheme of fluorescein and the nomenclature of ZP sensors are shown in Figure 1.4. A probe based on the asymmetric fluorescein platform used for the ZP4 series but incorporating an aminoquinoline binding unit has recently been developed.⁶⁰ This probe, called Quinozin-1 (QZ1, **21**), affords a much larger dynamic range and higher dissociation constant than the ZP1 or ZP4 series, and should be very useful in biological studies.

Ratiometric Small-Molecule Sensors

Ratiometric sensors for Zn²⁺ based on Fura-2 have been synthesized by Nagano et al, and by Molecular Probes. The Nagano probes, ZnAF-R1 and -R2 (**22**, **23**, Figure 1.5), are based on an internal charge transfer (ICT) mechanism. Binding of Zn²⁺ to the aniline nitrogen atom interferes with charge transfer and affords a blueshift in excitation wavelength. Metallation with Zn²⁺ also decreases the already-low quantum yield of the benzofuran-based sensors (Table 1.2).²⁶ Molecular Probes has described FuraZin-1 (**24**) and IndoZin-1 (**25**), which are based on 2-aryl benzofuran or indole, respectively, and

incorporate an iminodiacetate Zn^{2+} -binding moiety rather than the dipicolylamine of the ZnAF-R sensors. Like the ZnAF-R series, FuraZin-1 affords a blueshift in excitation wavelength on binding Zn^{2+} , whereas IndoZin-1 affords a blueshift in emission.⁶¹ Quantum yields for these compounds have not been reported, but are presumably also relatively low.

Emission ratiometric probes are preferable to excitation ratiometric probes, because excitation sources can vary in intensity at different wavelengths and may require the use of multiple lasers for two-photon or confocal imaging, which is often impractical. More recently, the concept of excited-state intramolecular proton transfer (ESIPT) has been applied to Zn^{2+} sensing.^{25,37} Fahrni and coworkers reported such benzimidazole probes (26-29) in which intramolecular proton transfer of the free probe lowers emission energy. Binding of Zn^{2+} blocks this mechanism and induces a blueshift in emission wavelength. Incorporation of additional binding moieties enables modulation of probe affinity. O'Halloran and co-workers recently reported a 2-arylbenzoxazole probe (30) containing a picolylamine binding moiety.⁶² Unlike the Nagano, Molecular Probes and Fahrni sensors, Zinbo-5 excitation and emission undergo a redshift on binding Zn^{2+} . For simplicity, data are acquired by using excitation at an isosbestic point in the absorption spectrum. The reason for redshifted emission of the metallated form is unclear. The dynamic range measured in vitro is relatively good; however, the intracellular dynamic range is quite low (faux-color scale range 0.96-1.25, ratio increase ~ 15%). The structures of UV-excitabile ratiometric probes are shown in Figure 1.5.

All of the fused 6, 5-heterocycle-based ratiometric probes described above require UV excitation, and many suffer from poor quantum yields. The 7-aminocoumarin-based

sensor **31** incorporates a dipicolylamine Zn^{2+} -binding moiety and affords a 21 nm bathochromic shift in emission maximum in methanolic solution, but the wavelength shift is minimal in aqueous solution.³⁶ To date, the only reported water-compatible small-molecule ratiometric sensing system with visible excitation and emission wavelengths is the tautomeric sensor ZNP-1 (**32**), reported by Lippard and co-workers.⁶³ ZNP-1 is an asymmetric fluorescein/naphthofluorescein hybrid, with a relatively weak emission band at 524-545 nm and a strongly Zn^{2+} -sensitive emission band at 604-624 nm. The wavelengths indicate that fluorescence is dominated by the naphthofluorescein-like fluorescence, an observation that is supported by the low quantum yield at physiological pH (Table 1.2). The affinity of the probe for Zn^{2+} is comparable to that of other fluorescein-based sensors with dipicolylamine binding moieties. ZNP-1 has been utilized in the imaging of endogenous Zn^{2+} in living cells using nitric oxide donors to induce release of Zn^{2+} from intracellular sources. Structures of **31** and **32** are shown in Figure 1.6.

Concluding Remarks

Biological Zn^{2+} plays many important roles, and the imaging of labile physiological Zn^{2+} is of great interest. Owing to the spectroscopically silent nature of the ion and the sensitivity of fluorescence techniques, fluorescent sensors are ideal to explore these processes. Recent years have seen an explosion in the number and nature of available fluorescent sensors for imaging intracellular Zn^{2+} , and small-molecule sensors based on PET, ICT, and ESIPT have been described. To date, none has been successful in meeting all of the criteria for an ideal Zn^{2+} sensor and there remains room for continued research in this field. The research described herein has focused on functionalization of

the known sensor ZP1 to include more of these desirable properties; specifically, on the inclusion of ester and acid moieties to control the subcellular localization of the sensor (Chapter 1), on the covalent attachment of a second, Zn²⁺-insensitive fluorophore to enable ratiometric sensing (Chapters 3 and 4), and on the development of methodology to covalently link biologically active molecules to ZP1 (Chapter 5). Approaches to other acid-functionalized fluorophores (Appendix 1) and the effect of alterations to the dipicolylamine binding units (Appendix 2) are also discussed.

References

- (1) Vallee, B. L.; Falchuk, K. H. The Biochemical Basis of Zinc Physiology. *Physiol. Rev.* **1993**, *73*, 79-118.
 - (2) Palmiter, R. D.; Huang, L. Efflux and compartmentalization of zinc by members of the SLC30 family of solute carriers. *Pflugers Arch. - Eur. J. Physiol.* **2004**, *447*, 744-751.
 - (3) Kambe, T.; Yamaguchi-Iwai, Y.; Sasaki, R.; Nagao, M. Overview of mammalian zinc transporters. *Cell. Mol. Life Sci.* **2004**, *61*, 49-68.
 - (4) Hambridge, M. Human Zinc Deficiency. *J. Nutr.* **2000**, *130*, 1344S-1349S.
 - (5) Lippard, S. J.; Berg, J. M. *Principles of Bioinorganic Chemistry*; 1 ed.; University Science Books: Mill Valley, 1994.
 - (6) Maret, W. Zinc and Sulfur: A Critical Biological Partnership. *Biochemistry* **2004**, *43*, 3301-3309.
 - (7) Jacob, C.; Maret, W.; Vallee, B. L. Control of zinc transfer between thionein, metallothionein, and zinc proteins. *Proc. Natl. Acad. Sci. USA* **1998**, *95*, 3489-3494.
-

- (8) Maret, W. Oxidative metal release from metallothionein via zinc-thiol/disulfide exchange. *Proc. Natl. Acad. Sci. USA* **1994**, *91*, 237-241.
- (9) Outten, C. E.; O'Halloran, T. V. Femtomolar Sensitivity of Metalloregulatory Proteins Controlling Zinc Homeostasis. *Science* **2001**, *292*, 2488-2492.
- (10) Palmiter, R. D. Protection against zinc toxicity by metallothionein and zinc transporter 1. *Proc. Natl. Acad. Sci. USA* **2004**, *101*, 4918-4923.
- (11) Choi, D. W.; Koh, J. Y. Zinc and Brain Injury. *Annu. Rev. Neurosci.* **1998**, *21*, 347-375.
- (12) Frederickson, C. J. Neurobiology of Zinc and Zinc-containing Neurons. *Int. Rev. Neurobiol.* **1989**, *31*, 145-238.
- (13) Frederickson, C. J.; Suh, S. W.; Silva, D.; Frederickson, C. J.; Thompson, R. B. Importance of Zinc in the Central Nervous System: The Zinc-Containing Neuron. *J. Nutr.* **2000**, *130*, 1471S-1483S.
- (14) Assaf, S. Y.; Chung, S.-H. Release of endogenous Zn²⁺ from brain tissue during activity. *Nature* **1984**, *308*, 734-736.
- (15) Koh, J.-Y.; Suh, S. W.; Gwag, B. J.; He, Y. Y.; Hsu, C. Y.; Choi, D. W. The Role of Zinc in Selective Neuronal Death After Transient Global Cerebral Ischemia. *Science* **1996**, *272*, 1013-1016.
- (16) Suh, S. W.; Chen, J. W.; Motamedi, M.; Bell, B.; Listiak, K.; Pons, N. F.; Danscher, G.; Frederickson, C. J. Evidence that synaptically-released zinc contributes to neuronal injury after traumatic brain injury. *Brain Res.* **2000**, *852*, 268-273.

- (17) Lee, J.-M.; Zipfel, G. J.; Park, K. H.; He, Y. Y.; Hsu, C. Y.; Choi, D. W. Zinc translocation accelerates infarction after mild transient focal ischemia. *Neuroscience* **2002**, *115*, 871-878.
- (18) Palmiter, R. D.; Cole, T. B.; Quaife, C. J.; Findley, S. D. ZnT-3, a putative transporter of zinc into synaptic vesicles. *Proc. Natl. Acad. Sci. USA* **1996**, *93*, 14934-14939.
- (19) Cole, T. B.; Wenzel, H. J.; Kafer, K. E.; Schwartzkroin, P. A.; Palmiter, R. D. Elimination of zinc from synaptic vesicles in the intact mouse brain by disruption of the ZnT3 gene. *Proc. Natl. Acad. Sci. USA* **1999**, *96*, 1716-1721.
- (20) Lopantsev, V.; Wenzel, H. J.; Cole, T. B.; Palmiter, R. D.; Schwartzkroin, P. A. Lack of vesicular zinc in mossy fibers does not affect synaptic excitability of CA3 pyramidal cells in zinc transporter 3 knockout mice. *Neuroscience* **2003**, *116*, 237-248.
- (21) Cole, T. B.; Robbins, C. A.; Wenzel, H. J.; Schwartzkroin, P. A.; Palmiter, R. D. Seizures and neuronal damage in mice lacking vesicular zinc. *Epilepsy Res.* **2000**, *39*, 153-169.
- (22) Danscher, G.; Juhl, S.; Stoltenberg, M.; Krunderup, B.; Schroder, H. D.; Andreasen, A. Autometallographic silver enhancement of zinc sulfide crystals created in cryostat sections from human brain biopsies: A new technique that makes it feasible to demonstrate zinc ions in tissue sections from biopsies and early autopsy material. *J. Histochem. Cytochem.* **1997**, *45*, 1503-1510.
- (23) Kimura, E.; Koike, T. Recent development of zinc-fluorophores. *Chem. Soc. Rev.* **1998**, *27*, 179-184.
-

- (24) Zalewski, P. D.; Millard, S. H.; Forbes, I. J.; Kapaniris, O.; Slavotinek, A.; Betts, W. H.; Ward, A. D.; Lincoln, S. F.; Mahadevan, I. Video Image Analysis of Labile Zinc in Viable Pancreatic Islet Cells Using a Specific Fluorescent Probe for Zinc. *J. Histochem. Cytochem.* **1994**, *42*, 877-884.
- (25) Henary, M. M.; Wu, Y.; Fahrni, C. J. Zn(II)-Selective Ratiometric Fluorescent Sensors Based on Inhibition of Excited-State Intramolecular Proton Transfer. *Chem. Eur. J.* **2004**, *10*, 3015-3025.
- (26) Maruyama, S.; Kikuchi, K.; Hirano, T.; Urano, Y.; Nagano, T. A Novel, Cell-Permeable, Fluorescent Probe for Ratiometric Imaging of Zinc Ion. *J. Am. Chem. Soc.* **2002**, *124*, 10650-10651.
- (27) Tsien, R. Y.; Pozzan, T.; Rink, T. J. Calcium Homeostasis in Intact Lymphocytes: Cytoplasmic Free Calcium Monitored With a New, Intracellularly Trapped Fluorescent Indicator. *J. Cell Biol.* **1982**, *94*, 325-334.
- (28) Frederickson, C. J.; Kasarskis, E. J.; Ringo, D.; Frederickson, R. E. A quinoline fluorescence method for visualizing and assaying the histochemically reactive zinc (bouton zinc) in the brain. *J. Neurosci. Methods* **1987**, *20*, 91-103.
- (29) Nasir, M. S.; Fahrni, C. J.; Suhy, D. A.; Kolodsick, K. J.; Singer, C. P.; O'Halloran, T. V. The chemical cell biology of zinc: structure and intracellular fluorescence of a zinc-quinolinesulfonamide complex. *J. Biol. Inorg. Chem.* **1999**, *4*, 775-783.
- (30) Fahrni, C. J.; O'Halloran, T. V. Aqueous Coordination Chemistry of Quinoline-Based Fluorescence Probes for the Biological Chemistry of Zinc. *J. Am. Chem. Soc.* **1999**, *121*, 11448-11458.

- (31) Koike, T.; Watanabe, T.; Aoki, S.; Kimura, E.; Shiro, M. A Novel Biomimetic Zinc(II)-Fluorophore, Dansylamidoethyl-Pendant Macrocyclic Tetraamine 1,4,7,10-Tetraazacyclododecane (Cyclen). *J. Am. Chem. Soc.* **1996**, *118*, 12696-12703.
- (32) Koike, T.; Abe, T.; Takahashi, M.; Ohtani, K.; Kimura, E.; Shiro, M. Synthesis and characterization of the zinc(II)-fluorophore, 5-dimethylaminonaphthalene-1-sulfonic acid [2-(1,5,9-triazacyclododec-1-yl)ethyl]amide and its zinc(II) complex. *J. Chem. Soc. Dalton Trans.* **2002**, 1764-1768.
- (33) Aoki, S.; Kaido, S.; Fujioka, H.; Kimura, E. A New Zinc(II) Fluorophore 2-(9-Anthrylmethylamino)ethyl-Appended 1,4,7,10-Tetraazacyclododecane. *Inorg. Chem.* **2003**, *42*, 1023-1030.
- (34) Czarnik, A. W. Chemical Communications in Water Using Fluorescent Chemosensors. *Acc. Chem. Res.* **1994**, *27*, 302-308.
- (35) Lim, N. C.; Yao, L.; Freake, H. C.; Brückner, C. Synthesis of a Fluorescent Chemosensor Suitable for the Imaging of Zinc(II) in Live Cells. *Bioorg. Med. Chem. Lett.* **2003**, *13*, 2251-2254.
- (36) Lim, N. C.; Brückner, C. DPA-substituted coumarins as chemosensors for zinc(II): modulation of the chemosensory characteristics by variation of the position of the chelate on the coumarin. *Chem. Commun.* **2004**, 1094-1095.
- (37) Henary, M. M.; Fahrni, C. J. Excited State Intramolecular Proton Transfer and Metal Ion Complexation of 2-(2'-Hydroxyphenyl)benzazoles in Aqueous Solution. *J. Phys. Chem. A* **2002**, *106*, 5210-5220.
-

- (38) Walkup, G. K.; Imperiali, B. Design and Evaluation of a Peptidyl Fluorescent Chemosensor for Divalent Zinc. *J. Am. Chem. Soc.* **1996**, *118*, 3053-3054.
- (39) Walkup, G. K.; Imperiali, B. Fluorescent Chemosensors for Divalent Zinc Based on Zinc Finger Domains. Enhanced Oxidative Stability, Metal Binding Affinity, and Structural and Functional Characterization. *J. Am. Chem. Soc.* **1997**, *119*, 3443-3450.
- (40) Pearce, D. A.; Jotterand, N.; Carrico, I. S.; Imperiali, B. Derivatives of 8-Hydroxy-2-methylquinoline are Powerful Prototypes for Zinc Sensors in Biological Systems. *J. Am. Chem. Soc.* **2001**, *123*, 5160-5161.
- (41) Shults, M. D.; Pearce, D. A.; Imperiali, B. Modular and Tunable Chemosensor Scaffold for Divalent Zinc. *J. Am. Chem. Soc.* **2003**, *125*, 10591-10597.
- (42) Godwin, H. A.; Berg, J. M. A Fluorescent Zinc Probe Based on Metal-Induced Peptide Folding. *J. Am. Chem. Soc.* **1996**, *118*, 6514-6515.
- (43) Fierke, C. A.; Thompson, R. B. Fluorescence-based biosensing of zinc using carbonic anhydrase. *BioMetals* **2001**, *14*, 205-222.
- (44) Chen, R. F.; Kernohan, J. C. Combination of Bovine Carbonic Anhydrase with a Fluorescent Sulfonamide. *J. Biol. Chem.* **1967**, *242*, 5813-5823.
- (45) Thompson, R. B.; Maliwal, B. P.; Felliccia, V. L.; Fierke, C. A.; McCall, K. Determination of Picomolar Concentrations of Metal Ions Using Fluorescence Anisotropy: Biosensing with a "Reagentless" Enzyme Transducer. *Anal. Chem.* **1998**, *70*, 4717-4723.

- (46) Thompson, R. B.; Cramer, M. L.; Bozym, R.; Fierke, C. A. Excitation ratiometric fluorescent biosensor for zinc ion at picomolar levels. *J. Biomed. Opt.* **2002**, *7*, 555-560.
- (47) Thompson, R. B.; Whetsell Jr., W. O.; Maliwal, B. P.; Fierke, C. A.; Frederickson, C. J. Fluorescence microscopy of stimulated Zn(II) release from organotypic cultures of mammalian hippocampus using a carbonic anhydrase-based biosensor system. *J. Neurosci. Meth.* **2000**, *96*, 35-45.
- (48) Sun, W. C.; Gee, K. R.; Klaubert, D. H.; Haugland, R. P. Synthesis of Fluorinated Fluoresceins. *J. Org. Chem.* **1997**, *62*, 6469-6475.
- (49) Qian, W.-J.; Gee, K. R.; Kennedy, R. T. Imaging of Zn²⁺ Release from Pancreatic beta-Cells at the Level of Single Exocytotic Events. *Anal. Chem.* **2003**, *75*, 3468-3475.
- (50) Haugland, R. P. *Handbook of Fluorescent Probes and Research Products, Ninth Edition*; Ninth ed.; Molecular Probes, Inc.: Eugene, Oregon, 2002.
- (51) Sensi, S. L.; Ton-That, D.; Weiss, J. H.; Rothe, A.; Gee, K. R. A new mitochondrial fluorescent zinc sensor. *Cell Calcium* **2003**, *34*, 281-284.
- (52) Hirano, T.; Kikuchi, K.; Urano, Y.; Higuchi, T.; Nagano, T. Highly Zinc-Selective Fluorescent Sensor Molecules Suitable for Biological Applications. *J. Am. Chem. Soc.* **2000**, *122*, 12399-12400.
- (53) Hirano, T.; Kikuchi, K.; Urano, Y.; Nagano, T. Improvement and Biological Applications of Fluorescent Probes for Zinc, ZnAFs. *J. Am. Chem. Soc.* **2002**, *124*, 6555-6562.
-

- (54) Hirano, T.; Kikuchi, K.; Urano, Y.; Higuchi, T.; Nagano, T. Novel Zinc Fluorescent Probes Excitable with Visible Light for Biological Applications. *Angew. Chem. Int. Ed.* **2000**, *39*, 1052-1054.
- (55) Walkup, G. K.; Burdette, S. C.; Lippard, S. J.; Tsien, R. Y. A New Cell-Permeable Fluorescent Probe for Zn²⁺. *J. Am. Chem. Soc.* **2000**, *122*, 5644-5645.
- (56) Burdette, S. C.; Walkup, G. K.; Spingler, B.; Tsien, R. Y.; Lippard, S. J. Fluorescent Sensors for Zn²⁺ Based on a Fluorescein Platform: Synthesis, Properties and Intracellular Distribution. *J. Am. Chem. Soc.* **2001**, *123*, 7831-7841.
- (57) Burdette, S. C.; Frederickson, C. J.; Bu, W.; Lippard, S. J. ZP4, an Improved Neuronal Zn²⁺ Sensor of the Zinpyr Family. *Journal of the American Chemical Society* **2003**, *125*, 1778-1787.
- (58) Frederickson, C. J.; Burdette, S. C.; Frederickson, C. J.; Sensi, S. L.; Weiss, J. H.; Yin, H. Z.; Balaji, R. V.; Truong-Tran, A. Q.; Bedell, E.; Prough, D. S.; Lippard, S. J. Method for Identifying Neuronal Cells Suffering Zinc Toxicity by Use of a Novel Fluorescent Sensor. *J. Neurosci. Meth.* **2004**, in press.
- (59) Chang, C. J.; Nolan, E. M.; Jaworski, J.; Burdette, S. C.; Sheng, M.; Lippard, S. J. Bright Fluorescent Chemosensor Platforms for Imaging Endogenous Pools of Neuronal Zinc. *Chem. Biol.* **2004**, *11*, 203-210.
- (60) Nolan, E. M.; Lippard, S. J. Quinozin-1. *J. Am. Chem. Soc.* **2004**, *126*, manuscript in preparation.

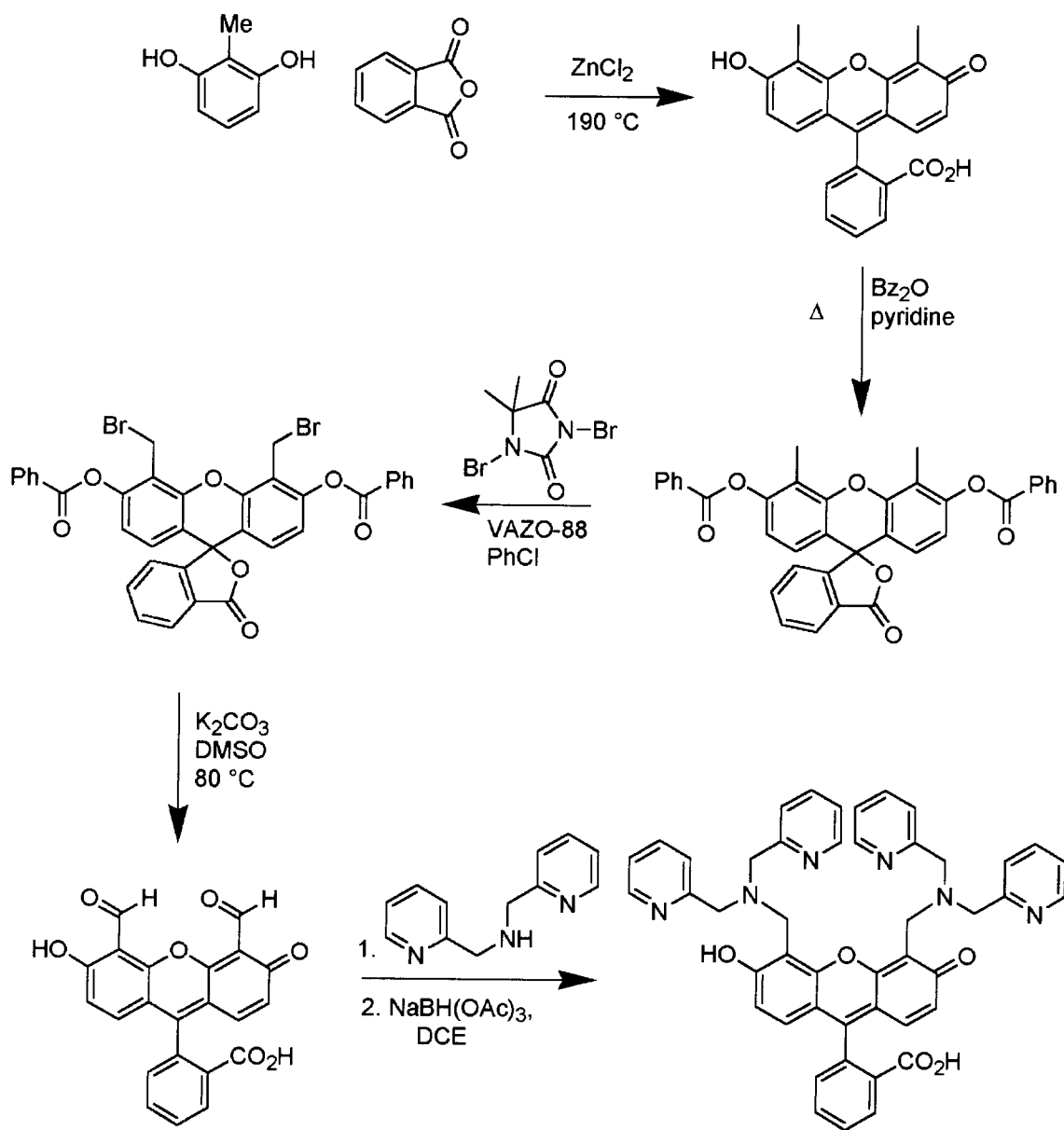
- (61) Gee, K. R.; Zhou, Z. L.; Ton-That, D.; Sensi, S. L.; Weiss, J. H. Measuring zinc in living cells. A new generation of sensitive and selective fluorescent probes. *Cell Calcium* **2002**, *31*, 245-251.
- (62) Taki, M.; Wolford, J. L.; O'Halloran, T. V. Emission Ratiometric Imaging of Intracellular Zinc: Design of a Benzoxazole Fluorescent Sensor and its Application in Two-Photon Microscopy. *J. Am. Chem. Soc.* **2004**, *126*, 712-713.
- (63) Chang, C. J.; Jaworski, J.; Nolan, E. M.; Sheng, M.; Lippard, S. J. A tautomeric zinc sensor for ratiometric fluorescence imaging: Application to nitric oxide-induced release of intracellular zinc. *Proc. Natl. Acad. Sci. USA* **2004**, *101*, 1129-1134.
-

Table 1.1 Thermodynamic and photophysical properties of small-molecule intensity-based Zn²⁺ sensors

Sensor	K _d	λ _{ex} (nm)	λ _{em} (nm)	Φ _{free} , Φ _{Zn}	Dynamic range
Zinquin (2)	log K' = 13.5	337	477		
2-Me-TSQ (3)	log β _{1,2} = 8.43, 18.2	362	485		>300
4	0.6 pM	330	528	0.03, 0.11	4.9
5	0.9 μM	320	568/538		5.2
6	20 pM	368	416	0.14, 0.44	3.1
7	< 1 μM	345	448	-, 0.26	4.4
8	0.5 μM	343		0.038, 0.88	
ESIPT(9)	logK = 3.93	347	411	0.26	50
FluoZin-1(10)	7.8 μM	491	520		~240
FluoZin-2(11)	2.1 μM	492	521		
FluoZin-3(12)	15 nM	494	516	<0.005, 0.43	>100
Newport Green(13)	40 μM	492	521		
RhodZin(14)	23 μM	548	589		
X-Rhodzin(15)	11 μM	575	604		
ZnAF-1(16a)	0.78nM	492	514	0.022, 0.23	
ZnAF-2(17a)	2.7 nM	492	514	0.023, 0.36	
ZnAF-1F(16b)	2.2 nM	492		0.004, 0.17	69
ZnAF-2F(17b)	5.5 nM	492		0.006, 0.24	60
ACF-1(18a)	-	495	515		14
ACF-2(18b)	-	505	525		26
ZP1 (19a)	0.7 nM	515/507	531/527	0.38, 0.87	2-3
ZP3 (19c)	0.7 nM	502/492	521/516	0.15, 0.92	> 6
ZP4 (20a)	0.65 nM	506/495	521/515	0.06, 0.34	5
QZ1 (21)	33 μM	505/498	520	0.024, 0.78	42

Table 1.2. Thermodynamic and photophysical properties of small-molecule ratiometric Zn²⁺ sensors

Sensor	λ_{ex} (nm)	λ_{em} (nm)	K_d	Φ_{free}	Φ_{Zn}	Dynamic range	Passive loading?
ZnAF-R1 (22)	359/329	532/528	0.79 nM	0.088	0.031		Ethyl Ester
ZnAF-R2 (23)	365/335	495/495	2.8 nM	0.17	0.10	3.5	Ethyl Ester
FuraZin-1 (24)	378/330	510	3.4 μ M			~1.7	Ester
IndoZin-1 (25)	350/350	480/395	3.0 μ M				Ester
26							
27	300-309/ 294-338	460-471/ 406-420	varied	0.09- 0.32	0.17- 0.23	19-82	Ester
28							
29							
Zinbo-5 (30)	337/376	407/443	2.2 nM	0.02	0.10	3.5?	Yes
31	410	484/505		0.64			
ZNP-1(32)	499	528, 604/ 545, 624	0.55 nM	0.02	0.05	18	Ester



Scheme 1.1. Synthesis of ZP2

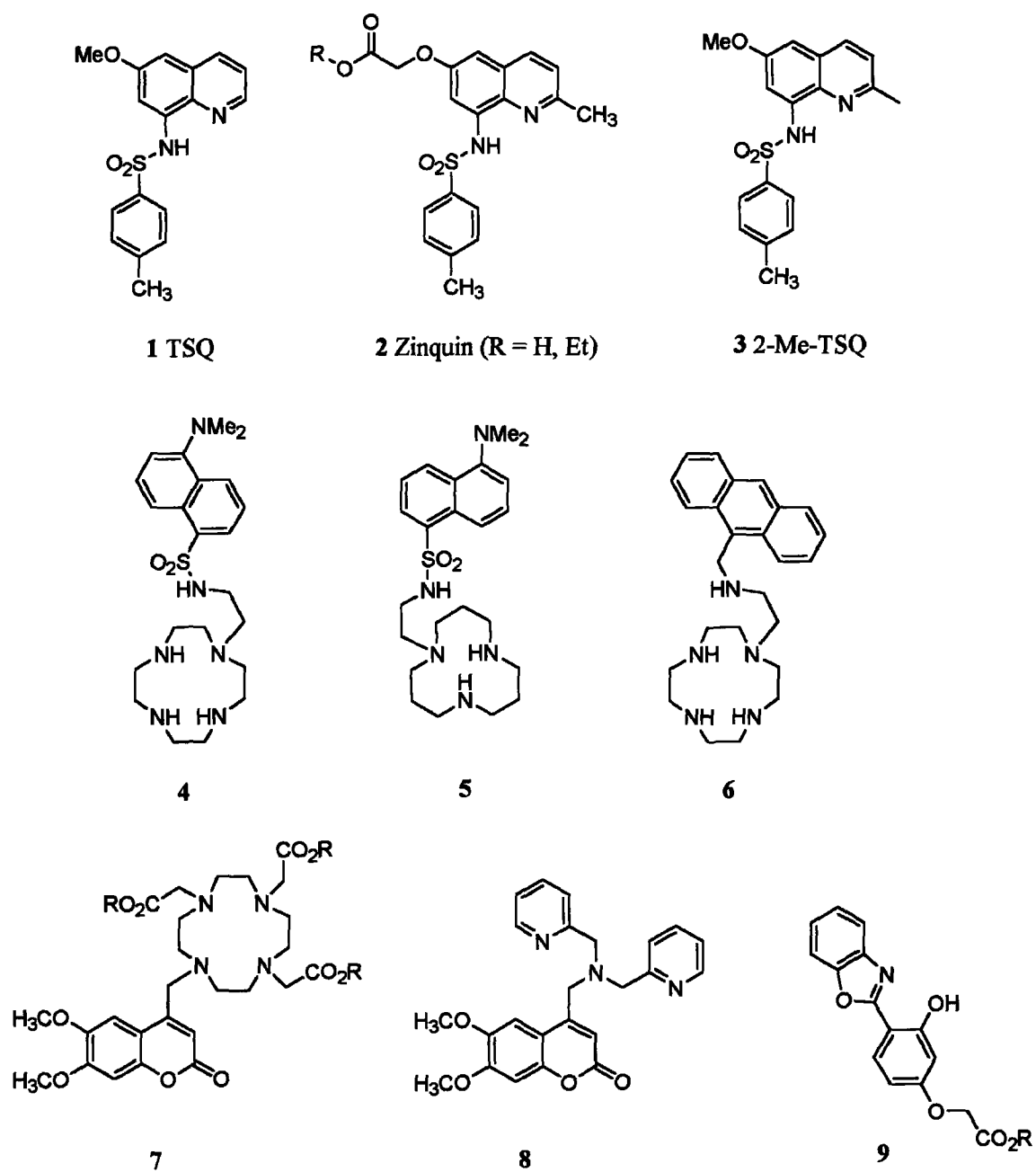


Figure 1.1. Small-molecule intensity-based sensors with UV excitation wavelengths

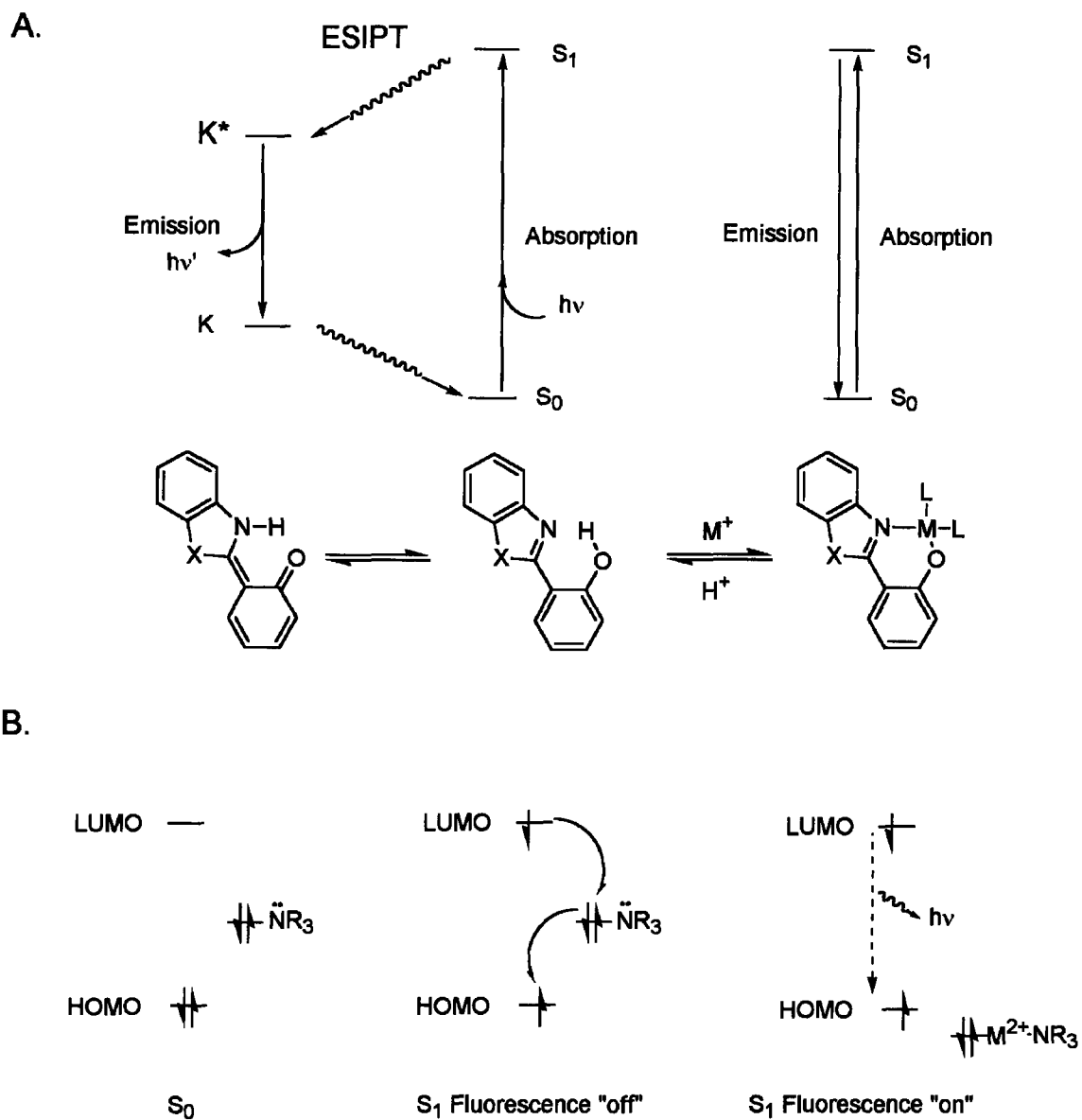


Figure 1.2. The mechanistic basis of some common sensing mechanisms: A. ESIPT,³⁷

B. PET

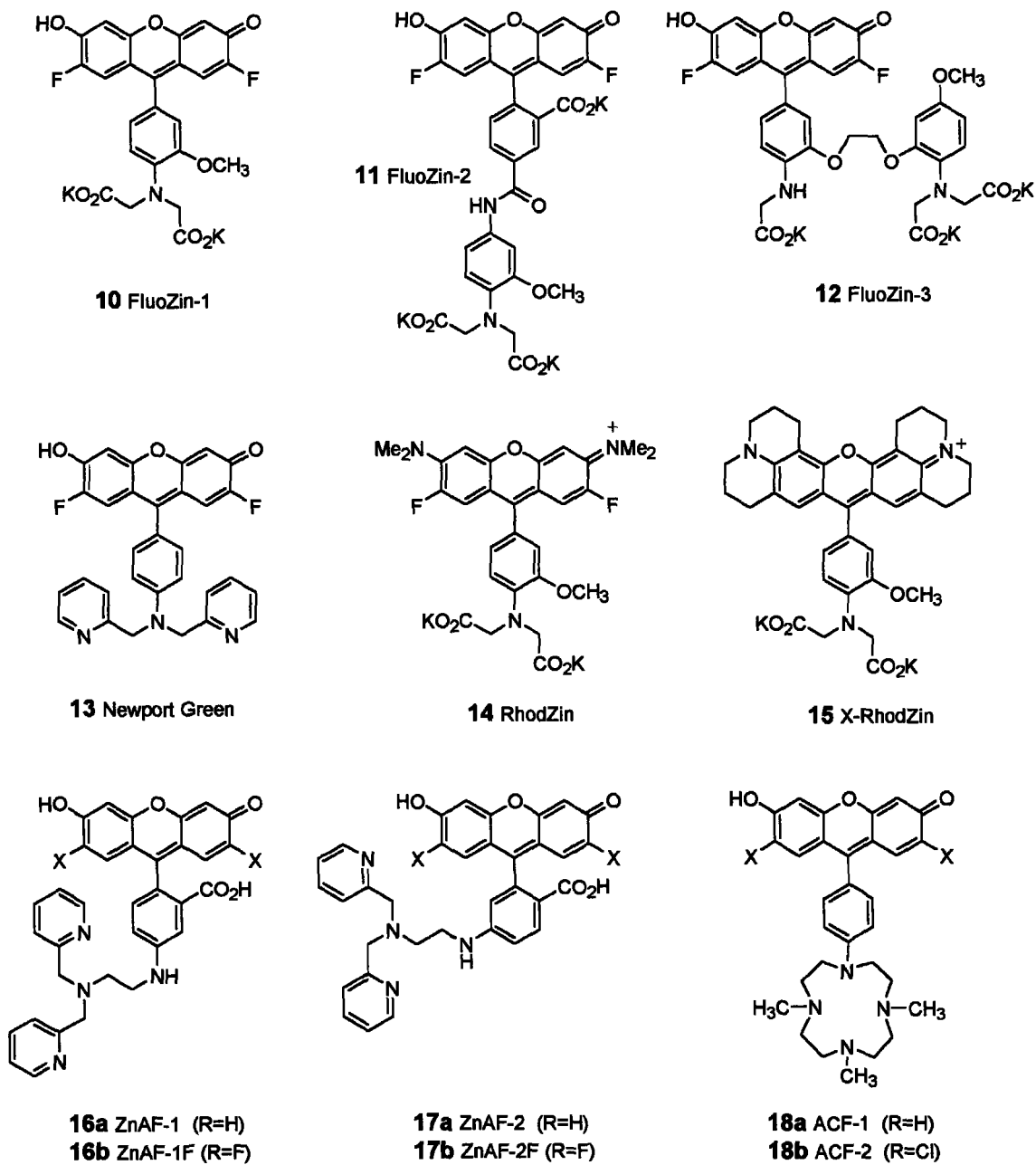
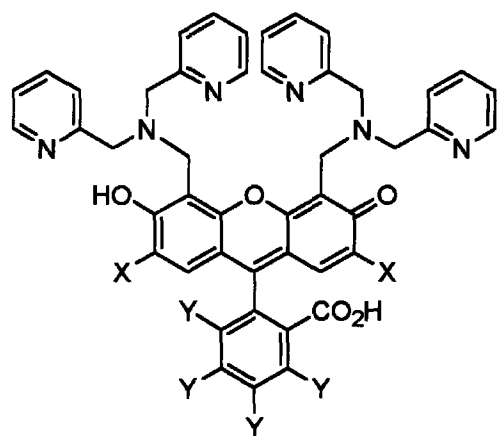
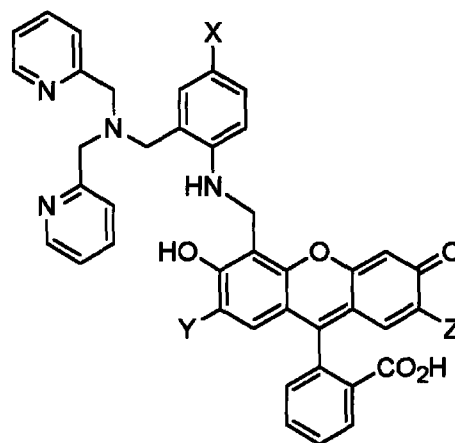


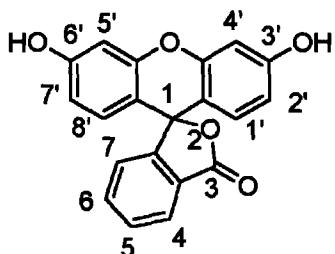
Figure 1.3. Small-molecule intensity-based sensors with visible excitation



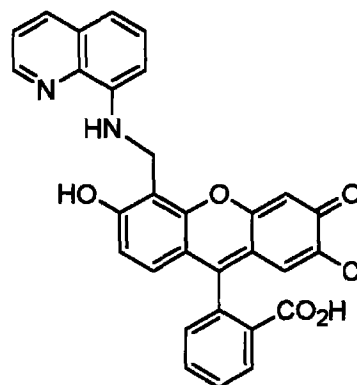
- 19a** ZP1 X = Cl, Y = H
19b ZP2 X = H, Y = H
19c ZP3 X = F, Y = H
19d ZPF1 X = Cl, Y = F
19e ZPCl1 X = Cl, Y = Cl
19f ZPBr1 X = Cl, Y = Br
19g ZP3 X = F, Y = F



- 20a** ZP4 X = H, Y = H, Z = Cl
20b ZP5 X = F, Y = H, Z = Cl
20c ZP6 X = Cl, Y = H, Z = Cl
20d ZP7 X = OMe, Y = H, Z = Cl
20e ZP8 X = H, Y = F, Z = F



Numbering system
of fluorescein



21 Quinolin-1 (QZ1)

Figure 1.4. Numbering and nomenclature of fluorescein and Zinpyr sensors

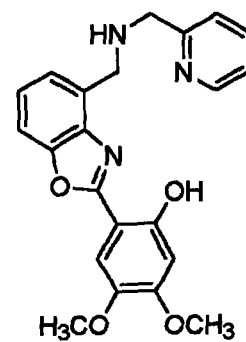
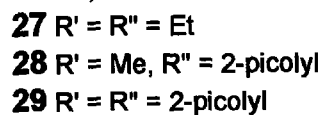
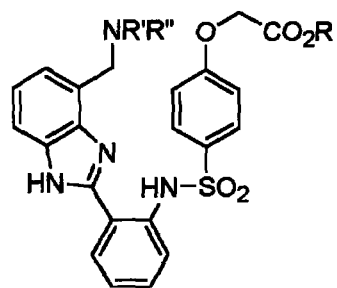
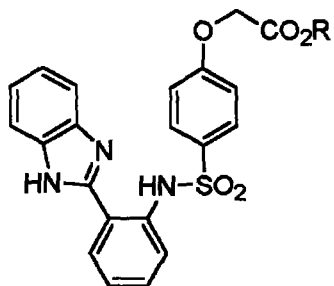
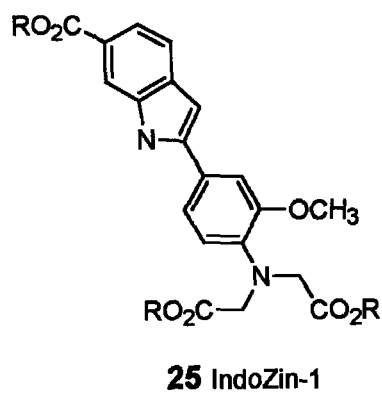
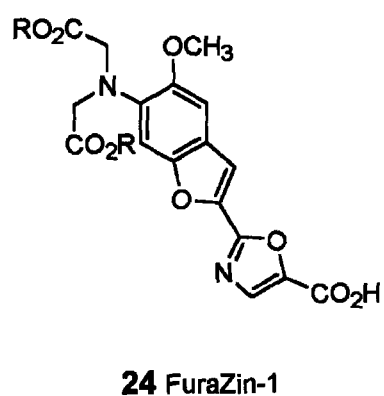
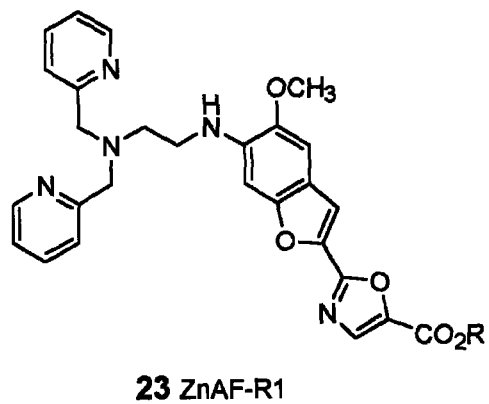
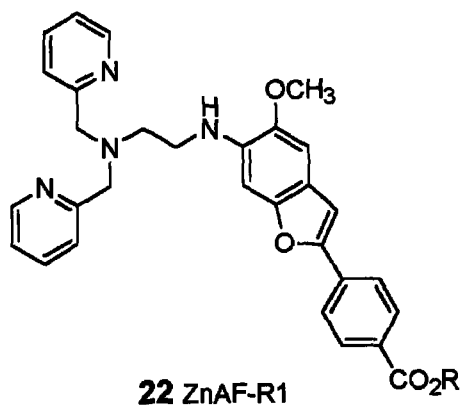


Figure 1.5. Ratiometric sensors with UV excitation wavelengths

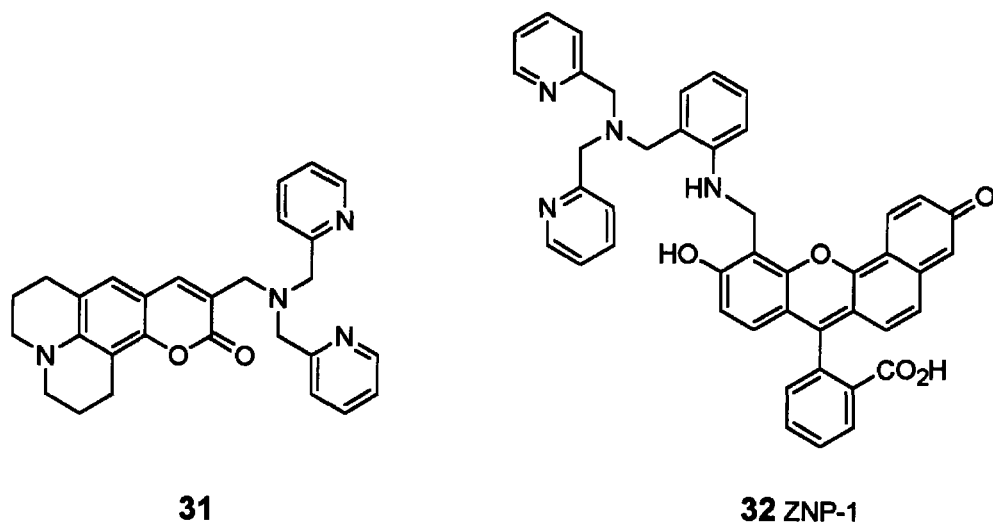


Figure 1.6. Ratiometric sensors with visible excitation

**Chapter 2 Membrane-Permeable and Impermeable Sensors of the Zinpyr Family
and Their Application to Imaging of Hippocampal Zinc in Vivo[†]**

Introduction[†]

The synthesis of fluorescent sensors for biological imaging of Zn^{2+} has drawn a great deal of recent attention.¹ Intracellular Zn^{2+} is a key structural or catalytic component of many proteins, with the overall intracellular concentration estimated to average 150 μM .² A complex system of zinc transporter proteins is employed in order to control Zn^{2+} homeostasis,^{3,4} and the vast majority of intracellular Zn^{2+} is sequestered or tightly bound to proteins such that cytosolic chelatable Zn^{2+} is essentially nonexistent.⁵ Certain specialized areas of the body accumulate Zn^{2+} . The presence of low millimolar concentrations of loosely bound Zn^{2+} in CA3 synaptic vesicles of mammalian cerebral cortex is of particular interest. This vesicular Zn^{2+} , which constitutes about 5% of total brain zinc, is conspicuous in hippocampal mossy fiber boutons and has been demonstrated by autometallographic and fluorescence techniques.⁶ Extensive experimentation has not established definitively the normal physiological roles of hippocampal synaptic zinc;^{7,8} however, a modulatory role in seizure conditions⁹ and subsequent neuronal damage is indicated.^{10,11} Because Zn^{2+} is a spectroscopically silent metal ion, fluorescent sensing approaches to studying the movements and functions of brain zinc ion are of great utility.

There are three areas in which rapidly exchangeable, loosely bound zinc may be imaged in the brain: the cytosol, secretory storage granules including neuronal vesicles, and the extracellular fluids. Membrane-impermeant dyes are useful for imaging extracellular Zn^{2+} released from presynaptic terminals,¹² whereas sequestered vesicular

[†] This work has been submitted for publication in slightly altered form (*Chem. Biol.* 2004, 11, in submission). Respective contributions were as follows: In vivo imaging of rat hippocampus was performed by Rafik Masalha and Christopher J. Frederickson, both of NeuroBioTex, Galveston, TX. HeLa cells and tissue culture expertise were provided by Katie R. Barnes.

Zn^{2+} is best imaged with a stably lipophilic probe. Cytosolic free Zn^{2+} , observed almost exclusively in injured or oxidatively stressed neurons, is best imaged with a trappable probe.

Among the list of desirable properties¹³ for a fluorescent biosensor is the ability to permeate into the cell and subsequently become trapped. This “trappable” property is most often achieved by the inclusion of an ester moiety. The lipophilic ester enters the cell and is hydrolyzed by intracellular esterases to a charged, membrane-impermeant carboxylate. Ethyl esters and the more hydrolytically labile acetoxymethyl esters¹⁴ are most commonly used for this purpose. One relevant example of this strategy is its application to the *p*-toluenesulfonamidoquinoline (TSQ) family of Zn^{2+} sensors. TSQ is lipophilic and penetrates both plasma and vesicular membranes, readily staining vesicular zinc; however, the staining protocol is not applicable to imaging zinc in live tissue.¹⁵ Consequently, the TSQ-based sensor Zinquin, which contains an ethyl ester to aid in solubility and intracellular retention of the sensor, was designed and synthesized.¹⁶ The presence of the ester group does not noticeably affect intracellular staining of mouse LTK fibroblasts compared to an analogous sensor containing a 6-methoxy group (2-Me-TSQ).¹⁷

The fluorescein-based Zn^{2+} sensor Zinpyr-1 (ZP1, Figure 2.1) has recently been reported.¹⁸ This sensor is excited by low-energy visible light ($\lambda_{\text{max}} > 500 \text{ nm}$), is extremely bright ($\Phi_{\text{Zn}} = 0.87$, $\epsilon_{\text{Zn}} = 8.4 \times 10^4 \text{ M}^{-1}\text{cm}^{-1}$), and is membrane-permeable without prior modification. A second generation of Zinpyr sensors, which do not enter intact cells, has been introduced and is exemplified by the asymmetric molecule ZP4 (Figure 2.1). Their permeability has been exploited in the selective imaging of damaged

neurons.^{19,20} By changing the substituent X (X = F, Cl, OMe) in the ZP4 family it has been possible to modulate their properties without altering the membrane permeability of these sensors.²¹ In the present article we describe chemical routes to a trappable ZP1 with a hydrolyzable ethyl ester in order to examine the effects of this modification on subcellular localization in vitro and in vivo. Our chemistry furnishes both membrane-permeable and -impermeable visible-excitation sensors, the preparation of which can be readily scaled up to afford multigram quantities of material. Applications to imaging hippocampal zinc ion are also reported.

Experimental

Materials and Methods.

Reagents were purchased from Aldrich and used without further purification. ¹H and ¹³C NMR spectra were acquired on a Varian 300 or 500 MHz or a Bruker 400 MHz spectrometer. Personnel at the DCIF at MIT acquired HRMS spectra on an FTMS electrospray instrument. Acetonitrile and dichloromethane were obtained from a dry-still solvent dispensation system. Fluorescence spectra were measured on a Hitachi F-3010 fluorimeter and UV-visible spectra on a Cary 1E UV-visible spectrophotometer. Both were analyzed by Kaleidagraph 3.0 for Windows.

Synthetic Procedures

2',7'-Dichloro-5(6)-Carboxyfluorescein (1a, b). 4-Chlororesorcinol (28.8 g, 200 mmol) and 1, 2, 4-benzenetricarboxylic acid (21.0 g, 100 mmol) were combined in 100 mL of methanesulfonic acid and stirred in a 90 °C oil bath for 18 h. The reaction mixture was then poured into 1500 mL of stirred ice water, and the resulting suspension was

filtered and washed with H₂O. The filtered solid was resuspended in 1 L of H₂O, filtered again, and dried under vacuum at 90 °C overnight to give 40.0 g of an orange solid (90% yield). ¹H NMR (methanol-d₄): δ 6.82 (s, 2 H), δ 6.85 (s, 2 H), δ 6.95 (s, 2 H), 6.99 (s, 2 H), δ 7.40 (d, 1 H), δ 7.85 (s, 1 H), δ 8.22 (d, 1 H), δ 8.39 (d, 1 H), δ 8.45 (d, 1 H), δ 8.70 (s, 1 H). The product was carried forward without further purification or characterization.

3',6'-Diacetyl-2',7'-dichloro-6-carboxyfluorescein pyridinium salt (2a). 2', 7'-Dichlorofluorescein-5(6)-carboxylic acid (40.0 g, 90 mmol) was stirred in 150 mL of acetic anhydride and 9 mL of pyridine and heated to reflux for 30 min. The reaction was allowed to cool to RT for 4 h and then filtered. The obtained solid was dried under vacuum to give 16.0 g (30%) of the desired product. ¹H NMR (CDCl₃): δ 11.13 (br s, 2 H); 8.70 (m, 2 H); 8.42 (d, 1 H); 8.14 (d, 1 H); 7.90 (m, 2 H); 7.46 (m, 2 H); 7.17 (s, 2 H); 6.87 (s, 2 H); 2.36 (s, 6 H). ¹³C NMR (CDCl₃): δ 168.4, 168.3, 152.4, 150.1, 149.0, 147.5, 139.2, 139.1, 132.6, 129.3, 129.1, 126.1, 125.8, 125.2, 123.2, 117.5, 113.3, 21.1., m.p. >300 °C (dec).

3',6'-Diacetyl-2',7'-dichloro-5-carboxyfluorescein (2b). The mother liquor from **2a** was added slowly to 300 mL of stirred H₂O, stirred for an additional 10 min, and extracted with 3 x 150 mL of ethyl acetate. The combined organic layers were washed with 1 x 100 mL of 3% HCl and 1 x 100 mL brine, dried over MgSO₄, and evaporated to give a light brown solid residue, which was recrystallized twice from CH₂Cl₂/EtOAc to give 13.5 g of the desired product (27% yield). ¹H NMR (CDCl₃): δ 8.84 (s, 1 H); 8.49 (d, 1 H); 7.35 (d, 1 H); 7.19 (s, 2 H); 6.89 (s, 2 H); 2.38 (s, 6 H). ¹³C NMR (CDCl₃): δ

169.7, 169.0, 167.4, 156.3, 149.6, 148.7, 137.3, 132.3, 128.9, 128.1, 126.3, 124.6, 123.0, 116.8, 113.0, 80.8, 66.3, 20.9. m.p. 178-180 °C.

3', 6'-Diacetyl-2', 7'-Dichlorofluorescein-6-Carboxylate Ethyl Ester (3a). 3', 6'-Diacetyl-2',7'-dichloro-6-carboxyfluorescein pyridinium salt (**2a**, 1.05 g, 1.7 mmol) was dissolved in 30 mL of dichloromethane and the solution was stirred at 0 °C. Dimethylformamide (400 µL) and oxalyl chloride (1.7 mL of a 2 M solution in dichloromethane) were added and the reaction was stirred overnight at RT. Sodium carbonate (180 mg, 1 mmol) and ethanol (10 mL) were added, and stirring was continued for 4 h. The solvents were removed by rotary evaporation and the resulting residue was taken up in CH₂Cl₂, filtered through a short plug (2 cm) of silica gel, and crystallized from dichloromethane/ethyl acetate to give 631 mg (67%) of off-white crystals. ¹H NMR (CDCl₃): δ 8.38 (d, 1 H); 8.13 (d, 1 H); 7.82 (s, 1 H); 7.17 (s, 2 H); 6.83 (s, 2 H); 4.40 (q, 2 H); 2.38 (s, 6 H); 1.41 (t, 3 H). ¹³C NMR (CDCl₃): δ 167.92; 167.55; 164.61; 151.91; 149.69; 148.68; 137.55; 132.03; 129.00; 125.83; 125.21; 122.91; 117.00; 113.00; 80.87; 62.41; 20.94; 14.56., m.p. 212-214 °C. HRMS(M+H): Calcd for C₂₇H₁₉Cl₂O₉ 557.0406; found 557.0393.

3', 6'-Diacetyl-2', 7'-Dichlorofluorescein-5-Carboxylate Ethyl Ester (3b). 3', 6'-Diacetyl-2',7'-dichloro-5-carboxyfluorescein (**2b**, 527 mg, 1 mmol) was dissolved in CH₂Cl₂ and stirred under nitrogen in a dry ice-acetone bath. DMF (200 µL) was added, followed by oxalyl chloride (1 mL of a 2 M solution in CH₂Cl₂) slowly over a period of 20 min. The solution was stirred for 12 h, at which time ethanol (10 mL) and NaHCO₃ (84 mg, 1 mmol) were added. The reaction was stirred for an additional 4 h, then evaporated under reduced pressure, taken up in CH₂Cl₂, and filtered through a 2-cm plug

of silica gel. Evaporation gave 390 mg of white crystalline residue (70% yield). ^1H NMR (CDCl_3): δ 8.75 (s, 1 H); 8.43 (d, 1 H); 7.32 (d, 1 H); 7.19 (s, 2 H); 6.85 (s, 2 H); 4.44 (q, 2 H); 2.33 (s, 6 H); 1.44 (t, 3 H). ^{13}C NMR (CDCl_3): δ 168.01, 167.82, 164.73, 155.40, 149.75, 148.80, 136.96, 133.68, 129.00, 127.38, 126.31, 124.45, 123.08, 117.08, 113.12, 80.84, 62.32, 21.05, 14.74. HRMS (M+H): Calcd for $\text{C}_{27}\text{H}_{19}\text{Cl}_2\text{O}_9$ 557.0406, found 557.0401.

ZP1(6-CO₂H) (4a). Dipicolylamine (640 mg, 3.2 mmol) was combined with paraformaldehyde (192 mg, 6.4 mmol) in 20 mL of acetonitrile and heated to reflux for 45 min. 3', 6'-Diacetyl-2',7'-dichloro-6-carboxyfluorescein pyridinium salt (**2a**, 304 mg, 0.5 mmol) was dissolved in 10 mL of MeCN and added, followed by 10 mL of H₂O, and reflux was continued for 24 h. The resulting suspension was cooled and filtered to yield 360 mg of a light pink powder, which was recrystallized from ethanol to give 282 mg (64% overall) after drying overnight at 60 °C under vacuum. The filtrate was acidified with several drops of glacial acetic acid, allowed to stand overnight, and filtered to yield an additional 65 mg (98% crude yield). ^1H NMR (DMSO-d_6): δ 8.55 (d, 4 H); 8.22 (d, 1 H); 8.10 (d, 1 H); 7.77 (m, 5 H); 7.39 (d, 4 H); 7.28 (m, 4 H); 6.63 (s, 2 H); 4.16 (s, 4 H); 4.01 (s, 8 H).; ^{13}C NMR (DMSO-d_6): 167.60, 166.11, 157.41, 155.49, 151.7, 148.69, 148.16, 137.45, 131.27, 129.52, 126.78, 125.65, 124.85, 123.23, 122.64, 116.25, 111.97, 109.36, 82.82, 58.65, 48.86. m.p. 215-218 °C. HRMS (M+H): Calcd for $\text{C}_{47}\text{H}_{37}\text{Cl}_2\text{N}_6\text{O}_7$ 867.2101; found 867.2080. Anal: Calcd for $\text{C}_{47}\text{H}_{36}\text{Cl}_2\text{N}_6\text{O}_7$: C, 65.06; H, 4.18; N, 9.69; Cl, 8.17. Found: C, 64.74; H, 3.96; N, 9.61; Cl, 8.29.

ZP1(5-CO₂H) (4b). 3', 6'-Diacetyl-2',7'-dichloro-6-carboxyfluorescein (264 mg, 0.5 mmol) was subjected to the reaction conditions described for **4a**. The resulting red

solution was acidified with several drops of glacial acetic acid, allowed to stand overnight at 4 °C, and filtered to yield 361 mg (83% crude yield) of a dark pink crystalline solid, which gave 318 mg on recrystallization from ethanol (73% overall yield). ¹H NMR (DMSO-d₆): δ 8.53 (d, 4 H); 8.37 (s, 1 H); 8.30 (d, 1 H); 7.77 (td, 4 H); 7.45 (d, 1 H); 7.37 (d, 4 H); 7.28 (m, 4 H); 6.67 (s, 2 H); 4.16 (s, 4 H); 4.00 (s, 8 H); ¹³C NMR (DMSO-d₆): 167.58, 166.16, 158.37, 155.77, 154.97, 149.17, 148.69, 137.20, 136.49, 133.25, 126.94, 126.15, 124.73, 123.23, 122.68, 116.47, 112.00, 109.25, 82.65, 58.49, 48.81. m.p. 195-195 °C. HRMS (M+H): Calcd for C₄₇H₃₇Cl₂N₆O₇: 867.2101; found 867.2108. Anal: Calcd for C₄₇H₃₆Cl₂N₆O₇: C, 65.06; H, 4.18; N, 9.69; Cl, 8.17. Found: C, 64.83; H, 4.02; N, 9.85; Cl, 8.33.

ZP1(6-CO₂Et) (5a). 3', 6'-Diacetyl-2', 7'-dichlorofluorescein-6-carboxylate ethyl ester (264 mg, 0.47 mmol) was subjected to the same reaction conditions as described for **4a**. The reaction solution was acidified with 5 drops of glacial acetic acid and cooled to -10 °C for 30 h. The resulting salmon-pink precipitate was filtered to give 233 mg (55%) after washing with water and acetonitrile. Recrystallization from ethanol gave 44% yield (185 mg). ¹H NMR (DMSO-d₆): δ 8.63 (d, 4 H); 8.35 (d, 1 H); 8.21 (d, 1 H); 7.90 (s, 1 H); 7.86 (t, 4 H); 7.47 (d, 4 H); 7.37 (m, 4 H); 6.71 (s, 2 H); 4.35 (q, 2 H); 4.25 (s, 4 H); 4.09 (s, 8 H); 1.32 (t, 3 H); m.p. 203-205 °C. HRMS(M+H): Calcd for C₄₉H₄₁Cl₂N₆O₇: 895.2414; found 895.2391. Anal: Calcd for C₄₉H₄₀Cl₂N₆O₇: C, 65.70; H, 4.50; N, 9.38; Cl, 7.92. Found: C, 65.63; H, 4.37; N, 9.61; Cl, 8.07.

ZP1(5-CO₂Et) (5b). 3', 6'-Diacetyl-2', 7'-dichlorofluorescein-5-carboxylate ethyl ester (141 mg, 0.25 mmol) was subjected to the same reaction conditions as reported for **4a**. The reaction solution was acidified with 5 drops of glacial acetic acid, concentrated on

the rotary evaporator, and the resulting pink residue was taken up in MeCN and filtered to give 113 mg of a pink powder (50%) after washing with water and acetonitrile. Recrystallization of 100 mg from EtOH gave 80 mg of a salmon-pink solid. ^1H NMR (DMSO- d_6): δ 8.54 (d, 4 H); 8.41 (s, 1 H); 8.33 (dd, 1 H); 7.77 (td, 4 H); 7.49 (d, 1 H); 7.38 (d, 4 H); 7.29 (m, 4 H); 6.67 (s, 2 H); 4.39 (q, 2 H); 4.16 (s, 4 H); 4.00 (s, 8 H); 1.37 (t, 3 H). ^{13}C NMR (DMSO- d_6): δ 168.53, 165.66, 158.45, 156.84, 156.24, 149.80, 149.23, 138.30, 137.19, 133.24, 128.03, 127.10, 126.05, 124.31, 123.78, 118.16, 117.51, 113.08, 110.20, 83.81, 62.62, 59.57, 49.88, 15.29. m.p. 178-180 °C. HRMS(M+H): Calcd for $\text{C}_{49}\text{H}_{41}\text{Cl}_2\text{N}_6\text{O}_7$: 895.2414; found 895.2406.

Spectroscopic Measurements

All glassware was washed sequentially with 20% HNO_3 , deionized water, and ethanol before use. Purified water (resistivity 18.2 Ohms) was obtained from a Millipore Milli-Q water purification system. Fluorophore stock solutions in DMSO were made up to concentrations of 1 mM and kept at 4 °C in 100-500 μL aliquots. Portions were thawed and diluted to the required concentrations immediately prior to each experiment. Fluorescence and absorption data were measured in HEPES buffer (50 mM, pH 7.5, KCl 100 mM) except for the fluorescein standard in quantum yield measurements. Solutions were transferred to clean, dry propylene containers for storage and were filtered (0.25 μm) before data acquisition. Fluorescence spectra were measured from 475 nm to 650 nm. All measurements were performed in triplicate. Dissociation constants were determined by using a dual-metal buffering system as previously described.²²

Extinction Coefficients. A 2 mL portion of HEPES buffer was titrated with 2 μL aliquots of 1 mM fluorophore stock solution and the absorption measured at each

concentration. The absorbance at the maximum was plotted as a function of concentration, and the slope was taken as the extinction coefficient. The procedure was repeated using 1.9-mL portions of HEPES buffer containing 100- μ L aliquots of 10 mM ZnCl₂ solution.

Quantum Yields. Quantum yields were calculated by recording UV-vis spectra of the fluorophore under study and a 1 μ M fluorescein standard in 0.1 N NaOH to determine the wavelength where the sample and fluorescein absorption were equal. The fluorescence spectrum of each was then recorded, exciting at the wavelength determined by UV-vis spectral comparison. The integrated emission of the sample was normalized to the fluorescein standard and multiplied by the standard quantum yield of 0.95.²³

Fluorescence-dependent pK_a determination. pK_a Titrations were performed in 100 mM KCl, 1 mM EDTA. A 1 mM stock solution of the fluorophore was diluted with 20 mL of this solution to a final concentration of 1 μ M. The pH was brought to 11.0 with 45% w/v KOH, then gradually lowered to pH 2, and the fluorescence spectrum was recorded at each half-unit step in pH. The integrated emission area F was normalized, plotted as a function of pH and fit to the expression in eq. 1. Where necessary, individual portions of the plot were fit as a function of a single pK_a in order to determine suitable initial values.

$$\frac{(F - F_0)}{(F_{\max} - F_0)} = \left(\frac{\Delta F_{1\max}}{[1 + e^{(pH - pK_{a1})}]} \right) + \left(\frac{\Delta F_{2\max}}{[1 + e^{(pH - pK_{a2})}]} \right) + \left(\frac{\Delta F_{3\max}}{[1 + e^{(pH - pK_{a3})}]} \right) \quad (1)$$

Dissociation constant determination. Solutions containing 1 μ M fluorophore, 2 mM CaCl₂, 1 mM EDTA, and 0 or 1 mM ZnCl₂ were prepared as previously described.²² These solutions were combined to give 3-mL aliquots containing 0-0.9 mM ZnCl₂, and

were allowed to equilibrate at RT for 20 min. The fluorescence spectrum of each aliquot was measured and the integrated emission was normalized and plotted as a function of effective free Zn^{2+} . The plots were then fit to eq. 2.

$$\frac{(F - F_0)}{(F_{\max} - F_0)} = k \frac{[Zn^{2+}]_{eff}}{K_d + [Zn^{2+}]_{eff}} \quad (2)$$

Metal ion selectivity. The fluorescence spectrum of a 2-mL aliquot of 1 μ M fluorophore excited at 512 nm was acquired by itself, after addition of a 4- μ L (CaCl₂, MgCl₂, 1.00 M) or 10- μ L (NaCl 2.00 M, MnSO₄, CoCl₂, NiCl₂, CuCl₂, CdCl₂ 10 mM) aliquot of metal stock solution, and after addition of a 10- μ L aliquot of ZnCl₂ (10 mM). The integrated emission of each spectrum was normalized to that of the metal-free control spectrum.

Imaging

HeLa cells were grown at 37 °C under a 5% CO₂ atmosphere in Dulbecco's modified Eagle's medium (DMEM, Gibco/BRL) supplemented with 10% fetal bovine serum, 1x penicillin/streptomycin and 2 mM L-glutamine. Cells were plated 24 h before study into 12-well plates containing 2 mL of DMEM per well. Cells were approximately 50% confluent at the time of study. A 10- μ L aliquot of dye (1 mM in DMSO) or control (DMSO) was added to each 2-mL well, and the cells were incubated for 30 min at 37 °C, at which point the medium was removed and the cells were washed twice with Hanks' buffered salt solution (HBSS) and suspended in 2 mL of DMEM. A 10- μ L aliquot of a solution containing 1 mM ZnCl₂ and 9 mM sodium-pyruvate in 9:1 DMSO:H₂O was added to selected wells, and the cells were incubated for 10 min at 37 °C. The cells were washed again with HBSS, resuspended in HBSS, and imaged by using a Nikon Eclipse TS100 microscope illuminated with a Chiu Mercury 100 W lamp, equipped with an RT

Diagnostics camera and operated with Spot Advanced software. Magnification was 20x. Fluorescence images were recorded with a FITC-HYQ filter cube (excitation 460-500, bandpass 510-560 nm).

Rats were deeply anesthetized with isoflurane, and a small burr hole was opened over the hippocampus (L3.0, P3.0) through which the dura was punctured. Stock solutions of ZP1 or ZP1(6-CO₂Et) (5 or 10 mM in DMSO) were micro-infused directly into the brains of the rats with either a Hamilton microliter syringe or a glass pipette (tip ~ 50-100µm) connected to a syringe-pump. Volumes of 2-4 µL were delivered at 0.5 µL/min by micro-syringe (27 gauge needle) or by a Harvard Apparatus syringe pump, using a glass micropipette with the tip broken to 100 µm diameter. All infusions were stereotaxically aimed at the dorsal hippocampus L3, P3, 4.0 sub dura. After infusion, wounds were closed and the rats were allowed to survive for 12-24 h. Roughly half of the rats were given pilocarpine after dye infusion (300 mg/kg; ip) and monitored for the occurrence of seizures and status epilepticus. In all, tissue from 12 rats was examined in the microscope (3 rats from each of ZP1 control and pilocarpine; ZP1(6-CO₂Et), control and pilocarpine). For brain removal, rats were rendered unconscious by inhalation of carbon dioxide or isoflurane, then decapitated, and the brains were removed quickly and frozen on a liquid CO₂ evaporation freezing stage. After cryotoming at 20 or 30 µm, the sections were allowed to dry briefly on clean glass slides, then viewed and imaged on a Zeiss Universal microscope, either with or without clearing in 100% glycerine and with or without a coverslip. Epi-illumination was provided by a 500 W halogen bulb with band-pass filtering at 480 nm, and images were acquired through a 530 nm bandpass and

500 nm dichroic filter using a SPOT II cooled CCD camera. Zeiss 25X (glycerin immersion) and an Olympus 10X planapo objectives were used.

Results and Discussion

Synthesis

The basic structure of Zinpyr-1, depicted in Figure 2.1, contains chlorine atoms at the 2' and 7' positions of the fluorescein platform. In its metal-free form, the lone pair of a benzylic amine largely quenches the fluorescence of ZP1. Coordination of this amine to Zn^{2+} or protonation affords an approximately 3-fold increase in fluorescence. The dipicolylamine Zn^{2+} -binding groups are installed via a Mannich reaction on the parent dichlorofluorescein. Substituents at the 2' and 7' positions are necessary to prevent Mannich reaction chemistry from occurring at these positions. A Mannich reaction of 5- or 6-carboxylate derivatives of 2',7'-dichlorofluorescein was therefore carried out as a desirable route to ester- and acid-functionalized ZP1 derivatives. The dichlorofluorescein-5(6)-carboxylates were synthesized as a mixture of isomers (1a, 1b) by methanesulfonic acid-catalyzed fluorescein condensation of 4-chlororesorcinol with benzene tricarboxylic acid.²⁴ This reaction affords two isomers, owing to lack of selectivity between the acid moieties at the 1- and 2-positions of the starting benzenetricarboxylic acid. The product mixture was protected and separated as the diacetates 2a and 2b. Activation of 2a and 2b with oxalyl chloride and subsequent reaction with ethanol gave the fluorescein ethyl ester diacetates (3a, 3b) in 65-70% yield, as shown in Scheme 2.1. Esterification of either carboxylate with ethanol under Mitsunobu conditions was also effective. The desired ZP1 carboxylates (4a, ZP1(6-CO₂H) and 4b, ZP1(5-CO₂H)) or esters (5a, ZP1(6-CO₂Et) and 5b, ZP1(5-CO₂Et)) were

isolated following Mannich reactions of the corresponding fluorescein diacetates 2a-b or 3a-b with dipicolylamine and paraformaldehyde (Scheme 2.1). The isolated yields of ethyl esters 5a and 5b were reproducibly much lower (40%, 44%) than those of the free carboxylates 4a and 4b (73%, 79%).

Photophysics and Thermodynamics

The physical properties of the new sensors and their zinc complexes were examined. Addition of Zn^{2+} to a 1 μM aqueous solution of each sensor afforded an increase in integrated emission up to 8-fold. The dissociation constant for the first binding event was determined by using a dual-metal EDTA buffered system, as previously described.²² Representative data for K_{d1} measurements are provided in Figure 2.2B. The presence of an electron-withdrawing carboxyl substituent at the 5- or 6-position has little effect on the binding affinity for Zn^{2+} relative to ZP1 (Table 2.1). Previous results have indicated that the first binding event is responsible for the large fluorescence increase and that the dissociation constant for binding a second zinc(II) ion to ZP1 is several orders of magnitude higher than the first.¹⁸ The second dissociation constants were not measured in the present study.

Quantum yields of the sensors in the bound and free states were determined relative to a fluorescein standard. All four sensors have lower background fluorescence ($\Phi = 0.13\text{-}0.21$) in the free state compared with the parent ZP1 ($\Phi = 0.38$). The brightness of the metal-bound sensors ZP1(5/6- CO_2R) is comparable to that of ZP1 (Table 2.1). Each sensor undergoes a blueshift in absorbance of ~ 10 nm upon Zn^{2+} binding. Extinction coefficients of the Zn^{2+} complex are increased over those of the free fluorophores in all cases by 10-15%. The extinction coefficient for the Zn^{2+} complex of

ZP1-6-CO₂H was determined at lower concentration, because the Beer's law plot is nonlinear above ~5 μM. This result may be due partly or wholly to formation of dye aggregates.²⁵ The brightness values of the free sensors are significantly reduced in comparison with the parent Zinpyr-1 sensor, whereas the brightness values of the Zn²⁺-bound sensors are comparable, representing a decrease in background fluorescence and an increase in sensor dynamic range. Measured values are listed in Table 2.1.

Equilibrium constants for three protonation events that affect fluorescence were determined by titration fluorimetry. The pK_a at 7 corresponds to protonation of the benzylic amine responsible for PET quenching of the fluorescence, as shown in Scheme 2.2. This value does not vary considerably among the carboxyl-substituted sensors reported here, but is significantly lower than that of the parent Zinpyr-1 molecule (pK_a = 8.4). The decrease in protonation of the benzylic amine at physiological pH has been suggested to result in a lower quantum yield of the free dye and thereby greatly decreased background fluorescence, offering a plausible explanation for the enhanced fluorescence response discussed above.²⁶ A ZP1 amide,²⁷ however, displays a similarly enhanced fluorescence response despite having a benzylic amine pK_a nearly identical to that of ZP1. This result suggests that the diminution in fluorescence following substitution of the bottom ring stems from another source. The energy of the benzoic acid moiety of fluorescein and its derivatives plays an important role in determining the fluorescence quantum yield,²⁸ and it is plausible that substitution with a carboxylate modulates the electron transfer driving force so as to give rise to the differences observed here. The pK_a value at 1.5-2.1 represents protonation of the xanthene system, which interrupts conjugation and quenches fluorescence. In this protonation state, the positive charge is

delocalized over the xanthene ring, but a significant portion resides on the carbon at the 1 position. Thus, an electron-withdrawing substituent at the 5-position destabilizes the cation, as reflected in the significantly lowered pK_a value of ZP1(5-CO₂R). Figure 2.2C displays pH profiles for **4a** and **4b**.

The selectivity of metal response mirrors that of other ZP1-like sensors based on symmetrically substituted fluorescein platforms, as biologically relevant metal ions produced no significant effect on Zn²⁺ response in background levels up to 10 mM.²⁶ Most first-row transition metal ions quenched fluorescence in a manner that was not reversed upon addition of excess Zn²⁺, with the exception of Mn²⁺, which quenched fluorescence reversibly. The Cd²⁺ ion also produced a large fluorescence enhancement, similar to that of the Zn²⁺ response. Representative data for ZP1(6-CO₂H) are provided in Figure 2.2D.

Biological Imaging Studies

Incubation of ZP1 with COS-7 cells affords a Golgi-associated punctate pattern with minimal staining of the remaining cell soma.¹⁸ Treatment of HeLa cells with 5 μ M dye and subsequent fluorescence microscopic imaging indicated that the ZP1(5/6-CO₂H) derivatives are not taken up by the cell (not shown). The ZP1(5/6-CO₂Et) esters, however, readily stained cells in a pattern similar that observed following ZP1 treatment (Figure 2.3). The relative in vivo staining of rat hippocampus with ZP1 or ZP1(6-CO₂Et), imaged 12-24 h after intracranial dye administration, was investigated (Figure 2.4). Pilocarpine seizures were induced in some rats, and the mechanically injured area near the injection site was examined in rats with or without prior seizures. ZP1 affords a bright granular staining in the zinc-rich neuropil of the hilus, whereas ZP1(6-CO₂Et) staining of

this area is much less intense. Hilar neurons injured by seizure accumulate Zn^{2+} in the cytosol and are stained brightly by both dyes, but the punctate staining of the surrounding neuropil obtained with ZP1 lowers the contrast relative to the somata and dendrites, affording little resolution of the underlying neuronal structure (Figure 2.4G). In contrast, injured neurons stained by ZP1(6-CO₂Et) are clearly delineated, and individual processes can be visualized (Figure 2.4 C). A similar contrast is observed in the staining patterns of the stratum lucidum (SL) and the stratum pyrimidale (SP). ZP1 affords bright punctate staining of the SL, presumably arising from giant (2-10 μ m) zinc-containing synaptic terminals of the mossy fibers (Figure 2.4 F, H). Much weaker punctate staining is observed in ZP1(6-CO₂Et)-stained SL (Figure 2.4 B, D) in comparison to the injured neurons. Figure 2.5 shows a detailed image of post-seizure CA3 staining by ZP1(6-CO₂Et) in which some punctate staining of vesicular Zn^{2+} is seen. We interpret these results to signify intracellular cleavage of the ethyl ester to give the membrane-impermeant species ZP1(6-CO₂H), which does not penetrate the vesicular membrane. The presence of some punctate staining probably reflects slow ester hydrolysis relative to passive diffusion of the sensor across vesicle membranes. In addition, axons coursing distal to the damage inflicted by the act of injection were brightly and clearly labeled by ZP1(6-CO₂Et), presumably reflecting injury-induced mobilization of zinc from cytosolic metalloproteins in degenerating axons. Seizure- or mechanically-injured neurons in the stratum pyrimidale are once again much more clearly delineated by ZP1(6-CO₂Et) than the parent ZP1 sensor.

Conclusions

A generally applicable synthetic route to Zinpyr-1 molecules containing an ester or acid functionality at the 5- or 6-position has been described. Physical characterization of these compounds indicates that the additional group modulates the photophysical properties of these sensors and significantly decreases background fluorescence from protonation. Both isomers are suitable for Zn^{2+} sensing. Comparison of sensors containing a free acid or analogous ethyl ester indicates that an additional negative charge renders the sensor membrane-impermeable. The presence of a hydrolyzable ester alters subcellular distribution of a sensor *in vivo* over a 12-24 h time scale, although no significant differences in subcellular distribution were observed in tissue culture imaging experiments with 30 min incubation periods. This result suggests that the incubation conditions are significant in the subcellular distribution of sensors containing alkyl esters. In summary, we have reported bright fluorescent Zn^{2+} sensors with low-energy visible excitation wavelengths and hybrid subcellular distribution properties. The sensors are mainly trapped in the cytosol, a property not previously available for the Zinpyr family of fluorescein-derivatized zinc ion sensors.

Acknowledgements

We acknowledge Rafik Masalha and Christopher J. Frederickson for performing *in vivo* imaging studies. We thank Katie R. Barnes for providing HeLa cells and tissue culture expertise. This work was supported by the NIGMS (GM65519 to S.J.L.) and by NINDS (NS38585, NS41682, and NS42882 to C. J. F.)

References

- (1) Kimura, E.; Aoki, S. Chemistry of zinc(II) fluorophore sensors. *BioMetals* **2001**, *14*, 191-204.
- (2) Frederickson, C. J. Neurobiology of Zinc and Zinc-containing Neurons. *Int. Rev. Neurobiol.* **1989**, *31*, 145-238.
- (3) Palmiter, R. D.; Huang, L. Efflux and compartmentalization of zinc by members of the SLC30 family of solute carriers. *Pflugers Arch. - Eur. J. Physiol.* **2004**, *447*, 744-751.
- (4) Kambe, T.; Yamaguchi-Iwai, Y.; Sasaki, R.; Nagao, M. Overview of mammalian zinc transporters. *Cell. Mol. Life Sci.* **2004**, *61*, 49-68.
- (5) Finney, L. A.; O'Halloran, T. V. Transition Metal Speciation in the Cell: Insights from the Chemistry of Metal Ion Receptors. *Science* **2003**, *300*, 931-936.
- (6) Frederickson, C. J.; Suh, S. W.; Silva, D.; Frederickson, C. J.; Thompson, R. B. Importance of Zinc in the Central Nervous System: The Zinc-Containing Neuron. *J. Nutr.* **2000**, *130*, 1471S-1483S.
- (7) Lopantsev, V.; Wenzel, H. J.; Cole, T. B.; Palmiter, R. D.; Schwartzkroin, P. A. Lack of vesicular zinc in mossy fibers does not affect synaptic excitability of CA3 pyramidal cells in zinc transporter 3 knockout mice. *Neuroscience* **2003**, *116*, 237-248.
- (8) Palmiter, R. D. Protection against zinc toxicity by metallothionein and zinc transporter 1. *Proc. Natl. Acad. Sci. USA* **2004**, *101*, 4918-4923.

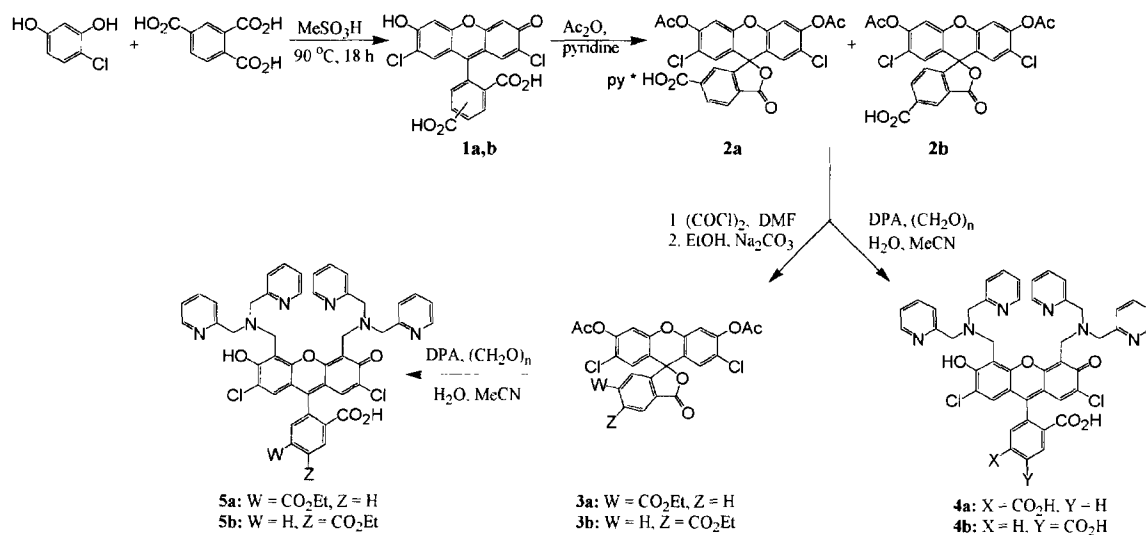
- (9) Cole, T. B.; Robbins, C. A.; Wenzel, H. J.; Schwartzkroin, P. A.; Palmiter, R. D. Seizures and neuronal damage in mice lacking vesicular zinc. *Epilepsy Res.* **2000**, *39*, 153-169.
- (10) Suh, S. W.; Chen, J. W.; Motamedi, M.; Bell, B.; Listiak, K.; Pons, N. F.; Danscher, G.; Frederickson, C. J. Evidence that synaptically-released zinc contributes to neuronal injury after traumatic brain injury. *Brain Res.* **2000**, *852*, 268-273.
- (11) Koh, J.-Y.; Suh, S. W.; Gwag, B. J.; He, Y. Y.; Hsu, C. Y.; Choi, D. W. The Role of Zinc in Selective Neuronal Death After Transient Global Cerebral Ischemia. *Science* **1996**, *272*, 1013-1016.
- (12) Thompson, R. B.; Whetsell Jr., W. O.; Maliwal, B. P.; Fierke, C. A.; Frederickson, C. J. Fluorescence microscopy of stimulated Zn(II) release from organotypic cultures of mammalian hippocampus using a carbonic anhydrase-based biosensor system. *J. Neurosci. Meth.* **2000**, *96*, 35-45.
- (13) Kimura, E.; Koike, T. Recent development of zinc-fluorophores. *Chem. Soc. Rev.* **1998**, *27*, 179-184.
- (14) Tsien, R. Y.; Pozzan, T.; Rink, T. J. Calcium Homeostasis in Intact Lymphocytes: Cytoplasmic Free Calcium Monitored With a New, Intracellularly Trapped Fluorescent Indicator. *J. Cell Biol.* **1982**, *94*, 325-334.
- (15) Frederickson, C. J.; Kasarskis, E. J.; Ringo, D.; Frederickson, R. E. A quinoline fluorescence method for visualizing and assaying the histochemically reactive zinc (bouton zinc) in the brain. *J. Neurosci. Methods* **1987**, *20*, 91-103.

- (16) Zalewski, P. D.; Millard, S. H.; Forbes, I. J.; Kapaniris, O.; Slavotinek, A.; Betts, W. H.; Ward, A. D.; Lincoln, S. F.; Mahadevan, I. Video Image Analysis of Labile Zinc in Viable Pancreatic Islet Cells Using a Specific Fluorescent Probe for Zinc. *J. Histochem. Cytochem.* **1994**, *42*, 877-884.
- (17) Nasir, M. S.; Fahrni, C. J.; Suhy, D. A.; Kolodsick, K. J.; Singer, C. P.; O'Halloran, T. V. The chemical cell biology of zinc: structure and intracellular fluorescence of a zinc-quinolinesulfonamide complex. *J. Biol. Inorg. Chem.* **1999**, *4*, 775-783.
- (18) Burdette, S. C.; Walkup, G. K.; Spingler, B.; Tsien, R. Y.; Lippard, S. J. Fluorescent Sensors for Zn^{2+} Based on a Fluorescein Platform: Synthesis, Properties and Intracellular Distribution. *J. Am. Chem. Soc.* **2001**, *123*, 7831-7841.
- (19) Burdette, S. C.; Frederickson, C. J.; Bu, W.; Lippard, S. J. ZP4, an Improved Neuronal Zn^{2+} Sensor of the Zinpyr Family. *Journal of the American Chemical Society* **2003**, *125*, 1778-1787.
- (20) Frederickson, C. J.; Burdette, S. C.; Frederickson, C. J.; Sensi, S. L.; Weiss, J. H.; Yin, H. Z.; Balaji, R. V.; Truong-Tran, A. Q.; Bedell, E.; Prough, D. S.; Lippard, S. J. Method for Identifying Neuronal Cells Suffering Zinc Toxicity by Use of a Novel Fluorescent Sensor. *J. Neurosci. Meth.* **2004**, in press.
- (21) Nolan, E. M.; Burdette, S. C.; Harvey, J. H.; Hilderbrand, S. A.; Lippard, S. J. Synthesis and Characterization of Zinc Sensors Based on a Monosubstituted Fluorescein Platform. *Inorg. Chem.* **2004**, *43*, 2624-2635.
-

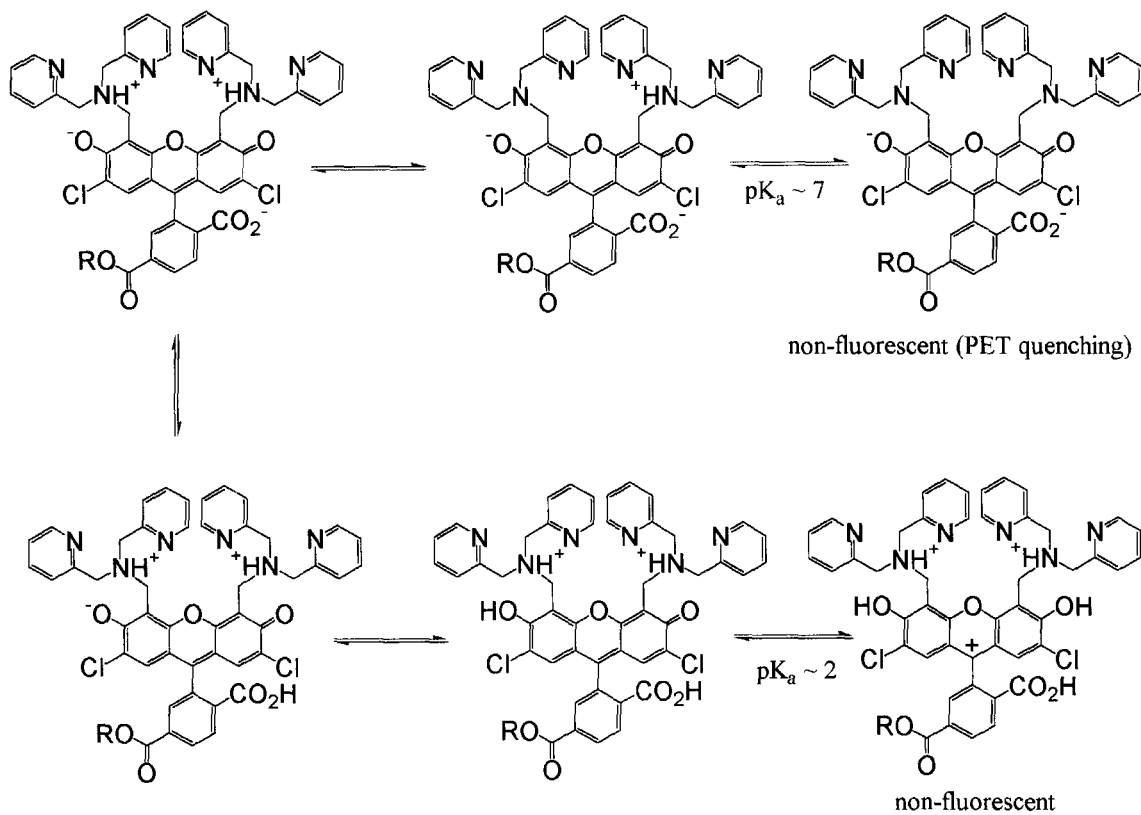
- (22) Walkup, G. K.; Burdette, S. C.; Lippard, S. J.; Tsien, R. Y. A New Cell-Permeable Fluorescent Probe for Zn^{2+} . *J. Am. Chem. Soc.* **2000**, *122*, 5644-5645.
- (23) Brannon, J. H.; Magde, D. Absolute Quantum Yield Determination by Thermal Blooming. Fluorescein. *J. Phys. Chem.* **1978**, *82*, 705-709.
- (24) Sun, W. C.; Gee, K. R.; Klaubert, D. H.; Haugland, R. P. Synthesis of Fluorinated Fluoresceins. *J. Org. Chem.* **1997**, *62*, 6469-6475.
- (25) Selwyn, J. E.; Steinfeld, J. I. Aggregation Equilibria of Xanthene Dyes. *J. Phys. Chem.* **1972**, *76*, 762-774.
- (26) Chang, C. J.; Nolan, E. M.; Jaworski, J.; Burdette, S. C.; Sheng, M.; Lippard, S. J. Bright Fluorescent Chemosensor Platforms for Imaging Endogenous Pools of Neuronal Zinc. *Chem. Biol.* **2004**, *11*, 203-210.
- (27) Woodroffe, C. C.; Lippard, S. J. A Novel Two-Fluorophore Approach to Ratiometric Sensing of Zn^{2+} . *J. Am. Chem. Soc.* **2003**, *125*, 11458-11459.
- (28) Miura, T.; Urano, Y.; Tanaka, K.; Nagano, T.; Ohkubo, K.; Fukuzumi, S. Rational Design Principle for Modulating Fluorescence Properties of Fluorescein-Based Probes by Photoinduced Electron Transfer. *J. Am. Chem. Soc.* **2003**, *125*, 8666-8671.

Table 2.1. Photochemical constants of ZP1(5/6-CO₂R) in the presence and absence of Zn²⁺

Sensor	λ_{\max} (Abs, nm)	ϵ_{\max} (M ⁻¹ cm ⁻¹)	Φ	Brightness	K_{d1} Zn ²⁺ (nM)	pK _{a1}	pK _{a2}	pK _{a3}
ZP1(5-CO ₂ Et)	517	66000	0.14	9.2 x 10 ³	0.26 ± 0.03	1.53(2)	4.02(3)	6.98(7)
+ Zn ²⁺	506	71000	0.58	4.1 x 10 ⁴				
ZP1(5-CO ₂ H)	520	81000	0.17	1.4 x 10 ⁴	0.22 ± 0.04	1.57(4)	3.7(4)	7.05(8)
+ Zn ²⁺	509	88000	0.62	5.5 x 10 ⁴				
ZP1(6-CO ₂ Et)	519	61000	0.13	7.9 x 10 ³	0.37 ± 0.04	2.1(1)	4.0(1)	7.00(4)
+ Zn ²⁺	509	72000	0.67	4.8 x 10 ⁴				
ZP1(6-CO ₂ H)	516	76000	0.21	1.6 x 10 ⁴	0.16 ± 0.02	2.12(1)	4.07(4)	7.12(7)
+ Zn ²⁺	506	81000	0.63	5.1 x 10 ⁴				
ZP1 ²⁶	515	79500	0.38	3.0 x 10 ⁴	0.7 ± 0.1	2.75		8.37
+ Zn ²⁺	507	84000	0.87	7.3 x 10 ⁴				



Scheme 2.1. Synthesis of ZP1(5/6-CO₂R)



Scheme 2.2. Protonation equilibria of ZP1(6-CO₂R)

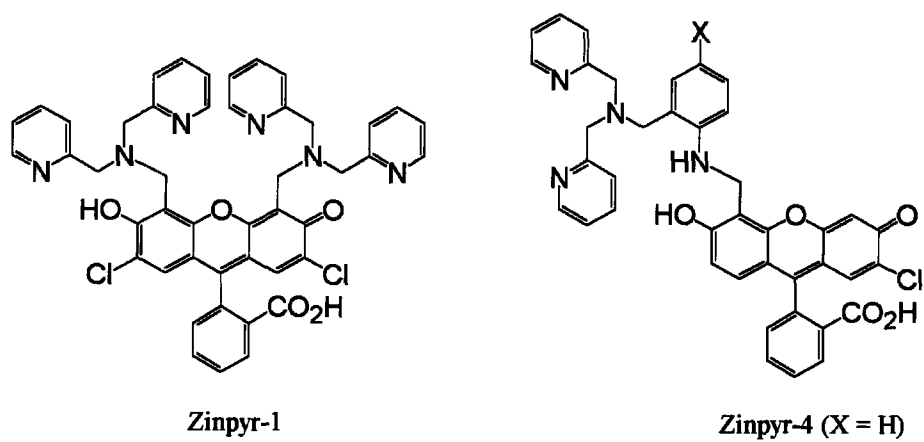


Figure 2.1. Structural diagrams of ZP1 and ZP4.

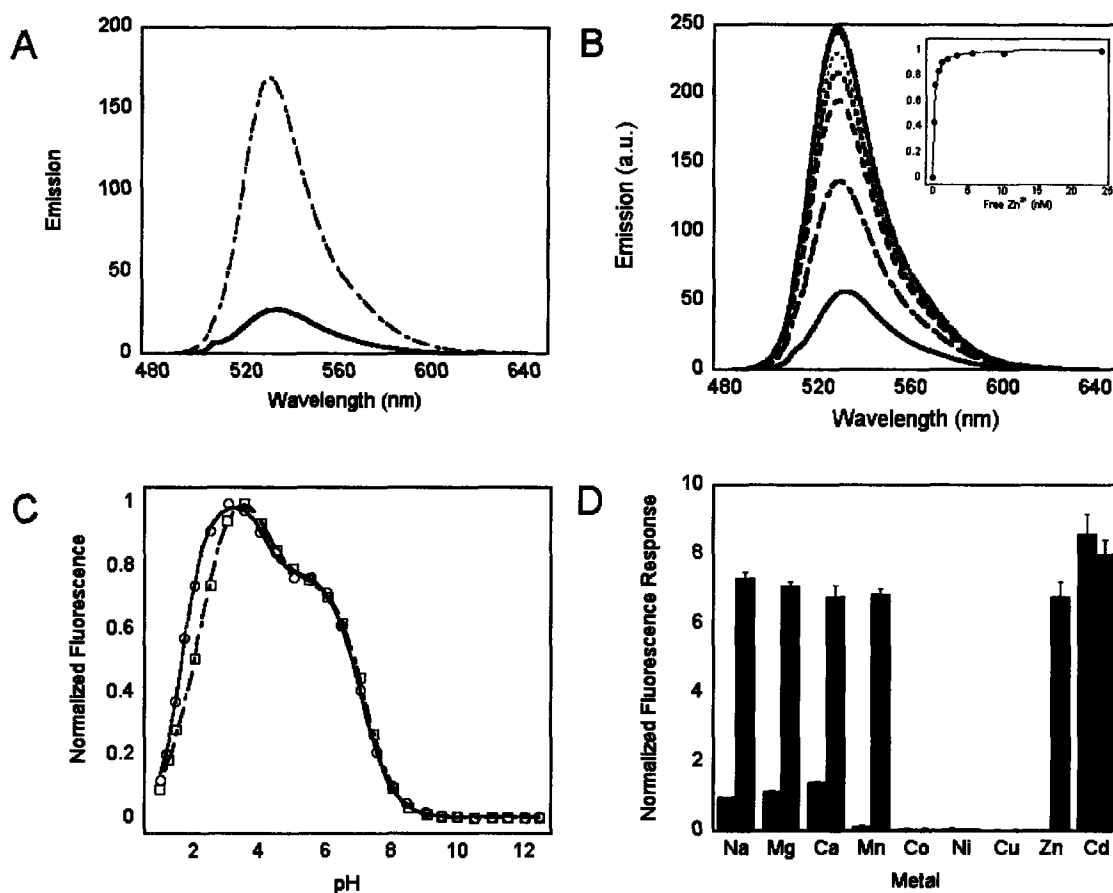


Figure 2.2. Photophysical and thermodynamic characterization of ZP1(6-CO₂R).

(A) Zn²⁺ response of ZP1(6-CO₂H) with excitation at 505 nm, pH 7.4 (B) ZP1(6-CO₂H) response to nanomolar levels of free Zn²⁺, inset shows K_d fit (C) Fluorescence pH profile of ZP1(5-CO₂H) (circles) and ZP1(6-CO₂H)(squares) (D) Selectivity of Zn²⁺ response: treatment of 1 μM dye with 50 μM –2 mM of shown metal ion (red bars) followed by addition of 50 μM ZnCl₂ (blue bars).

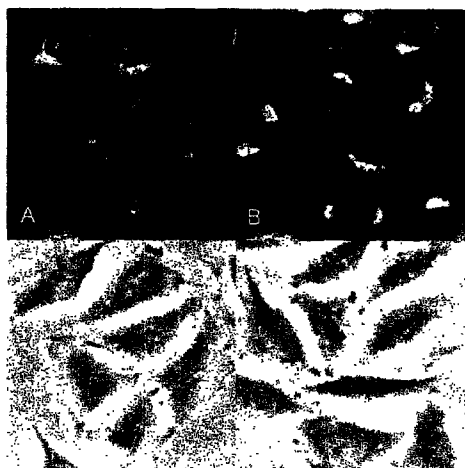


Figure 2.3. Comparison of ZP1-CO₂Et and ZP1 staining.

HeLa cells were incubated for 30 min at 37 °C with 5 μM ZP1(6-CO₂Et) (A, C) or 5 μM ZP1 (B, D) washed twice with HBSS, incubated with 45 μM sodium pyrithione and 5 μM ZnCl₂, washed again, and imaged. Epifluorescence (A, B) and phase contrast (C, D) images are shown. Scale bar 20 μm.

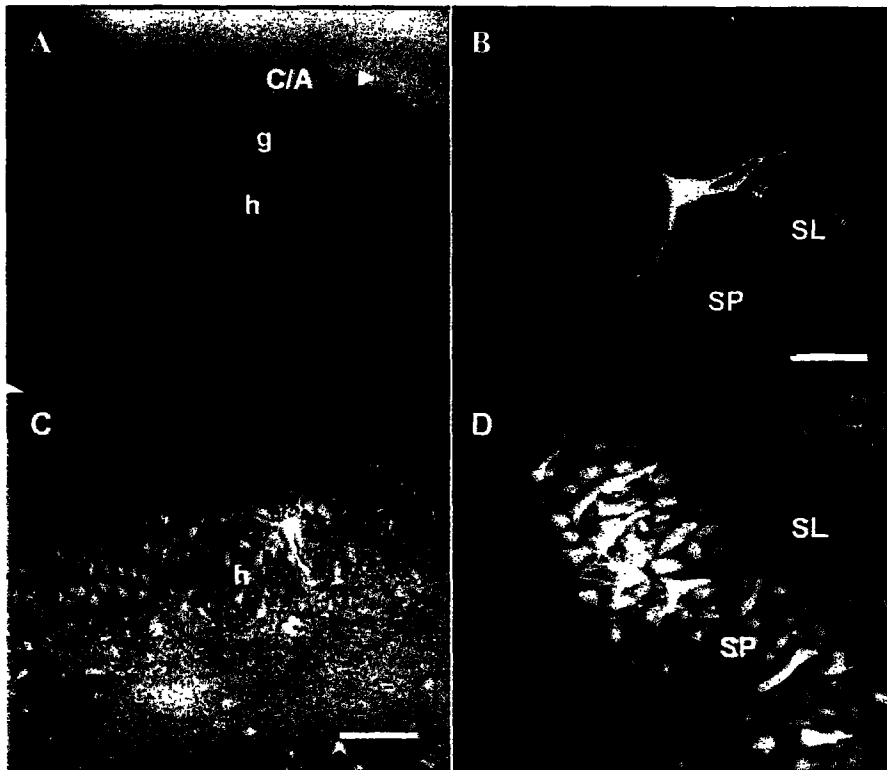


Figure 2.4 (A-D). Imaging of ZP1(6-CO₂Et) (A, B, C, D) and ZP1 (E, F, G, H)-stained rat hippocampus.

Images of normal (A, B, E, F) and post seizure (C, D, G, H) brains are shown. Very weak staining of hilar and CA1 neuropil is seen in A, just discriminable from the granule stratum (g). Neurons injured by the dye injection and sequella stain vividly (B) ZP1 treatment of normal rat (E, F) and post-seizure rat (G, H) affords bright punctate staining of the zinc rich neuropil in the hilus (h), stratum radiatum (SR) and stratum lucidum (SL) and in the commissural/associational neuropil (C/A), while the granule neuron stratum (g) remains unstained. Scattered stained pyramidal neurons are seen in the hilus of C and G and stratum pyramidale (SP) of D and H. Scale bars 125 μm, A, C, E, and G; 50 μm, B, D, F, and H.



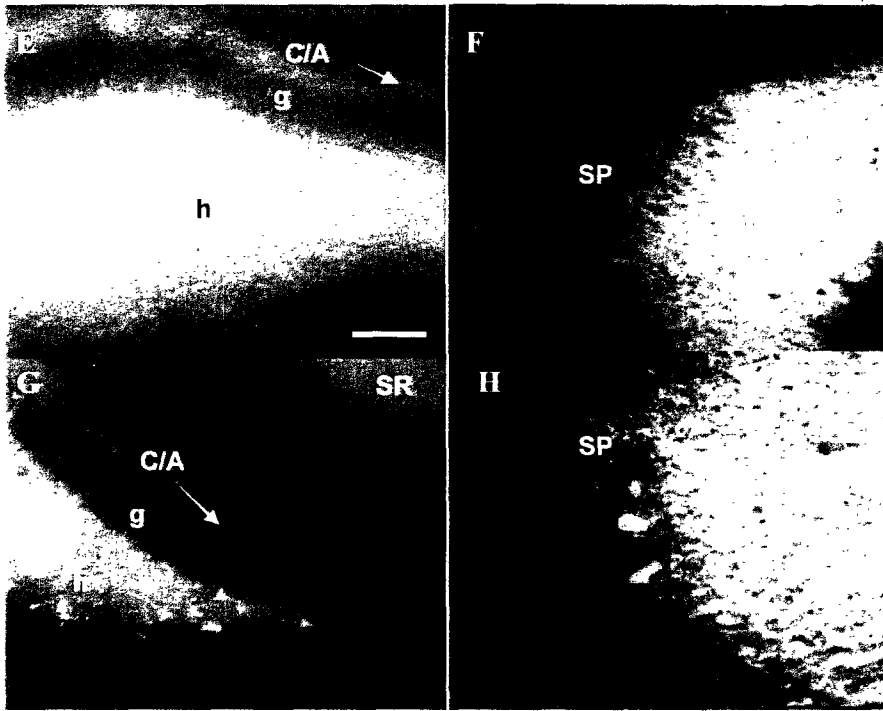


Figure 2.4(E-H).



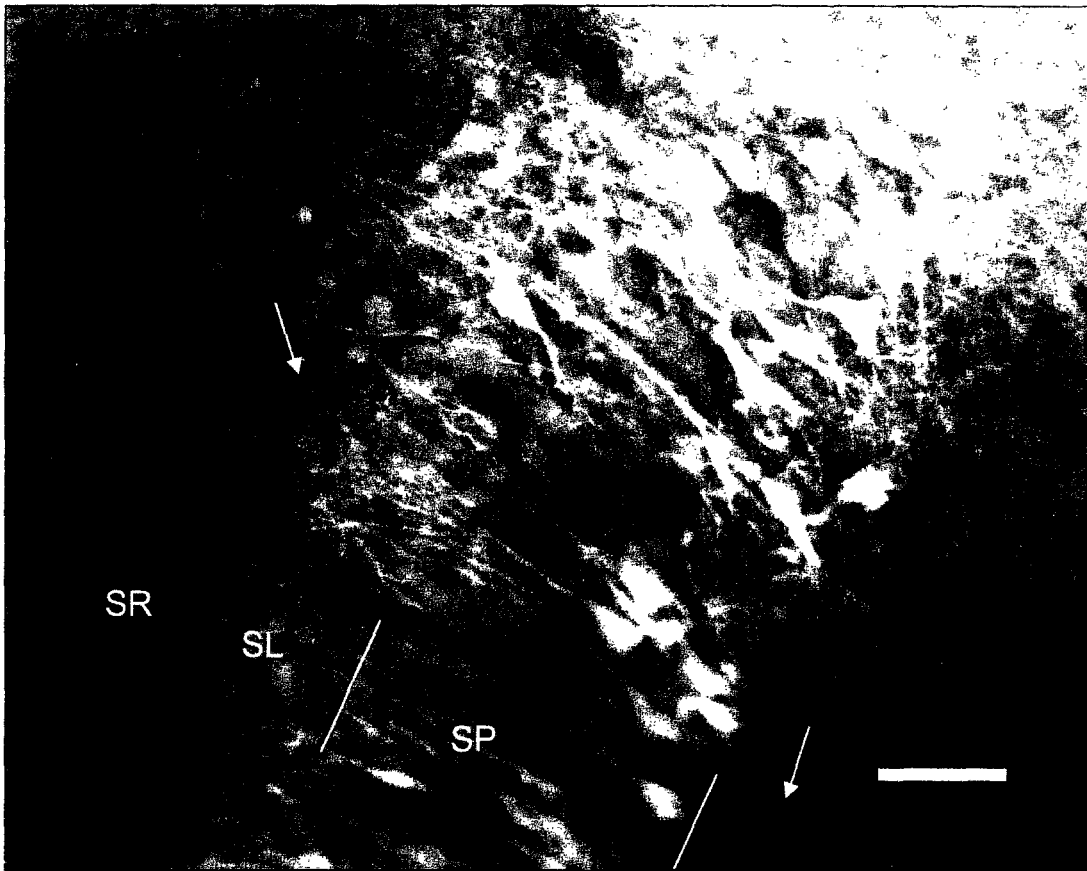


Figure 2.5. Detail of Zn(6-CO₂Et) imaging of the CA3 region after pilocarpine-induced seizure.

The stratum radiatum (SR), stratum lucidum (SL), and stratum pyramidale (SP) are labeled. Scale bar 50 μ m. Note stained pyramidal neurons, unstained stratum lucidum. Arrows indicate examples of single puncta (right) or areas of punctate staining (left).



**Chapter 3 A Two-Fluorophore Esterase-Based Ratiometric Sensing System for
Intracellular Zinc(II)[†]**

Introduction[†]

The application of fluorescent sensors to biological systems has traditionally been complicated by an inability to assess the local concentration of the sensor. Hence, a localized bright fluorescent signal may reflect a large amount of analyte in that area, or it may be an artifact of high local dye concentration. Ratiometric sensors that display two distinctly different measurable signals in the presence and absence of analyte are thus of great interest and utility because they can eliminate such ambiguities.¹

Several ratiometric fluorescent probes for biological zinc(II) ion have recently been described. The majority of these are based on fluorophores requiring relatively short-wavelength, high-energy excitation sources, such as 2-aryl benzimidazoles², benzoxazoles³, indoles and benzofurans.^{4,5} Binding of Zn^{2+} affords a wavelength shift in excitation or emission, based on interruption of fluorophore conjugation or on excited-state intramolecular proton transfer (ESIPT). Excitation wavelengths for these probes range from about 300-380 nm, and emission wavelengths vary between 395-532 nm. ZNP-1, a ratiometric probe with visible excitation and relatively dim fluorescence, has been reported.⁶ These sensors and mechanisms of sensing are reviewed in Chapter 1.

We envisioned a ratiometric two-fluorophore sensing system in which a zinc-sensitive fluorophore was linked to a zinc-insensitive reporter fluorophore such that the two fluorophores would separate upon entering the cell. An ester-linked system seemed ideal for this application, because carboxylate esterification is a common strategy in

[†] A portion of this work has been published elsewhere, in slightly altered form (*J. Am. Chem. Soc.* **2003**, *125*, 11458-11459). Respective contributions were as follows: The initial synthesis of 3',6'-diacetyl-dichlorofluorescein-6-carboxysuccinimidyl ester and studies on the Mitsunobu condensation of coumarin 343 with 6-(3-hydroxypropylamido)-3',6'-diacetyldichloro-fluorescein were carried out Annie C. Won (UROP student).

preparing cell-permeable sensors. The lipophilic esterified sensor can passively diffuse across the cell membrane, and once inside the cell the esters can be hydrolyzed by cytoplasmic esterases, regenerating the parent carboxylates.

In the previous chapter we described the synthesis of ZP1 species containing carboxylate functionalities on the bottom ring. ZP1 is a fluorescein-based Zn^{2+} sensor that is cell-permeable without prior modification;^{7,8} however, fluorescein-based compounds are typically membrane-impermeable owing to the predominance of a charged tautomer in neutral pH aqueous solutions. Such fluorescein species are permeabilized by protecting the phenolic hydroxyl groups as hydrolytically-labile acetates,⁹ trapping the fluorescein moiety in the cell-permeable lactone form.¹⁰ Esterification of carboxylates with alkyl or functionalized alkyl groups is widely used for sensors in which the carboxylate is an integral part of the analyte-binding system or is introduced to increase solubility. Acetoxymethyl esters are particularly susceptible to hydrolysis,^{10,11} but ethyl esters^{2,12,13} are also commonly used, implying that alkyl esters are acceptable substrates for cytoplasmic esterases.

Coumazin-1 and -2 (CZ1, **1**; CZ2, **2**) are ZP1 analogues containing coumarin 343 (**3**) as the reporter fluorophore bound via a hydrolyzable alkyl-amidoester or -diester linker. Permeation of **1** or **2** into the cell and subsequent cleavage by intracellular esterases thus regenerates the parent fluorophores **3** and **4** or **5**, and enables two-fluorophore ratiometric sensing of Zn^{2+} , as shown in Scheme 3.1. In this chapter, we describe our synthesis and physical characterization of these two molecules as well as biological applications. A preliminary communication describing CZ1 has appeared previously.¹⁴

Experimental

Materials and Methods.

Reagents were purchased from Aldrich and used without further purification except for coumarin 343, which was recrystallized from MeOH and CH₂Cl₂ before use. The pyridinium salt of 3',6'-diacetyl-2',7'-dichloro-6-carboxyfluorescein (**6**) was prepared as described in Chapter 2. A porcine liver esterase (PLE) suspension was purchased from Sigma and used as supplied. Acetonitrile and dichloromethane were obtained from a dry-still solvent dispensation system. Fluorescence spectra were acquired on a Hitachi F-3010 fluorimeter and UV-visible absorption spectra were recorded on a Cary 1E UV-visible spectrophotometer at 25 °C. Both were analyzed by using Kaleidagraph 3.0 for Windows. ¹H and ¹³C NMR spectra were acquired on a Varian 300 or 500 MHz or a Bruker 400 MHz spectrometer. High-resolution mass spectra were acquired on an FTMS electrospray apparatus by personnel at the MIT DCIF. LCMS analysis was performed on an Agilent Technologies 1100 Series LCMS with a Zorbax Extend C-18 column using a linear gradient of 100% A (95:5 H₂O:MeCN, 0.05% HCO₂H) to 100% B (95:5 MeCN:H₂O; 0.05% HCO₂H) over 30 min at a flow rate of 0.250 mL/min. Detector wavelengths were set at 240 nm and 500 nm, and the MS detector was set to positive ion mode scanning the range $m/z = 100-2000$.

Synthetic Procedures

3',6'-Diacetyl-2',7'-Dichloro-6-(4-Hydroxybutyl)fluoresceinamide (7). The pyridinium salt of 3',6'-diacetyl-2',7'-dichloro-6-carboxyfluorescein (**6**, 2.44 g, 4 mmol) was dissolved in 40 mL of dry CH₂Cl₂ and 800 μL of DMF and stirred under N₂ in a dry

ice-acetone bath. Oxalyl chloride (4 mL of a 2 M solution in CH₂Cl₂) was added over 2 h, and the reaction was stirred overnight. The solvents were then removed under reduced pressure. The residue was taken up in CH₂Cl₂ and NaHCO₃ (336 mg, 4 mmol) was added. A portion of 4-aminobutanol (400 μL) was dissolved in CH₂Cl₂ and added slowly using an addition funnel. The reaction was stirred for 4 h at RT, then washed with 2 x 40 mL H₂O and 1 x 50 mL brine, dried over MgSO₄ and the solvent was removed under reduced pressure. The glassy yellow residue was purified by flash chromatography on silica gel eluting with 98:2 → 96:4 CHCl₃:MeOH, and dried under vacuum to give 650 mg (27%) of a glassy colorless foam. ¹H NMR (CDCl₃): δ 8.08 (s, 2 H); 7.49 (s, 1 H); 7.14 (br s, 1 H); 7.11 (s, 2 H); 6.85 (s, 2 H); 3.62 (t, 2 H); 3.38 (m, 2 H); 2.38 (s, 6 H); 1.61-1.69 (m, 4 H). ¹³C NMR (CDCl₃): δ 168.22, 167.78, 165.49, 149.52, 148.58, 142.13, 130.10, 129.01, 127.35, 126.10, 122.97, 122.31, 117.14, 112.95, 80.54, 62.64, 40.54, 30.02, 26.29, 20.95. m.p. 118-119 °C. HRMS(M+Na): Calcd for C₂₈H₂₁Cl₂O₉N₁Na₁: 608.0491; Found 608.0481

3',6'-Diacetyl-2',7'-Dichloro-6-(4-(Coumarin-343-carboxybutyl)fluoresceinamide

(8). 3',6'-Diacetyl-2',7'-dichloro-6-(4-hydroxybutyl)fluoresceinamide (7, 600 mg, 1 mmol) was combined with coumarin 343 (290 mg, 1.02 mmol) in dry CH₂Cl₂. Triphenyl phosphine (290 mg, 1.11 mmol) and diisopropyl azodicarboxylate (DIAD, 210 μL) were added, and the reaction was stirred at RT for 2.5 h. Most of the solvent was then removed by rotary evaporation, and the residue was diluted with diethyl ether and allowed to stand at RT overnight. The resulting yellow precipitate was filtered and washed with diethyl ether to give 781 mg (90%) of a yellow crystalline powder. ¹H NMR (CDCl₃): δ 8.36 (s, 1 H); 8.26 (d, 1 H); 8.06 (d, 1 H); 7.99 (br t, 1 H); 7.78 (s, 1 H); 7.09 (s, 2 H); 6.95 (s, 1

H); 6.85 (s, 2 H); 4.30 (br s, 2 H); 3.50 (br t, 2 H); 3.36 (br s, 4 H); 2.74-2.86 (m, 4 H); 2.34 (s, 6 H); 1.98 (br s, 4 H); 1.83 (br s, 4 H). ^{13}C NMR (CDCl_3): δ 168.19, 167.97, 165.75, 165.28, 159.55, 153.64, 152.15, 150.44, 149.74, 149.11, 148.63, 142.27, 129.88, 129.07, 127.34, 125.85, 125.61, 123.59, 122.84, 119.77, 117.30, 112.84, 107.95, 106.34, 105.69, 80.87, 65.73, 53.64, 50.48, 50.08, 39.82, 27.57, 26.34, 25.43, 21.20, 20.22. m.p. dec > 170 °C. HRMS(M-H): Calcd for $\text{C}_{45}\text{H}_{35}\text{Cl}_2\text{N}_2\text{O}_{12}$: 865.1567, Found 865.1561.

Coumazin-1 (1). Dipicolylamine (320 mg, 1.6 mmol) and paraformaldehyde (96 mg, 3.2 mmol) were combined in 20 mL of MeCN and heated to reflux for 45 min. 3',6'-Diacetyl-2',7'-dichloro-6-(4-(coumarin-343-carboxybutyl)fluoresceinamide (**8**, 217 mg, 0.25 mmol) was suspended in 10 mL of MeCN and added to the refluxing solution, and 10 mL of H_2O was then added. The reaction was removed from heat after 24 h, and the solvents were removed under reduced pressure. Several drops of glacial acetic acid were added, followed by H_2O , and a red precipitate formed, which was filtered to give 120 mg of the crude product. The filtrate was allowed to stand for 48 h at RT and then filtered to afford 54 mg additional product. Recrystallization from $\text{CHCl}_3/\text{MeOH}$ yielded 99 mg (33%) of a red solid. ^1H NMR (CDCl_3): δ 8.57 (d, 4 H); 8.39 (s, 1 H); 8.20 (d, 1 H); 8.02 (d, 1 H); 7.86 (br t, 1 H); 7.77 (s, 1 H); 7.64 (m, 4 H); 7.33 (d, 4 H); 7.17 (m, 4 H); 6.96 (s, 1 H); 6.62 (s, 2 H); 4.31 (br s, 2 H); 4.17 (s, 4 H); 4.00 (s, 8 H); 3.48 (br s, 2 H); 3.35 (br s, 4 H); 2.87 (t, 2 H); 2.76 (t, 2 H); 1.97 (br m, 4 H); 1.83 (br m, 4 H). ^{13}C NMR (CDCl_3): δ 168.69, 166.01, 165.47, 159.56, 157.70, 156.04, 153.71, 152.50, 150.45, 149.09, 148.79, 148.62, 148.40, 141.59, 138.30, 137.33, 128.96, 128.69, 127.90, 127.31, 124.01, 123.50, 122.66, 121.90, 119.72, 117.76, 111.82, 109.56, 107.95, 105.82, 65.81,

59.30, 50.48, 50.10, 49.34, 39.70, 27.58, 26.50, 25.29, 21.23, 20.25, 20.19. m.p. dec > 149 °C. HRMS(M+H): Calcd for C₆₇H₅₉Cl₂N₈O₁₀: 1205.3731; Found 1205.3770.

N-(2-Hydroxyethyl)-3',6'-Diacetyl-2',7'-Dichlorofluorescein-6-amide (9). The pyridinium salt of 3',6'-diacetyl-2',7'-dichloro-6-carboxyfluorescein (6, 1.22 g, 2 mmol) was dissolved in dry CH₂Cl₂ containing 400 μL of DMF and stirred in a dry ice-acetone bath. Oxalyl chloride (1.5 mL, 2 M solution in CH₂Cl₂) was diluted with 25 mL of dry CH₂Cl₂ and added dropwise over 30 min. The reaction was stirred for an additional 30 min, and then concentrated under reduced pressure. The resulting residue was dissolved in CH₂Cl₂, NaHCO₃ (336 mg, 4 mmol) was added, and the suspension was stirred at -78 °C as a solution of ethanolamine (390 μL, 409 mg, 6.6 mmol) in 15 mL of CH₂Cl₂ was added dropwise. The reaction was stirred overnight, at which time 40 mL of H₂O was added and the layers were separated. The aqueous layer was washed with 2 x 40 mL CH₂Cl₂; the combined organic layers were washed with saturated NaCl solution, dried over MgSO₄, and evaporated. The resulting residue was purified by flash chromatography on silica gel eluting with 98:2 → 96:4 CHCl₃:MeOH to give 450 mg (42%) of **9** as a colorless solid. ¹H NMR(CDCl₃): δ 8.10 (s, 2 H); 7.56 (s, 1 H); 7.11 (s, 2 H); 7.08 (t, 1 H); 6.84 (s, 1 H); 3.70 (t, 2 H); 3.49 (m, 2 H); 2.37 (s, 6 H). ¹³C NMR(CDCl₃): δ 168.40, 167.79, 166.32, 152.42, 149.72, 148.82, 141.52, 130.37, 129.15, 128.02, 126.27, 123.09, 122.53, 117.09, 113.04, 80.67, 61.79, 43.03, 20.82. m.p. 159-162 °C. HRMS(M+H): Calcd for C₂₇H₂₀Cl₂NO₉: 572.0515; Found 572.0529.

Mitsunobu Reaction of N-(2-Hydroxyethyl)-3',6'-Diacetyl-2',7'-Dichlorofluorescein-6-amide. N-(2-Hydroxyethyl)-3',6'-diacetyl-2',7'-dichlorofluorescein-6-amide (**9**, 55 mg, 0.1 mmol) was combined with coumarin 343 (29 mg, 0.1 mmol),

triphenylphosphine (30 mg, 0.11 mmol), and DIAD (21 μ L, 0.1 mmol) in dry CH_2Cl_2 and stirred 45 min at RT. The reaction was concentrated in vacuo, the residue was dissolved in minimal CH_2Cl_2 and Et_2O was added. The resulting orange crystalline solid was filtered off and one half of the filtrate was loaded onto a preparative scale TLC plate. Compound **10** was isolated as the major product (17 mg, corresponds to 64% overall yield). $^1\text{H NMR}(\text{CDCl}_3)$: δ 8.28 (d, 1 H); 8.12 (d, 1 H); 7.76 (s, 1 H); 7.16 (s, 2 H); 6.87 (s, 2 H); 4.47 (t, 2 H); 4.08 (t, 2 H); 2.38 (s, 6 H). HRMS(M+Na): Calcd for $\text{C}_{27}\text{H}_{17}\text{Cl}_2\text{NO}_8\text{Na}$: 576.0229; Found 576.0216.

Coumarin 343 4-Hydroxybutyl Ester (11). Coumarin 343 (**3**, 285 mg, 1 mmol) was combined with 4-benzyloxy-1-butanol (190 μ L, 1.03 mmol), triphenylphosphine (280 mg, 1.07 mmol), and DIAD (210 μ L, 1.01 mmol) in 20 mL of dry CH_2Cl_2 . The reaction was stirred at RT for 90 min and then quenched with 20 mL of MeOH. Pd/C was added and the suspension was stirred under a H_2 atmosphere for 2 h and then filtered through Celite and concentrated in vacuo. The viscous residue was purified by flash chromatography on silica gel eluting with 93:7 CHCl_3 :MeOH, and then crystallized from CHCl_3 layered with Et_2O . Filtration gave 277 mg of **11** (78% yield). $^1\text{H NMR}(\text{CDCl}_3)$: δ 8.36 (s, 1 H); 6.95 (s, 1 H); 4.35 (t, 2 H); 3.74 (t, 2 H); 3.34 (m, 4 H); 2.87 (t, 2 H); 2.77 (t, 2 H); 1.98 (m, 4 H); 1.75 (m, 4 H). $^{13}\text{C NMR}(\text{CDCl}_3)$: δ 165.11, 159.20, 153.64, 149.76, 148.82, 127.19, 119.47, 107.76, 107.18, 105.82, 65.39, 62.06, 50.43, 50.04, 29.91, 27.57, 25.00, 21.27, 20.29, 20.18. m.p. 135-137 $^\circ\text{C}$. HRMS(M+Na) Calcd for $\text{C}_{20}\text{H}_{23}\text{NO}_5\text{Na}$: 380.1474; Found 380.1463.

Coumarin 343 4-(6-Carboxy-3',6'-Diacetyl-2',7'-Dichlorofluorescein)Butyl Ester (12). Coumarin 343 4-hydroxybutyl ester (**11**, 268 mg, 0.75 mmol) was combined with 6-

carboxy-2',7'-dichlorofluorescein-3',6'-diacetate pyridinium salt (479 mg, 0.78 mmol), triphenylphosphine (206 mg, 0.78 mmol), and DIAD (158 μ L) in 30 mL of dry CH_2Cl_2 at RT and stirred overnight. More DIAD (79 μ L) was then added. After 24 h the reaction was concentrated in vacuo and the desired product was isolated by flash chromatography on silica gel eluting with 98:2 \rightarrow 90:10 CHCl_3 :MeOH, followed by trituration with MeOH to give 185 mg (28%) of **12**. ^1H NMR(CDCl_3): δ 8.38 (d, 1 H); 8.31 (s, 1 H); 8.14 (d, 1 H); 7.84 (s, 1 H); 7.18 (s, 2 H); 6.94 (s, 1 H); 6.85 (s, 2 H); 4.42 (t, 2 H); 4.35 (t, 2 H); 3.34 (m, 4 H); 2.88 (t, 2 H); 2.76 (t, 2 H); 2.38 (s, 6 H); 1.9-2.0 (m, 8 H). ^{13}C NMR(CDCl_3): δ 168.08, 167.78, 164.88, 158.81, 153.70, 152.12, 149.86, 149.49, 148.85, 148.78, 137.57, 132.16, 129.17, 129.06, 127.18, 126.02, 125.39, 123.02, 119.37, 117.09, 113.11, 107.71, 107.38, 105.93, 80.95, 65.03, 64.44, 50.46, 50.07, 26.61, 24.60, 24.56, 21.33, 20.83, 20.35, 20.25. m.p. dec $>$ 159 $^\circ\text{C}$. HRMS(M+Na): Calcd for $\text{C}_{45}\text{H}_{35}\text{Cl}_2\text{NO}_{13}\text{Na}$: 890.1383; Found 890.1414.

Coumazin-2 (2). Dipicolylamine (128 mg, 0.64 mmol) and paraformaldehyde (40 mg, 1.32 mmol) were combined in 10 mL of dry MeCN and heated to reflux for 45 min. A portion of **12** (87 mg, 0.1 mmol) was suspended in 5 mL of MeCN and added to the refluxing solution, followed by 5 mL of H_2O . The reaction was heated at reflux for 24 h, at which time it was cooled to RT, concentrated in vacuo, acidified with 5 drops of glacial acetic acid, and stored at 4 $^\circ\text{C}$ overnight. The resulting red precipitate was filtered to afford 87 mg (72%) of **2**. ^1H NMR(CDCl_3): δ 8.60 (d, 4 H); 8.38 (d, 2 H); 8.33 (s, 1 H); 8.10 (d, 1 H); 7.85 (s, 1 H); 7.67 (td, 4 H); 7.36 (d, 4 H); 7.20 (m, 4 H); 6.97 (s, 1 H); 6.60 (s, 2 H); 4.40 (t, 2 H); 4.32 (t, 2 H); 4.20 (s, 4 H); 4.01 (m, 8 H); 3.34 (m, 4 H); 2.86

(t, 2 H); 2.75 (t, 2 H); 1.80-1.98 (m, 12 H). m.p. dec > 151 °C. HRMS(M+H): Calcd for $C_{67}H_{58}Cl_2N_7O_{11}$: 1206.3571; Found 1206.3564.

2',7'-Dichloro-6-(2-Hydroxyethyl)fluoresceinamide (14). The pyridinium salt of 3',6'-Diacetyl-2',7'-dichloro-6-carboxyfluorescein (**6**, 4.75 g, 9 mmol) was suspended in ethyl acetate (dried over $MgSO_4$) and stirred in an ice bath. Oxalyl chloride (2 M in CH_2Cl_2 , 5 mL) and DMF (1 mL) were added, and the solution was stirred for 16 h. The solvents were removed on the rotary evaporator and the yellow residue was taken up in 25 mL of CH_2Cl_2 . The resulting solution was stirred in an ice bath and ethanolamine (2.9 mL, 2.87 g, 47 mmol) was added. A red suspension was formed immediately upon addition of ethanolamine. The reaction was stirred 2 h at RT, then 30 mL of H_2O were added, the layers separated, and the organic layer extracted with 2 x 30 mL H_2O . The combined aqueous layers were washed with 1 x 30 mL of CH_2Cl_2 , acidified with 2 N HCl, and filtered to give an orange solid which was dried in air overnight. Yield 2.04 g, 47%. m.p. dec > 290 °C. 1H NMR(DMSO- d_6): δ 11.08 (br s, 2 H); 8.66 (t, 1 H); 8.18 (d, 1 H); 8.10 (d, 1 H); 7.72 (s, 1 H); 6.95 (s, 2 H); 6.78 (s, 2 H); 3.49 (t, 2 H); 3.17 (m, 2 H). ^{13}C NMR (DMOS- d_6): δ 167.79, 164.78, 155.32, 151.82, 150.02, 141.10, 129.81, 128.48, 127.87, 125.36, 122.32, 116.42, 110.01, 103.70, 81.71, 59.44, 42.41. m.p. dec > 290 °C HRMS(M+H): Calcd for $C_{23}H_{16}Cl_2NO_7$: 488.0304; found 488.0285.

ZP1(6-CONH(CH₂)₂OH) (13). Dipicolylamine (5.12 g, 25.6 mmol) and paraformaldehyde (680 mg, 22.6 mmol) were refluxed together in dry MeCN for 45 min. 2',7'-Dichloro-6-(2-hydroxy-ethyl)fluoresceinamide (**14**, 1.92 g, 4 mmol) was dissolved in 1:1 H_2O :MeCN and added, and the reaction was refluxed for 24 h. The reaction was then cooled to RT, the MeCN was removed under reduced pressure, and the remaining

solution was stored at $-25\text{ }^{\circ}\text{C}$ overnight. The resulting precipitate was filtered, washed with H_2O , and dried to give 1.35 g (38%) of **13** as an orange-pink solid. ^1H NMR (MeOH-d_4): δ 8.50 (d, 4 H); 8.12 (m, 2 H); 7.75 (td, 4 H); 7.64 (s, 1 H); 7.47 (d, 4 H); 7.28 (m, 4 H); 6.71 (s, 2 H); 4.32 (s, 4 H); 4.16 (m, 8 H); 3.66 (t, 2 H); 3.48 (t, 2 H). ^{13}C NMR (DMSO-d_6): δ 167.68, 164.92, 157.28, 155.67, 151.41, 148.68, 148.10, 141.13, 137.17, 129.65, 128.15, 126.85, 125.28, 123.18, 122.65, 116.34, 111.90, 109.32, 82.55, 64.95, 59.35, 58.41, 48.78, 42.38. m.p. 123-125 $^{\circ}\text{C}$ HRMS(M+H): Calcd for $\text{C}_{49}\text{H}_{42}\text{Cl}_2\text{N}_7\text{O}_7$: 910.2523; Found 910.2491. Anal. Calcd for $\text{C}_{49}\text{H}_{41}\text{Cl}_2\text{N}_7\text{O}_7$: C, 64.62; H, 4.54; N, 10.76; Cl, 7.78. Found: C, 64.47; H, 4.27; N, 10.60; Cl, 7.53.

6-Carboxy-2',7'-Dichlorofluorescein-3',6'-diacetatesuccinimidyl Ester (15). The pyridinium salt of 6-Carboxy-2',7'-dichlorofluorescein-3',6'-diacetate (**6**, 945 mg, 1.5 mmol) was combined with 1-[3-(dimethylamino)propyl]-3-ethylcarbodiimide hydrochloride (EDC) (300 mg, 1.56 mmol) and N-hydroxysuccinimide (200 mg, 1.74 mmol) in 10 mL of 1:1 ethyl acetate:DMF and stirred at RT for 6 h. Brine (75 mL) and CH_2Cl_2 (50 mL) were added, and the layers were separated. The aqueous layer was extracted with 2 x 50 mL CH_2Cl_2 ; the combined organics were washed with 2 x 50 mL of 0.1 N HCl and 1 x 50 mL of brine, dried over MgSO_4 , and evaporated. The resulting residue was purified by flash chromatography on silica gel eluting with 99:1 CHCl_3 : MeOH to give 647 mg (0.48 mmol, 69%) of **15** as a glassy foam. ^1H NMR(CDCl_3): δ 8.44 (d, 1 H); 8.22 (d, 1 H); 7.93 (s, 1 H); 7.19 (s, 2 H); 6.84 (s, 2 H); 2.90 (dd, 4 H); 2.37 (s, 6 H). ^{13}C NMR (CDCl_3): δ 168.90, 167.90, 167.00, 162.61, 160.43, 152.17, 149.62, 148.88, 132.72, 132.07, 130.66, 128.89, 126.30, 123.07, 116.36, 113.06, 80.84, 25.61,

20.67. m.p. 84-86 °C. HRMS(M+H): Calcd for $C_{29}H_{18}Cl_2NO_{11}$: 626.0257; Found 626.0220

N-(4-Hydroxybutyl)-2',7'-Dichlorofluorescein-6-amide (16). 6-Carboxy-2',7'-dichlorofluorescein-3',6'-diacetate succinimidyl ester (**15**, 312 mg, 0.5 mmol) was dissolved in 1:1 CH_2Cl_2 :MeOH and stirred at RT with 4-aminobutanol (230 μ L, 222 mg, 2.5 mmol) overnight. The resulting red solution was concentrated on the rotary evaporator, taken up in 10 mL of H_2O , acidified with conc. HCl, and filtered to afford an orange solid, which was dried overnight to give 235 mg of **16** (91% yield). 1H NMR(MeOH- d_4): δ 8.15 (s, 2 H); 7.62 (s, 1 H); 6.85 (s, 2 H); 6.68 (s, 2 H); 3.57 (t, 2 H); 3.35 (m, 2 H); 1.50-1.65 (m, 4 H). m.p. 179-180 °C (dec). HRMS(M-H): Calcd for $C_{25}H_{18}Cl_2NO_7$: 514.0460; Found 514.0474.

ZP1(6-CONH(CH₂)₄OH) (4). Dipicolylamine (256 mg, 1.3 mmol) was combined with paraformaldehyde (36 mg, 2.6 mmol) in 10 mL of dry MeCN and heated to reflux for 45 min. N-(4-Hydroxybutyl)-2',7'-dichlorofluorescein-6-amide (103 mg, 0.2 mmol) was suspended in 15 mL of 1:1 MeCN: H_2O and added to the reaction, and reflux was continued for 24 h. The reaction was cooled to RT, acidified with 0.5 mL of glacial acetic acid, and concentrated under reduced pressure. The residue was diluted with MeOH and H_2O and stored at 4 °C overnight. Filtration afforded the desired product (19 mg, 10%). 1H NMR(MeOH- d_4): δ 8.53 (d, 4 H); 8.12 (s, 2 H); 7.63 (s, 1 H); 7.48 (d, 4 H); 7.30 (m, 4 H); 7.26 (t, 4 H); 6.67 (s, 2 H); 4.34 (s, 4 H); 4.18 (m, 8 H); 3.52 (t, 2 H); 3.37 (t, 2 H); 1.52-1.68 (m, 4 H). m.p. 157-159 °C (dec). HRMS(M+H): Calcd for $C_{51}H_{46}Cl_2N_7O_7$: 938.2836; Found 938.2843

Spectroscopic Measurements

Solutions, buffers, and protocols were as described in Chapter 2. Extinction coefficients, quantum yields, fluorescence-dependent pK_a values, and dissociation constants were measured as described in Chapter 2. All measurements were performed in triplicate.

Zn²⁺ Response of Esterase-Treated CZ Dyes. A 10 mL portion of a 4 μ M solution of CZ1 in pH 7.5 HEPES buffer was incubated with a 10- μ L aliquot of PLE (10 mg/mL in 3.2 M $(NH_4)_2SO_4$) at RT for 12 h. A 2 mL aliquot was withdrawn and the fluorescence spectrum from 425-650 nm was acquired with excitation first at 445 nm, then at 505 nm. A 4 μ L aliquot of 10 mM $ZnCl_2$ was added and the fluorescence spectra were recorded as before. The procedure was repeated for CZ2 with incubation times varying from 1 to 6 h.

Preparation of Esterase-Treated Coumazin-1 for Physical Measurements. A 50 μ L aliquot of PLE suspension was added to 50 mL of 2 μ M Coumazin-1 in pH 7.5 HEPES buffer. The solution was incubated for 10 h at 25 °C before use in metal ion selectivity or dissociation constant measurements. Dissociation constants were measured as previously described.⁷

Metal Selectivity of Esterase-Treated Coumazin-1. Fluorescence spectra of 2 mL aliquots were acquired between 425-650 nm with excitation first at 445 nm, then at 505 nm. A 10 μ L aliquot of 2.00 M NaCl or 10 mM $MnCl_2$, $CoCl_2$, $NiCl_2$, $CuCl_2$, $CdCl_2$, or a 4 μ L aliquot of 1.00 M $CaCl_2$ or $MgCl_2$ was added, the fluorescence spectra were re-acquired, and a 10 μ L aliquot of 10 mM $ZnCl_2$ was added and the fluorescence spectra were acquired once more. The ratio of ZP1 integrated emission to coumarin integrated emission was calculated for each metal concentration.

Michaelis-Menten Kinetics of Esterase Hydrolysis of CZ Dyes. A 10 μL aliquot of PLE was added to a fluorescence cuvette containing 2 mL of pH 7.5 HEPES buffer and various concentrations (0.05 nM – 4 μM) of CZ1. The cuvette was shaken vigorously and the emission intensity at 488 nm (excitation 445 nm) was monitored for 5 min at 25 $^{\circ}\text{C}$. The rate of increase in emission intensity between 100-200 sec was determined and converted to $\mu\text{mol}/\text{min}$ of coumarin 343 produced using a standard curve. The rate of increase in concentration of coumarin 343 was plotted as a function of substrate concentration and fit by using a Michaelis-Menten model. The procedure was repeated for CZ2 using a dye concentration range from 0.5 nM-25 μM and with addition of 5 μL aliquots of PLE.

LCMS Determination of CZ1 and CZ2 Ester Hydrolysis Products. A 10 μM solution of CZ1 (20 μL of a 1 mM DMSO stock solution of CZ1 and 5 μL PLE suspension in 2 mL HEPES buffer (50 mM, pH 7.5)) was incubated 19 h at 22 $^{\circ}\text{C}$ in a polystyrene tube covered with aluminum foil, filtered, and analyzed by LCMS. The major peaks observed were at 10.8 min (no assignable mass), 13.0 min ($m/z = 469.9$), and 18.4 min ($m/z = 593.1$). A 10- μM solution of CZ2 was similarly prepared and incubated for 1 h before LCMS analysis. The major peaks observed were at 14.8 min ($m/z = 939.2$) and 18.1 min ($m/z = 593.1$). Retention times were determined for 10 μM standard solutions of expected metabolites for comparison and were as follows: **3** 18.5 min ($m/z = 593.1$; Calcd for $2\text{M}+\text{Na} = 593.2$); **4** 12.9 min ($m/z = 469.2$; Calcd for $(\text{M}+2\text{H})/2 = 469.2$); **11** 17.2 min ($m/z = 380.3$; Calcd for $\text{M}+\text{Na} = 380.2$).

Absorption Spectroscopy of PLE-Treated CZ1 and CZ2. A 20 μL aliquot of 1 mM CZ1 stock solution (DMSO) was added to 2 mL of HEPES buffer. A 10 μL aliquot of

PLE suspension was added, and the absorbance spectrum was acquired periodically over 6 h. The procedure was repeated for CZ2.

Imaging

Human cortical neurons (HCN-A94-02) were cultured in 1:1 DMEM:F12 containing N2 supplements (Gibco, 1 mL/100 mL media). Basic fibroblast growth factor (bFGF, Invitrogen, 20 ng/mL) was added to the medium immediately prior to use. The medium was replaced every 2-4 days, and cells were passaged after reaching 90% confluency. Cells were cultured in vessels that had been previously coated with poly-L-ornithine and mouse laminin according to the following procedure. A 10 µg/mL solution of poly-L-ornithine (PORN, Sigma) was added to culture flasks or plates, and the vessels were incubated for 24 h at 22 °C. The PORN solution was aspirated; the vessels were washed 2x with sterile H₂O, and a 1 µg/mL solution of mouse laminin (BD Bioscience) was added to the vessels. After incubation at 37 °C for 24 h, the vessels were wrapped in two layers of sterile aluminum foil and stored at -80 °C. Plates and flasks were thawed and washed 2x with sterile H₂O immediately prior to use.

HeLa cells were grown at 37 °C under a 5% CO₂ atmosphere in Dulbecco's modified Eagle's medium (DMEM, Gibco/BRL) supplemented with 10% fetal bovine serum, 1x penicillin/streptomycin and 2 mM L-glutamine. Cells were plated 24 h before study into 2-mL imaging dishes. Cells were approximately 50% confluent at the time of study. A 20-µL aliquot of dye (1 mM DMSO) was added to each 2-mL dish, and the cells were incubated for 30 min at 37 °C, at which point the medium was aspirated and the cells were washed twice with phosphate-buffered saline solution (PBS), resuspended in dye-free EMEM (Mediatech) and examined on a Zeiss Axiovert 200M inverted

epifluorescence microscope with differential interference contrast (DIC), operated by OpenLab software (Improvision, Lexington, MA). Images were collected at 30-sec intervals for 30 min during the course of the experiment, as a 10 μ L aliquot of a solution containing 1 μ M ZnCl₂ and 9 μ M sodium pyruvate was added. The fluorescence response reached a maximum at about 10-15 min after addition of ZnCl₂, at which time a 10 μ L aliquot of 10 μ M TPEN was added. At each time point, four images were collected in rapid succession: a DIC image (775DF50 emission) and three fluorescence images using a CFP filter (420DF20 excitation, 450DRLP dichroic, 475DF40 emission), a FRET filter (420DF20 excitation, 450DRLP dichroic, 530DR30 emission), and a YFP filter (495DF10 excitation, 515DRLP dichroic, 530DF30 emission). Fluorescence images were background-corrected. Acquisition times were in the range of 100 to 250 msec.

Results and Discussion

Synthesis

The compounds Coumazin-1 and -2 were synthesized as shown in Scheme 3.2. Oxalyl chloride-mediated coupling of 3',6'-diacetyl-2',7'-dichloro-fluorescein-6-carboxylate pyridinium salt **6** with 4-aminobutanol afforded the desired protected hydroxybutylamidofluorescein **7** in 42% yield. Moderate to poor yields are typical of such reactions owing to the relative lability of the phenolic acetyl protecting groups. Subsequent Mitsunobu condensation of the hydroxyl group with coumarin 343 furnishes the linked coumarin-fluorescein **8** in excellent yield, and Mannich reaction of **8** with paraformaldehyde and dipicolylamine affords the desired CZ1. The choice of an n-butyl linker was not arbitrary. Our initial approach involved the hydroxyethylamide **9**; however, the Mitsunobu reaction conditions gave primarily the intramolecular cyclization

product **10**, as shown in Scheme 3.3. Oxazole formation of β -hydroxyethyl amides under Mitsunobu conditions is well precedented in the literature,¹⁵⁻¹⁷ notably in syntheses of paclitaxel and related compounds. Similar problems were encountered with a propyl linker (data not shown). The butyl linker would form a thermodynamically unfavorable seven-membered ring as the product of such an intramolecular condensation, allowing the desired intermolecular reaction to dominate.

The approach to Coumazin-2 (CZ2) was slightly different and is illustrated in Scheme 3.4. The most effective route was Mitsunobu condensation of coumarin 343 with 4-benzyloxyl-1-butanol followed by hydrogenation, which furnishes the requisite coumarin hydroxy ester **11** in 78% yield over two steps. Removal of the diisopropyl hydrazidodicarboxylate byproduct from the intermediate benzyl ether was extremely difficult and reduced the overall yield; hence the most expedient route was to carry the undesired byproduct through and remove it from the deprotected **11** by crystallization. A second Mitsunobu reaction of **11** with the diacetyldichlorofluorescein carboxylate **6** was sluggish, proceeding only to 28% conversion. The reaction yield was not improved by using the free acid of the fluorescein moiety rather than the pyridinium salt. The resulting diester-linked fluorescein-coumarin compound **12** was subjected to standard Mannich conditions and furnished the desired compound CZ2 (**2**) in 72% crude yield.

The expected ZP hydrolysis product **4** and an ethyl analogue **13** of CZ1 were synthesized as shown in Scheme 3.5 and their photophysical and thermodynamic properties were examined. Oxalyl chloride activation of **6** followed by reaction with excess ethanolamine afforded the intermediate fluoresceinamide **14**. Oxalyl chloride activation, however, was sensitive to a variety of experimental factors and the extent of

conversion to the acid chloride was found to be somewhat variable, leading to mixtures that included deprotected starting material. Because column chromatography of unprotected fluorescein species is tedious, alternative methods of activation were sought. EDC-mediated coupling of **6** to *N*-hydroxy-succinimide proceeded in reasonable yield to give the succinimidyl ester **15**, an activated intermediate that can be purified by column chromatography. Subsequent reaction with a threefold or greater excess of amine in mixed $\text{CH}_2\text{Cl}_2/\text{MeOH}$ yielded the deprotected fluoresceinamide **16**, which can be isolated by simple precipitation after removal of organic solvents, providing a straightforward and efficient route to simple fluoresceinamides. Subsequent Mannich reaction of **14** and **16** furnished the desired amide-substituted ZP1 adducts **4** and **13**. Extinction coefficients and quantum yields for **4** and **13** with and without Zn^{2+} were measured, and the dissociation constants and fluorescence response of both species to Zn^{2+} are comparable to the ester- and acid-containing ZP1 sensors described in Chapter 2. CZ2 contains two possible sites for ester hydrolysis. Esterase digestion can therefore produce ZP1 hydroxybutyl ester **5** or ZP1(6- CO_2H) (**17**), as shown in Scheme 3.6. The Zn^{2+} -sensing properties of ester- or acid-functionalized ZP1 carboxylates have been described in the previous chapter. Measured constants for putative CZ fragments or analogues thereof are listed in Table 3.1. All of these ZP1-like hydrolysis products may be expected to function effectively as Zn^{2+} sensors.

Photophysics and Thermodynamics

The photophysical properties of CZ1 and CZ2 have been examined, and relevant data are listed in Table 3.1. Both coumazin compounds fluoresce extremely weakly prior to esterase processing, regardless of the fluorophore excited. Whereas a Förster resonance

energy transfer (FRET) mechanism might account for quenching of the putative donor, such a process would require a concomitant increase in the fluorescence emission of the putative acceptor, which is not observed. ZP1 fluorescence in both cases is similarly quenched, indicating that the Förster interaction is not the major mechanism of quenching.¹⁸ In addition, the extinction coefficients of CZ1 and CZ2 are significantly reduced in comparison to their ZP counterparts (Table 3.1). Treatment of either CZ1 or CZ2 with porcine liver esterase (PLE) effects an increase in intensity of nearly 100% and a blueshift from 526 nm to 519 nm in the absorption band corresponding to the ZP1 absorbance (Figure 3.1). The coumarin absorption band similarly undergoes a blueshift from 450 nm to 435 nm, but the intensity of the band decreases by approximately 40%. The lack of a clean isosbestic point at 480 nm for CZ2 compared to CZ1 is indicative of multiple reactions, presumably owing to the potential for hydrolysis at two sites. This extreme change is further evidence that the Förster mechanism, which requires little to no alteration in the absorption spectrum, is not operative.¹⁹ Other reports of such extreme quenching in the case of covalently linked FRET-capable fluorophores, combined with significant changes in the absorption spectrum, have been accounted for by exciton theory,^{18,20} and such may be the case here.

The change in absorption spectrum occurred much more quickly for CZ2 than for CZ1, and the kinetics of PLE action on both compounds were examined by fluorometric assay (data shown in Figure 3.2). Hydrolysis of either ester in CZ2 will afford roughly the same fluorescence increase. Similarly, after the first hydrolysis event for each CZ2 molecule, the second hydrolysis event will show no fluorescence response but may act as a competing substrate. Although the Michaelis-Menten values measured for CZ2 are

valid for comparison of the fluorescence response with values measured for CZ1, the fluorescence response may arise from more than one reaction and the measured values are therefore considered to be pseudo-constants. Hydrolysis of CZ2 is much more efficient than hydrolysis of CZ1, with significantly greater pseudo- k_{cat} (12.4-fold) and pseudo- $k_{\text{cat}}/K_{\text{M}}$ (4.7-fold) values (Table 3.2). Such a large effect cannot be explained by the statistical presence of twice as many substrates and was initially attributed to greater activity of PLE on the ZP1 ester compared to the coumarin ester. In order to examine this possibility, the CZ2 PLE cleavage products were analyzed by LCMS after 1 h of incubation. The major peaks observed appeared with retention times of 14.8 min (m/z (M+ H) = 939.2) and 18.1 min (m/z (2M + H + Na)/2 = 593.1), corresponding to **5** and **3**, respectively. These products are expected from hydrolysis at the coumarin ester (Scheme 3.6). Since no peak or signal for **17** could be observed during a standard run, its absence in the CZ2 product mix is not conclusive. However, the lack of detectable amounts of the complementary product **11**, which gives a clear signal at 17.2 min (m/z (M + Na) = 380.3) when run in a control, is strong circumstantial evidence that the coumarin ester is cleaved first with good selectivity. Thus the increase in rate of hydrolysis appears to stem primarily from enhanced activity of the enzyme on **2** over **1**. LCMS analysis of CZ1 after 19 h exposure to PLE showed products of hydrolysis at the single ester functionality, as expected (**4**, 13.0 min, (M + 2H) = 469.9 and **3**, 18.4 min, (2 M + Na) = 593.1)

The fluorescence responses of esterase-treated CZ1 and CZ2 were also examined. As expected, excitation at 445 nm afforded coumarin fluorescence at 490 nm, and the coumarin emission spectrum was largely unaltered upon addition of excess ZnCl_2 . Some ZP1 fluorescence at 535 nm is observed for both compounds and increases significantly

after addition of Zn^{2+} , but can be excluded by measuring fluorescence intensity at 488 nm or by instituting a cutoff of 500 nm in measuring integrated fluorescence emission area for coumarin. This ZP1 emission band arises from the ability of fluorescein to absorb some photons even when excited at 445 nm. Excitation at 505 nm affords a classic ZP1 emission band, which increases severalfold in response to addition of $ZnCl_2$. Surprisingly, addition of saturating $ZnCl_2$ to esterase-treated CZ2 results in only a 4-fold increase in the ratio of ZP1 integrated emission to coumarin 343 integrated emission compared with the ratio in the absence of Zn^{2+} , whereas an 8-fold increase is observed for CZ1 (Figure 3.3). The ratio of ZP1:coumarin fluorescence for CZ2 remains relatively constant over several hours.

Biological Imaging

Comparison of CZ1 to CZ2 in the staining of human cortical neurons indicated that fluorescence of the latter develops more quickly and with better image quality than that of CZ1. For CZ2, sufficient fluorescence for analysis develops within 2 hours, although the brightness of staining continues to increase somewhat through 4 hours (Figure 3.4). High background fluorescence is particularly problematic for coumarin fluorescence with our apparatus; thus the coumarin fluorescence images are more valuable in terms of assessing stain quality. For both compounds, the 1 mM DMSO stock solution was diluted with an equal volume of water in order to ensure even application of the dye across the well.

For quantitative ratiometric studies, HeLa cells were stained by the application of a 1 mM solution of CZ2 in DMSO without prior dilution. Using this protocol, the area immediately surrounding the site of application is brightly stained at the expense of the

remaining area, implying a role for DMSO in permeabilizing cellular membranes to the probe. The brightly stained area was imaged (Figure 3.5), and the application of ZnCl₂-sodium pyrithione resulted in a hyperbolic increase in ZP1 emission over approximately ten minutes with no change in coumarin emission (Figure 3.6). TPEN was added after ZP1 emission had reached an apparent maximum, and the ZP1 emission decreased to slightly lower than initial levels. Coumarin emission was not affected throughout the experiment. The intracellular distribution of each dye appears to be reasonably consistent as assessed by the images after treatment with zinc-pyrithione and after treatment with TPEN. An oval-shaped area in each cell displays somewhat different intensity ratios as compared to the surrounding area, and probably corresponds to the cell nucleus. Both dyes are concentrated in the perinuclear area, and relatively good colocalization is observed, based on the Zn²⁺- and TPEN-treated images (Figure 3.5 B, C). The TPEN-induced decrease of ZP1:coumarin fluorescence ratio to below initial levels appears to reflect the presence of some Zn²⁺-bound dye before zinc ion and ionophore are added, because addition of TPEN to CZ2-treated cells without prior addition of Zn²⁺ and pyrithione also causes a slight decrease in the intensity ratio (data not shown).

Conclusions

We describe a new approach to ratiometric sensing of intracellular Zn²⁺ based on the well-known phenomenon of intracellular hydrolysis of esterases. The compounds CZ1 and CZ2 are based on ZP1 sensors linked to the Zn²⁺-insensitive reporter fluorophore coumarin 343 via an amido-ester or diester moiety. The CZ compounds have very low fluorescence, and upon treatment with porcine liver esterase the ZP1-based Zn²⁺ sensor and reporter fluorophore are regenerated. CZ2 activation occurs more rapidly than

CZ1 activation, although the same ester moiety is hydrolyzed first in both cases. CZ2 has been applied to image exogenous Zn^{2+} in HeLa cells, and displays an increase in fluorescence ratio upon treatment with Zn^{2+} and an ionophore. The fluorescence ratio decreases below initial levels upon treatment with TPEN, a result that is in accord with other recent reports.³

Acknowledgements

We are indebted to Alice Y. Ting and Chi-Wang Lin for providing training on and use of the epifluorescence microscope. Human cortical neuron tissue culture stock was kindly supplied by Prof. Fred Gage of the Salk Institute. HeLa cells were graciously provided by Katie R. Barnes and Caroline Sauoma. Synthetic assistance was provided by Annie C. Won.

References

- (1) Tsien, R. Y.; Poenie, M. Fluorescence ratio imaging: a new window into intracellular ionic signaling. *Trends Biochem. Sci.* **1986**, *11*, 450-455.
- (2) Henary, M. M.; Wu, Y.; Fahrni, C. J. Zn(II)-Selective Ratiometric Fluorescent Sensors Based on Inhibition of Excited-State Intramolecular Proton Transfer. *Chem. Eur. J.* **2004**, *10*, 3015-3025.
- (3) Taki, M.; Wolford, J. L.; O'Halloran, T. V. Emission Ratiometric Imaging of Intracellular Zinc: Design of a Benzoxazole Fluorescent Sensor and its Application in Two-Photon Microscopy. *J. Am. Chem. Soc.* **2004**, *126*, 712-713.
- (4) Gee, K. R.; Zhou, Z. L.; Ton-That, D.; Sensi, S. L.; Weiss, J. H. Measuring zinc in living cells. A new generation of sensitive and selective fluorescent probes. *Cell Calcium* **2002**, *31*, 245-251.

- (5) Maruyama, S.; Kikuchi, K.; Hirano, T.; Urano, Y.; Nagano, T. A Novel, Cell-Permeable, Fluorescent Probe for Ratiometric Imaging of Zinc Ion. *J. Am. Chem. Soc.* **2002**, *124*, 10650-10651.
- (6) Chang, C. J.; Jaworski, J.; Nolan, E. M.; Sheng, M.; Lippard, S. J. A tautomeric zinc sensor for ratiometric fluorescence imaging: Application to nitric oxide-induced release of intracellular zinc. *Proc. Natl. Acad. Sci. USA* **2004**, *101*, 1129-1134.
- (7) Walkup, G. K.; Burdette, S. C.; Lippard, S. J.; Tsien, R. Y. A New Cell-Permeable Fluorescent Probe for Zn^{2+} . *J. Am. Chem. Soc.* **2000**, *122*, 5644-5645.
- (8) Burdette, S. C.; Walkup, G. K.; Spingler, B.; Tsien, R. Y.; Lippard, S. J. Fluorescent Sensors for Zn^{2+} Based on a Fluorescein Platform: Synthesis, Properties and Intracellular Distribution. *J. Am. Chem. Soc.* **2001**, *123*, 7831-7841.
- (9) Adamczyk, M.; Chan, C. M.; Fino, J. R.; Mattingly, P. G. Synthesis of 5- and 6-Hydroxymethylfluorescein Phosphoramidites. *J. Org. Chem.* **2000**, *65*, 596-601.
- (10) Haugland, R. P. *Handbook of Fluorescent Probes and Research Products, Ninth Edition*; Ninth ed.; Molecular Probes, Inc.: Eugene, Oregon, 2002.
- (11) Tsien, R. Y.; Pozzan, T.; Rink, T. J. Calcium Homeostasis in Intact Lymphocytes: Cytoplasmic Free Calcium Monitored With a New, Intracellularly Trapped Fluorescent Indicator. *J. Cell Biol.* **1982**, *94*, 325-334.
- (12) Zalewski, P. D.; Millard, S. H.; Forbes, I. J.; Kapaniris, O.; Slavotinek, A.; Betts, W. H.; Ward, A. D.; Lincoln, S. F.; Mahadevan, I. Video Image Analysis of

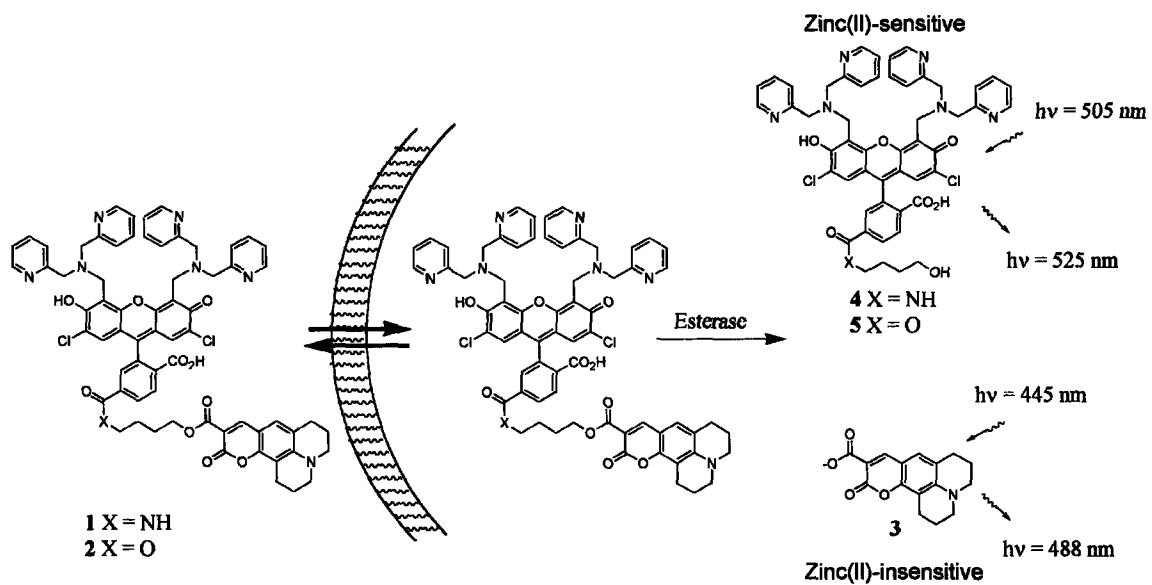
- Labile Zinc in Viable Pancreatic Islet Cells Using a Specific Fluorescent Probe for Zinc. *J. Histochem. Cytochem.* **1994**, *42*, 877-884.
- (13) Nasir, M. S.; Fahrni, C. J.; Suhy, D. A.; Kolodsick, K. J.; Singer, C. P.; O'Halloran, T. V. The chemical cell biology of zinc: structure and intracellular fluorescence of a zinc-quinolinesulfonamide complex. *J. Biol. Inorg. Chem.* **1999**, *4*, 775-783.
- (14) Woodroffe, C. C.; Lippard, S. J. A Novel Two-Fluorophore Approach to Ratiometric Sensing of Zn^{2+} . *J. Am. Chem. Soc.* **2003**, *125*, 11458-11459.
- (15) Hamamoto, H.; Mamedov, V. A.; Kitamoto, M.; Hayashi, N.; Tsuboi, S. Chemomenzymatic synthesis of the C-13 side chain of paclitaxel (Taxol) and docetaxel (Taxotere). *Tet. Asymm.* **2000**, *11*, 4485-4497.
- (16) Cevallos, A.; Rios, R.; Moyano, A.; Pericàs, M. A.; Riera, A. A convenient synthesis of chiral 2-alkynyl-1,3-oxazolines. *Tet. Asymm.* **2000**, *11*, 4407-4416.
- (17) Mandai, T.; Kuroda, A.; Okumoto, H.; Nakanishi, K.; Mikuni, K.; Hara, K.; Hara, K. A semisynthesis of paclitaxel via a 10-deacetylbaccatin III derivative bearing a β -keto ester appendage. *Tet. Lett.* **1999**, *41*, 243-246.
- (18) Packard, B. Z.; Toptygin, D. D.; Komoriya, A.; Brand, L. Characterization of fluorescence quenching in bifluorophoric protease substrates. *Biophys. Chem.* **1997**, *67*, 167-176.
- (19) Foerster, T. In *Modern Quantum Chemistry*; Sinanoglu, O., Ed., 1965.
- (20) Packard, B. Z.; Toptygin, D. D.; Komoriya, A.; Brand, L. Profluorescent protease substrates: Intramolecular dimers described by the exciton model. *Proc. Natl. Acad. Sci. USA* **1996**, *93*, 11640-11645.

Table 3.1. Photochemical properties of CZ dyes and their expected cleavage fragments

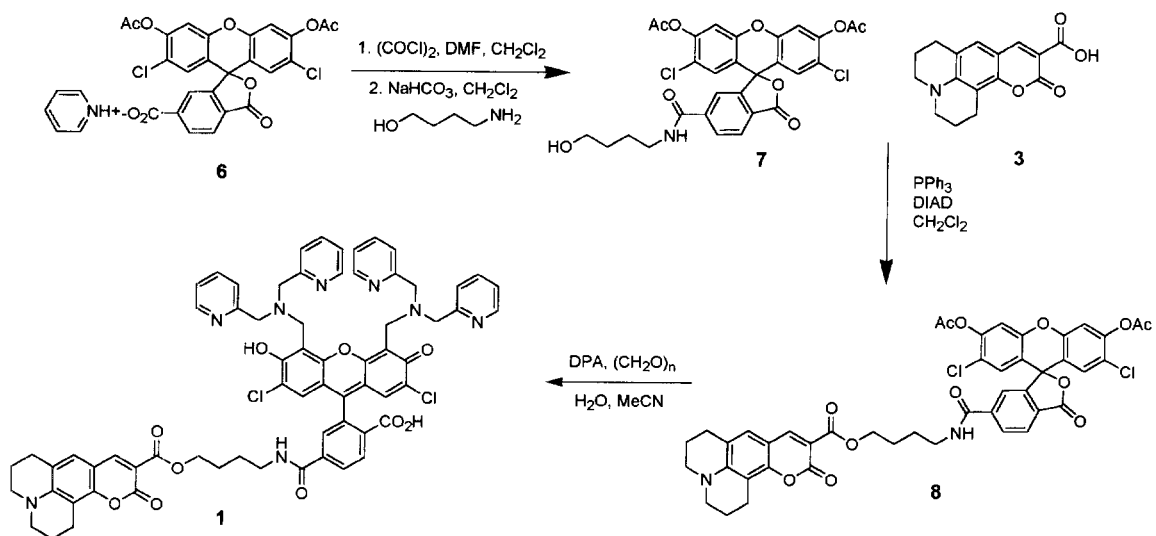
	ϵ ($M^{-1}cm^{-1}$)	λ_{max} (nm) Absorbance	Φ_{ZP1}	$\Phi_{Coumarin}$	K_d (nM)	pK_a
4	62000	519	0.22		0.25	-
4 + Zn	65000	509	0.69			
13	71100	518	0.21		0.20	8.43
13 + Zn	78600	508	0.67			
17	76000	516	0.21		0.16	7.12
17 + Zn	81000	506	0.63			
ZP1-6-CO ₂ Et	61000	519	0.13		0.37	7.00
	72000	509	0.67			
CZ1	37200	451,	0.02	0.01	0.25	
	38600	526				
	41000	449,	0.04	0.01		
	38100	518				
CZ2	26000	450,	0.02	0.01		
	22400	526				
	26567	448,	0.04	0.01		
	24333	521				

Table 3.2. Michaelis-Menten constants for CZ dyes

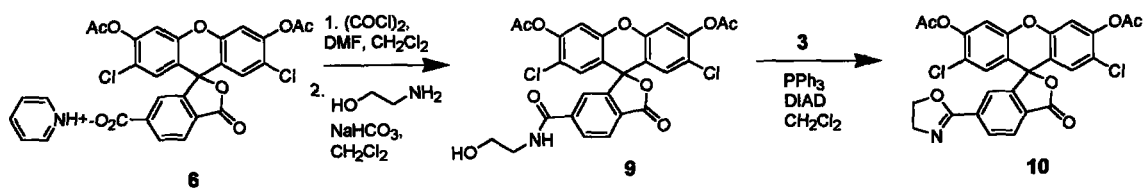
	k_{cat} (min^{-1})	k_{cat}/K_M ($\mu\text{M}^{-1}\text{min}^{-1}$)
CZ1	0.017	0.027
CZ2	0.211	0.128



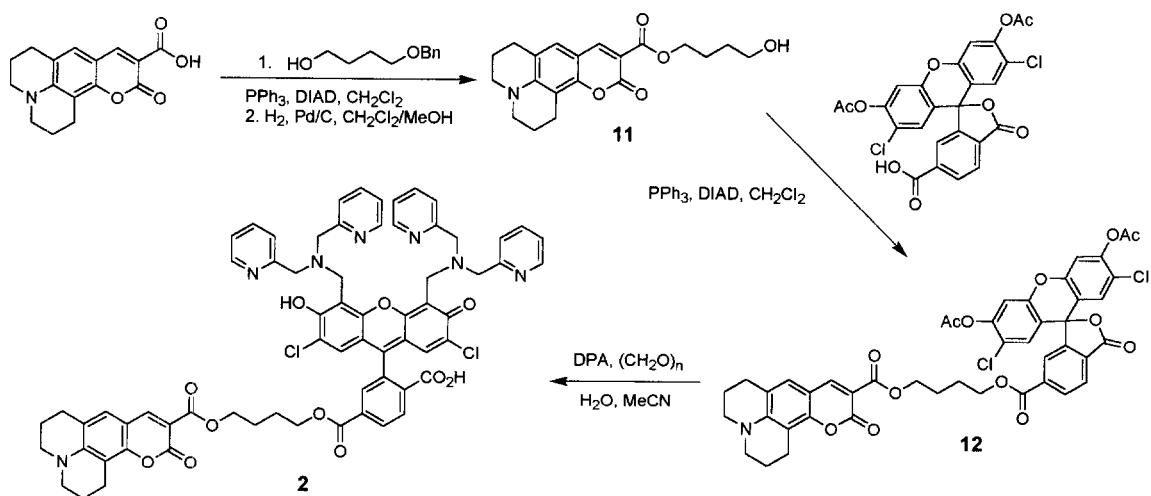
Scheme 3.1. Proposed mechanism of ratiometric Zn^{2+} sensing



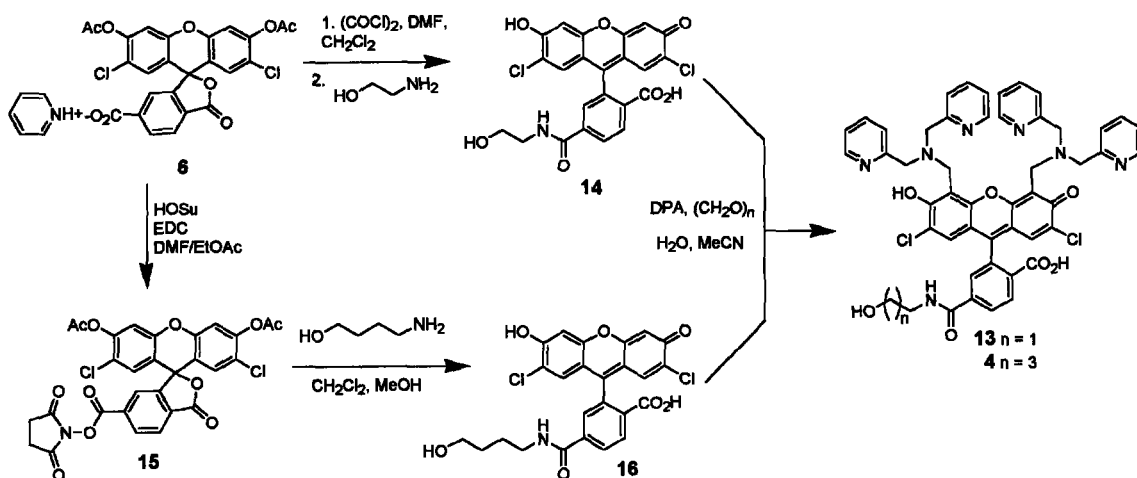
Scheme 3.2. Synthesis of CZI



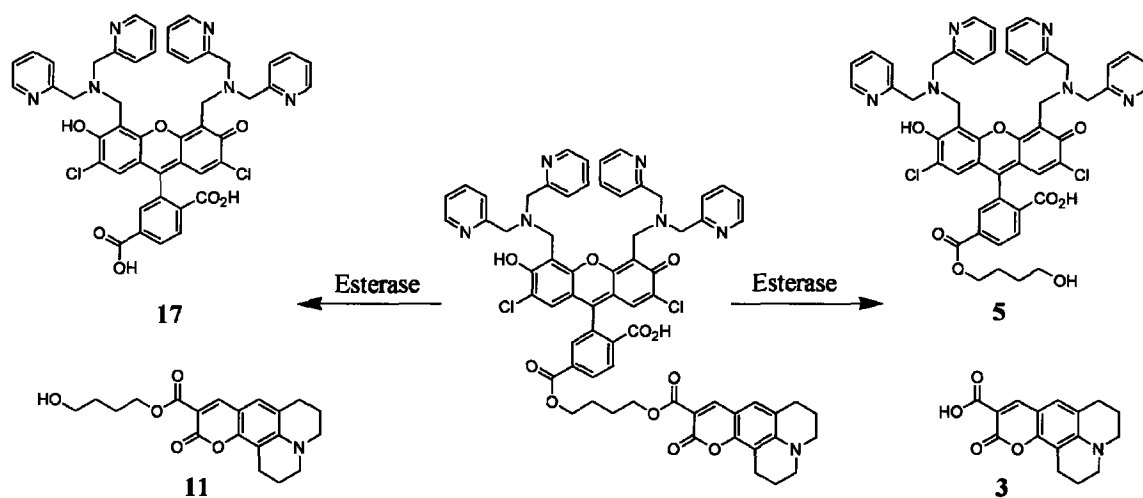
Scheme 3.3. Intramolecular cyclization under Mitsunobu conditions.



Scheme 3.4. Synthesis of CZ2



Scheme 3.5. Synthesis of putative ZP1 metabolites



Scheme 3.6. Possible esterase digestion products of CZ2.

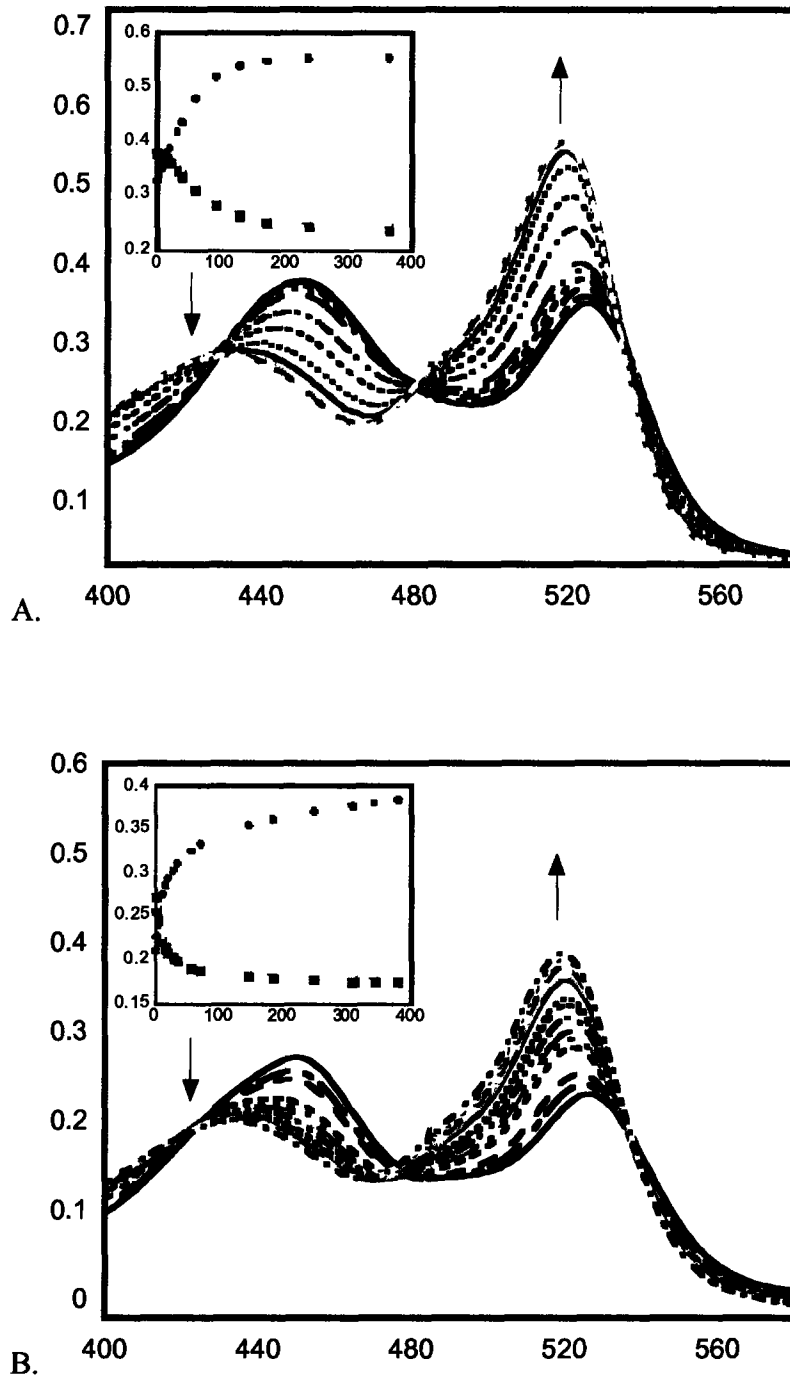


Figure 3.1. Time-dependent changes in absorption spectra for CZ1 over 6 h (A) and CZ2 over 3 h (B) on treatment with porcine liver esterase.

Insets: changes in absorption at 519 nm (red circles) and 450 nm (blue squares) as a function of time (min).

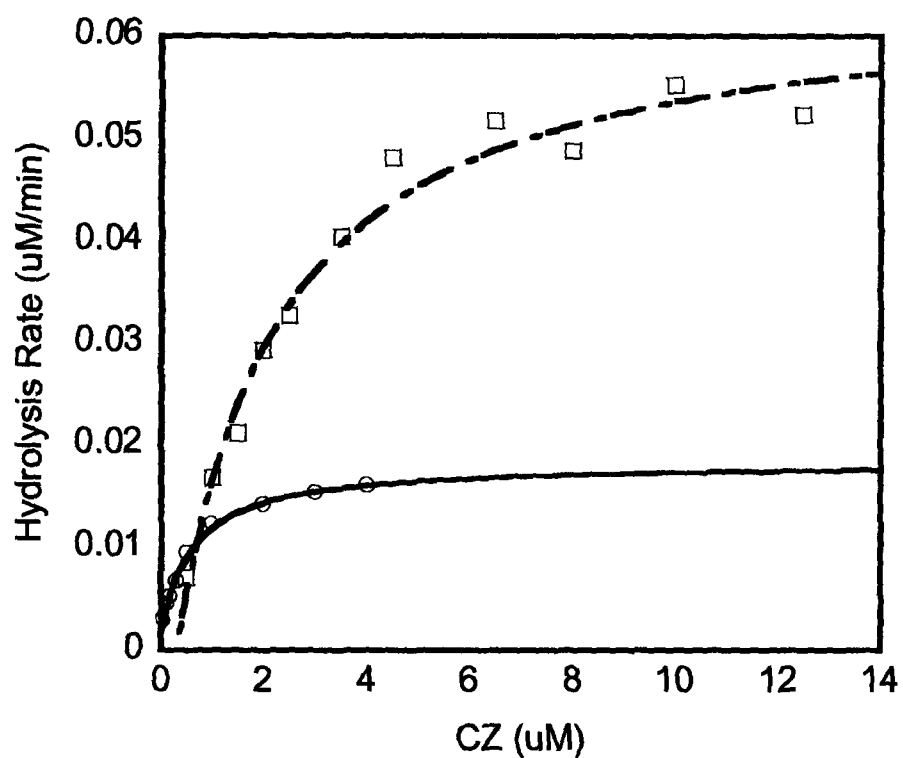


Figure 3.2. Michaelis-Menten fit of CZ esterase hydrolysis rate.

CZ1 (red circles) was treated with 75 nM PLE, and CZ2 (blue squares) was treated with 37.5 nM PLE; both at 25 °C in HEPES buffer (pH 7.5). Hydrolysis rate was assumed to be the rate of production of coumarin 343, which was determined using a standard curve.



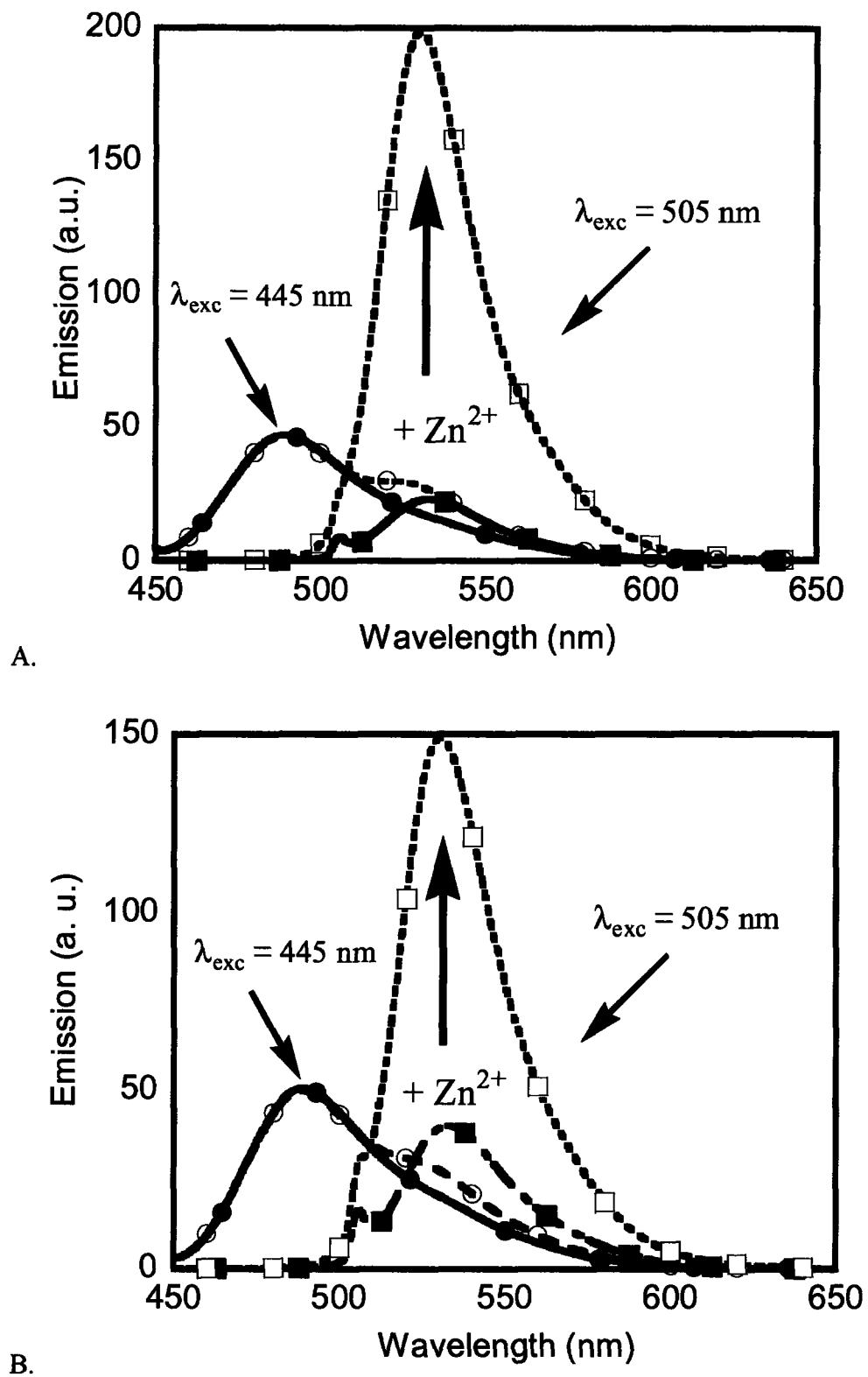
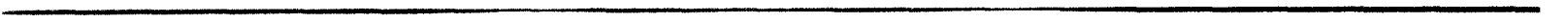


Figure 3.3. Fluorescence response of esterase-treated CZ1 (A) and CZ2 (B).



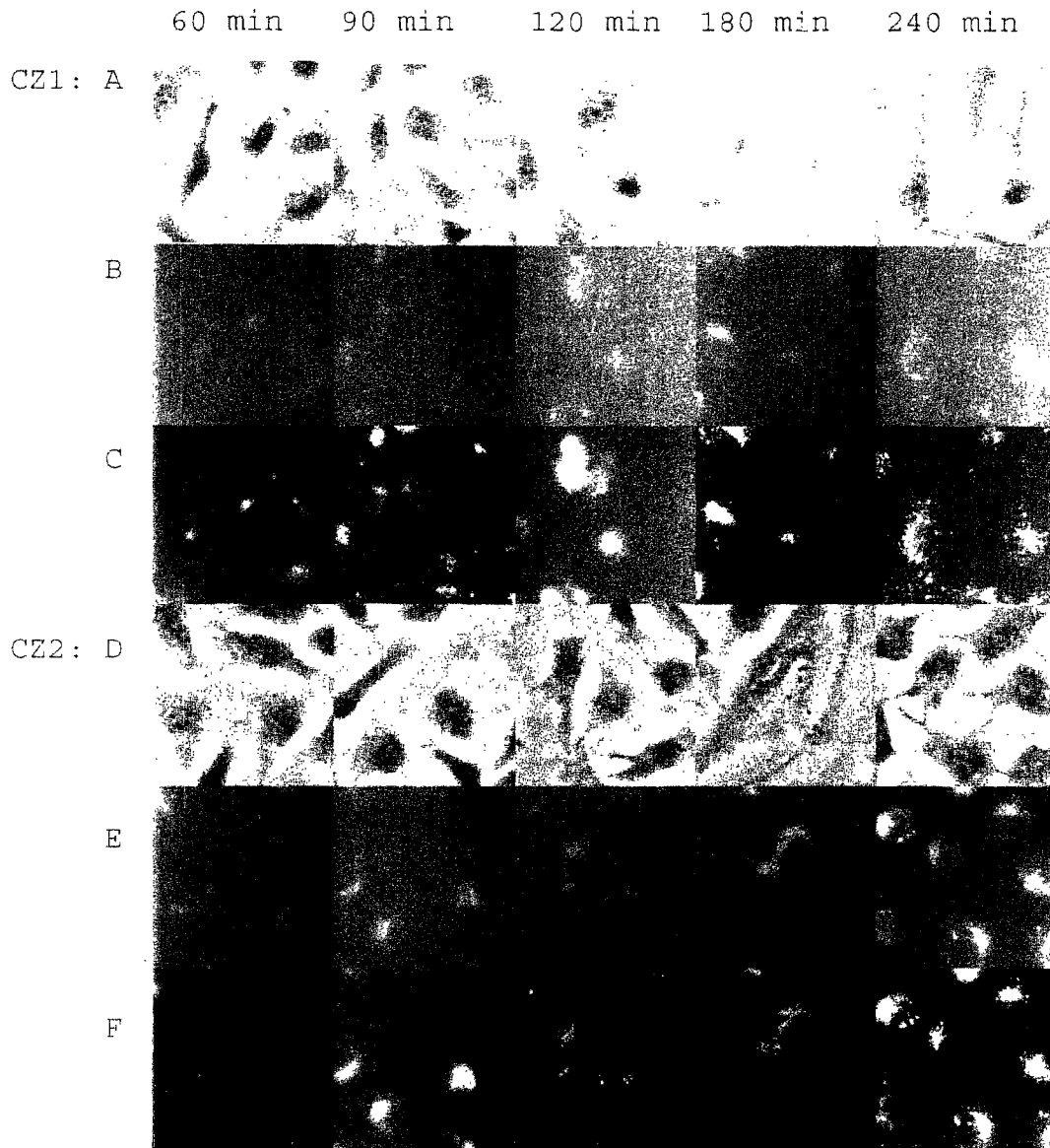


Figure 3.4. Time course of CZ staining in HCN-A94-02 cells.

A, B, C: phase contrast, coumarin fluorescence, and ZP fluorescence, respectively, of CZ1-stained cells; D, E, F: phase contrast, coumarin fluorescence, and ZP fluorescence of CZ2-stained cells.

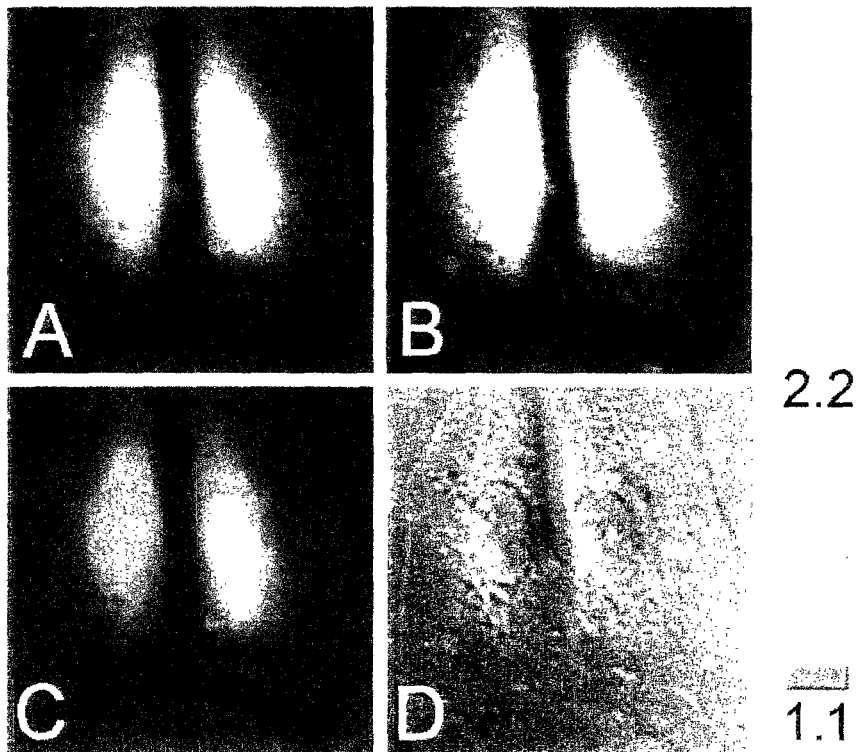


Figure 3.5. Fluorescence ratio images of HeLa cells treated with CZ2 after addition of ZnCl_2 and sodium pyrithione (A, 0 min; B, 8 min), and after subsequent treatment with TPEN (C, 8 min). D: DIC image.

Images were acquired at 40x magnification, and the faux-color ratio range was 1.1 (blue)-2.2 (red).

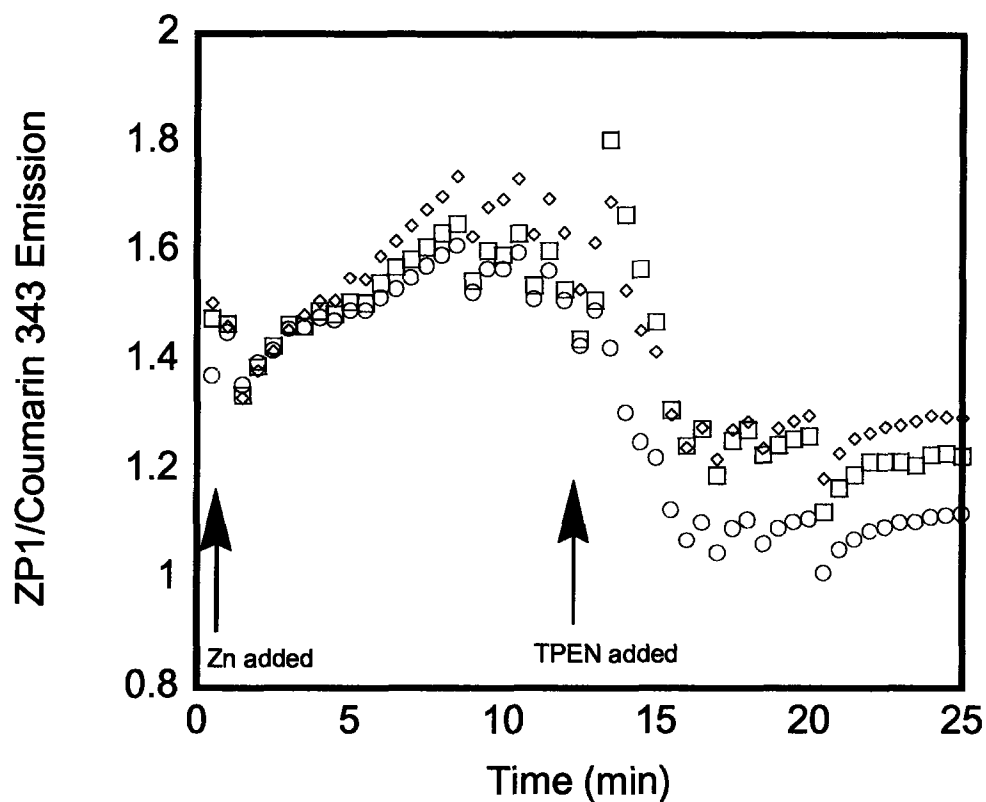


Figure 3.6. Intensity ratios of ZP1 emission divided by coumarin emission as a function of time.

Three separate regions of interest were defined at the start of the experiment and total integrated emission of ZP1 divided by integrated emission of coumarin 343 was measured at 30 sec intervals. ZnCl_2 ($5 \mu\text{M}$ final concentration) and sodium pyridithione ($45 \mu\text{M}$) were added at 5 min, and TPEN ($50 \mu\text{M}$) was added at 17 min.

Chapter 4 Bisfluorophore Approaches to Ratiometric ZP1 Sensors

Introduction

We have described the synthesis and application of esterase-activated two-fluorophore ratiometric Zn^{2+} sensors in the previous chapter.¹ These sensors afforded a ratiometric response to exogenously applied Zn^{2+} when incubated with HeLa cells; however, this system is complicated by the long incubation period, reliance on intracellular esterases, and the possibility that the two fluorophores could diffuse away from each other after hydrolysis. It would be preferable to design two-fluorophore ratiometric sensors that do not rely on intracellular activation. Flexible n-alkyl linkers between the fluorophores allow for intramolecular interaction that enables efficient quenching of both fluorescent moieties, as reported by our group and others.¹⁻³ Use of one or more rigid cyclohexyl groups or *para*-substituted phenyl rings as the linker between fluorescein and coumarin fluorophores decreases or prevents intramolecular quenching of such compounds.^{4,5} We therefore sought to produce ZP1-type sensors linked to calibrating fluorophores via a *trans*-1, 4-cyclohexanediamido moiety.

We report here the synthesis and photochemical properties of model dichlorofluorescein compounds linked to naphthofluorescein, X-rhodamine, and coumarin 343 by a cyclohexylamide moiety at the 6-position of the fluorescein. These three fluorophores are shown in Figure 4.1, and represent potential donor and acceptor fluorophores with regard to the fluorescein, with varying degrees spectral overlap. The data gleaned from these model compounds have been applied to the design and synthesis of a novel two-fluorophore ratiometric sensor for biological Zn^{2+} .

Experimental

Materials and Methods

Reagents were purchased from Aldrich and used without further purification except for coumarin 343, which was recrystallized from MeOH and CH₂Cl₂ before use. 5(6)-Carboxy-X-rhodamine succinimidyl esters and 5(6)-carboxynaphthofluorescein succinimidyl esters were purchased from Molecular Probes as mixed isomers and used as received. 3',6'-Diacetyl-2',7'-dichloro-5-carboxyfluorescein and the pyridinium salt of 3',6'-diacetyl-2',7'-dichloro-6-carboxyfluorescein were prepared as described in Chapter 2, and the succinimidyl ester of 3',6'-diacetyl-2',7'-dichloro-6-carboxyfluorescein was synthesized as described in Chapter 3. Acetonitrile and dichloromethane were obtained from a dry-still solvent dispensation system. ¹H and ¹³C NMR spectra were acquired on a Bruker 400 MHz or a Varian 500 MHz spectrometer. Fluorescence spectra were acquired on a Hitachi F-3010 fluorimeter and UV-visible absorption spectra on a Cary 1E UV-visible spectrophotometer. Absorbance and fluorescence data were analyzed by using Kaleidagraph 3.0 for Windows. LCMS analysis was performed on an Agilent Technologies 1100 Series LCMS with a Zorbax Extend C-18 column using a linear gradient of 100% A (95:5 H₂O:MeCN, 0.05% HCO₂H) to 100% B (95:5 MeCN:H₂O; 0.05% HCO₂H) over 30 min at a flow rate of 0.250 mL/min. Detector wavelengths were set at 240 nm and 500 nm, and the electrospray MS detector was set to positive ion mode scanning the range $m/z = 100-2000$. Low-resolution mass spectra were acquired on the same instrument. Preparative high-performance liquid chromatography (HPLC) was performed on a Waters 600 pump with a Waters 600E systems controller monitored by a Waters 486 tunable absorbance detector. A Higgins Analytical, Inc. reverse-phase C18

column measuring 250 mm x 20 mm was used for HPLC, with a flow rate of 10 mL/min. Solvents A and B were purified water (resistivity 18.2 ohms) obtained from a Millipore Milli-Q water purification system or low-water acetonitrile (Mallinckrodt), respectively, each containing 0.1 % v/v trifluoroacetic acid.

Synthetic Procedures

N-(4-Amino-cyclohexyl)-2-(2',7'-dichlorofluorescein) hydrochloride salt (1). 3', 6'-Diacetyl-2', 7'-dichlorofluorescein-6-carboxylate succinimidyl ester (0.92 g, 1.47 mmol) was dissolved in 40 mL of CH₂Cl₂ and added dropwise to a stirred solution of 1, 4-*trans*-cyclohexanediamine (4.56 g, 40 mmol) in 50 mL of 1:1 CH₂Cl₂:MeOH. After stirring overnight, the bright orange suspension was concentrated under reduced pressure, and the bright red residue was taken up in 40 mL of H₂O. Concentrated HCl was added until an orange precipitate formed. The precipitate was filtered, redissolved in saturated NaHCO₃ and precipitated once again by addition of HCl. The orange solid was dried under vacuum to afford 0.419 g of the desired product (52.8% yield). ¹H NMR (MeOH-d₄): δ 8.16 (d, 1 H); 8.14 (d, 1 H); 7.63 (s, 1 H); 6.86 (s, 2 H); 6.67 (s, 2 H); 3.85 (t, 1 H); 3.06 (t, 1 H); 2.06 (m, 4 H); 1.51 (m, 4 H). HRMS(M+H): Calcd for C₂₇H₂₃Cl₂N₂O₆: 541.0933; Found 541.0900.

***trans*-(4-Amino-cyclohexyl)-carbamic acid benzyl ester (2).** *trans*-1,4-Cyclohexanediamine (5.71 g, 50 mmol) was dissolved in 10 mL of H₂O and 14 mL of ethanol, and 1 mg of bromocresol green indicator was added. A 50% w/v solution of methanesulfonic acid in H₂O was added in a dropwise manner until the blue color of the solution disappeared. Benzyl chloroformate (7.8 g, 45.7 mmol) was dissolved in 10 mL of dimethoxyethane and added in a dropwise fashion to the stirred solution. A 50% w/v

aqueous solution of potassium acetate was added concomitantly to maintain a slight green tinge in the reaction. Stirring was continued for 1 h at RT after the addition was completed. The volatile solvents were then removed and the residue was suspended in 100 mL of H₂O, shaken, and filtered to remove solid precipitate. The filtrate was washed with 3 x 40 mL portions of Et₂O and the aqueous layer was then basified with excess 40% w/v NaOH and extracted with 3 x 40 mL Et₂O. The combined organic layers were washed with brine, dried over MgSO₄, and evaporated to afford 2.56 g (22.5% yield) of a white waxy solid after drying. ¹H NMR (CDCl₃): δ 7.36 (m, 5 H); 5.09 (s, 2 H); 4.57 (br d, 1 H); 3.48 (br s, 1 H); 2.67 (m, 1 H); 2.02 (m, 4 H); 1.87 (m, 2 H); 1.20 (m, 4 H).

3',6'-Diacetyl-2',7'-Dichlorofluorescein-6-Carboxamido-N-Carboxybenzyl-*trans*-1, 4-Cyclohexanediamine (3). 3',6'-Diacetyl-2',7'-dichlorofluorescein-6-carboxylate pyridinium salt (457 mg, 0.75 mmol) was combined with EDC (160 mg, 0.83 mmol) in dry CH₂Cl₂ and stirred at RT for 20 min. N-Carboxybenzyl-*trans*-1, 4-cyclohexane-diamine (186 mg, 0.75 mmol) was dissolved in CH₂Cl₂ and added dropwise via pipet. The reaction was stirred overnight, then washed with 2 x 50 mL portions of 0.1 N HCl. The organic layer was washed with 50 mL of brine, dried over MgSO₄ and concentrated under reduced pressure. Purification on a silica gel column eluting with 96.5:3.5 CHCl₃:MeOH afforded 232 mg of the desired product (40.7%). ¹H NMR (CDCl₃): δ 8.10 (m, 2 H); 7.47 (s, 1 H); 7.36 (m, 6 H); 7.14 (s, 2 H); 6.83 (s, 2 H); 6.38 (d, 1 H); 5.06 (s, 2 H); 4.73 (d, 1 H); 3.84 (m, 1 H); 3.46 (m, 1 H); 2.38 (s, 6 H); 2.03 (m, 4 H); 1.21-1.39 (m, 4 H). ¹³C NMR (CDCl₃): δ 169.2, 168.6, 165.7, 156.7, 153.2, 150.6, 149.7, 142.8, 137.6, 131.3, 130.1, 129.6, 129.23, 129.19, 128.9, 128.7, 128.1, 127.1, 124.0, 123.2, 118.0, 114.0, 81.6, 67.7, 66.4, 54.5, 50.4, 49.9, 32.9, 32.4, 21.7.

ZP1(6-CONH-Cy-NHCbz) (4). Paraformaldehyde (54 mg, 3.8 mmol) and dipicolylamine (384 mg, 1.92 mmol) were combined in dry acetonitrile and heated to reflux for 30 min. 3',6'-Diacetyl-2',7'-dichlorofluorescein-6-carboxy amido-N-carboxybenzyl-*trans*-1,4-cyclohexanediamine (232 mg, 0.3 mmol) was dissolved in 1 mL of CHCl₃, diluted with 8 mL of MeCN, and added along with 10 mL of H₂O. The reaction was heated at reflux for 24 h, removed from heat, and concentrated under reduced pressure to afford a dark red residue. Addition of MeCN afforded a pink precipitate, which was filtered to give 172 mg (52.2%) of a pink powder after washing with MeCN. ¹H NMR (MeOH-d₄): δ 8.53 (m, 4 H); 8.42 (d, 1 H); 8.10 (m, 2 H); 7.74 (m, 4 H); 7.62 (s, 1 H); 7.42 (d, 4 H); 7.25-7.31 (m, 9 H); 6.70 (d, 1 H); 6.59 (s, 2 H); 5.03 (s, 2 H); 4.27 (s, 4 H); 4.07 (m, 8 H); 3.79 (br s, 1 H); 3.35 (br s, 1 H); 1.97 (m, 4 H); 1.24-1.40 (m, 4 H). MS(M+H): Calcd for C₆₁H₅₅Cl₂N₈O₈: 1097.4; Found 1097.4.

ZP1(6-CONH-Cy-NH₂) (5). A portion of 4 (11 mg, 10 μmol) was stirred with ZnCl₂ (41 mg, 0.30 mmol) in MeOH under N₂ for 20 min. A portion of Pd black (50 mg) was added, and the reaction was then stirred under a hydrogen atmosphere for 10 min and then filtered through Celite. The resulting solution was stirred vigorously with 0.5 g of Chelex (50-100 mesh) for 2 h at RT. The Celite was removed by filtration to afford a pale pink solution. LCMS analysis showed a peak eluting at 8.7 min and another at 11.3 min, both with a mass corresponding to the desired product. MS(M+H): Calcd for C₅₃H₄₉Cl₂N₈O₆: 963.3; Found 963.4. ¹H NMR analysis demonstrated the absence of a peak at 5.2 ppm, confirming the loss of the benzyl protecting group.

2',7'-Dichlorofluorescein-6-carboxamidocyclohexane-4-amido-5-carboxynaphthofluorescein (7). 2',7'-Dichlorofluorescein-6-carboxamido(4-amino)cyclohexane (1, 11.8

mg, 20.4 μmol) was combined with 5(6)-carboxynaphthofluorescein succinimidyl ester (11.4 mg, 20 μmol) and triethylamine (10 μL) in 2 mL of DMF and stirred for 6 h at RT over activated molecular sieves. The reaction was concentrated under reduced pressure at 70 °C and lyophilized. The residue was purified by preparative HPLC to afford 8.4 mg of the desired product (42% overall yield). ^1H NMR (MeOH- d_4): δ 8.68 (m, 3 H); 8.62 (d, 1 H); 8.51 (s, 1 H); 8.17 (m, 3 H); 7.65 (s, 1 H); 7.40 (d, 2 H); 7.35 (dd, 2 H); 7.28 (d, 1 H); 7.17 (s, 2 H); 6.86 (s, 2 H); 6.73 (d, 2 H); 6.68 (s, 2 H), 3.91 (br m, 2 H); 1.99 (br m, 4 H); 1.53 (m, 4 H). HRMS(M+H): Calcd for $\text{C}_{56}\text{H}_{37}\text{Cl}_2\text{N}_2\text{O}_{12}$: 999.1723; Found 999.1732

2', 7'-Dichlorofluorescein-6-carboxamidocyclohexane-4-amido-5-carboxy-X-rhodamine (8). Compound 1 (23.2 mg, 40.2 μmol) and 5(6)-carboxy-X-rhodamine succinimidyl ester (23.1 mg, 36.6 μmol) were combined with triethylamine (10 μL) and activated molecular sieves in 2 mL of DMF. The reaction was stirred for 21 h, then lyophilized. The residue was purified by preparative HPLC (70:30 A:B \rightarrow 0:100 A:B over 25 min, retention time 21.5 min) to afford 13.4 mg of the desired product (34%). ^1H NMR (MeOH- d_4): δ 8.67 (m, 2 H), 8.63 (d, 1 H); 8.18 (m, 3 H); 7.65 (s, 1 H); 7.43 (d, 1 H); 6.86 (s, 2 H); 6.68 (s, 2 H); 6.61 (s, 2 H); 3.95 (br s, 2 H); 3.48-3.56 (m, 8 H); 3.11 (m, 4 H); 2.67 (m, 4 H); 2.09 (m, 8 H); 2.03 (m, 4 H); 1.55 (m, 4 H). HRMS(M+H): Calcd for $\text{C}_{60}\text{H}_{51}\text{Cl}_2\text{N}_4\text{O}_{10}$: 1057.2982; Found 1057.2977

Coumarin 343 Succinimidyl Ester (10). Coumarin 343 (285 mg, 1 mmol) was combined with EDC (380 mg, 2 mmol) and N-hydroxysuccinimide (200 mg, 1.74 mmol) in 2 mL of DMF and 10 mL of CH_2Cl_2 . The reaction was stirred for 6 h, at which time the orange solution had become a yellow suspension. The reaction was diluted with 140 mL of CH_2Cl_2 and washed with 2 x 100 mL of H_2O and 1 x 100 mL brine, dried over

MgSO₄, and concentrated under reduced pressure. The resulting orange sludgy residue was taken up in Et₂O, allowed to stand overnight, and filtered to afford 353 mg of orange crystals (92% yield). ¹H NMR (CDCl₃): δ 8.55 (s, 1 H); 6.95 (s, 1 H); 3.39 (m, 4 H); 2.86 (m, 6 H); 2.77 (t, 2 H); 1.99 (m, 4 H). m.p. dec > 204 °C. MS(M+Na): Calcd for C₂₀H₁₈N₂O₆Na: 405.1; Found 405.1.

2',7'-Dichlorofluorescein-6-carboxamidocyclohexane-4-amido-(3-coumarin 343) (9).

Coumarin 343 succinimidyl ester (**10**, 45.8 mg, 0.12 mmol) was combined with 2',7'-dichlorofluorescein-6-carboxamido(4-amino)cyclohexane hydrochloride salt (**1**, 57.7 mg, 0.1 mmol) and Na₂CO₃ (21.2 mg, 0.2 mmol) in 2 mL of DMF and stirred overnight. Diethyl ether was added, and the resulting precipitate was collected by filtration, suspended in 20 mL of H₂O, filtered, and precipitated again by addition of conc HCl. Filtration and drying afforded 46.5 mg of a dark brown solid (57.6 %). A portion was recrystallized from CHCl₃ and trace MeOH prior to use in spectroscopic studies. ¹H NMR(MeOH-d₄): δ 8.58 (d, > 1 H); 8.50 (s, 1 H); 8.11-8.17 (m, 2 H); 7.62 (s, 1 H); 7.11 (s, 1 H); 6.84 (s, 2 H); 6.66 (s, 2 H); 3.88 (br s, 1 H); 3.81 (br m, 1 H); 3.33 (m, 4 H); 2.84 (t, 2 H); 2.77 (t, 2 H); 1.95-2.08 (m, 8 H); 1.46 (m, 4 H). MS: Calcd for C₄₃H₃₆Cl₂N₃O₉: 808.2; Found 808.2.

ZP1-6-carboxamidocyclohexane-4-amido-(3-coumarin 343) (11). Dipicolylamine (29 mg, 0.15 mmol) was combined with paraformaldehyde (8.7 mg, 0.29 mmol) in 5 mL of MeCN and heated to reflux for 30 min. 2', 7'-Dichlorofluorescein-6-carboxamidocyclohexane-4-amido-(3-coumarin 343) (**9**, 46 mg, 0.057 mmol) was suspended in 10 mL of 1:1 MeCN:H₂O and added, and the reaction was heated at reflux for 14 h. The solvents were removed under reduced pressure, and the resulting pink solid was suspended in

MeCN and filtered to afford 72 mg (103% crude yield) of 11. A portion of the crude material was purified for spectroscopic studies by preparative HPLC using a gradient of 30% B → 100% B over 25 min. Lyophilization afforded an orange solid. ^1H NMR(MeOH- d_4): δ 8.62 (m, 5 H); 8.52 (s, 1 H); 8.29 (d, 1 H); 8.18 (d, 1 H); 7.95 (td, 4 H); 7.62 (s, 1 H); 7.52 (d, 4 H); 7.46 (dd, 4 H); 7.14 (s, 1 H); 6.72 (s, 2 H); 4.48–4.59 (m, 12 H); 3.95 (br s, 1 H); 3.84 (br m, 1 H); 3.39 (m, 4 H); 2.85 (t, 2 H); 2.77 (t, 2 H); 2.09 (m, 4 H); 1.96 (m, 4 H); 1.45–1.53 (m, 4 H). HRMS(M+H): Calcd for $\text{C}_{69}\text{H}_{62}\text{Cl}_2\text{N}_9\text{O}_9$: 1230.4048; Found 1230.4065.

Spectroscopic Measurements

Protocols were as described in Chapter 2, with the following exceptions. Fluorescence and absorption data were acquired in HEPES buffer (50 mM, pH 7.5, KCl 100 mM) unless otherwise noted. Experiments done at pH 10 were performed in CABS buffer (50 mM, pH 10.0, KCl 100 mM). Fluorescein standard solutions were made up to a concentration of 1 μM in 0.1 N NaOH ($\Phi_{\text{std}} = 0.95$)⁶ and rhodamine 6G standard solutions were 1 μM in ethanol ($\Phi_{\text{std}} = 0.94$)⁷ for quantum yield determinations. Extinction coefficients and quantum yields were measured as described in Chapter 2. Spectral overlap integrals were calculated by normalizing the emission spectrum of the donor fluorophore and the absorbance spectrum of the acceptor fluorophore such that the total integration for each was 1. The area of overlap was then integrated. All measurements were performed in triplicate.

Results and Discussion

Experimental Design

In a system containing a ZP1 moiety bound via a rigid linker to a second fluorophore, at least two photophysical processes must be considered. They are the photoinduced electron transfer (PET) upon which the ZP1 turn-on response to Zn^{2+} depends, and potential fluorescence resonance energy transfer between the two fluorophores (FRET). Based on distance, it is likely that PET quenching of free ZP1 by benzylic amines, separated from the ZP1 xanthene system by less than 2 Å, would compete effectively with energy transfer from or to a second fluorophore separated from the xanthene system by 10 Å or more. The PET process is governed by Marcus theory,⁸⁻¹⁰

$$k(r) = k_0 e^{-\beta(r-r_0)} e^{[-(\Delta G + \lambda)^2 / 4\lambda RT]} \quad (1)$$

and the primary distance dependence¹¹ of the rate constant for electron transfer is defined by eq. 1, where r is the separation between donor and acceptor, r_0 is the close contact distance, usually set at 3.0 Å, and β is on the order of 0.3-2.0 Å⁻¹ and is typically low (< 1.0 Å⁻¹) for photoexcited systems. R is the gas constant, T is temperature, ΔG is the driving force, k_0 is the characteristic oscillatory frequency of the nuclei about their equilibrium positions, generally taken to be 10¹³ s⁻¹ and λ is the reorganizational energy. The Förster resonance energy transfer rate constant is inversely proportional to the sixth power of the distance between fluorophores. Important factors in determining the rate of energy transfer are shown in eq. 2¹² and include the quantum yield of the donor Φ_D , the

$$k_{FRET} \propto \frac{\Phi_D K^2}{\tau_D r^6} J \quad (2)$$

fluorescence lifetime of the donor τ_D , a factor describing the relative orientations of the two transition state dipoles κ^2 , and the spectral overlap integral J , which describes the overlap between donor emission and acceptor absorbance. The quantity R_0 , referred to as

$$R_0 = \left(8.785 \times 10^{-5} \frac{\kappa^2 \Phi_D J}{\eta^4} \right)^{\left(\frac{1}{6}\right)} \quad (3)$$

the Förster radius, is defined as the distance between fluorophores that affords half-maximal efficiency of energy transfer¹³ and can be calculated according to the expression in eq 3, where η is the refractive index, generally taken to be 1.4 in aqueous solution.

It was expected that a system in which the excitation energy of the calibrating fluorophore was lower than the ZP1 fluorescein moiety would be most advantageous for several reasons. In addition to greater biocompatibility, lower-energy fluorophores could act as acceptors in a fluorescence resonance energy transfer (FRET) pairing. In contrast, a system in which the calibrating fluorophore excitation energy was higher than that of the ZP1 fluorophore might transfer all of its energy to the latter, resulting in a simple blueshift of sensor excitation with no change in emission shape upon binding Zn^{2+} . Schematics of expected fluorophore behavior are diagrammed in Figure 4.2.

Acceptor fluorophores with varying degrees of spectral overlap J were chosen for evaluation. Naphthofluorescein has little to no spectral overlap with dichlorofluorescein, whereas X-rhodamine has moderate spectral overlap. A coumarin 343-dichlorofluorescein fluorophore pair has excellent spectral overlap, although in this case the coumarin is the donor fluorophore and the fluorescein the acceptor. Measured values of J for **1** with X-rhodamine and coumarin 343, and literature values for fluorophore photophysical characteristics, are listed in Table 4.1.

Synthesis

Several routes toward the synthesis of ZP1-reporter fluorophore structures were explored. The initial synthetic approach was the synthesis of a ZP1 analogue containing a pendant aminocyclohexane, which could then be subjected to reaction with commercially available N-hydroxysuccinimidyl esters of various fluorophores. Mannich reaction of an unprotected fluorescein-cyclohexylamine precursor **1** with paraformaldehyde and dipicolylamine produced an insoluble red precipitate, possibly owing to a competing reaction of the primary amine. The Zinpyr family is incompatible with acid-labile protecting groups, because the Mannich reaction used to prepare ZP1-type sensors is reversible in strong acid.¹⁴ Accordingly, a Cbz-monoprotected cyclohexyl-amine **2** was prepared¹⁵ and coupled with diacetyldichlorofluorescein. The product **3** was subjected to Mannich reaction conditions, affording the Cbz-protected ZP1 cyclohexylamine **4**. Hydrogenolytic removal of the Cbz group proved to be unexpectedly difficult; several palladium catalysts were screened and only palladium black was effective. Concomitant hydrogenolysis of the N-picolyl groups was problematic. Metallation of **4** with ZnCl₂ prior to hydrogenolysis, short reaction times (< 15 min), and subsequent treatment with Chelex resin afforded primarily the desired product **5**, as analyzed by LCMS, in very low yield. Reaction of the obtained residue with 5(6)-carboxynaphthofluorescein succinimidyl ester gave a mixture of products in which the proportion of linked fluorescein-naphthofluorescein was relatively small. As a result of these difficulties, the synthetic approach was reevaluated, and the fluorescein cyclohexylamine **6** was coupled with the succinimidyl esters of 5(6)-carboxynaphthofluorescein and 5(6)-carboxyl-X-rhodamine to afford potential synthons **7** and **8** (Figure 4.3) for subsequent Mannich reactions. The

coupled two-fluorophore products were purified by preparative HPLC. ^1H NMR analysis indicated that, although the succinimidyl esters of both X-rhodamine and naphthofluorescein were obtained as a mixture of isomers, isomerically pure products were isolated, possibly owing to steric effects. The obtained isomer **7** was assigned as the 5-carboxynaphthofluorescein adduct based on the presence of a doublet at 7.3 ppm and a singlet at 8.5 ppm, integrating to 1 H each. Integration patterns in the ^1H NMR spectrum of **8** were also consistent with a single isomer, and a similar doublet at 7.4 ppm and apparent singlet at 8.7 ppm supported the same assignment of substitution pattern for **8**. A second doublet at or above 8.5 ppm is consistent with the third aromatic proton of a 5-carboxy bottom ring or with a cyclohexylamide proton. The spectra of **7** and **8** are complicated by overlapping signals; however, both appear to have two doublets in the region from 8.6-8.7 ppm. Proton NMR spectra of **1**, **7**, and **8** are shown in Figure 4.4. The proton NMR spectrum of a 5-carboxy-2',7'-dichlorofluorescein species, reported in Chapter 1, is included for comparison.

In order to examine further the nature of the fluorescein-cyclohexyl-fluorophore system, an analogous compound **9** containing a 7-amino coumarin in place of the long-wavelength fluorophores was prepared by a route similar to that for **7** and **8** (Scheme 4.2). Coumarin 343 succinimidyl ester **10** was synthesized using EDC to couple the parent acid with N-hydroxysuccinimide, and subsequent reaction with **1** afforded the parent bis-fluorophore **9**. Based on its favorable photophysical characteristics, **9** was subjected to Mannich reaction conditions with dipicolylamine and paraformaldehyde, and the ZP1 analogue **11** was isolated by preparative HPLC and characterized.

Photophysical Characterization of the Two-Fluorophore Compounds

Evaluation of the photophysical properties of the resulting bisfluorophoric compounds revealed that **7** and **8** displayed very low fluorescence quantum yields (Table 4.2), making them impractical for fluorescent sensing applications. Compound **8** proved to be noticeably fluorescent in methanolic solution, evincing both fluorescein and rhodamine fluorescence bands. Although the quantum yield of rhodamines is much higher in alcoholic solution than in aqueous buffer,¹⁶ the manifestation of this effect is evident in the relative decrease of the rhodamine emission of **8** in methanol, as compared to the fluorescein emission. The overall decrease in fluorescence quantum yield probably arises from different conformational distances between fluorophores and/or alteration of electronic interactions in different solvent environments. Emission spectra of **8** in methanolic solution or aqueous buffer are shown in Figure 4.5. Fluorescein-rhodamine dyes linked via a 4-aminobenzoic acid moiety have been reported and used as energy-transfer dyes; however, fluorescence measurements were performed in mixed acetonitrile-buffer solutions, or in aqueous solutions containing 8 M urea as a denaturant.¹⁷ The naphthofluorescein-fluorescein linked compound **7** was also examined in methanol. No naphthofluorescein absorption band was observed, and the compound was non-fluorescent. These model compounds suggest that the analogous ZP1-linked rhodamine or naphthofluorescein compounds are poor candidates for ratiometric sensing.

Examination of the photophysical properties of **9** indicated that the fluorescein moiety retained its fluorescence, with a quantum yield of 0.70 when excited in the fluorescein absorption region. Excitation of the coumarin at 445 nm afforded primarily fluorescein emission as assessed by emission wavelength and shape, but a slight shoulder

below 500 nm arises from coumarin emission. This result suggested that a system based on **9** might be applicable to ratiometric measurements, given a suitable Zn^{2+} response by the fluorescein moiety.

Literature values of the Förster radius for fluorescein-rhodamine pairs are generally between 45-55 Å, and values observed for 7-aminocoumarin-fluorescein pairs are in the same range.¹⁸ Although the distance between fluorophores in these systems is expected to be significantly less than 55 Å, it is unclear why such disparity is observed between the fluorescein-rhodamine and fluorescein-coumarin fluorophore pairs. Formally, an additional aromatic ring is present in the moiety linking the two xanthene systems of **8** compared to the system linking the xanthene moiety to the coumarin in **9** and **11**. Similar extensions in coumarin-fluorophore energy transfer pairs have been reported to increase significantly the efficiency of energy transfer. Preliminary AM1 calculations estimate the minimum separation between fluorophores in **8** to be approximately 17 Å, as compared to approximately 14 Å for **9** (Figure 4.6). The Dexter mechanism of energy transfer is operative at distances closer than those effective for

$$k(r) = KJe^{\left(\frac{-2r}{L}\right)} \quad (4)$$

FRET; however, Dexter energy transfer mechanisms¹⁹ display exponential distance dependences and generally require fluorophore separation of 10 Å or less. The distance dependence of Dexter energy transfer rate is shown in eq. 4, where K is an empirically determined constant, L represents the van der Waals radii, and r and J are as previously defined. Photoinduced electron transfer from extended π systems bound directly to the xanthene system has been reported to quench fluorescein fluorescence,^{10,20} and a similar mechanism may obtain here. In contrast to Dexter theory, the exponential nature of

Marcus electron transfer distance dependence is mitigated somewhat by r_0 and β , and the process may occur at distances greater than 10 Å. The propensity for electron transfer is also controlled by the driving force ΔG and the reorganizational term λ , both terms that vary according to solvent and donor-acceptor properties, and that may account for the differences in photophysical behavior.

Two-Fluorophore-Based Ratiometric Zn²⁺ Sensing

Examination of the photophysical properties of **11** indicates that both the extinction coefficients and quantum yields are significantly lower than the parent coupled fluorophore **9**. The fluorescence spectrum is dominated by fluorescein emission; however, as in the model compound, a low-intensity shoulder below 500 nm is consistent with coumarin emission. Addition of excess ZnCl₂ to the solution causes a 90% increase in ZP1 fluorescence, whereas the coumarin emission decreases by about 5%. The decrease in coumarin emission prompted an examination of the dependence of spectral overlap J for coumarin 343 with a 6-carboxamido ZP1 species in the presence or absence of Zn²⁺. A slight blueshift in ZP1 absorbance upon binding Zn²⁺ occurs for all members of the ZP1 family, and accordingly the spectral overlap integral for coumarin 343 emission with ZPA3 is 0.72 ± 0.01 , increasing to 0.76 ± 0.006 upon addition of excess ZnCl₂ (Figure 4.8). The metal ion selectivity of ZP1-based sensors, including one ZP1-coumarin sensing system, has been reported extensively elsewhere^{1,21-23} and does not differ noticeably between sensors. Similarly, all ZP1-based sensors bind Zn²⁺ with dissociation constants between 0.2 and 1.1 nM. The corresponding properties of **11** are expected to be similar to these previously reported sensors, and were therefore not investigated.

Conclusions

We have prepared dichlorofluorescein derivatives that are attached to orthogonally excited fluorophores via a rigid cyclohexane linker. Compounds in which the fluorophore is naphthofluorescein or X-rhodamine evince greatly diminished fluorescence, suggesting that a larger separation between fluorophores is necessary in order to implement these long-wavelength reporter fluorophores. Appending coumarin 343 enables near-quantitative energy transfer to the dichlorofluorescein, with a slight shoulder below 500 nm that is consistent with coumarin emission. Based on these results, we have synthesized a ZP1 sensor linked via a rigid cyclohexylamide moiety to coumarin 343 that enables ratiometric sensing of Zn^{2+} with a dynamic range of 0.9.

Acknowledgement

This work was supported by the NIGMS (GM65519 to S.J.L.)

References

- (1) Woodroffe, C. C.; Lippard, S. J. A Novel Two-Fluorophore Approach to Ratiometric Sensing of Zn^{2+} . *J. Am. Chem. Soc.* **2003**, *125*, 11458-11459.
- (2) Packard, B. Z.; Toptygin, D. D.; Komoriya, A.; Brand, L. Profluorescent protease substrates: Intramolecular dimers described by the exciton model. *Proc. Natl. Acad. Sci. USA* **1996**, *93*, 11640-11645.
- (3) Kawanishi, Y.; Kikuchi, K.; Takakusa, H.; Mizukami, S.; Urano, Y.; Higuchi, T.; Nagano, T. Design and Synthesis of Intramolecular Resonance-Energy Transfer Probes for Use in Ratiometric Measurements in Aqueous Solution. *Angew. Chem. Int. Ed.* **2000**, *39*, 3438-3440.

- (4) Takakusa, H.; Kikuchi, K.; Urano, Y.; Kojima, H.; Nagano, T. A Novel Design Method of Ratiometric Fluorescent Probes Based on Fluorescence Resonance Energy Transfer Switching by Spectral Overlap Integral. *Chem. Eur. J.* **2003**, *9*, 1479-1485.
 - (5) Takakusa, H.; Kikuchi, K.; Urano, Y.; Sakamoto, S.; Yamaguchi, K.; Nagano, T. Design and Synthesis of an Enzyme-Cleavable Sensor Molecule for Phosphodiesterase Activity Based on Fluorescence Resonance Energy Transfer. *J. Am. Chem. Soc.* **2002**, *124*, 1653-1657.
 - (6) Brannon, J. H.; Magde, D. Absolute Quantum Yield Determination by Thermal Blooming. Fluorescein. *J. Phys. Chem.* **1978**, *82*, 705-709.
 - (7) Kubin, R. F.; Fletcher, A. N. Fluorescence Quantum Yields of Some Rhodamine Dyes. *J. Luminescence* **1982**, *27*, 455-462.
 - (8) Marcus, R. A. Electron Transfer Reactions in Chemistry: Theory and Experiment (Nobel Lecture). *Angew. Chem. Int. Ed.* **1993**, *32*, 1111-1121.
 - (9) Marcus, R. A. Chemical and Electrochemical Electron-Transfer Theory. *Annu. Rev. Phys. Chem.* **1964**, *15*, 155-196.
 - (10) Miura, T.; Urano, Y.; Tanaka, K.; Nagano, T.; Ohkubo, K.; Fukuzumi, S. Rational Design Principle for Modulating Fluorescence Properties of Fluorescein-Based Probes by Photoinduced Electron Transfer. *J. Am. Chem. Soc.* **2003**, *125*, 8666-8671.
 - (11) Marcus, R. A.; Sutin, N. Electron transfers in chemistry and biology. *Biochim. Biophys. Acta* **1985**, *811*, 265-322.
-

- (12) Lakowicz, J. R. *Principles of Fluorescence Spectroscopy*; 2nd ed.; Kluwer Academic/Plenum Publishers: New York, 1999.
- (13) Haugland, R. P. *Handbook of Fluorescent Probes and Research Products, Ninth Edition*; Ninth ed.; Molecular Probes, Inc.: Eugene, Oregon, 2002.
- (14) Walkup, G. K. personal communication.
- (15) Atwell, G. J.; Denny, W. A. Monoprotection of α, ω -Alkanediamines with the N-Benzyloxycarbonyl Protecting Group. *Synthesis* **1984**, 1032-1033.
- (16) Frank, A. J.; Otvos, J. W.; Calvin, C. Quenching of Rhodamine 101 Emission in Methanol and in Colloidal Suspensions of Latex Particles. *J. Phys. Chem.* **1979**, *83*, 716-722.
- (17) Lee, L. G.; Spurgeon, S. L.; Heiner, C. R.; Benson, S. C.; Rosenblum, B. B.; Menchen, S. M.; Graham, R. J.; Constantinescu, A.; Upadhyya, K. G.; Cassel, J. M. New energy transfer dyes for DNA sequencing. *Nucl. Acids Res.* **1997**, *25*, 2816-2822.
- (18) Wu, P.; Brand, L. Resonance Energy Transfer: Methods and Applications. *Anal. Biochem.* **1994**, *218*, 1-13.
- (19) Lamola, A. A. *Energy Transfer and Organic Photochemistry*; Interscience Publishers: New York, 1969.
- (20) Tanaka, K.; Miura, T.; Umezawa, N.; Urano, Y.; Kikuchi, K.; Higuchi, T.; Nagano, T. Rational Design of Fluorescein-Based Fluorescence Probes. Mechanism-Based Design of a Maximum Fluorescence Probe for Singlet Oxygen. *J. Am. Chem. Soc.* **2001**, *123*, 2530-2536.

- (21) Chang, C. J.; Nolan, E. M.; Jaworski, J.; Burdette, S. C.; Sheng, M.; Lippard, S. J. Bright Fluorescent Chemosensor Platforms for Imaging Endogenous Pools of Neuronal Zinc. *Chem. Biol.* **2004**, *11*, 203-210.
- (22) Burdette, S. C.; Walkup, G. K.; Spingler, B.; Tsien, R. Y.; Lippard, S. J. Fluorescent Sensors for Zn^{2+} Based on a Fluorescein Platform: Synthesis, Properties and Intracellular Distribution. *J. Am. Chem. Soc.* **2001**, *123*, 7831-7841.
- (23) Walkup, G. K.; Burdette, S. C.; Lippard, S. J.; Tsien, R. Y. A New Cell-Permeable Fluorescent Probe for Zn^{2+} . *J. Am. Chem. Soc.* **2000**, *122*, 5644-5645.
-

Table 4.1. Photophysical characteristics of potential calibrating fluorophores

	λ_{exc} (nm)	ϵ ($\text{M}^{-1}\text{cm}^{-1}$)	λ_{em} (nm)	Φ^{a}	J^{f}
Naphthofluorescein ^{a, b}	598	10,000	668	0.14 ^e	-
X-Rhodamine ^{a, c}	567	92,000	591	0.96	0.46
Coumarin 343 ²³	443	44,300 ^c	490	0.68	0.73

^aFree dye carboxylate, ^bIn pH 10 aqueous solution ^cIn MeOH, ^dDextran or protein conjugate, ^eAt pH 9.5, ^fSpectral overlap with 1.

Table 4.2. Photophysical characteristics of bisfluorophore rigid linker compounds.

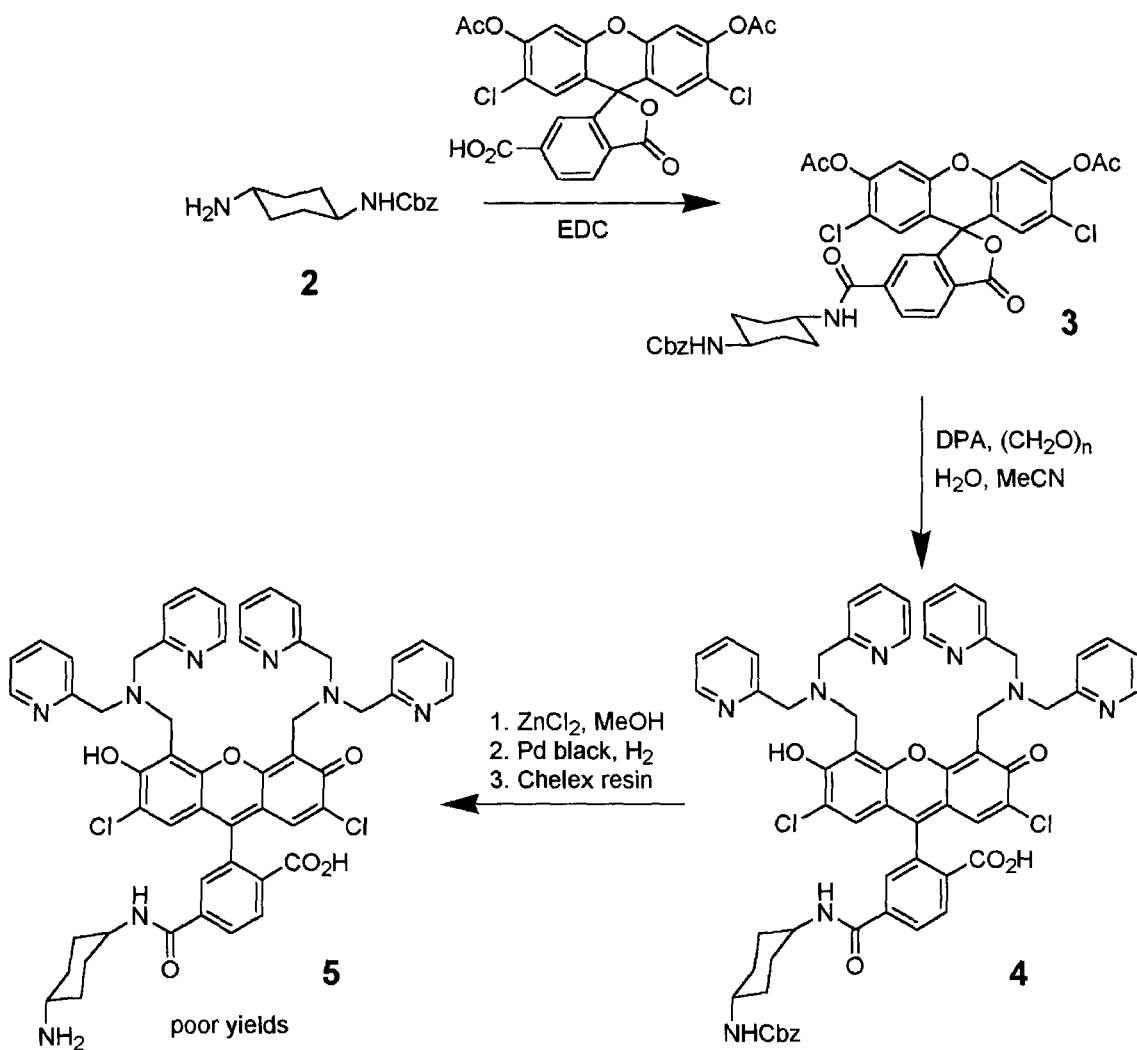
	λ_{exc1} (nm)	ϵ_1 ($\text{M}^{-1}\text{cm}^{-1}$)	λ_{exc2} (nm)	ϵ_2 ($\text{M}^{-1}\text{cm}^{-1}$)	Φ^a
7 (pH 7.5)	512	49,000	601	10,000	-
7 (pH 10)	511	52,000	621	23,000	0.04
8 (pH 7.5)	506	77,000	597	22,000	0.02
8 (MeOH) ^c			574	60,000	0.24 0.29
9 (pH 7.5)	472	33,000	509	67,000	0.70 0.64

^aQuantum yields listed are determined from excitation of fluorescein moiety,
^bDetermined from excitation of other fluorophore, ^cThe concentration dependence of fluorescein absorption is nonlinear above 2 μM and an extinction coefficient was not determined.

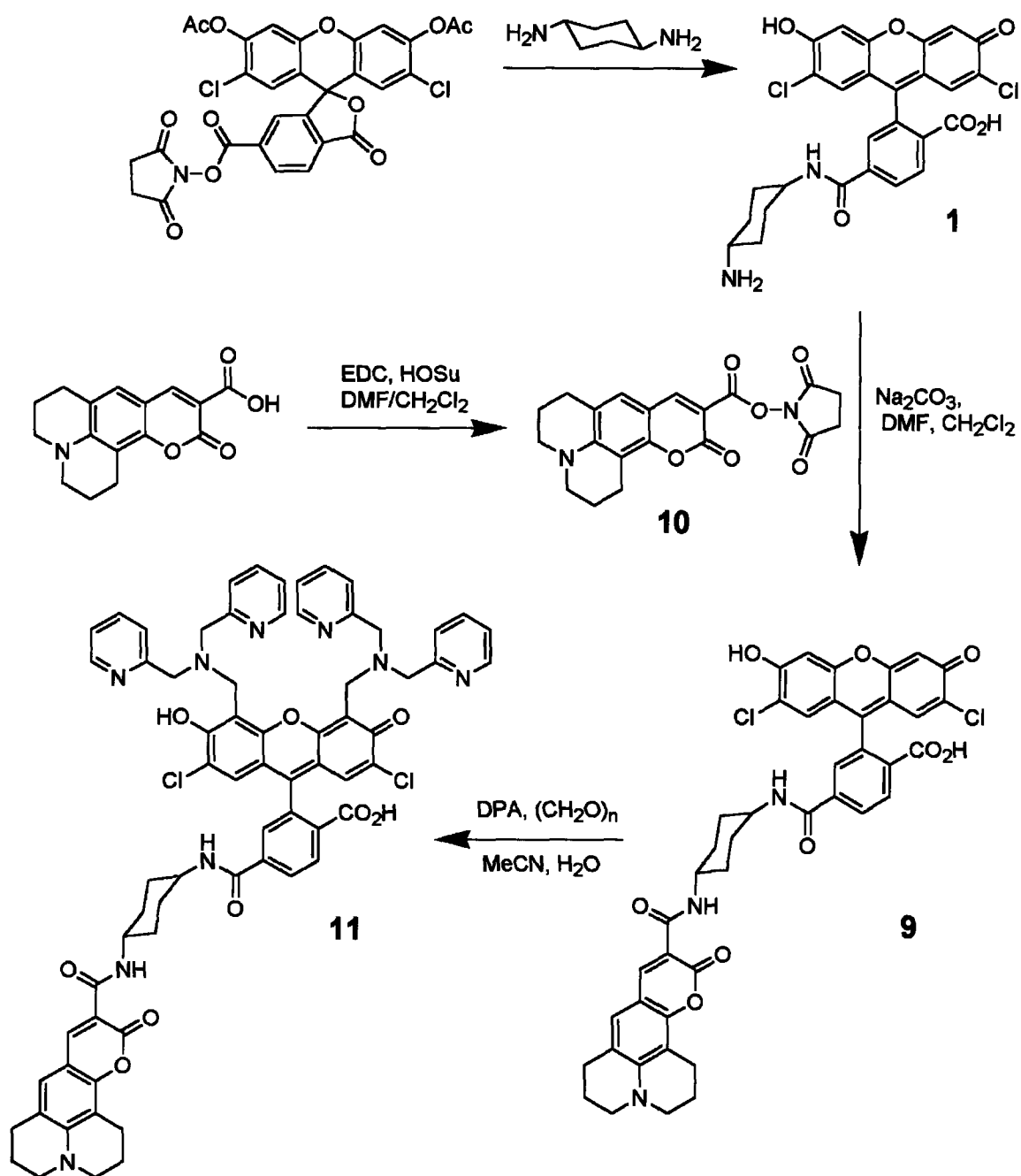
Table 4.3. Photophysical characteristics of 11.

	λ_{exc1} (nm)	ϵ_1 ($\text{M}^{-1}\text{cm}^{-1}$)	λ_{exc2} (nm)	ϵ_2 ($\text{M}^{-1}\text{cm}^{-1}$)	Φ^{a}	Φ^{b}	Ratio ^c
235b	452	9900	518	20,000	0.11	0.18	20
+ Zn ²⁺	448 (sh)	11,000	510	22,000	0.25	0.40	38

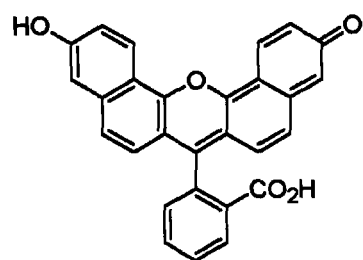
^aExcitation of coumarin fluorophore; ^bExcitation of fluorescein fluorophore; ^cCalculated by dividing integrated emission from 500-650 nm by integrated emission from 455-500 nm.



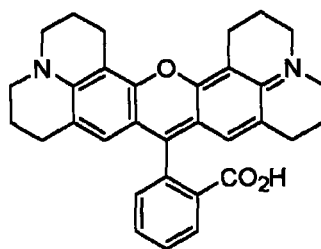
Scheme 4.1. Synthesis of ZP1-cyclohexylamine.



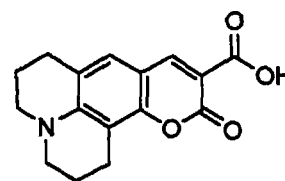
Scheme 4.2. General synthetic approach



Naphthofluorescein



X-Rhodamine



Coumarin 343

Figure 4.1. Structures of naphthofluorescein, X-rhodamine, and coumarin 343.

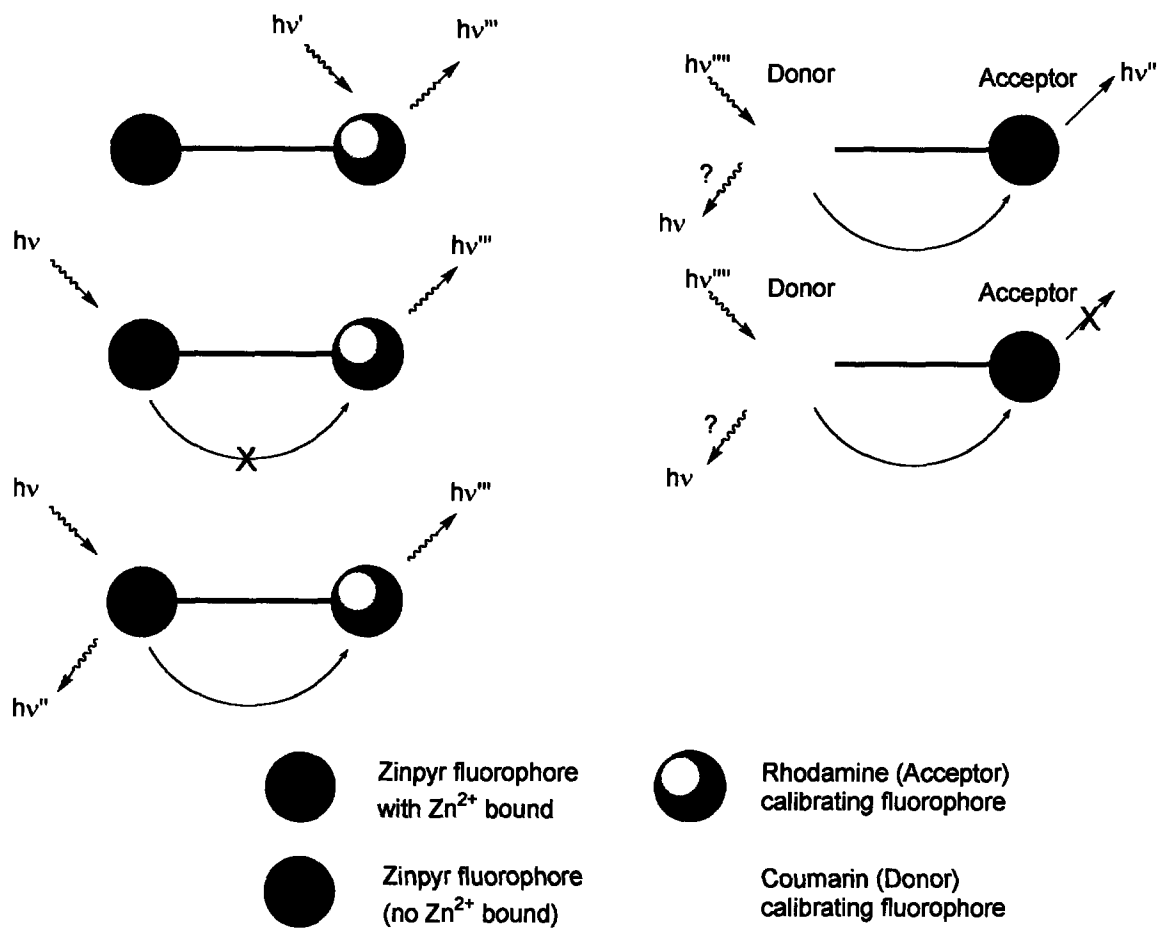


Figure 4.2. Schematics of expected fluorophore interaction

.



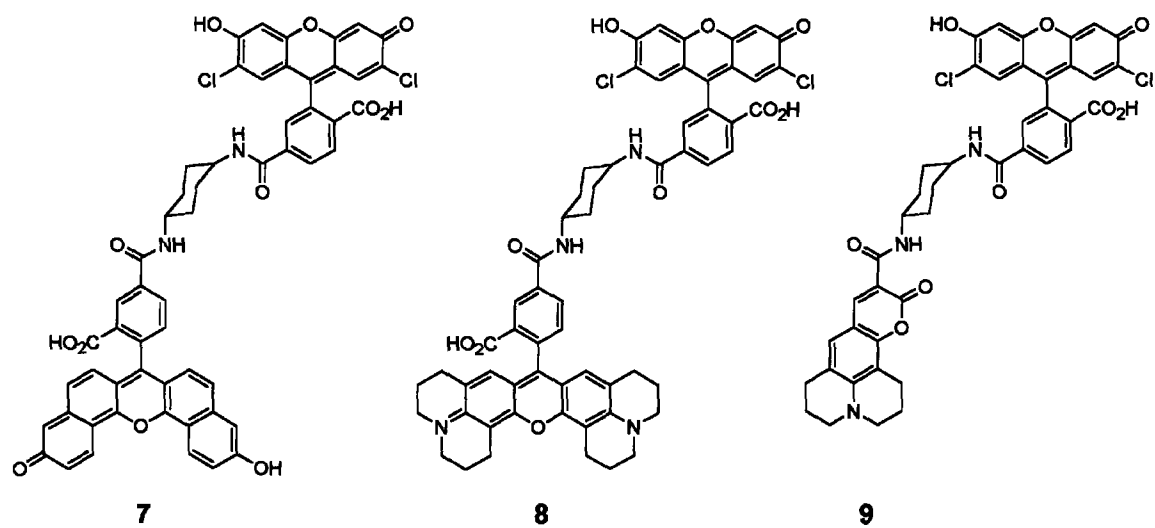


Figure 4.3. Dichlorofluorescein-cyclohexamide-linked reporter fluorophores

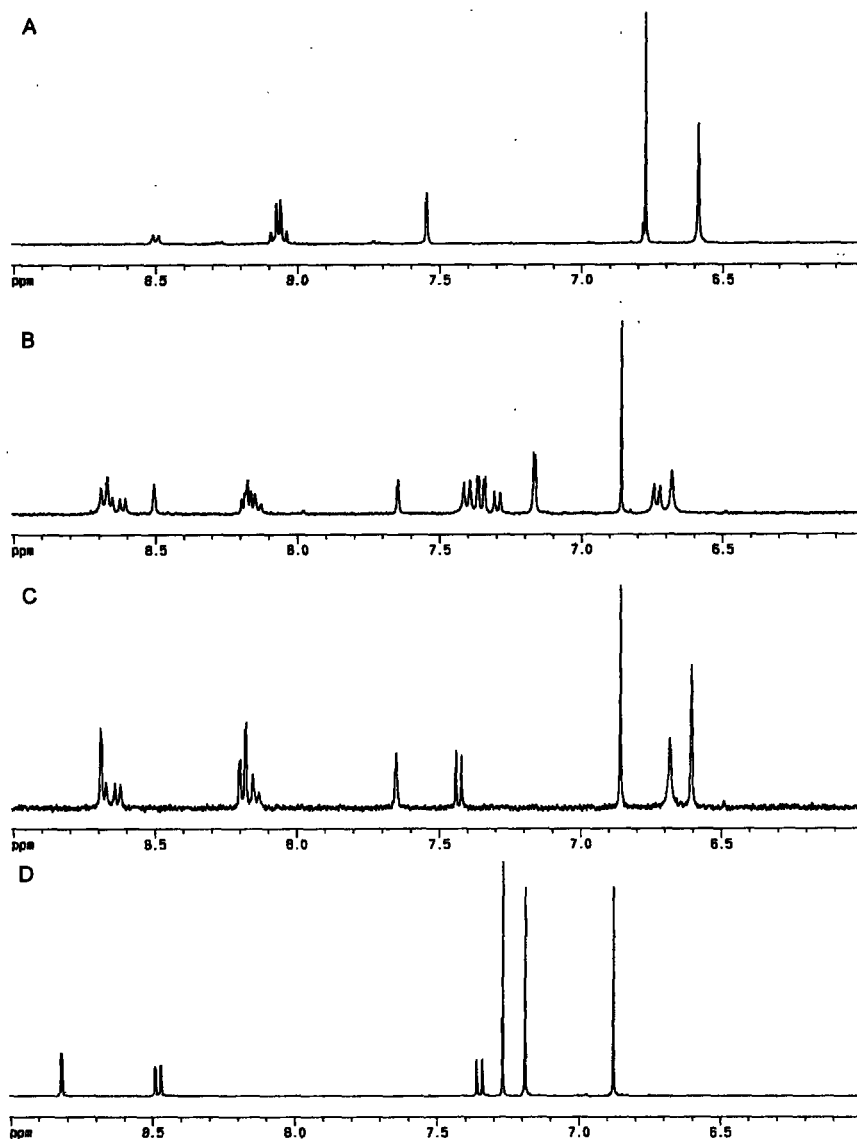


Figure 4.4. Proton NMR spectra of **7** and **8**

A. ^1H NMR of **1** (MeOH-d_4), B. ^1H NMR of **7** (MeOH-d_4), C. ^1H NMR of **8** (MeOH-d_4), D. ^1H NMR of 3',6'-diacetyl-2',7'-dichlorofluorescein-5-carboxylate (CDCl_3). 6-carboxy-2',7'-dichlorofluoresceins give rise to a pseudo-quartet at or above 8.0 ppm and a singlet at or above 7.5 ppm. 5-carboxy-2',7'-dichlorofluoresceins afford two doublets separated by 1 ppm or more, and a singlet at higher field. The amide proton of **1** appears as a broad doublet at 8.5 ppm.

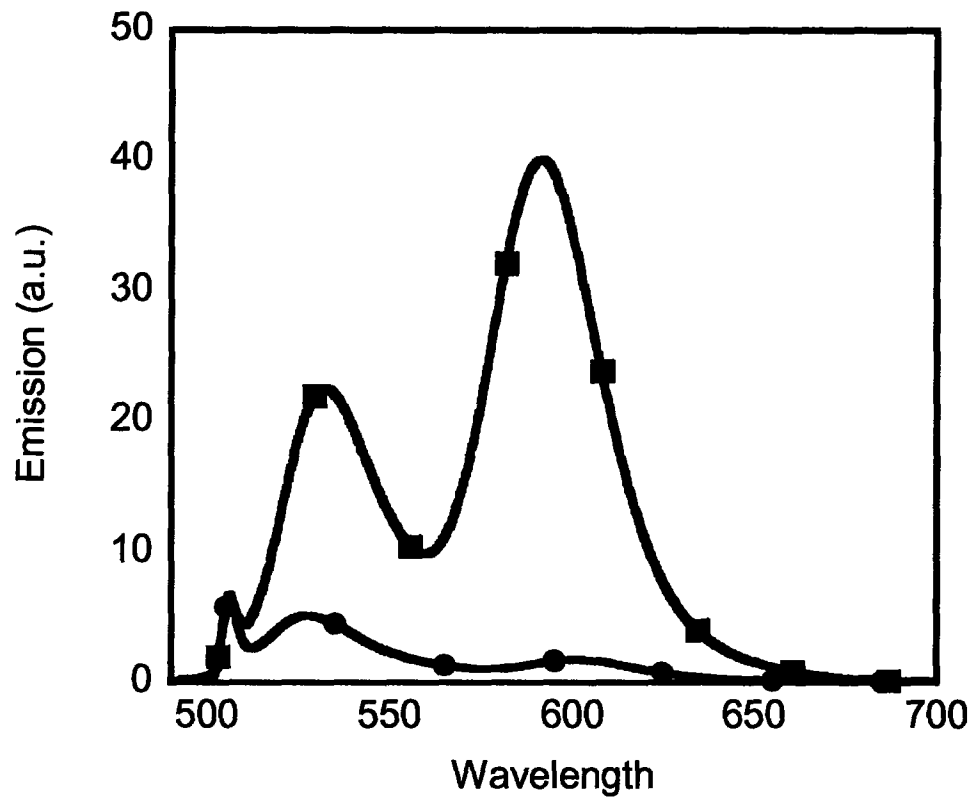


Figure 4.5. Comparative emission spectra of **8** (1 μM) in aqueous HEPES buffer (pH 7.5, red circles) and methanolic solution (blue squares).



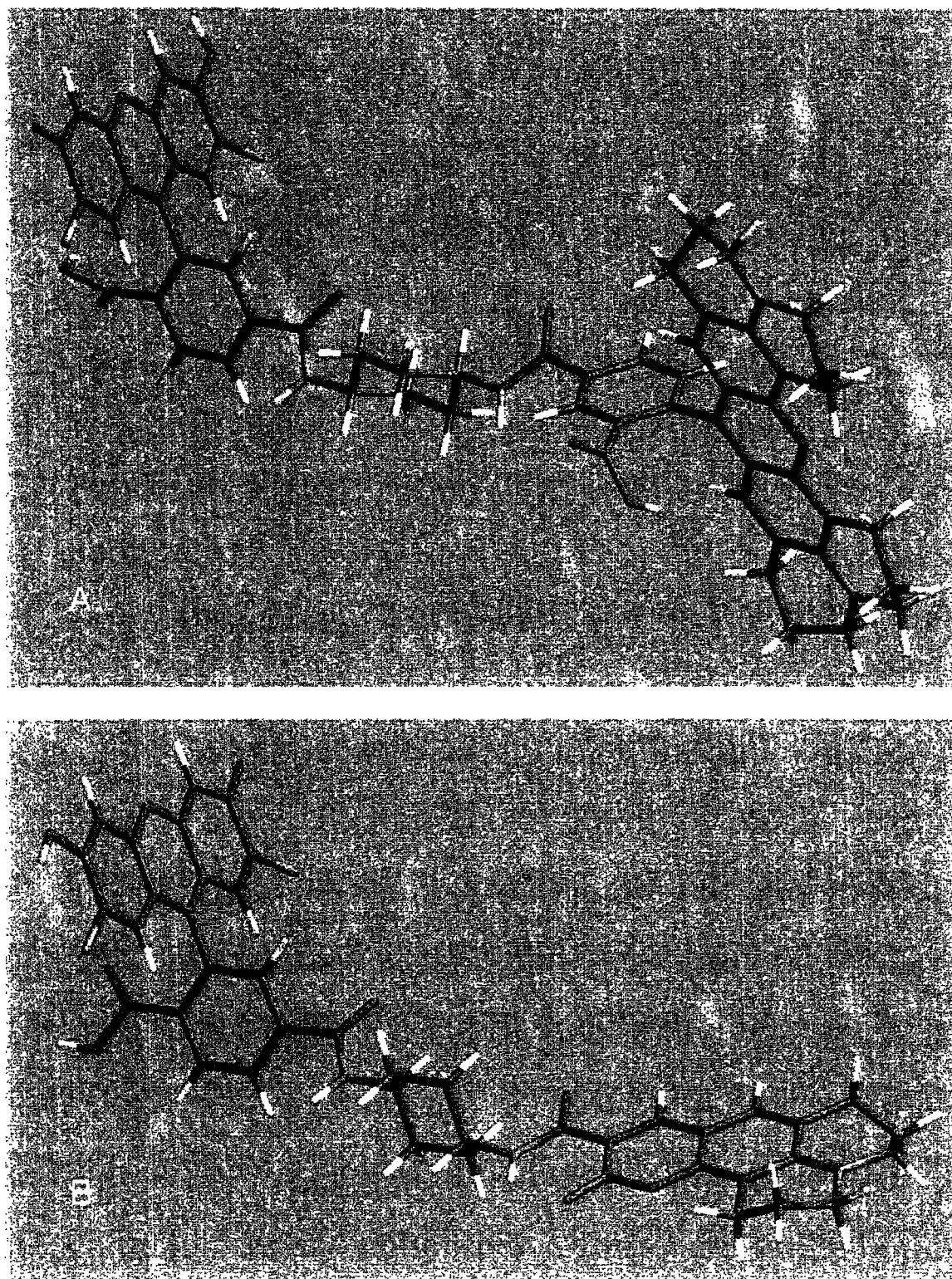


Figure 4.6. AM1 optimized equilibrium geometries of **8** (A) and **9** (B).

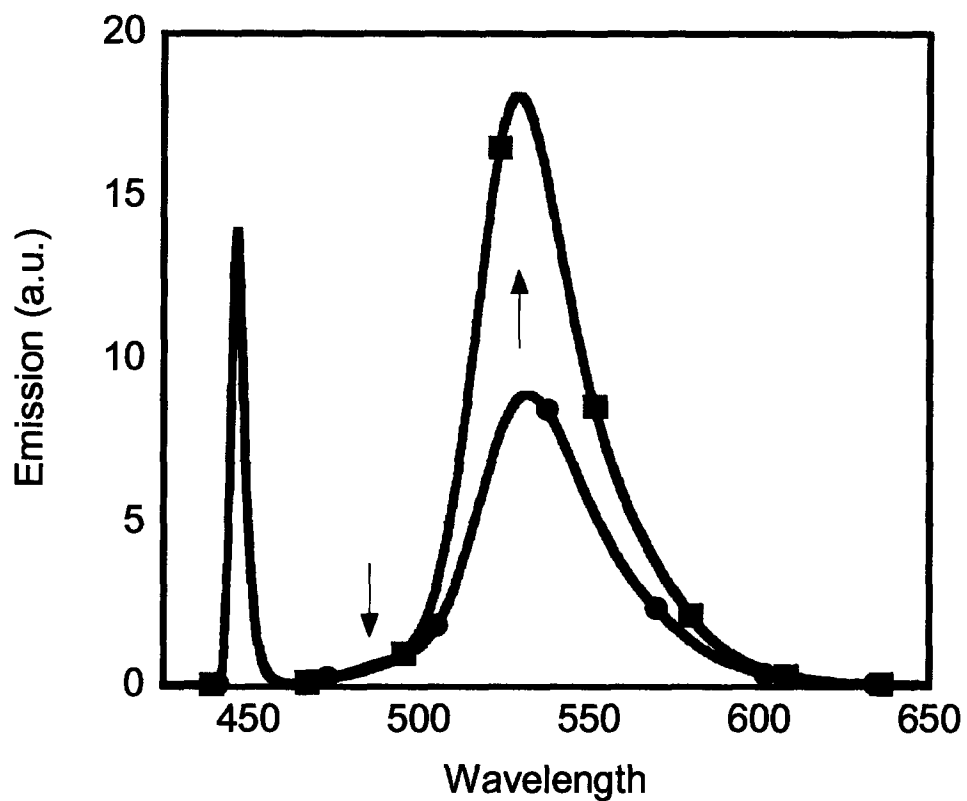


Figure 4.7. Fluorescence response of 11 to excess ZnCl₂.

The emission spectrum of a 4 μ M solution of 11 was acquired with excitation at 445 nm, before and after the addition of a 4 μ L aliquot of ZnCl₂.

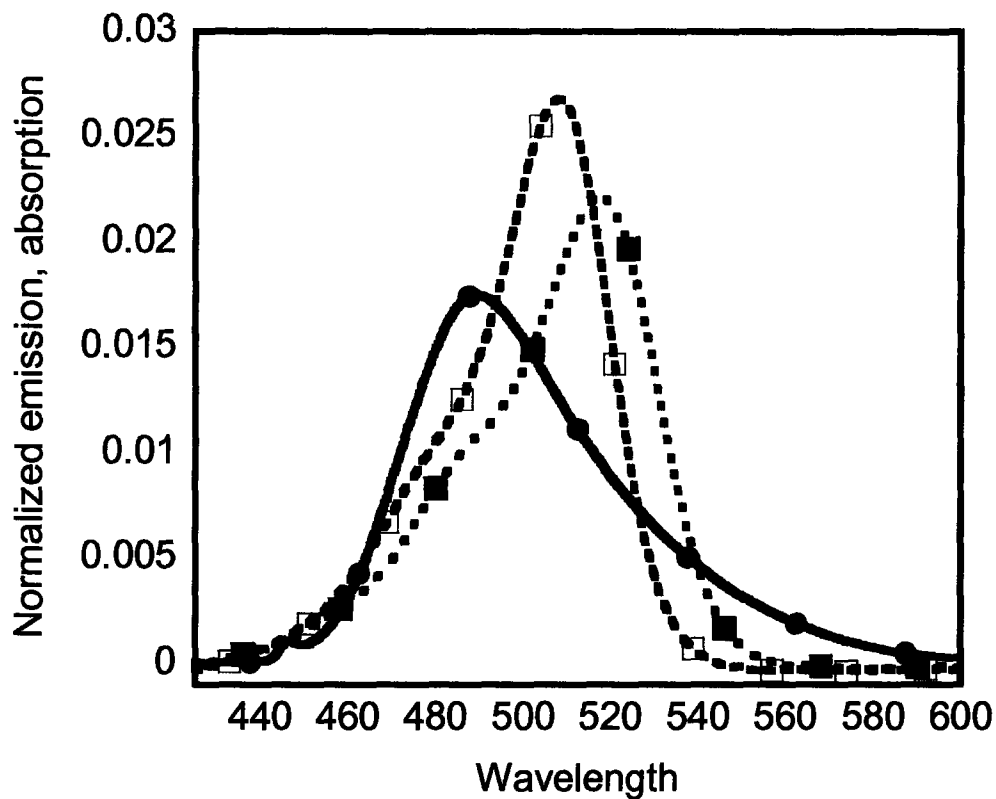


Figure 4.8. Change in spectral overlap integral J of coumarin 343 emission with ZPA3 absorbance upon addition of Zn^{2+} .

Coumarin emission (red solid circles) was measured at a concentration of $1 \mu\text{M}$, as was ZPA3 absorbance in the presence (green open squares) and absence (blue solid squares) of $20 \mu\text{M ZnCl}_2$. Spectra were normalized to a total integrated emission of 1.

Chapter 5 ZP1 Synthons for Direct Functionalization of Biological Targets[†]

Introduction[†]

The ability to monitor zinc(II) flux in particular areas of the cell or synapse would be of great utility. Hence, approaches to ZP1 sensors functionalized with biological targeting agents have been considered. Compounds that bind to postsynaptic receptors of Zn^{2+} -containing presynaptic terminals would be capable of sensing local Zn^{2+} fluxes after synapse firing. Because Zn^{2+} -enriched neurons are typically glutamatergic¹ and because N-methyl-D-aspartate-sensitive glutamate receptors are widely implicated in Zn^{2+} -mediated modulation of glutamate response,²⁻⁵ ZP1 sensor adducts of NMDA receptor agonists and antagonists were targeted.

Functionalized ZP1 sensors have thus far relied on preparation of dichlorofluorescein-5(6)-carboxylate derivatives containing the desired group, followed by Mannich reaction of the derivatized fluorescein.⁶ Although this approach is useful in some cases, it is inefficient for expensive or chemically sensitive coupling partners. Many groups may not tolerate Mannich reaction conditions, or may be Mannich substrates themselves. Hence, we sought a ZP1 synthon that would enable direct access to functionalized ZP1 sensors. We present here two orthogonal approaches for direct functionalization of ZP1 with biologically active groups.

Click chemistry—the copper-catalyzed coupling of a terminal alkyne with an azide to form a 1, 4-substituted triazole—has undergone a surge in popularity in recent years.^{7,8} The reaction is very reliable and specific, with near-quantitative yields and synthons that are relatively inert to side reactions under typical biological conditions.

[†] Respective contributions were as follows: Investigation of click chemistry reactions of **1** with azidopropanol and other azide substrates was carried out by Annie C. Won (UROP student).

Hence, we have prepared a ZP1 alkyne (1) and examined its reactivity with azides under click chemistry conditions.

Although the paucity of azides in biological systems can be used to advantage in matters of selectivity, the comparative lack of readily available azido-functionalized substrates is sometimes a hindrance. A ZP1 synthon reactive towards the ubiquitous amino functional group was deemed a worthwhile target, and thus a ZP1 succinimidyl ester (2) has been prepared. Succinimidyl esters react readily and smoothly with amines.⁹ We have applied this approach to the synthesis of ZP1 adducts of a putative NMDA receptor antagonist, and of simple diamines for further functionalization.

Experimental

Materials and Methods.

Reagents were purchased from Aldrich and used without further purification, except for pyBOP, which was obtained from Novabiochem, and Chelex resin, which was obtained from Sigma. Azidopropanol was prepared as previously described.¹⁰ ZP1(6-CO₂H) (5) and the pyridinium salt of 3',6'-diacetyl-2',7'-dichloro-6-carboxyfluorescein were synthesized as described in Chapter 2. Acetonitrile was obtained from a dry-still solvent dispensation system. ¹H NMR and ¹³C spectra were acquired on a Bruker 400 MHz or a Varian 500 MHz spectrometer. LCMS analysis was performed on an Agilent Technologies 1100 Series LCMS with a Zorbax Extend C-18 column using a linear gradient of 100% A (95:5 H₂O:MeCN, 0.05% HCO₂H) to 100% B (95:5 MeCN:H₂O; 0.05% HCO₂H) over 30 min at a flow rate of 0.250 mL/min. Detector wavelengths were set at 240 nm and 500 nm, and the electrospray MS detector was set to positive ion mode scanning the range m/z = 100-2000. Low-resolution MS spectra were acquired on the

same instrument. Preparative high-performance liquid chromatography (HPLC) was performed on a Waters 600 pump with a Waters 600E systems controller monitored by a Waters 486 tunable absorbance detector, using a Higgins Analytical, Inc. reverse-phase C18 column measuring 250 mm x 20 mm. Solvents A and B were purified water (resistivity 18.2 Ohms) obtained from a Millipore Milli-Q water purification system, or low-water acetonitrile (Mallinckrodt), respectively; each containing 0.1 % v/v trifluoroacetic acid. Isolated compounds were stored at 4 °C or -25 °C.

Synthetic Procedures

3',6'-Diacetyl-6-Carboxy-2',7'-Dichlorofluorescein Propargylamide (3a). The pyridinium salt of 3',6'-diacetyl-5-carboxy-2',7'-dichlorofluorescein (1.22 g, 2 mmol) was combined with pyBOP (1.56 g, 3 mmol), propargylamine (280 μ L) and triethylamine (280 μ L) in 50 mL of dry CH_2Cl_2 and stirred at RT. After 90 min, the reaction was concentrated on the rotary evaporator and purified by flash chromatography on silica gel, eluting with 98:2 CHCl_3 :MeOH. The resulting residue was recrystallized from MeOH to give 423 mg (35% yield). $^1\text{H NMR}$ (CDCl_3): δ 8.12 (m, 2 H); 7.54 (s, 1 H); 7.14 (s, 2 H); 6.84 (s, 2 H); 6.63 (br t, 1 H); 4.18 (m, 2 H); 2.37 (s, 6 H); 2.24 (br t, 1 H).

3',6'-Diacetyl-5-Carboxy-2',7'-Dichlorofluorescein Propargylamide (3b). 3',6'-Diacetyl-5-carboxy-2',7'-dichlorofluorescein (527 mg, 1 mmol) was combined with pyBOP (1.04 g, 2 mmol), propargylamine (140 μ L) and triethylamine (140 μ L) in 50 mL of dry CH_2Cl_2 and stirred at RT. After 90 min, the solution was concentrated under reduced pressure and purified by flash chromatography on silica gel, eluting with 98:2 CHCl_3 :MeOH, to give 394 mg (70% yield) of 3b. $^1\text{H NMR}$ (CDCl_3): δ 8.49 (s, 1 H); 8.28 (d, 1 H); 7.33 (d, 1 H); 7.18 (s, 2 H); 6.84 (s, 2 H); 4.31 (m, 2 H); 2.39 (s, 6 H); 2.31

(br t, 1 H). ^{13}C NMR (CDCl_3): δ 168.03, 167.76, 165.11, 154.38, 149.82, 148.84, 136.94, 135.53, 129.00, 126.46, 124.87, 124.15, 123.09, 116.98, 113.14, 81.11, 79.15, 72.64, 30.50, 21.05. HRMS(M-H): Calcd for $\text{C}_{28}\text{H}_{16}\text{Cl}_2\text{NO}_8$: 564.0253; Found 564.0242.

ZP1-6-(CONHCH₂CCH) (1). Dipicolylamine (640 mg, 3.2 mmol) was combined with paraformaldehyde (192 mg, 6.4 mmol) in 15 mL of MeCN and heated to reflux for 30 min. 3',6'-Diacetyl-5-carboxy-2',7'-dichlorofluorescein propargylamide (283 mg, 0.5 mmol) was dissolved in 6 mL of MeCN and the solution was added. After addition of H₂O (6 mL), the reaction was heated for an additional 16 h, cooled, and filtered. The filtrand was washed with H₂O and MeCN to afford 371 mg (82%) of a pale pink solid. ^1H NMR ($\text{DMSO}-d_6$): δ 9.16 (t, 1 H); 8.55 (d, 4 H); 8.16 (d, 1 H); 8.09 (d, 1 H); 7.75 (m, 5 H); 7.39 (d, 4 H); 7.28 (m, 4 H); 6.62 (s, 2 H); 4.19 (s, 4 H); 4.01 (s, 10 H); 3.08 (t, 1 H). HRMS(M+H): Calcd for $\text{C}_{50}\text{H}_{40}\text{Cl}_2\text{N}_7\text{O}_6$: 904.2417; Found 904.2435.

N-[1-(3-hydroxy-propyl)-1H-[1,2,3]triazol-4-ylmethyl]-ZP1-6-carboxamide (4). Azidopropanol (2.2 mg, 0.022 mmol) was combined with copper(II) sulfate pentahydrate (2.8 mg, 0.011 mmol), sodium ascorbate (21.8 mg, 0.11 mmol) and 1 in 6 mL of a 1:1 H₂O:MeOH mixture. The reaction was stirred at RT for 24 h, then concentrated under reduced pressure and lyophilized overnight. The resulting residue was stirred vigorously in CH_2Cl_2 with Chelex resin (1 g) for 2 h, then gravity filtered and concentrated under reduced pressure to yield a pink residue. ^1H NMR (CDCl_3): 8.59 (dd, 4 H); 8.11 (d, 1 H); 8.06 (d, 1 H); 7.66 (td 4 H); 7.59 (s, 1 H); 7.38 (d, 4 H); 7.20 (m, 4 H); 6.62 (s, 2 H); 6.48 (br t, 1 H); 4.19 (s, 4 H); 4.01 (s, 8 H); 3.79 (m, 4 H); 3.52-3.63 (m, 12 H)^{*}; 3.50 (s, 1 H); 3.4 (t, 2 H); 1.86 (m, > 2H). MS(M+2H): Calcd for $\text{C}_{53}\text{H}_{48}\text{Cl}_2\text{N}_{10}\text{O}_7$: 503.2; Found 503.2

ZP1-6-CO₂Su (2). A portion of ZP1(6-CO₂H) (**5**, 86.6 mg, 0.1 mmol) was combined with disuccinimidyl dicarbonate (52.5 mg, 0.2 mmol), activated molecular sieves, and triethylamine (160 μ L) in 3 mL of DMF and 15 mL of MeCN. The reaction was stirred for 48 h at RT, and then concentrated under reduced pressure and quenched by addition of glacial acetic acid. The product was isolated by preparative HPLC eluting with a gradient of 0 \rightarrow 100% B over 30 min. The peak eluting at 19 min was collected and the combined fractions were lyophilized to afford 50.2 mg of the desired product (52% yield). Remaining starting material (18 mg, 21%) was also recovered (retention time 16.8 min). ¹H NMR (MeOH-d₄): δ 8.62 (d, 4 H); 8.51 (dd, 1 H); 8.40 (d, 1 H); 7.96 (td, 4 H); 7.90 (d, 1 H); 7.42-7.55 (m, 8 H); 6.75 (s, 2 H); 4.49-4.58 (m, 12 H); 2.90 (br s, 4 H). MS(M + H): Calcd for C₅₁H₄₀Cl₂N₇O₉: 964.2; Found 964.3

ZP1-Cy-NH₂ (6). A portion of ZP1(6-CO₂H) (17.3 mg, 20 μ mol) was combined with disuccinimidyl dicarbonate (15.7 mg, 60 μ mol), activated molecular sieves, and triethylamine (20 μ L) in 0.5 mL of DMF and 3 mL of MeCN. The reaction was stirred for 24 h at RT and then concentrated under reduced pressure. The dark pink residue was diluted with CHCl₃, and the solution was washed with 2 x 50 mL of 1:1 H₂O:brine, then with 1 x 50 mL brine. The solvents were removed under reduced pressure, and the residue was dissolved in 0.5 mL of DMF and added to a solution of *trans*-1, 4-cyclohexanediamine (22 mg, 0.2 mmol). The reaction was stirred for 3 h, and the desired product was isolated by preparative-scale HPLC (0 \rightarrow 50% B over 20 min). Lyophilization afforded 4.5 mg (23.4%) of a dark pink solid. ¹H NMR (MeOH-d₄): δ 8.65 (d, 4 H); 8.29 (d, 1 H); 8.17 (dd, 1 H); 8.02 (td, 4 H); 7.65 (d, 1 H); 7.60 (d, 4 H); 7.53 (m, 4 H); 6.69 (s, 2 H); 4.48-4.63 (m, 12 H); 3.90 (br m, 1 H); 3.13 (br m, 1 H); 2.09

(br m, 4 H); 1.51 (br m, 4 H). MS(M + H): Calcd for $C_{53}H_{49}Cl_2N_8O_6$: 963.3; Found 963.2

ZP1-Diaminopimelic Acid (7). A portion of compound **2** (9.6 mg, 0.01 mmol) was dissolved in 0.5 mL of DMF and added to a solution of diaminopimelic acid (38.0 mg, 0.2 mmol) and triethylamine (30 μ L) in 3 mL of H_2O . The reaction was stirred for 2 h at RT, then quenched by addition of 20 μ L of glacial acetic acid. The desired product was isolated by preparative HPLC, eluting with a gradient of 0 \rightarrow 100% B over 35 min. Lyophilization gave 2.5 mg (37.6%) of a pink solid. 1H NMR (MeOH- d_4): δ 8.63 (d, 4 H); 8.31 (d, 1 H); 8.22 (d, 1 H); 7.97 (m, 4 H); 7.66 (s, 1 H); 7.41-7.54 (m, 9 H); 6.73 (s, 1 H); 6.69 (s, 1 H); 4.57 (m, 1 H); 4.48-4.56 (m, 12 H); 3.96 (m, 1 H); 1.89-2.06 (m, 4 H); 1.65 (m, 2 H). MS(M+H): Calcd for $C_{54}H_{49}Cl_2N_8O_{10}$: 1039.3; Found 1039.2.

Results and Discussion

Synthesis

A ZP1 alkyne **1** for click chemistry coupling was prepared by pyBOP mediated coupling of propargylamine with 3',6'-diacetyl-2',7'-dichlorofluorescein to give **3a** and subsequent Mannich reaction with dipicolylamine and paraformaldehyde (Scheme 5.1). A model click chemistry reaction of **1** with azidopropanol proceeds uneventfully; however, the metal-binding sites of ZP1 bind copper with higher affinity than for Zn^{2+} , and treatment with Chelex resin was necessary in order to remove the metal. The product **4** adsorbs onto the resin, such that the desired product is obtained in poor yields, and is contaminated by apparent leaching of ligands from the resin. Click chemistry reactions of ZP1 alkyne with aromatic azides did not proceed detectably.

Succinimidyl esters are commonly used as activated coupling partners in reactions with amines. A ZP1 succinimidyl ester was identified as a desirable synthon for modular synthesis of functionalized ZP1 compounds. Unsurprisingly, Mannich reaction of 3',6'-diacetyl-2',7'-dichlorofluorescein-6-carboxysuccinimidyl ester furnished none of the esterified product. Similarly, reaction of ZP1(6-CO₂H) with N-hydroxysuccinimide and EDC failed to afford the desired **2**.¹¹ Use of disuccinimidyl carbonate as the esterification reagent in the presence of triethylamine, in contrast, gave **2** in 52% yield after purification. When the esterification reaction was conducted in DMF, two overlapping product peaks with mass signals corresponding to the desired product were observed in the LCMS trace, a result that may signify indiscriminate esterification of either the 3- or 6-carboxylate. Use of MeCN as the primary solvent reduces environmental polarity and presumably increases the population of the lactone conformer, in which the 3-carboxylate cannot undergo esterification. A single symmetric product peak was observed by LCMS when a 6:1 MeCN:DMF solvent system was employed; however, this solvent mixture also reduces conversion. No di-esterified product was observed by LCMS under either set of conditions. The ZP1 succinimidyl ester was isolated from the reaction mixture by preparative-scale HPLC, and can be reacted with a selection of amines to afford ZP1 conjugates of biologically active molecules. Coupling reactions, when conducted in aqueous solutions, afford significant amounts of both desired product and the hydrolysis product, ZP1(6-CO₂H).

HPLC purification of the ZP1 succinimidyl ester **2** can be somewhat tedious. In cases where the ultimate amido product incorporates a positive charge, such as a pendant amine, chromatographic separation of the product from the ZP1(6-CO₂H) starting

material **5** is good and purification of the intermediate succinimidyl ester **2** is unnecessary. Direct reaction of crude **2** with *trans*-1,4-cyclohexanediamine and subsequent HPLC purification of the product **6** affords a useful intermediate for the chemistry described in Chapter 4, in fewer steps and better overall yield than the protocol reported there.

Choice of Biological Targets

Glutamate is the primary mediator of fast excitatory synaptic transmission in the central nervous system. Glutamate receptors are classified according to the pharmacology of their antagonists, and the three major classes of glutamate receptors are the α -amino-3-hydroxy-5-methyl-4-isoxazole (AMPA)-sensitive channels, the kainate-sensitive channels, and the N-methyl-D-aspartate (NMDA)-sensitive channels. NMDA receptors are of interest with respect to synaptic Zn^{2+} because there is a regulatory Zn^{2+} binding site² and because Zn^{2+} is believed to modulate NMDA receptor-mediated excitotoxic insult.^{2,5} Like many neural receptor proteins, NMDA receptors are composed of combinations of various subunits, and the precise characteristics of a given channel are defined by the combination of the subunits that comprise it. Physiologically relevant agonists and antagonists of the NMDA receptor channel include glutamate itself, glycine, Mg^{2+} , protons, spermine, Ca^{2+} , and histamine.¹² The polyamines spermidine and spermine also stimulate NMDA receptors via the so-called polyamine binding site.

We chose diaminopimelic acid and spermine as coupling partners for **2** for several reasons. Both compounds are commercially available and both are symmetric polyamines, reducing the number of possible products. A variety of α -amino- α,ω -dicarboxyalkanes and bioisosteres thereof have been reported to antagonize NMDA

receptor activity reversibly, with micromolar affinities.¹³ Alkyl chains containing two to six carbons with varying substituents and rigidities have been successfully employed. Spermine potentiates NMDA receptor response with half-maximal response obtained at concentrations below 100 μM .¹⁴ Other polyamines, including spermidine, also bind to NMDA receptors, suggesting that the conversion of one terminal amine to an amide would not abolish receptor affinity for the resulting compound. However, the reaction of **2** with spermine at 0 °C and subsequent HPLC purification furnishes an apparent mixture of products as assessed by proton NMR, most likely arising from non-selective reaction of the succinimidyl ester with both primary and secondary amines. In contrast, the coupling reaction with diaminopimelic acid affords a single adduct (**7**) that is easily isolated by preparative HPLC.

Conclusions

We have described the synthesis and application of two orthogonal ZP1 synthons for direct coupling with amines or azides. Click chemistry reactions of a ZP1 alkyne proceeds with an aliphatic azide, but removal of stoichiometric copper after the reaction severely reduces yield. The carboxylate-substituted compound ZP1(6-CO₂H) is available in gram quantities via three steps as described in Chapter 2, and can be readily converted to the amine-reactive succinimidyl ester. This intermediate enables access to ZP1 adducts of delicate or expensive amines in a single reaction.

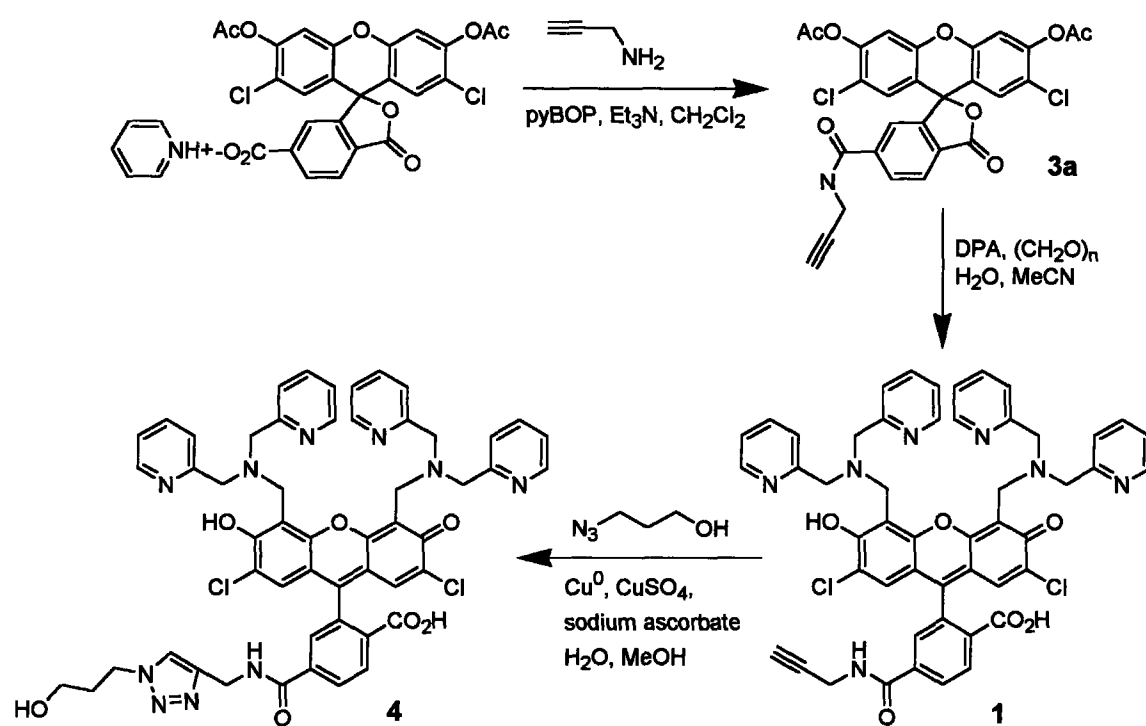
Acknowledgement

We thank Annie Won for investigating click chemistry reactions of ZP1 alkyne and for aid in investigating NMDA receptor antagonists.

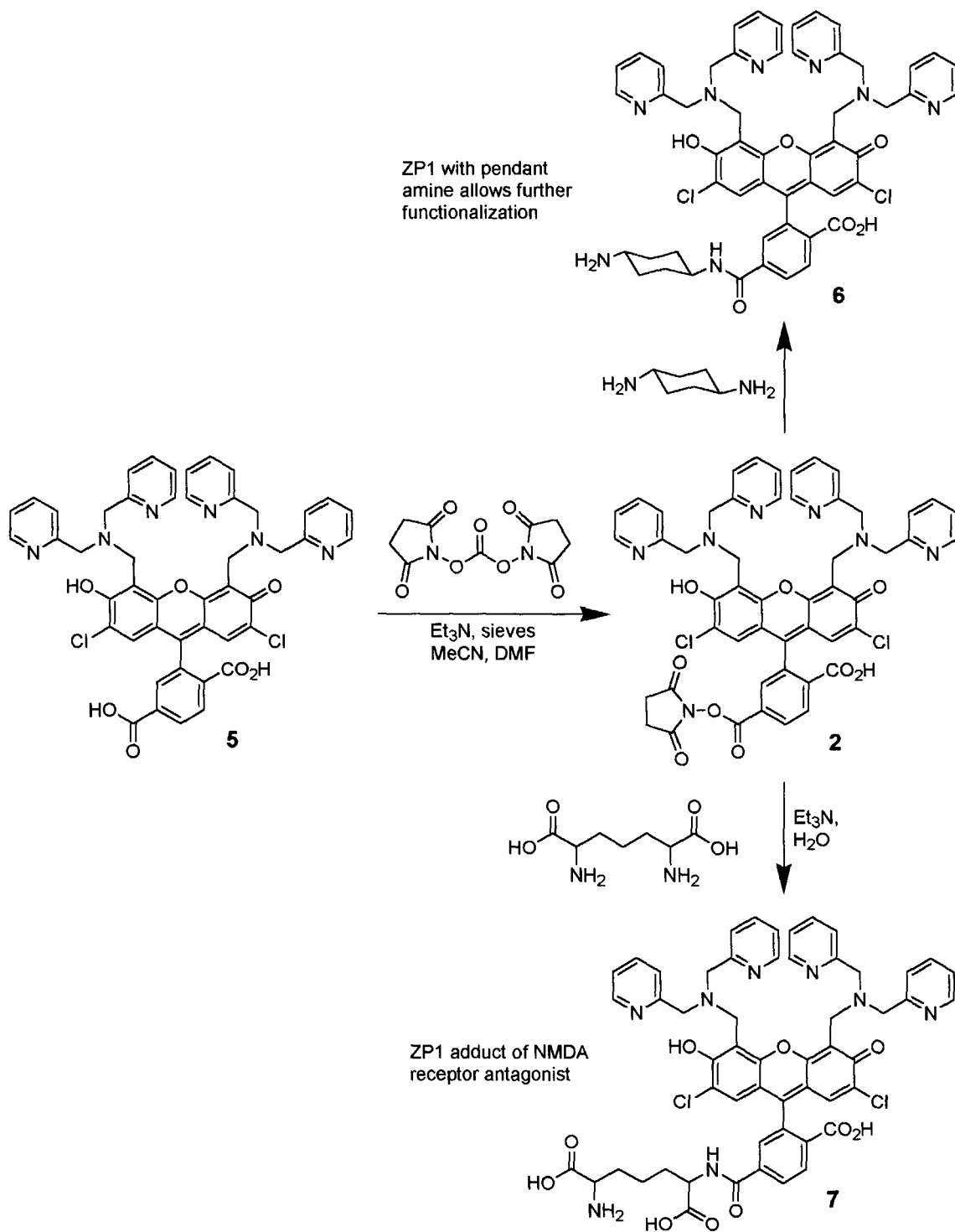
References

- (1) Frederickson, C. J. Neurobiology of Zinc and Zinc-containing Neurons. *Int. Rev. Neurobiol.* **1989**, *31*, 145-238.
- (2) Westbrook, G. L.; Mayer, M. L. Micromolar concentrations of Zn^{2+} antagonize NMDA and GABA responses of hippocampal neurons. *Nature* **1987**, *328*, 640-643.
- (3) Manzerra, P.; Behrens, M. M.; Canzoniero, L. M. T.; Wang, X. Q.; Heidinger, V.; Ichinose, T.; Yu, S. P.; Choi, D. W. Zinc induces a Src family kinase-mediated up-regulation of NMDA receptor activity and excitotoxicity. *Proc. Natl. Acad. Sci. USA* **2001**, *98*, 11055-11061.
- (4) Sensi, S. L.; Canzoniero, L. M.; Yu, S. P.; Ying, H. S.; Koh, J. Y.; Kershner, G. A.; Choi, D. W. Measurement of Intracellular Free Zinc in Living Cortical Neurons: Routes of Entry. *J. Neurosci.* **1997**, *17*, 9554-9564.
- (5) Peters, S.; Koh, J. Y.; Choi, D. W. Zinc Selectively Blocks the Action of N-Methyl-d-Aspartate on Cortical Neurons. *Science* **2004**, *236*, 589-593.
- (6) Woodrooffe, C. C.; Lippard, S. J. A Novel Two-Fluorophore Approach to Ratiometric Sensing of Zn^{2+} . *J. Am. Chem. Soc.* **2003**, *125*, 11458-11459.
- (7) Kolb, H. C.; Finn, M. G.; Sharpless, K. B. Click Chemistry: Diverse Chemical Function from a Few Good Reactions. *Angew. Chem. Int. Ed.* **2001**, *40*, 2004-2021.
- (8) Kolb, H. C.; Sharpless, K. B. The growing impact of click chemistry on drug discovery. *Drug Disc. Today* **2003**, *8*, 1128-1137.

- (9) Haugland, R. P. *Handbook of Fluorescent Probes and Research Products, Ninth Edition*; Ninth ed.; Molecular Probes, Inc.: Eugene, Oregon, 2002.
 - (10) Badiang, J. G.; Aubé, J. One-Step Conversion of Aldehydes to Oxazolines and 5,6-Dihydro-4*H*-1,3-oxazines Using 1,2- and 1,3-Azido Alcohols. *J. Org. Chem.* **1996**, *61*, 2484-2487.
 - (11) Won, A. C.; Choi, A.; Chang, C. J.; Lippard, S. J., unpublished results.
 - (12) Yamakura, T.; Shimoji, K. Subunit- and Site-Specific Pharmacology of the NMDA Receptor Channel. *Prog. Neurobiol.* **1999**, *59*, 279-298.
 - (13) Kinney, W. A.; Lee, N. E.; Garrison, D. T.; Podlesny, E. J. J.; Simmonds, J. T.; Bramlett, D.; Notvest, R. R.; Kowal, D. M.; Tasse, R. P. Bioisosteric Replacement of the α -Amino Carboxylic Acid Functionality in 2-Amino-5-phosphonopentanoic Acid Yields Unique 3,4-Diamino-3-cyclobutene-1,2-dione Containing NMDA Antagonists. *J. Med. Chem.* **1992**, *35*, 4720-4726.
 - (14) McGurk, J. F.; Bennett, M. V. L.; Zukin, R. S. Polyamines potentiate responses of N-methyl-D-aspartate receptors expressed in *Xenopus* oocytes. *Proc. Natl. Acad. Sci. USA* **1990**, *87*, 9971-9974.
-



Scheme 5.1. Synthesis of ZP1 alkyne and subsequent click chemistry reaction



Scheme 5.2. Synthesis of ZP1-OSu and adducts

Retrospective

This thesis has been primarily concerned with the modification of an existing intensity-based sensor for zinc ion, Zinpyr-1 (ZP1), to meet selected items on the list of requirements for an ideal sensor, as outlined in Chapter 1 (page 23-24). The selectivity of fluorescence response for Zn^{2+} over other relevant physiological metal ions is excellent for the parent ZP1 and was not significantly modified in this work. Similarly, the low-energy excitation and emission wavelengths and the intensity of fluorescence response were not greatly altered, although in some cases the background fluorescence and dynamic range have been improved. Alteration of subcellular sensor distribution has been achieved by ester- and acid-substitution of the parent sensor, with concomitant enhancement of dynamic range, as described in Chapter 2. Synthetic methodology for the preparation of ZP1 adducts of biological targeting agents is reported in Chapter 5, offering the potential for directing sensors to a region of interest, such as a subcellular organelle or membrane-bound receptor protein. Ratiometric sensing strategies based on the inclusion of a second, calibrating fluorophore have been described in Chapters 3 and 4. These systems include coumarin 343, an intensely fluorescent dye with visible excitation and emission, which functions as an internal reference. The photophysical and thermodynamic properties of sensors reported in this thesis are listed in the summary table on page 168.

Ideally, the sensor dissociation constant should approximate the median concentration of analyte under study, and the wide range of biological Zn^{2+} concentrations makes desirable a variety of probe affinities. The dissociation constants of ZP1-based sensors fall within a relatively narrow subnanomolar range. Modulation of

binding units, and thereby affinity, has been explored to some extent, as described in Appendices 1 and 2, but these efforts have not yielded effective sensors. The approaches reported here are relatively modular, however, and may be applied to other intensity-based probes in order to address this issue.

Summary Table of Sensor Properties

Compound name	ϵ ($M^{-1}cm^{-1}$)	λ_{max} (nm) Absorbance	Φ_{ZP1}	$\Phi_{Coumarin}$	K_d (nM)	pK _a	ZP1: Coumarin Fluorescence ratio
2.4a ZP1(6-CO ₂ H) + Zn ²⁺	76000	516	0.21		0.16	7.12	
	81000	506	0.63				
2.4b ZP1(5-CO ₂ H) + Zn ²⁺	81000	520	0.17		0.22	7.05	
	88000	509	0.62				
2.5a ZP1(6-CO ₂ Et) + Zn ²⁺	61000	519	0.13		0.37	7.00	
	72000	509	0.67				
2.5b ZP1(5-CO ₂ Et) + Zn ²⁺	66000	517	0.14		0.26	6.98	
	71000	506	0.58				
3.1 CZ1 + Zn ²⁺	37200	451,	0.02	0.01	0.25		0.5
	38600	526					
	41000	449,	0.04	0.01			4.0
3.2 CZ2 + Zn ²⁺	38100	518					
	26000	450,	0.02	0.01			0.6
	22400	526					
3.4 + Zn ²⁺	26567	448,	0.04	0.01			2.0
	24333	521					
	62000	519	0.22		0.25		
3.13 + Zn ²⁺	65000	509	0.69				
	71100	518	0.21		0.20	8.43	
4.11 + Zn ²⁺	78600	508	0.67				
	9900	452,	0.18	0.11			20
	20000	518					
	11000	448(sh),	0.40	0.25			38
	22000	510					

Appendix 1 Isomerically Specific Approaches to Other Substituted Fluorophores[†]

Introduction[†]

The previous chapters have dealt with sensors based on 2',7'-dichlorofluorescein carboxylates. In addition to this platform, approaches to fluorescein sulfonamides, carboxylate-substituted rhodamines, and carboxylate-substituted rhodafluors and asymmetric fluoresceins have been explored. Sulfonamides are a relatively common binding motif for Zn^{2+} , and have formed the basis for several Zn^{2+} sensing approaches, such as the quinoline sulfonamide (TSQ) family of sensors,¹⁻⁴ macrocyclic scorpionate complexes,^{5,6} and carbonic anhydrase-based sensing systems.⁷⁻¹² We considered that a fluorescein-based sulfonamide might represent an interesting target for Zn^{2+} sensing. Chapter 4 has dealt with applications of carboxy rhodamines, among other fluorophores. Carboxylate-substituted rhodamines form by acid-catalyzed condensation of the appropriate 3-aminophenol with 1,2,4-benzenetricarboxylic acid, a reaction analogous to the fluorescein condensation. Like the fluorescein condensation, this reaction affords the desired product as an equal mixture of two isomers; however, unlike fluorescein carboxylate isomeric mixtures,^{13,14} there is no general reported method of separating the two isomers by crystallization. Chromatographic separation of isomers is particularly tedious with these polar, charged compounds. Finally, asymmetrically substituted fluoresceins¹⁵⁻¹⁸ and various hybrid rhodamine-fluorescein compounds,¹⁹⁻²¹ termed "rhodafluors", have been prepared by our group. These compounds share a 2',4'-dihydroxybenzophenone-2-carboxylate as a synthon, but the preparation of isomerically pure dicarboxy-substituted analogues of these benzophenones has not been reported. In

[†] Respective Contributions were as follows: Crystal structures were solved by Weiming Bu and Mi Hee Lim.

this chapter, we describe methodology to prepare isomerically pure carboxylate- or sulfonate-substituted analogues of these fluorophores.

Experimental

Materials and Methods.

Reagents were obtained from Aldrich, except for 4-sulfophthalic acid, which was obtained from Lancaster, and palladium dibenzylideneacetone, sodium *tert*-butoxide, and 2'-dimethylamino-2-dicyclohexyl-phosphinobiphenyl, which were obtained from Strem. 4-Sulforesorcinol was prepared as previously described.²² The synthesis of 3',6-diacetyl-2',7'-dichlorofluorescein-5(6)-carboxylates were described in Chapter 2. ¹H and ¹³C NMR spectra were acquired on a 300 or 500 MHz Varian or 400 MHz Bruker instrument. HRMS data were acquired by personnel at the MIT DCIF. Low-resolution electrospray mass spectra were acquired on an Agilent Technologies 1100 Series LCMS. Crystals for X-ray crystallography were covered with Infineum V8512 (formerly called Paratone N oil) and mounted on a quartz fiber. Data were collected by using a Bruker CCD X-ray diffractometer with Mo K α radiation ($\lambda = 0.71073 \text{ \AA}$) using the SMART software package²³ and corrected for absorption using the SADABS program.²⁴ Data were integrated using the SAINTPLUS software package,²⁵ and structures were solved and refined using SHELXTL.²⁶ Procedures for data collection and structural work have been reported in detail elsewhere.²⁷

Synthetic Procedures

Condensation of 4-Sulforesorcinol with Phthalic Anhydride. 4-Sulforesorcinol (424 mg, 2 mmol) was ground together with phthalic anhydride (148 mg, 1 mmol) and ZnCl₂

(41 mg, 0.3 mmol) with a mortar and pestle, and the resulting mixture was heated in a 190 °C oil bath for 30 min. Water and MeOH were added and the resulting solution was extracted with 3 x 20 mL portions of CH₂Cl₂. The combined organic layers were washed with 1 x 20 mL of brine, dried over MgSO₄, and evaporated to afford a dark orange-brown solid residue. ¹H NMR analysis indicated unsubstituted fluorescein as the major product. ¹H NMR (MeOH-d₄): δ 8.05 (dd, 1 H); 7.77 (td, 1 H); 7.70 (td, 1 H); 7.21 (dd, 1 H); 6.70 (d, 2 H); 6.60 (d, 2 H); 6.54 (dd, 2 H).

Fluorescein-5(6)-Sulfonic Acid (1). A 1.14-mL portion of a 50% aqueous solution of 4-sulfophthalic acid (0.736 g, 3 mmol, 80% pure) was neutralized with potassium hydroxide (45% w/v in water) and the solvent was evaporated to give a purple semi-solid residue, which was combined with resorcinol (0.661 g, 6 mmol) in 6 mL of methanesulfonic acid. The reaction mixture was stirred in an 85 °C oil bath for 18 h, then poured into 40 mL of H₂O. A reddish-brown precipitate was filtered and dried under vacuum to afford 696 mg of a brown powder (71% yield), which was carried on without further purification. ¹H NMR (MeOH-d₄): δ 8.81 (s, 1 H); 8.46 (d, 1 H); 8.23-8.30 (m, 2 H); 7.84 (d, 1 H); 7.5 (d, 1 H); 7.5 (s, 2 H); 7.46 (s, 2 H); 7.36 (dd, 4 H); 7.2 (m, 4 H).

Diisopropylethylammonium Salt of 3',6'-Dipivaloylfluorescein-6-Sulfonate (2a). Fluorescein-5(6)-sulfonic acid (9.08 g, 22 mmol) was dissolved in 35 mL of trimethylacetic anhydride, 17.5 mL of diisopropylethylamine, and 30 mL of DMF. The solution was heated to reflux for 4 h and then quenched by addition of ethanol. The solvents were removed on the rotary evaporator and the resulting light brown viscous oil was taken up in 200 mL of CH₂Cl₂ and 400 mL of ethyl acetate, and washed with 3 x 300 mL of 1 M phosphate buffer (pH 7.0). The organic phase was dried over MgSO₄ and

evaporated. Diethyl ether was added, and a heavy fine precipitate formed. The filtered solid was recrystallized from dichloromethane and diethyl ether to give 2.10 g (13.5%) of fluorescein 6-sulfonic acid dipivaloate diisopropylethylammonium salt. ^1H NMR (CDCl_3): δ 9.00 (br s, 1 H); 8.17 (d, 1 H); 8.04 (d, 1 H); 7.64 (s, 1 H); 7.04 (d, 2 H); 6.84 (d, 2 H); 6.76 (dd, 2 H); 3.60 (m, 2 H); δ 3.03 (m, 2 H); 1.36 (s, 18 H); 1.30-1.34 (m, 15 H). HRMS(M-H): Calcd for $\text{C}_{30}\text{H}_{27}\text{O}_{10}\text{S}$: 579.1325; Found 579.1330.

Diisopropylethylammonium Salt of 3',6'-Dipivaloylfluorescein-5-Sulfonate (2b). The filtrate from **2a** was allowed to stand at room temperature overnight, and the resulting light yellow crystals were filtered to give 0.91 g (5.8% overall) of the diisopropylethylammonium salt of fluorescein 5-sulfonic acid dipivaloate. ^1H NMR (CDCl_3): δ 9.25 (br s, 1 H); 8.33 (s, 1 H); 8.06 (d, 1 H); 6.97 (d, 1 H); 6.86 (d, 2 H); 6.61 (d, 2 H); 6.56 (dd, 2 H); 3.56 (m, 2 H); 2.98 (m, 2 H); 1.35 (m, 9 H); 1.26 (d, 6 H); 1.17 (s, 18 H). Continued fractional crystallization brought the final yields to 3.31 g, 21% for the 6-isomer; and 1.59 g, 10.1% for the 5-isomer.

Optimized Purification of Diisopropylethylammonium Salt of 3',6'-Dipivaloylfluorescein-6-Sulfonate (2a). Fluorescein 5(6)-sulfonic acid (6.20 g, 15 mmol) was combined with trimethylacetic anhydride (35 mL) and diisopropylethylamine (18 mL) in dimethylformamide (20 mL) and heated to reflux 4 h. The reaction was allowed to cool, then taken up in 200 mL of CH_2Cl_2 and 400 mL of ethyl acetate. The organic solution was washed with 3 x 300 mL of phosphate buffer (1 M, pH 7.0), dried over MgSO_4 , evaporated, and the resulting residue was crystallized from diethyl ether and CH_2Cl_2 at -25 °C overnight. Filtration gave 2.49 g (23.4%) of the desired product. The mother

liquor was placed in the freezer and a second crop of crystals was obtained (800 mg) for a total yield of 3.29 g (31% overall).

Fluorescein 6-Sulfonic Acid (3a). 3',6'-Dipivaloylfluorescein 6-sulfonic acid diisopropylethylammonium salt (177 mg, 0.25 mmol) was dissolved in 10 mL of 50:50 v/v ethanol/H₂O. Potassium hydroxide was added (0.40 g) and the reaction was heated to reflux overnight. The ethanol was then removed under reduced pressure, the dark red solution was acidified, and the resulting orange precipitate (71 mg, 69%) was collected by filtration and dried overnight. ¹H NMR (DMSO-d₆): δ 7.95 (d, 1 H); 7.87 (d, 1 H); 7.25 (s, 1 H); 6.70 (s, 2 H); 6.55-6.62 (m, 4 H). IR: 3400-2500 cm⁻¹ (br, s), 1707 cm⁻¹ (m), 1638 cm⁻¹ (m), 1603 cm⁻¹ (s), 1457 cm⁻¹ (s), 1314-1122 cm⁻¹ (br, s), 1037 cm⁻¹ (s). HRMS(M+H): Calcd for C₂₀H₁₃O₈S: 413.0331; Found 413.0320. The acidic filtrate obtained was allowed to stand at RT for two weeks, at the end of which time small bright-orange X-ray quality crystals of **3a** had formed.

3',6'-Dichlorofluoran-6-Sulfonyl Chloride (4a). Fluorescein 6-sulfonic acid (412 mg, 1 mmol) was added to thionyl chloride (2.6 mL, 6 g, 5 mmol) and dimethylformamide (6 mg, 6 μL, 82 μmol) and the reaction was heated to reflux under Ar for 4 h. The resulting solution was poured into 150 mL of stirred ice water and stirred for an additional 10 min. The yellow grainy solid obtained was lyophilized to give a final mass of 360 mg (87% yield). ¹H NMR (DMSO-d₆): δ 8.02 (d, 1 H); 6.94 (d, 2 H); 7.92 (d, 1 H); 7.58 (s, 2 H); 7.39 (s, 1 H); 7.22 (d, 2 H). FTIR(KBr, cm⁻¹): 3422 (br, m), 1777 (s), 1599 (m), 1566 (w), 1482 (m), 1411 (s), 1266-1060 (br, s), 955 (m).

Fluorescein 5-Sulfonic Acid (3b). 3',6'-Dipivaloylfluorescein 5-sulfonic acid diisopropylethyl ammonium salt (1.42 g, 2 mmol) and potassium hydroxide (3.2 g) were

dissolved in 30 mL of 50:50 v/v ethanol/H₂O and heated to reflux overnight. The ethanol was removed under reduced pressure, and the aqueous solution was acidified with concentrated HCl, causing the product to precipitate. Filtration and drying overnight afforded the desired product as 696 mg (84%) of a yellow solid. ¹H NMR (DMSO-d₆) δ 8.06 (s, 1 H); 7.98 (d, 1 H); 7.22 (d, 1 H); 6.67 (d, 2 H); 6.60 (d, 2 H); 6.55 (dd, 2 H). FTIR(KBr, cm⁻¹): 3500-2500 (br, s), 1714 (s), 1639-1538 (br, s) 1463 (s), 1383 (m), 1326 (s), 1220-1126 (s), 1039 (m). HRMS(M-H): Calcd for C₂₀H₁₁O₈S: 411.0175; Found 411.0155.

3',6'-Dichlorofluoran-5-Sulfonyl Chloride (4b). Fluorescein 5-sulfonic acid (618 mg, 1.5 mmol) was combined with thionyl chloride (4 mL) and dimethylformamide (10 μL) and heated to reflux for 4 h. The reaction was poured into 150 mL of stirred ice water, affording a dark yellow solid that was filtered and lyophilized to give a final mass of 549 mg (82% yield). ¹H NMR (DMSO-d₆): δ 8.10 (s, 1 H); 8.00 (d, 1 H); 7.58 (d, 2 H); 7.33 (d, 1 H); 7.20 (dd, 2 H); 6.95 (d, 2 H). IR: 3091 cm⁻¹ (br, w), 1779 cm⁻¹ (s), 1599 cm⁻¹ (s), 1564 cm⁻¹ (s), 1481 cm⁻¹ (s), 1425-1384 cm⁻¹ (br, s), 1318 cm⁻¹ (m), 1251-1083 cm⁻¹ (br, m), 954 cm⁻¹ (s). HRMS(M-Cl + OH): Calcd for C₂₀H₉Cl₂O₆S: 446.9497; Found 446.9503.

3', 6'-Dichlorofluoran-6-Sulfonamido-2-Methylpyridine (5a). 3',6'-Dichlorofluoran-6-sulfonyl chloride (**4a**, 86 mg, 0.2 mmol) was dissolved in 15 mL of CH₂Cl₂ and added dropwise to a stirred suspension of 2-aminomethylpyridine (43 mg, 0.4 mmol) and NaHCO₃ (84 mg, 1 mmol) in CH₂Cl₂. After stirring overnight, the reaction suspension was filtered and evaporated; the product was purified by flash chromatography on silica gel (10 mm x 17 cm) eluting with 9:1 CHCl₃:MeOH, and then recrystallized from

methanol to give 30 mg (30%) of an off-white powder. ^1H NMR (DMSO- d_6): δ 8.59 (t, 1 H), 8.31 (m, 1 H), 8.20 (d, 1 H), 8.08 (dd, 1 H), 7.76 (s, 1 H), 7.66 (td, 1 H), 7.61 (d, 2 H), 7.15-7.26 (m, 3 H), 6.91 (d, 2 H), 4.12 (d, 2 H). X-ray quality crystals were obtained by slow evaporation of a saturated acetonitrile solution of **5a** at RT over 2 d.

3',6'-Divaloylfluorescein-6-Sulfonyl Chloride (6). 3',6'-Divaloylfluorescein-6-sulfonate diisopropylethylammonium salt (708 mg, 1 mmol) was stirred in 10 mL of ethyl acetate (dried over MgSO_4) in an ice bath. Oxalyl chloride (1 mL of 2 M solution in CH_2Cl_2) was added, followed by 200 μL of DMF. The ice bath was removed, and the reaction was stirred for 16 h. The reaction was then placed on ice and quenched with 10 mL of H_2O . The layers were separated, and the organic layer was washed with 1 x 10 mL H_2O and 1 x 10 mL brine, dried, and evaporated to give a yellow solid residue. ^1H NMR (CDCl_3): δ 8.68 (s, 1 H); 8.31 (d, 1 H); 7.45 (d, 1 H); 7.18 (s, 2 H); 6.84 (s, 2 H); 1.37 (s, 18 H). HRMS(M+H): Calcd for $\text{C}_{30}\text{H}_{28}\text{ClO}_9\text{S}$: 599.1143; Found 599.1114

6-Fluoresceinsulfonamido-2-Methylpyridine (7). The product from **5** was dissolved in 20 mL of CHCl_3 and stirred in an ice bath. 2-Aminomethylpyridine (300 μL) was added and the reaction was stirred overnight. The reaction was then extracted with 2 x 20 mL of H_2O , the combined aqueous layers were washed with 1 x 20 mL CHCl_3 , concentrated on the rotary evaporator to 5 mL, and the bright red viscous solution was acidified with 2 mL of 1 N HCl. The resulting yellow precipitate was filtered and the resulting solid (485 mg) was chromatographed on silica (20 mm x 16 cm), eluting with 89:10:1 CHCl_3 :MeOH: AcOH. The desired product (43 mg, 8.5%) was isolated as a bright yellow-orange solid. ^1H NMR (MeOH- d_4): δ 8.38 (m, 2 H); 8.09 (dd, 1 H); 7.74 (td, 1 H); 7.43 (d, 1 H); 7.30 (d, 1 H); 7.23 (m, 1 H); 6.69 (s, 2 H); 6.60 (s, 4 H); 4.35 (s, 2 H).

HRMS(M+H): Calcd for $C_{26}H_{19}N_2O_7S$: 503.0913; Found 503.0912. The dipivaloyl-protected sulfonamide product **8** was also isolated from the organic reaction extract by flash chromatography on silica eluted with 94:6 $CHCl_3$:MeOH. 1H NMR ($CDCl_3$): δ 8.42 (d, 2 H); 8.05 (dd, 1 H); 7.61 (td, 1 H); 7.12-7.19 (m, 3 H); 7.05 (d, 2 H); 6.84 (br t, 1 H); 6.79 (dd, 2 H); 6.69 (d, 2 H). HRMS (M+H): Calcd for $C_{36}H_{35}N_2O_9S$: 671.2063; Found 671.2071.

3',6'-Dibromofluoran (9). 3-Bromophenol (1.73 g, 10 mmol) and phthalic anhydride (740 mg, 5 mmol) were combined in 5 mL of methanesulfonic acid and heated in a 140 °C oil bath for 16 h. The reaction was poured into 120 mL of stirred ice water, stirred 20 min, and then filtered. The resulting damp gray solid was taken up in $CHCl_3$ and filtered through a short plug of silica gel, evaporated, and recrystallized from CH_2Cl_2 and MeOH to afford the desired product as 990 mg of off-white crystals (43% yield). 1H NMR($CDCl_3$): δ 8.05 (dd, 1 H); 7.70 (td, 1 H); 7.65 (td, 1 H); 7.50 (d, 2 H); 7.20 (dd, 2 H); 7.14 (dd, 1 H); 6.71 (d, 2 H). ^{13}C NMR($CDCl_3$): δ 169.40, 153.18, 151.53, 135.88, 130.65, 129.64, 127.92, 126.17, 125.85, 124.61, 124.07, 120.80, 118.31, 81.52. HRMS(M+H): Calcd for $C_{20}H_{11}Br_2O_3$: 456.9075; Found 456.9084.

3',6'-Pyrrolidinorhodamine (10)-Method A. 3',6'-Dibromofluoran (46 mg, 0.1 mmol) was combined with $ZnCl_2$ (68 mg, 0.5 mmol) and pyrrolidine (83 μ L, 71 mg, 1 mmol) and heated in a 170 °C oil bath for 4 h. The reaction was removed from heat, and allowed to cool. Water and concentrated HCl were added; the suspension was stirred, filtered, and the solid was washed twice with dilute HCl to afford a purple solid (42 mg, 95% yield). 1H NMR(MeOH- d_4): δ 8.34 (d, 1 H); 7.81 (m, 2 H); 7.41 (d, 1 H); 7.12 (d, 2 H); 6.90

(dd, 2 H); 6.82 (d, 2 H); 3.61 (m, 8 H); 2.14 (m, 8 H). MS (M+H): Calcd for $C_{28}H_{27}N_2O_3$: 439.2; Found 439.4.

3',6'-Pyrrolidinofluoran (10)-Method B. 3',6'-Dibromofluoran (229 mg, 0.5 mmol) was combined with palladium dibenzylideneacetone (11.5 mg, 0.0125 mmol; 0.025 mmol Pd), sodium *tert*-butoxide (101 mg, 1.05 mmol), and 2'-dimethylamino-2-dicyclohexylphosphinobiphenyl (10.3 mg, 0.025 mmol) in a thick-walled tube fitted with a rubber septum. The tube was thrice evacuated and back-filled with N_2 , and 1.5 mL of dry toluene was added, followed by 90 μ L (77 mg, 1.08 mmol) of pyrrolidine. The septum was replaced with a Teflon screw cap and the reaction was stirred in an 80 °C oil bath for 15 h, then removed from heat and allowed to cool. Hexanes were added to the purple slurry, and a purple solid was isolated by filtration (350 mg, wet.) LCMS and 1H NMR analysis of the solid supported a single product identical to those produced by method A.

Pyridinium Salt of 3',6'-Dibromo-6-Carboxyfluoran (11c). 3-Bromophenol (3.46 g, 20 mmol) and 1, 2, 4-benzenetricarboxylic acid (2.10 g, 10 mmol) were combined in 10 mL of methanesulfonic acid and heated in a 140 °C oil bath for 3 d. The reaction was poured into 200 mL of stirred ice water, stirred vigorously with warming for 30 min, and then filtered to yield a greenish solid which was dried in air to give 3.83 g of **11a** and **11b** as a mixture of isomers. Crystallization from 30 mL of acetic anhydride and 10 mL of pyridine afforded 1.35 g of white solid, which was recrystallized from 2:1 Ac_2O :pyridine to furnish the desired compound **11c** as 1.07 g (18%) of fine white crystals. 1H NMR(DMSO- d_6): δ 8.58 (m, 2 H); 8.25 (dd, 1 H); 8.16 (d, 1 H); 7.86 (d, 1 H); 7.76 (tt, 1 H); 7.71 (d, 2 H); 7.39 (m, 2 H); 7.33 (dd, 2 H); 6.87 (d, 2 H). HRMS(M-H): Calcd for $C_{21}H_9Br_2O_5$: 498.8817; Found 498.8804.

3',6'-Dibromo-5-Carboxyfluoran (11b). The filtrate from the initial crystallization of 11c was concentrated and recrystallized from pyridine to afford 906 mg of an off-white solid. Further recrystallization from CHCl_3 :MeOH afforded the desired product as 571 mg of white crystals (11.4% yield). $^1\text{H NMR}(\text{DMSO-}d_6)$: δ 8.44 (d, 1 H); 8.31 (dd, 1 H); 7.72 (d, 2 H); 7.51 (d, 1 H); 7.34 (dd, 2 H); 6.90 (d, 2 H).

3',6'-Dipyrrolidino-6-Carboxyrhodamine (12). 3',6'-Dibromo-6-carboxyfluoran (116 mg, 0.2 mmol) was combined with ZnCl_2 (136 mg, 1 mmol) and pyrrolidine (332 μL , 5 mmol) and heated in a 140 °C oil bath for 4 h. The dark purple residue was dissolved in 15 mL of concentrated HCl, and the resulting dark red solution was filtered and then diluted with 30 mL of H_2O , allowed to stand at RT for two hours, and filtered to yield 98 mg (94%) of the desired product HCl salt. $^1\text{H NMR}(\text{MeOH-}d_4)$: δ 8.42 (d, 1 H); 8.39 (d, 1 H); 7.98 (s, 1 H); 7.11 (d, 2 H); 6.94 (d, 2 H); 6.84 (s, 2 H); 3.62 (br s, 8 H); 2.14 (s, 8 H). HRMS(M-H): Calcd for $\text{C}_{29}\text{H}_{25}\text{N}_2\text{O}_5$: 481.1763; Found 481.1744.

2, 5-Dicarboxy-5'-Chloro-2',4'-Dihydroxybenzophenone (14a). 3',6'-Diacetyl-2',7'-dichlorofluorescein-6-carboxylic acid pyridinium salt (2.44 g, 4 mmol) was suspended in 60 mL of 50% aqueous NaOH (w/v) and heated at 165 °C for 60 min. The reaction was removed from the heating bath, poured into 400 mL of cold H_2O , acidified with conc HCl, and allowed to stand at RT for two hours. The suspension was filtered, and the pale yellow solid was taken up in MeOH, filtered to remove residual NaCl, and evaporated to afford 1.19 g of the desired product (89% yield). $^1\text{H NMR}(\text{MeOH-}d_4)$: δ 8.20 (m, 2 H); 7.98 (s, 1 H); 6.97 (s, 1 H); 6.49 (s, 1 H). $^{13}\text{C NMR}(\text{MeOH-}d_4)$: δ 201.18, 168.00, 167.96, 164.79, 161.97, 141.57, 135.70, 134.58, 134.46, 132.09, 132.00, 129.58, 115.42, 113.53, 105.01.

2, 4-Dicarboxy-5'-Chloro-2',4'-Dihydroxybenzophenone (14b). 3',6'-Diacetyl-2',7'-dichlorofluorescein-5-carboxylic acid (2.12 g, 4 mmol) was suspended in 60 mL of 50% aqueous NaOH (w/v) and heated at 165 °C for 60 min. The reaction was removed from heat, poured into 400 mL of cold H₂O, acidified with conc HCl, and allowed to stand at RT overnight. The suspension was filtered, and the dirty-brown solid was resuspended in 50 mL of H₂O, stirred, and filtered again. The resulting solid was then taken up in MeOH, filtered to remove residual NaCl, and evaporated to afford 1.14 g of the desired product (85% yield). ¹H NMR(MeOH-d₄): δ 8.72 (s, 1 H); 8.34 (d, 1 H); 7.51 (d, 1 H); 6.95 (s, 1 H); 6.49 (s, 1 H). ¹³C NMR(CDCl₃): δ 201.36, 168.11, 167.86, 164.78, 162.03, 145.24, 134.66, 134.59, 133.77, 132.91, 131.19, 129.09, 115.37, 113.56, 104.95. HRMS(M-H): Calcd for C₁₅H₈ClO₇: 334.9959; Found 334.9944.

6-Carboxy-2'-Chloroseminaphthofluorescein (15). 1,6-Dihydroxynaphthofluorescein (24 mg, 0.15 mmol) was combined with benzophenone **14a** (34 mg, 0.1 mmol) in 200 μL of methanesulfonic acid in a 180 °C oil bath. After 14 h, 5 mL of H₂O was added and the resulting suspension was filtered and washed twice with H₂O. The resulting purple solid was dissolved in MeOH, the solution was filtered, and H₂O was added to the filtrate to induce precipitation. The product was collected by filtration and dried in air to give 42 mg (91%) of the desired compound. ¹H NMR (DMSO-d₆): δ 11.2 (br s, 1 H); 10.2 (br s, 1 H); 8.40 (d, 1 H); 8.24 (d, 1 H); 8.16 (d, 1 H); 7.72 (s, 1 H); 7.38 (d, 1 H); 7.27 (d, 1 H); 7.15 (s, 1 H); 7.14 (s, 1 H); 6.91 (s, 1 H); 6.62 (s, 1 H). MS(M-H): Calcd for C₂₅H₁₂ClO₇: 459.0; Found 459.0.

Results and Discussion

Fluorescein Sulfonamides

In the synthesis of fluorescein sulfonamides, sulfonation of the xanthene system was considered most likely to afford a derivative that would exhibit a Zn^{2+} -induced change in fluorescence. Direct sulfonation of unsubstituted fluorescein with fuming sulfuric acid provided only unreacted starting material. Reaction of sulfonated resorcinol with phthalic anhydride provided unsubstituted fluorescein as the major product (Scheme A1.1). Hence, condensation of resorcinol with 4-sulfophthalic acid was explored. As with benzenetricarboxylic acid, this reaction produced a mixture of two isomers (**1**) in roughly equal amounts.^{28,29} The mixture could be separated by protection as the dipivaloyl esters and subsequent crystallization of the 6-isomer **2a** followed by crystallization of the 5-isomer **2b**, each as its diisopropylethylammonium salt. Basic hydrolysis of **2a, b** yielded the deprotected fluorescein sulfonic acids **3a, b**. A crystal structure of fluorescein-6-sulfonic acid (**3a**) was obtained and is shown in Figure A1.1. The crystal formed under strongly acidic conditions and consequently the fluorescein is in the lactone-opened form, presumably with a positive charge conjugated over the xanthene system. The C-O bonds of the phenolic hydroxyls are approximately the same length (1.34, 1.33) and are each consistent with a single bond, rather than a ketone tautomer. Three solvent molecules are included in the unit cell. Crystallographic parameters for all crystal structures are listed in Table A1.1, and bond lengths and angles for **3a** are listed in Table A1.2.

Coupling of the sulfonic acids with amines was first attempted following activation with thionyl chloride (Scheme A1.2); however, reaction of both protected and

unprotected fluoresceins under these conditions gave a non-fluorescent material **4a, b**, which was determined to be the 3', 6'-dichlorofluoran by X-ray crystallographic analysis of the 2-picolyamine adduct **5a** (Figure A1.2, bond lengths and angles listed in Table A1.3). Use of the milder oxalyl chloride as an activating agent to generate sulfonyl chloride **6** and subsequent reaction with an amine affords the desired sulfonamide product as a mixture of unprotected (**7**) and protected (**8**) material (Scheme A1.3).

Rhodamines and Rhodamine Carboxylates

The conversion of 3',6'-dichlorofluoran into rhodamines by direct ZnCl₂-catalyzed condensation with excess amine has been reported.^{30,31} This reaction suggested that, since 3',6'-dihalofluorans are quite similar to 3',6'-diacetyl- or dipivaloyl-fluorescein in that both types of compounds contain the basic fluorescein motif that has been trapped in the lactone form, it might be possible to separate 3',6'-dihalofluoran-5(6)-carboxylates by selective crystallization, similar to the resolution of 2',7'-dichlorofluorescein-5(6)-carboxylates. Alternatively, reaction of previously resolved fluorescein carboxylates with thionyl chloride or thionyl bromide could provide the desired isomerically pure dihalofluoran carbonyl halide (vide supra).

We chose to work with the more reactive dibromofluoran species, rather than the reported dichlorofluoran substrate. 3',6'-Dibromofluoran **9** was synthesized by acid-catalyzed condensation of bromophenol with phthalic anhydride and used as a model for the less readily available dibromofluoran carboxylates. 3',6'-Dibromofluoran reacted smoothly with excess pyrrolidine under literature conditions to afford the desired rhodamine **10**. Palladium-catalyzed reductive coupling under reaction conditions described by Buchwald and co-workers³² also furnished the same product. This work is

summarized in Scheme A1.4. Reaction of **9** with a single equivalent of pyrrolidine under Buchwald conditions gave primarily a mixture of rhodamine and starting material, with the monoamine adduct formed as a minor product. Dibromofluoran **9** is more soluble in chlorinated hydrocarbon solvents, but use of dichloroethane as the reaction solvent did not improve the yield of monoadduct.

3',6'-Dibromo-5(6)-carboxylate (**11a,b**) was synthesized similarly. Selective crystallization from pyridine and acetic anhydride afforded the pure 6-isomer pyridinium salt **11c** in 15% yield, and further recrystallization of the mother liquor furnished the pure 5-isomer **11b** in 11% yield. Unsurprisingly, Buchwald coupling conditions were not compatible with a carboxylate-containing substrate. Nevertheless, heating **11c** at 140 °C with 5 equiv of ZnCl₂ and 10 equiv of pyrrolidine, followed by treatment with hydrochloric acid, furnished the desired rhodamine **12** in > 80% yield with no apparent mixing of isomers. The strongly acidic workup is necessary in order to hydrolyze any amide byproduct that arises from carboxylate-amine condensation. The harsh conditions required for the reaction preclude the use of all but the most robust amines in the condensation.

Toward Isomerically Pure Asymmetric Fluorescein or Rhodafluor Carboxylates

The syntheses of ZP1 sensors containing a carboxylate or an amide functionality have been described in previous chapters. To date, no such methodology exists for preparing similarly functionalized ZP4 sensors. In the synthesis of a ratiometric probe containing two fluorophores, a single Zn²⁺-binding site would be ideal. The probe Quinonin-1,³³ with micromolar affinity and vastly improved dynamic range, is a prime target for further functionalization. We therefore turned our attention to the synthesis of

dihydroxydicarboxybenzophenones, which would be the logical starting material for the synthesis of asymmetric carboxylate-containing fluoresceins. Although subjecting 1,2,4-benzenetricarboxylic acid to aluminum chloride-catalyzed condensation with 4-chlororesorcinol³⁴ resulted in quantitative recovery of starting material, the hydrolysis of previously-resolved fluorescein carboxylates **13a** and **b** under harshly basic conditions furnished the desired benzophenone **14a, b** as isomerically pure compounds. The hydrolysis of dichlorofluorescein-5(6)-carboxylate to give **14a** and **14b** as a mixture and subsequent condensation with 3-aminophenols has been reported,³⁵ but the potential mixing of isomers during the fluorescein condensation has not been explored. Preliminary results from condensation of **14a** with 1,6-dihydroxynaphthalene indicate that seminaphthofluorescein **15** can be obtained in excellent yield with no apparent scrambling of isomers.

Conclusions

We describe here the synthesis and separation of fluorescein 5(6)-sulfonic acid. Oxalyl chloride activation of the separated isomers affords the fluorescein sulfonyl chloride, whereas thionyl chloride converts the phenolic hydroxyls to chlorine atoms. Such dihalofluorans may also be synthesized by acid-catalyzed condensation of 3-halophenol with phthalic anhydride or analogues, and can be converted to rhodamines via Lewis acid- or palladium-catalyzed reaction with simple amines. Carboxylate-substituted dihalo-fluorans are similar to diacetyl- or dipivaloyl-fluoresceins in that they are formed as a mixture of isomers, are trapped in lactone form, and may be readily separated by fractional crystallization. This methodology can be applied as a route to isomerically pure carboxylate-substituted rhodamines. Strongly basic hydrolysis of previously resolved

fluorescein carboxylates affords the appropriate synthon for isomerically pure asymmetric fluorescein or rhodafluor carboxylates.

Acknowledgements

This work was supported by the McKnight Foundation for the Neurosciences, by NIGMS (GM65519 to S. J. L.) and by Merck/MIT (predoctoral fellowship to C. C. W.) We thank Matthew A. Clark for helpful synthetic discussions with regard to the rhodamine and rhodafluor carboxylate work, and Weiming Bu and Mi Hee Lim for solving crystal structures.

References

- (1) Frederickson, C. J.; Kasarskis, E. J.; Ringo, D.; Frederickson, R. E. A quinoline fluorescence method for visualizing and assaying the histochemically reactive zinc (bouton zinc) in the brain. *J. Neurosci. Methods* **1987**, *20*, 91-103.
- (2) Fahrni, C. J.; O'Halloran, T. V. Aqueous Coordination Chemistry of Quinoline-Based Fluorescence Probes for the Biological Chemistry of Zinc. *J. Am. Chem. Soc.* **1999**, *121*, 11448-11458.
- (3) Nasir, M. S.; Fahrni, C. J.; Suhy, D. A.; Kolodsick, K. J.; Singer, C. P.; O'Halloran, T. V. The chemical cell biology of zinc: structure and intracellular fluorescence of a zinc-quinolinesulfonamide complex. *J. Biol. Inorg. Chem.* **1999**, *4*, 775-783.
- (4) Zalewski, P. D.; Millard, S. H.; Forbes, I. J.; Kapaniris, O.; Slavotinek, A.; Betts, W. H.; Ward, A. D.; Lincoln, S. F.; Mahadevan, I. Video Image Analysis of Labile Zinc in Viable Pancreatic Islet Cells Using a Specific Fluorescent Probe for Zinc. *J. Histochem. Cytochem.* **1994**, *42*, 877-884.

- (5) Koike, T.; Watanabe, T.; Aoki, S.; Kimura, E.; Shiro, M. A Novel Biomimetic Zinc(II)-Fluorophore, Dansylamidoethyl-Pendant Macrocyclic Tetraamine 1,4,7,10-Tetraazacyclododecane (Cyclen). *J. Am. Chem. Soc.* **1996**, *118*, 12696-12703.
- (6) Koike, T.; Abe, T.; Takahashi, M.; Ohtani, K.; Kimura, E.; Shiro, M. Synthesis and characterization of the zinc(II)-fluorophore, 5-dimethylaminonaphthalene-1-sulfonic acid [2-(1,5,9-triazacyclododec-1-yl)ethyl]amide and its zinc(II) complex. *J. Chem. Soc. Dalton Trans.* **2002**, 1764-1768.
- (7) Chen, R. F.; Kernohan, J. C. Combination of Bovine Carbonic Anhydrase with a Fluorescent Sulfonamide. *J. Biol. Chem.* **1967**, *242*, 5813-5823.
- (8) Thompson, R. B.; Cramer, M. L.; Bozym, R.; Fierke, C. A. Excitation ratiometric fluorescent biosensor for zinc ion at picomolar levels. *J. Biomed. Opt.* **2002**, *7*, 555-560.
- (9) Thompson, R. B.; Maliwal, B. P.; Zeng, H.-H. Zinc biosensing with multiphoton excitation using carbonic anhydrase and improved fluorophores. *J. Biomed. Opt.* **2000**, *5*, 17-22.
- (10) Thompson, R. B.; Whetsell Jr., W. O.; Maliwal, B. P.; Fierke, C. A.; Frederickson, C. J. Fluorescence microscopy of stimulated Zn(II) release from organotypic cultures of mammalian hippocampus using a carbonic anhydrase-based biosensor system. *J. Neurosci. Meth.* **2000**, *96*, 35-45.
- (11) Thompson, R. B.; Jones, E. R. Enzyme-Based Fiber Optic Zinc Biosensor. *Anal. Chem.* **1993**, *65*, 730-734.

- (12) Fierke, C. A.; Thompson, R. B. Fluorescence-based biosensing of zinc using carbonic anhydrase. *BioMetals* **2001**, *14*, 205-222.
 - (13) Rossi, F. M.; Kao, J. P. Y. Practical Method for the Multigram Separation of the 5- and 6-Isomers of Carboxyfluorescein. *Bioconj. Chem.* **1997**, *8*, 495-497.
 - (14) Sun, W. C.; Gee, K. R.; Klaubert, D. H.; Haugland, R. P. Synthesis of Fluorinated Fluoresceins. *J. Org. Chem.* **1997**, *62*, 6469-6475.
 - (15) Burdette, S. C.; Frederickson, C. J.; Bu, W.; Lippard, S. J. ZP4, an Improved Neuronal Zn²⁺ Sensor of the Zinpyr Family. *Journal of the American Chemical Society* **2003**, *125*, 1778-1787.
 - (16) Chang, C. J.; Jaworski, J.; Nolan, E. M.; Sheng, M.; Lippard, S. J. A tautomeric zinc sensor for ratiometric fluorescence imaging: Application to nitric oxide-induced release of intracellular zinc. *Proc. Natl. Acad. Sci. USA* **2004**, *101*, 1129-1134.
 - (17) Chang, C. J.; Nolan, E. M.; Jaworski, J.; Okamoto, K.; Hayashi, Y.; Sheng, M.; Lippard, S. J. ZP8, an Improved Neuronal Zinc Sensor of the ZP Family: Application to Imaging Zinc in Hippocampal Slices with Two-Photon Microscopy. *Inorg. Chem.* **2004**, *43*, submitted.
 - (18) Nolan, E. M.; Burdette, S. C.; Harvey, J. H.; Hilderbrand, S. A.; Lippard, S. J. Synthesis and Characterization of Zinc Sensors Based on a Monosubstituted Fluorescein Platform. *Inorg. Chem.* **2004**, *43*, 2624-2635.
 - (19) Clark, M. A.; Hilderbrand, S. A.; Lippard, S. J. Synthesis of Fluorescein Derivatives Containing Metal-Coordinating Heterocycles. *Tet. Lett.* **2004**, submitted.
-

- (20) Clark, M. A.; Duffy, K.; Tibrewala, J.; Lippard, S. J. Synthesis and Metal-Binding Properties of Chelating Fluorescein Derivatives. *Org. Lett.* **2003**, *5*, 2051-2054.
- (21) Burdette, S. C.; Lippard, S. J. The Rhodafluor Family. An Initial Study of Potential Ratiometric Fluorescent Sensors for Zn²⁺. *Inorg. Chem.* **2002**, *41*, 6816-6823.
- (22) Evans, D. F.; Iki, N. Nuclear Magnetic Resonance Studies of Complexes of Aluminium(III), Gallium(III), and Indium(III) with Disulphonated 2,2'-Dihydroxyazobenzene Ligands in Aqueous Solution. *J. Chem. Soc. Dalton Trans.* **1990**, 3773-3779.
- (23) *SMART: Software for the CCD Detector System*, 5.65; Bruker Advanced X-ray Solutions: Madison, WI, 2001.
- (24) Sheldrick, G. M. *SADABS: Area-Detector Absorption Correction*, University of Göttingen: Göttingen, Germany, 2001.
- (25) *SAINTPLUS: Software for the CCD Detector System*, version 5.01; Bruker AXS: Madison, WI, 1998.
- (26) *SHELXTL: Program Library for Structure Solution and Molecular Graphics*, version 6.2; Bruker AXS: Madison, WI, 2001.
- (27) Kuzelka, J.; Mukhopadhyay, S.; Spingler, B.; Lippard, S. J. Synthesis and Characterization of Cu₂(I,I), Cu₂(I,II), and Cu₂(II,II) Compounds Supported by Two Phthalazine-Based Ligands: Influence of a Hydrophobic Pocket. *Inorg. Chem.* **2004**, *43*, 1751-1761.

- (28) Ioffe, I. S.; Devyatova, N. I.; Roskulyak, L. A. Sulfonic acids of fluorescein. I. Condensation of sulfophthalic acids with resorcinol. *Zh. Obsh. Khim.* **1962**, *32*, 2107-11.
- (29) Roskulyak, L. A.; Zelenin, K. N. Sulfonic acids of fluorescein. V. Structure of isomeric sulfofluoresceins formed by condensation of sulfophthalic acid with resorcinol. *Zh. Obsh. Khim.* **1965**, *1*, 1030-1.
- (30) Corrie, J. E. T.; Craik, J. S.; Munasinghe, V. R. N. A Homobifunctional Rhodamine for Labeling Proteins with Defined Orientations of a Fluorophore. *Bioconj. Chem.* **1998**, *9*, 160-167.
- (31) Werner, T.; He, H.; Kessler, M. A.; Wolfbeis, O. S. New Lipophilic Rhodamines and Their Application to Optical Potassium Sensing. *J. Fluorescence* **1992**, *2*, 93-98.
- (32) Zhang, X.-X.; Buchwald, S. L. Efficient Synthesis of *N*-Aryl-Aza-Crown Ethers via Palladium-Catalyzed Amination. *J. Org. Chem.* **2000**, *65*, 8027-8031.
- (33) Nolan, E. M.; Lippard, S. J. Quinozin-1. *J. Am. Chem. Soc.* **2004**, *126*, manuscript in preparation.
- (34) Smith, G. A.; Metcalfe, J. C.; Clarke, S. D. The Design and Properties of a Series of Calcium Indicators which Shift from Rhodamine-like to Fluorescein-like Fluorescence on Binding Calcium. *J. Chem. Soc. Perkin Trans. 2* **1993**, 1195-1204.
- (35) Whitaker, J. E.; Haugland, R. P.; Ryan, D.; Hewitt, P. C.; Haugland, R. P.; Prendergast, F. G. Fluorescent Rhodol Derivatives: Versatile, Photostable Labels and Tracers. *Anal. Biochem.* **1992**, *207*, 267-279.
-

Table A1.1. Crystallographic parameters.

	3a	5a
Empirical formula	C ₂₀ H ₁₈ O ₁₁ S	C ₂₈ H ₁₆ Cl ₂ N ₃ O ₅ S
Molecular weight	466.40	577.40
space group	P2 ₁ /c	C2/c
a (Å)	10.4324(12)	26.608(4)
b (Å)	16.854(2)	11.0908(16)
c (Å)	11.9615(14)	18.447(3)
β, deg	109.516(2)	105.444(3)
V, Å ³	1982.3(4)	5247.2(13)
Z	4	8
ρ _{calc} , g/cm ³	1.563	1.462
T, °C	-85	-70
μ (Mo Kα), mm ⁻¹	0.228	0.372
θ limits, deg	2.07 to 28.29	1.59 to 28.29
total no. of data	12393	15877
no. of unique data points	4568	6031
no. of parameters	357	352
R ^a	0.0678	0.0553
wR ^{2b}	0.1392	0.1320
max, min peaks, e/Å ³	0.451, -0.452	0.681, -0.428

$${}^a R = \Sigma ||F_o| - F_c| / \Sigma |F_o|, {}^b wR^2 = \{w (F_o^2 - F_c^2)^2 / \Sigma [w (F_o^2)^2]\}^{1/2}$$

Table A1.2. Bond lengths and angles for **3a**.

Bond lengths	[Å]	Bond angles	[°]
S(1)-O(2)	1.437(3)	O(2)-S(1)-O(1)	113.36(15)
S(1)-O(1)	1.452(3)	O(2)-S(1)-O(3)	112.89(17)
S(1)-O(3)	1.453(3)	O(1)-S(1)-O(3)	112.10(16)
S(1)-C(5)	1.781(3)	O(2)-S(1)-C(5)	105.73(16)
O(8)-C(14)	1.352(4)	O(1)-S(1)-C(5)	106.00(16)
O(8)-C(16)	1.362(4)	O(3)-S(1)-C(5)	106.00(15)
O(7)-C(3)	1.341(4)	C(14)-O(8)-C(16)	120.4(3)
O(6)-C(2)	1.328(4)	C(15)-C(20)-C(19)	119.9(3)
O(5)-C(8)	1.309(4)	C(15)-C(20)-C(18)	118.7(3)
C(20)-C(15)	1.393(5)	C(19)-C(20)-C(18)	120.9(3)
C(20)-C(15)	1.393(5)	C(20)-C(19)-C(10)	124.3(3)
C(20)-C(19)	1.400(4)	C(20)-C(19)-C(14)	118.3(3)
C(20)-C(18)	1.500(4)	C(10)-C(19)-C(14)	117.4(3)
C(19)-C(10)	1.413(5)	C(1)-C(18)-C(9)	119.1(3)
C(19)-C(14)	1.415(4)	C(1)-C(18)-C(20)	114.4(3)
O(4)-C(8)	1.219(4)	C(9)-C(18)-C(20)	126.5(3)
C(18)-C(1)	1.388(5)	C(2)-C(17)-C(14)	119.7(3)
C(18)-C(9)	1.400(5)	O(8)-C(16)-C(12)	117.0(3)
C(17)-C(2)	1.378(5)	O(8)-C(16)-C(15)	120.6(3)
C(17)-C(14)	1.383(5)	C(12)-C(16)-C(15)	122.4(3)
C(16)-C(12)	1.376(5)	C(20)-C(15)-C(16)	119.1(3)
C(16)-C(15)	1.413(5)	C(20)-C(15)-C(11)	124.4(3)
C(15)-C(11)	1.423(5)	C(16)-C(15)-C(11)	116.5(3)
C(13)-C(10)	1.354(5)	O(8)-C(14)-C(17)	117.1(3)
C(13)-C(2)	1.417(5)	O(8)-C(14)-C(19)	121.5(3)
C(12)-C(3)	1.377(5)	C(17)-C(14)-C(19)	121.4(3)
C(11)-C(4)	1.342(5)	C(10)-C(13)-C(2)	120.5(3)
C(9)-C(7)	1.403(5)	C(16)-C(12)-C(3)	118.7(3)
C(9)-C(8)	1.488(5)	C(4)-C(11)-C(15)	121.7(3)
C(7)-C(6)	1.376(5)	C(13)-C(10)-C(19)	121.1(3)
C(6)-C(5)	1.372(5)	C(18)-C(9)-C(7)	118.7(3)
C(5)-C(1)	1.388(5)	C(18)-C(9)-C(8)	123.5(3)
C(4)-C(3)	1.412(5)	C(7)-C(9)-C(8)	117.8(3)
		O(4)-C(8)-O(5)	124.5(3)
		O(4)-C(8)-C(9)	121.2(3)
		O(5)-C(8)-C(9)	114.2(3)
		C(6)-C(7)-C(9)	121.7(3)
		C(5)-C(6)-C(7)	119.1(3)
		C(6)-C(5)-C(1)	120.6(3)
		C(6)-C(5)-S(1)	121.9(3)
		C(1)-C(5)-S(1)	117.4(3)
		C(11)-C(4)-C(3)	119.8(3)
		O(7)-C(3)-C(12)	117.3(3)
		O(7)-C(3)-C(4)	121.8(3)
		C(12)-C(3)-C(4)	120.9(3)
		O(6)-C(2)-C(17)	118.7(3)
		O(6)-C(2)-C(13)	121.5(3)
		C(17)-C(2)-C(13)	119.8(3)
		C(5)-C(1)-C(18)	120.8(3)

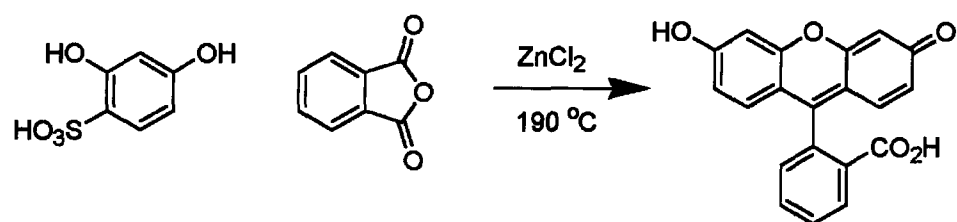
Symmetry transformations used to generate equivalent atoms

Table A1.3. Bond lengths and angles for **5a**.

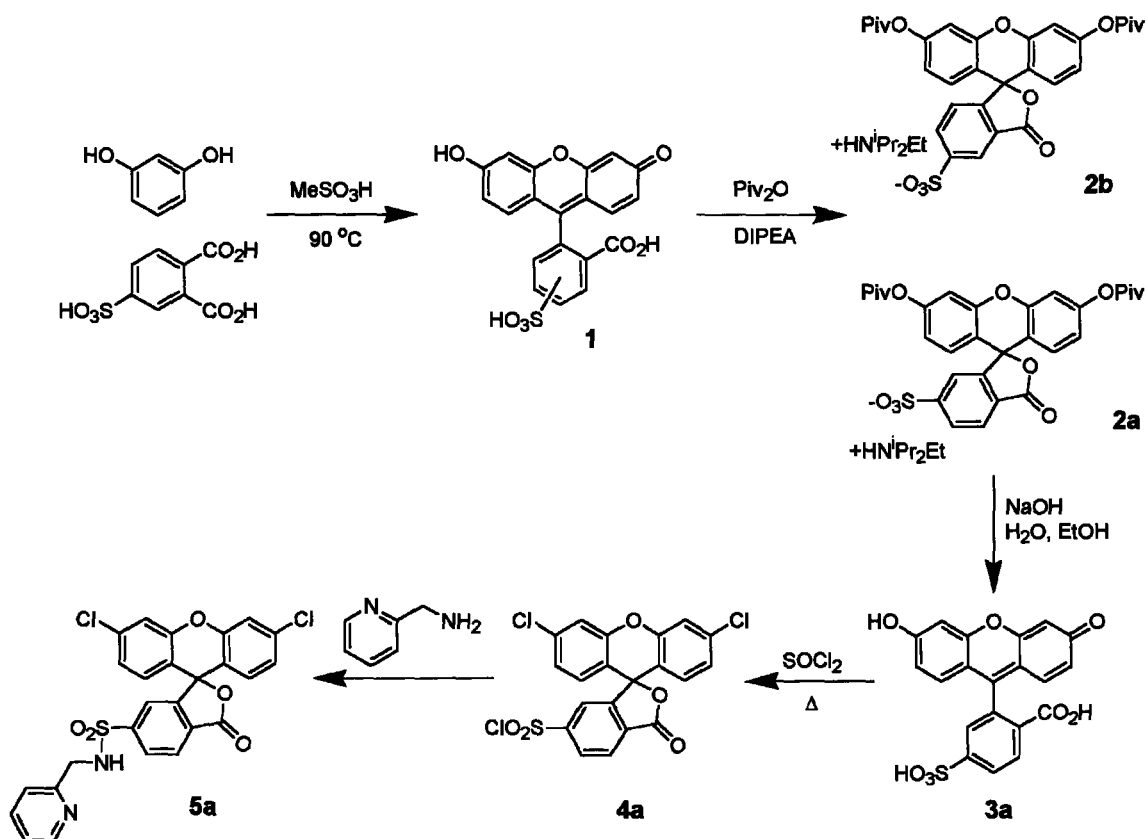
Bond lengths	[Å]	Bond angles	[°]
S(1)-O(1)	1.425(3)	O(1)-S(1)-O(2)	121.18(16)
S(1)-O(2)	1.431(3)	O(1)-S(1)-N(1)	108.02(16)
S(1)-N(1)	1.600(3)	O(2)-S(1)-N(1)	106.63(17)
S(1)-C(12)	1.780(3)	O(1)-S(1)-C(12)	106.55(15)
O(3)-C(16)	1.208(4)	O(2)-S(1)-C(12)	106.20(15)
O(4)-C(16)	1.365(4)	N(1)-S(1)-C(12)	107.62(14)
O(4)-C(19)	1.498(3)	C(16)-O(4)-C(19)	111.2(2)
O(5)-C(26)	1.372(4)	C(26)-O(5)-C(14)	118.3(2)
O(5)-C(14)	1.376(4)	C(5)-N(1)-S(1)	121.5(3)
Cl(1)-C(13)	1.739(3)	C(9)-N(2)-C(2)	115.1(4)
Cl(2)-C(20)	1.736(3)	C(4)-C(1)-C(9)	119.2(3)
N(1)-C(5)	1.456(4)	C(3)-C(2)-N(2)	120.2(4)
N(2)-C(9)	1.422(5)	C(2)-C(3)-C(4)	118.4(4)
N(2)-C(2)	1.425(5)	C(1)-C(4)-C(3)	124.1(4)
C(1)-C(4)	1.305(5)	N(1)-C(5)-C(9)	114.8(3)
C(1)-C(9)	1.310(5)	C(15)-C(6)-C(22)	122.0(3)
C(2)-C(3)	1.354(6)	C(13)-C(7)-C(14)	118.5(3)
C(3)-C(4)	1.371(5)	C(21)-C(8)-C(10)	120.5(3)
C(5)-C(9)	1.512(5)	C(21)-C(8)-C(19)	129.5(3)
C(6)-C(15)	1.378(4)	C(10)-C(8)-C(19)	109.9(3)
C(6)-C(22)	1.401(4)	C(1)-C(9)-N(2)	123.0(3)
C(7)-C(13)	1.373(5)	C(1)-C(9)-C(5)	117.8(3)
C(7)-C(14)	1.392(4)	N(2)-C(9)-C(5)	119.2(4)
C(8)-C(21)	1.376(4)	C(8)-C(10)-C(18)	122.4(3)
C(8)-C(10)	1.378(4)	C(8)-C(10)-C(16)	108.5(3)
C(8)-C(19)	1.514(4)	C(18)-C(10)-C(16)	129.0(3)
C(10)-C(18)	1.382(4)	C(24)-C(11)-C(25)	121.7(3)
C(10)-C(16)	1.469(4)	C(23)-C(12)-C(21)	121.9(3)
C(11)-C(24)	1.369(4)	C(23)-C(12)-S(1)	119.4(2)
C(11)-C(25)	1.394(4)	C(21)-C(12)-S(1)	118.7(2)
C(12)-C(23)	1.378(4)	C(7)-C(13)-C(15)	121.7(3)
C(12)-C(21)	1.394(4)	C(7)-C(13)-Cl(1)	118.4(3)
C(13)-C(15)	1.387(5)	C(15)-C(13)-Cl(1)	119.9(3)
C(14)-C(22)	1.384(4)	O(5)-C(14)-C(22)	123.4(3)
C(17)-C(20)	1.372(4)	O(5)-C(14)-C(7)	114.6(3)
C(17)-C(26)	1.389(4)	C(22)-C(14)-C(7)	122.0(3)
C(18)-C(23)	1.386(4)	C(6)-C(15)-C(13)	118.4(3)
C(19)-C(22)	1.496(4)	O(3)-C(16)-O(4)	121.4(3)
C(19)-C(25)	1.510(4)	O(3)-C(16)-C(10)	130.3(3)
C(20)-C(24)	1.381(4)	O(4)-C(16)-C(10)	108.3(3)
C(25)-C(26)	1.383(4)	C(20)-C(17)-C(26)	118.8(3)
		C(10)-C(18)-C(23)	117.4(3)
		C(22)-C(19)-O(4)	107.4(3)
		C(22)-C(19)-C(25)	111.7(3)
		O(4)-C(19)-C(25)	107.1(2)
		C(22)-C(19)-C(8)	115.7(3)
		O(4)-C(19)-C(8)	101.8(2)
		C(25)-C(20)-C(24)	112.3(3)
		C(17)-C(20)-C(24)	121.2(3)
		C(17)-C(20)-Cl(2)	119.5(3)
		C(24)-C(20)-Cl(2)	119.3(3)
		C(8)-C(21)-C(12)	117.4(3)
		C(14)-C(22)-C(6)	117.3(3)
		C(14)-C(22)-C(19)	121.5(3)
		C(6)-C(22)-C(19)	121.1(3)

C(12)-C(23)-C(18)	120.4(3)
C(11)-C(24)-C(20)	119.1(3)
C(26)-C(25)-C(11)	117.7(3)
C(26)-C(25)-C(19)	121.2(3)
C(11)-C(25)-C(19)	121.0(3)
O(5)-C(26)-C(25)	123.5(3)
O(5)-C(26)-C(17)	114.9(3)
C(25)-C(26)-C(17)	121.5(3)

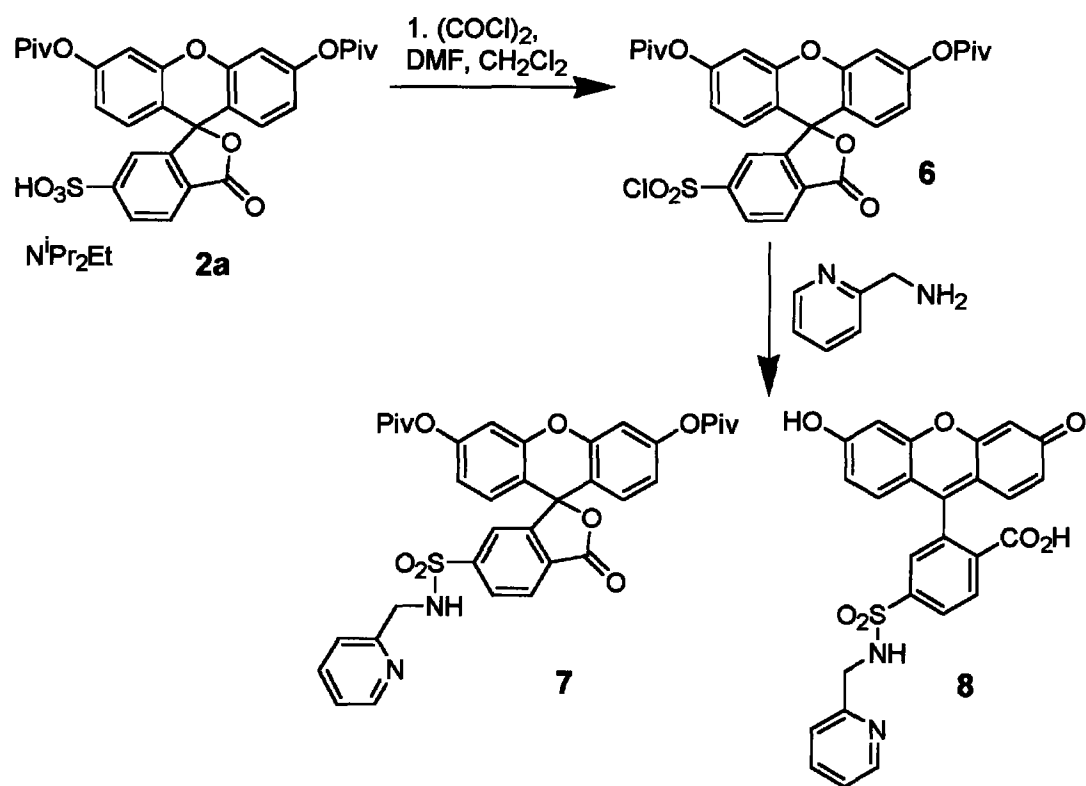
Symmetry transformations used to generate equivalent atoms



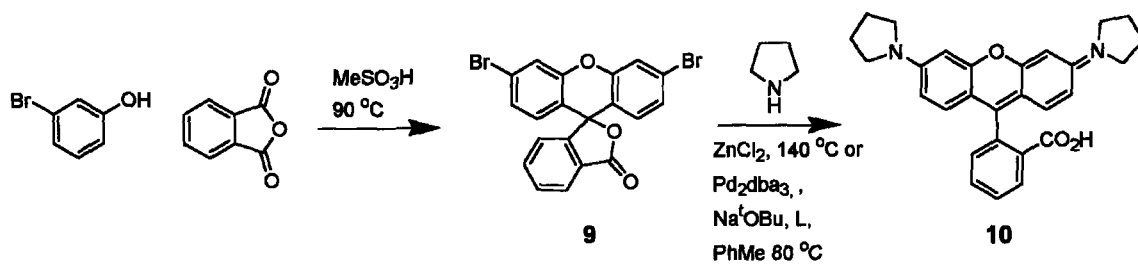
Scheme A1.1. Attempted synthesis of fluorescein-2',7'-disulfonate.



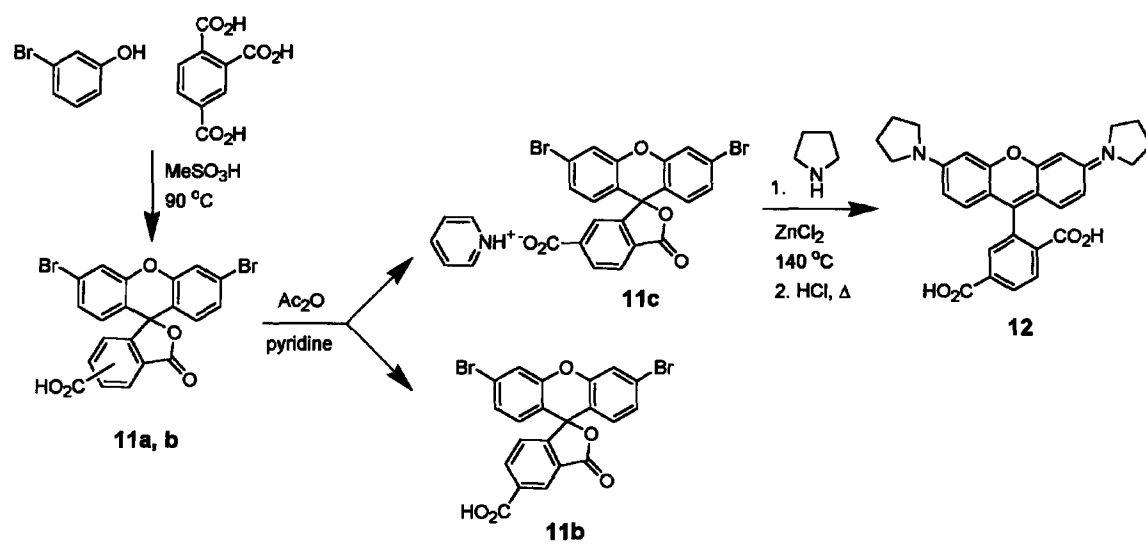
Scheme A1.2. Synthesis, separation and attempted activation of fluorescein-5(6)-sulfonic acid.



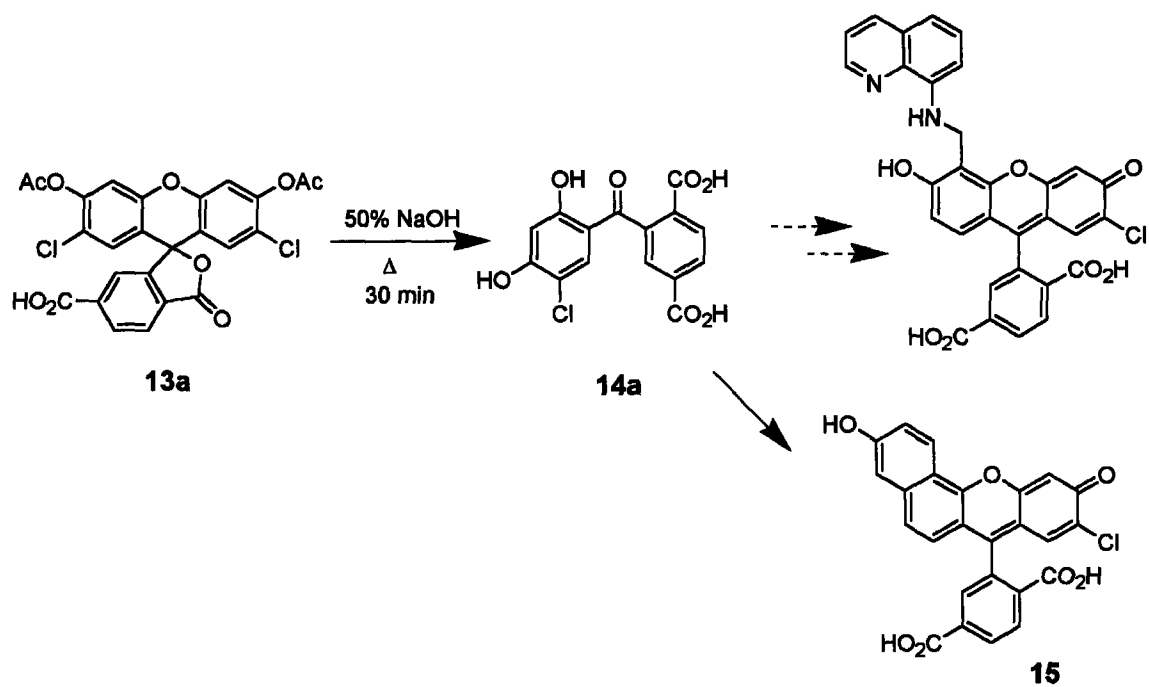
Scheme A1.3. Oxalyl chloride-mediated coupling of fluorescein sulfonic acid.



Scheme A1.4. Dibromofluoran route to rhodamine synthesis.



Scheme A1.5. Separation of dibromofluoran carboxylates and conversion to rhodamine.



Scheme A1.6. Synthesis and potential applications of carboxylate-substituted benzophenone synthon.

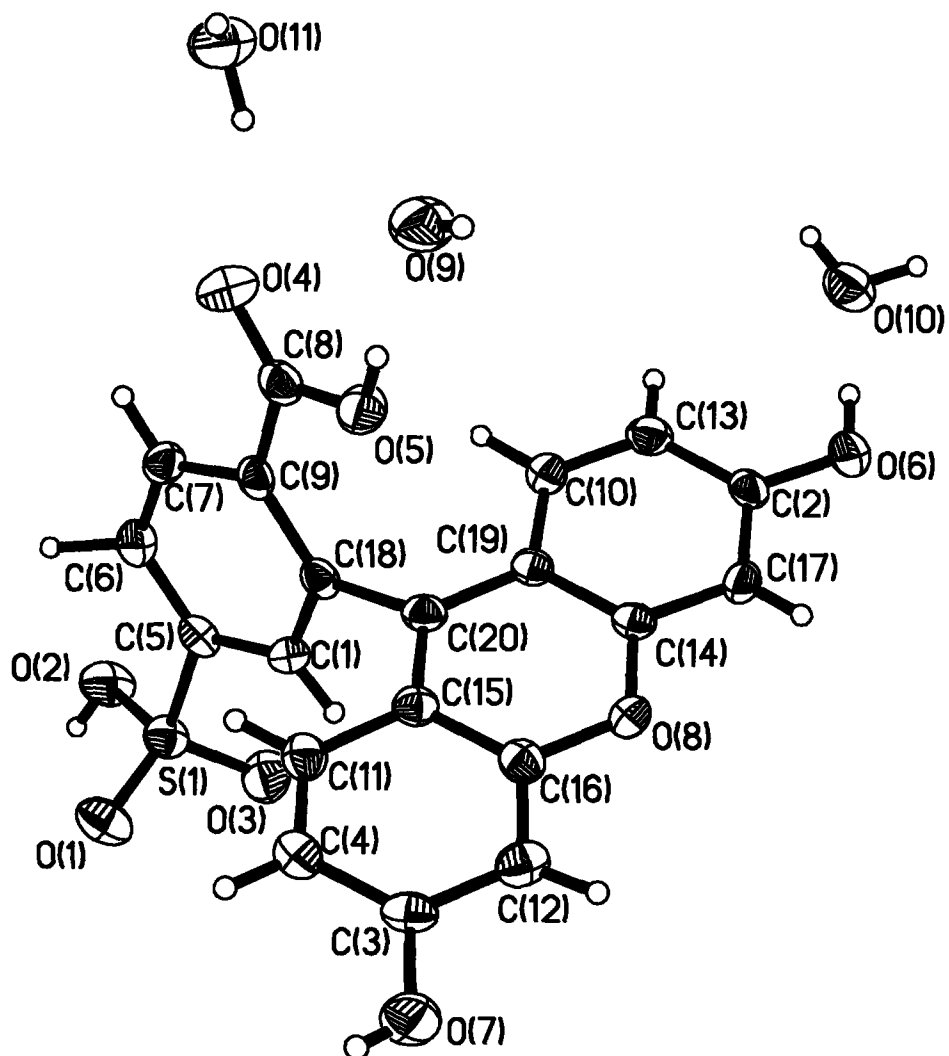


Figure A1.1. Crystal structure of fluorescein-6-sulfonic acid.

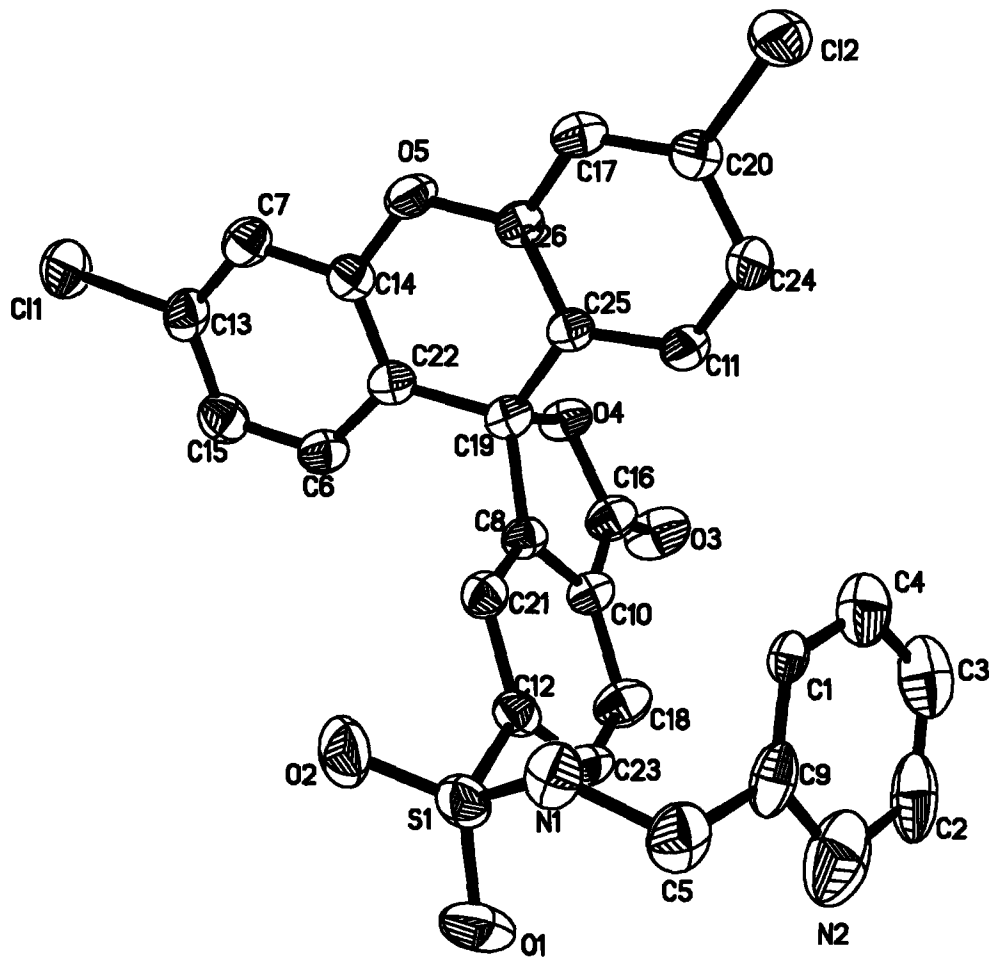


Figure A1.2. Crystal structure of fluorescein-6-sulfonamidopicoline.

Appendix 2 Modulation of Zn²⁺ Affinity By Modification of ZP1

Introduction

Binding affinity is an important consideration in biological sensing.¹ Dissociation constants should ideally be similar to the median concentration of analyte under study, since high-affinity sensors may become saturated and imply an artificially high analyte concentration, whereas low-affinity sensors may lack the requisite sensitivity. Biological Zn^{2+} concentrations range from sub-nanomolar in cytosol² to near millimolar concentrations in synaptic vesicles of the hippocampus,³ and therefore multiple sensors with varying affinities are desirable. The ZP1 family of sensors binds Zn^{2+} with sub-nanomolar affinity. We sought to reduce the binding affinity of ZP1 by replacing the pyridyl ligands with carboxylates.

Zinpyr-1 (ZP1, **1**)^{4,5} bears a close resemblance to the known high-pH calcium ion sensor calcein (Figure A2.1).⁶ Calcein is synthesized in a manner similar to ZP1, but the use of unsubstituted fluorescein rather than dichlorofluorescein affords the product as a mixture of isomers. We have prepared **2**, an isomerically pure analogue of calcein, from dichlorofluorescein, as well as **3**, a hybrid of ZP1 and calcein in which each amine is substituted with one picolyl and one acetate group. The synthesis, metal ion response, and protonation constants of these compounds are reported here.

Experimental

Materials and Methods.

Reagents were purchased from Aldrich and used without further purification except for pyridine carboxaldehyde, which was distilled before use. Methanol was distilled from MgI_2 under a nitrogen atmosphere. 1H NMR data were collected on a 300 MHz Varian or a 400 MHz Bruker instrument. Fluorescence spectra were acquired on a

Hitachi F-3010 fluorimeter and UV-visible absorption spectra were acquired on a Cary 1E UV-visible spectrophotometer. Both were analyzed using Kaleidagraph 3.0 for Windows.

Synthetic Procedures

[(Pyridin-2-ylmethyl)-amino]-acetic acid ethyl ester (4). Glycine ethyl ester hydrochloride (14.0 g, 100 mmol) was stirred with potassium carbonate (6.91 g, 50 mmol) in 200 mL of MeOH until gas no longer evolved (ca 45 min). Pyridine carboxaldehyde was added dropwise, and the mixture was stirred for an addition 45 min under an Ar atmosphere. A 1.5-g portion of 10% Pd/C was then added, and the mixture was stirred overnight under an atmosphere of hydrogen. The reaction was filtered through Celite, concentrated under reduced pressure, and distilled in vacuo to yield 8.2 g of a yellow oil (42.2%). $^1\text{H NMR}(\text{CDCl}_3 + \text{D}_2\text{O})$: δ 8.54 (d, 1 H); 7.64 (td, 1 H); 7.32 (d, 1 H); 7.18 (dd, 1 H); 4.82 (br s, < 1 H); 4.18 (q, 2 H); 3.93 (s, 2 H); 3.46 (s, 2 H); 1.27 (t, 3 H). The NMR data obtained are in good agreement with literature values⁷ and the product was not further characterized.

4',5'-Bis-[(carboxymethyl-pyridin-2-ylmethyl-amino)-methyl]- 2',7'-dichlorofluorescein (3). Paraformaldehyde (204 mg, 6.4 mmol) and [(pyridin-2-ylmethyl)-amino]acetic acid ethyl ester (1.24 g, 6.4 mmol) were combined in 60 mL MeCN under Ar and heated to reflux for 30 min. 2',7'-Dichlorofluorescein (804 mg, 2 mmol) was suspended in 80 mL of 1:1 MeCN:H₂O and added, and the reaction mixture was heated to reflux for 24 h. The acetonitrile was removed under reduced pressure, and a solution of 12 g of NaOH in 60 mL of H₂O and 40 mL of EtOH was added. The basic solution was heated to reflux overnight and then allowed to cool and acidified slightly. The organic

solvents were removed under reduced pressure, and the cloudy aqueous solution was stored at 4 °C overnight, then filtered through Celite. The filtrate was made slightly basic (pH ~ 8) and concentrated, cooled at 4 °C for several hours, then filtered through Celite. The red precipitate was extracted with boiling EtOH and H₂O, filtered, and evaporated to afford 0.5 g of red solid (33% yield). ¹H NMR(DMSO-d₆): δ 8.50 (d, 2 H); 8.00 (d, 1 H); 7.71 (td, 2 H); 7.46 (m, 2 H); 7.33 (d, 2 H); 7.25 (dd, 2 H); 7.07 (d, 1 H); 6.73 (s, 2 H); 3.80 (s, 4 H); 3.72 (s, 4 H); 2.95 (s, 4 H). HRMS(M+H): Calcd for C₃₈H₃₁Cl₂N₄O₉: 757.1468; Found 757.1466.

4',5'-Bis-[(bis-ethoxycarbonylmethyl-amino)-methyl]-2',7'-dichlorofluorescein (5).

Diethyl iminodiacetate (1.21 g, 6.4 mmol) and paraformaldehyde (204 mg, 6.4 mmol) were refluxed together for 30 min in 60 mL of MeCN. 2',7'-Dichlorofluorescein (804 mg, 2 mmol) was suspended in 80 mL of 1:1 MeCN:H₂O and added, and the reaction was heated to reflux for 24 h. The solvents were removed under reduced pressure, and the resulting product was purified on a silica gel column eluting with CHCl₃:PhMe:MeOH 60:35:5 to afford 1.53 g of a crude orange solid, which was recrystallized from hexanes and toluene to afford 0.686 g (51.6% yield) of fluffy light-orange crystals that turned red on contact with water. ¹H NMR(CDCl₃): δ 8.05 (d, 2 H); 7.75 (t, 1 H); 7.69 (t, 1 H); 7.21 (d, 1 H); 6.65 (s, 2 H); 4.48 (d, 2 H); 4.25 (m, 10 H); 3.60 (s, 8 H); 1.20 (t, 12 H).

4',5'-Bis-[(bis-carboxymethyl-amino)-methyl]-2',7'-fluorescein (2).

4',5'-Bis-[(bis-ethoxycarbonylmethyl-amino)-methyl]-2',7'-dichlorofluorescein (133 mg, 0.2 mmol) and NaOH (110 mg, 2.8 mmol) were dissolved in 5 mL of EtOH and 10 mL of H₂O and heated to reflux overnight. The ethanol was then removed under reduced pressure, and the aqueous solution was acidified to pH 3 with 4-5 drops of 12 M HCl to afford a bright

red precipitate, which was filtered, washed with 3 x 5 mL portions of H₂O, and lyophilized to give 81.5 mg (59%) of the desired product. ¹H NMR(DMSO-d₆): δ 8.03 (d, 1 H); 7.84 (t, 1 H); 7.76 (t, 1 H); 7.37 (d, 1 H); 6.63 (s, 2 H); 4.21 (m, 8 H); 3.52 (s, 4 H). HRMS(M-H): Calcd for C₃₀H₂₃Cl₂N₂O₁₃: 689.0577; Found 689.0559.

Spectroscopic Measurements

Purified water (resistivity 18.2 Ohms) was obtained from a Millipore Milli-Q water purification system. Fluorophore stock solutions in DMSO were made up to concentrations of 1 mM and kept at 4 °C. Portions were thawed and diluted to the required concentrations immediately prior to each experiment. Fluorescence data were acquired in HEPES buffer (50 mM, pH 7.5, KCl 100 mM) or in unbuffered KCl solution at pH 12.5. Quantum yields and pK_a values were measured as described in Chapter 2 or as described elsewhere.⁴ Physical data reported are the result of a single measurement.

Results and Discussion

Synthesis

The synthesis of dicarboxylate and tetracarboxylate analogues of ZP1 has been accomplished by a similar synthetic approach, as shown in Scheme A2.1. Reductive amination of glycine ethyl ester with pyridine carboxaldehyde furnished the appropriate Mannich amine **4** for synthesis of **3**, whereas iminodiacetate diethyl ester is commercially available. Subsequent basic ester hydrolysis affords the desired compounds. The intermediate tetraethyl ester **5** was isolated by column chromatography and subsequent recrystallization; the corresponding intermediate for **3** was not isolated.

Photophysics and Thermodynamics

Addition of ZnCl_2 to **2** or **3** at pH 7.5 afforded no fluorescence increase. Addition of CaCl_2 to **2** afforded a very small increase in fluorescence at pH 7.5, consistent with literature reports that the related calcein functions as a calcium sensor at high pH. Examination of fluorescence-dependent protonation equilibria indicated very high pK_a values for both **2** and **3** (Figure A2.2, Table A2.1), and subsequently the quantum yield of fluorescence was determined at pH 12. An 8-fold increase was observed for **2** upon addition of CaCl_2 at pH 12. The fluorescence response of **3** to a variety of metal ions was examined at pH 10.5, and it was found that most transition metals including Zn^{2+} induced a decrease in fluorescence (Figure A2.3). Cadmium(II) and mercury(II) afforded a 16% and an 6% increase in fluorescence, respectively. Even at high pH values the fluorescence of **3** was not appreciably quenched, as seen in Figure A2.2, indicating that protonation equilibria arguments do not satisfactorily explain fluorescence response mechanisms of these and related compounds. A recent communication suggests that the subtleties underlying the mechanism of fluorescence quenching in aminomethyl-functionalized dichlorofluorescein compounds are not fully understood.⁸

Conclusions

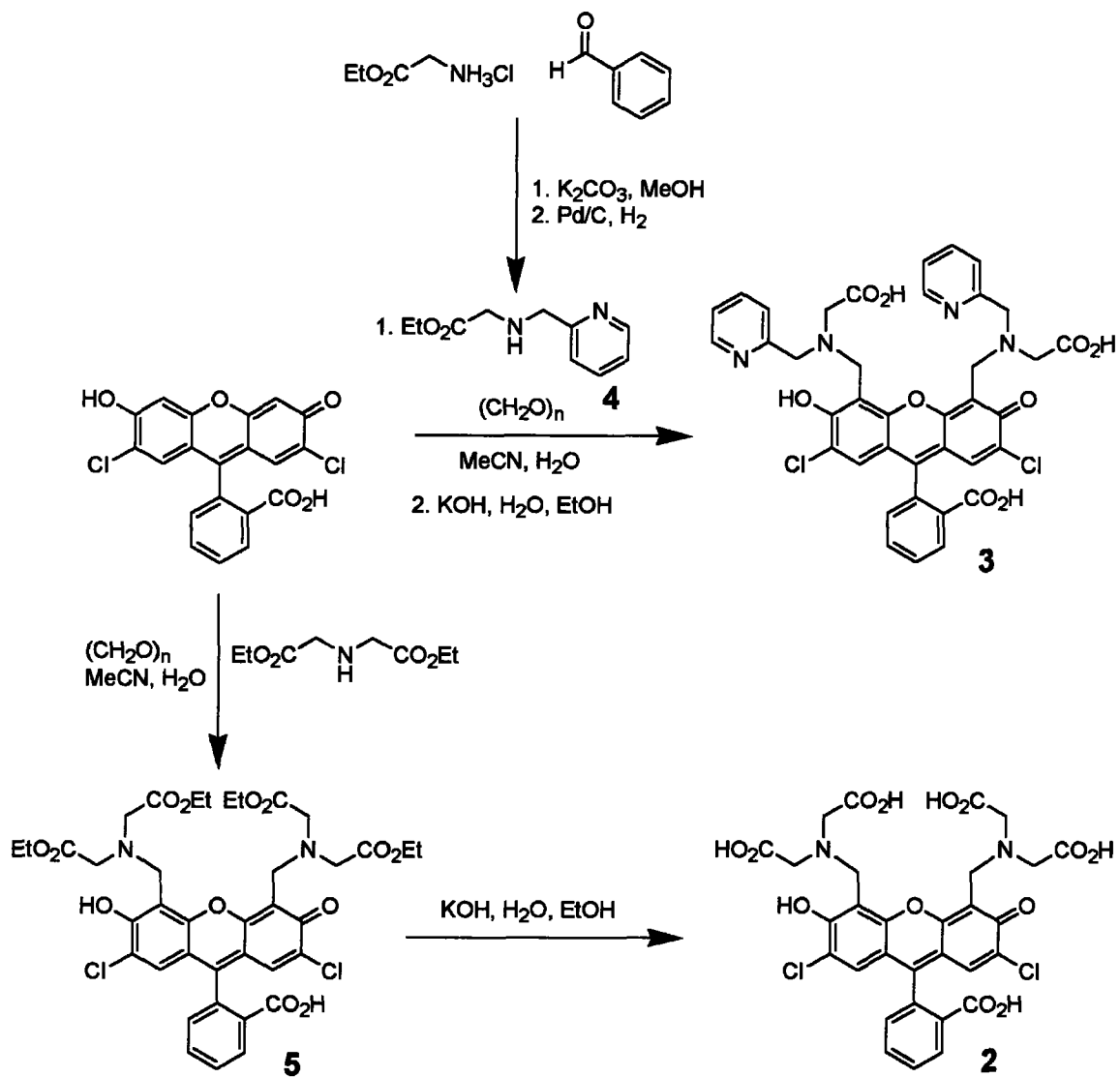
ZP1 analogues containing carboxylates in place of pyridyl ligands have been prepared with the goal of tuning Zn^{2+} affinity. Replacing all four pyridyl ligands with carboxylates produces an analogue of the high-pH calcium sensor calcein, and an increased pK_a value for fluorescence-dependent protonation equilibria. Replacing two of the four pyridyl ligands with carboxylates produces a fluorophore that is largely unresponsive to added transition metal ions and has a similarly increased pK_a value.

References

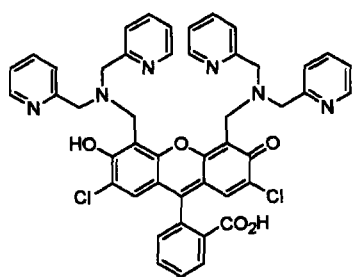
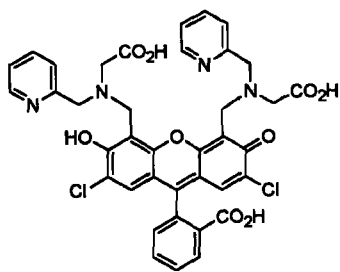
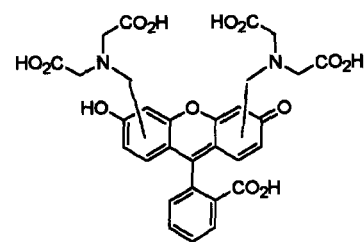
- (1) Kimura, E.; Koike, T. Recent development of zinc-fluorophores. *Chem. Soc. Rev.* **1998**, *27*, 179-184.
- (2) Outten, C. E.; O'Halloran, T. V. Femtomolar Sensitivity of Metalloregulatory Proteins Controlling Zinc Homeostasis. *Science* **2001**, *292*, 2488-2492.
- (3) Frederickson, C. J. Neurobiology of Zinc and Zinc-containing Neurons. *Int. Rev. Neurobiol.* **1989**, *31*, 145-238.
- (4) Walkup, G. K.; Burdette, S. C.; Lippard, S. J.; Tsien, R. Y. A New Cell-Permeable Fluorescent Probe for Zn²⁺. *J. Am. Chem. Soc.* **2000**, *122*, 5644-5645.
- (5) Burdette, S. C.; Walkup, G. K.; Spingler, B.; Tsien, R. Y.; Lippard, S. J. Fluorescent Sensors for Zn²⁺ Based on a Fluorescein Platform: Synthesis, Properties and Intracellular Distribution. *J. Am. Chem. Soc.* **2001**, *123*, 7831-7841.
- (6) Diehl, H.; Ellingboe, J. L. Indicator for Titration of Calcium in Presence of Magnesium using Disodium Dihydrogen Ethylenediamine Tetraacetate. *Anal. Chem.* **1956**, *28*, 882-884.
- (7) Policar, C.; Lambert, F.; Cesario, M.; Morgenstern-Badarau, I. An Inorganic Helix [Mn(IPG)(MeOH)_n][PF₆]_n^[f]: Structural and Magnetic Properties of a *syn-anti* Carboxylate-Bridged Manganese(II) Chain Involving a Tetradentate Ligand. *Eur. J. Inorg. Chem.* **1999**, 2201-2207.
- (8) Sparano, B. A.; Shahi, S. P.; Koide, K. Effect of Binding and Conformation on Fluorescence Quenching in New 2',7'-Dichlorofluorescein Derivatives. *Org. Lett.* **2004**, *6*, 1947-1949.

Table A2.1. Photophysical and thermodynamic constants

Compound	Φ (pH 7.5)	Φ (pH 12.5)	pK_{a1}	pK_{a2}	pK_{a3}
ZP1	0.38		2.8		8.4
ZP1 + Zn ²⁺	0.87				
3	0.56		3.4		9.4
3 + Zn ²⁺	0.49				
2	0.53	0.08	3.1	5.9	10.2
2 + Zn ²⁺	0.55	0.63			



Scheme A2.1. Synthesis of ZP1 analogues

**Zinpyr-1 (1)****3****Calcein****Figure A2.1.** Structures of ZP1 and analogues

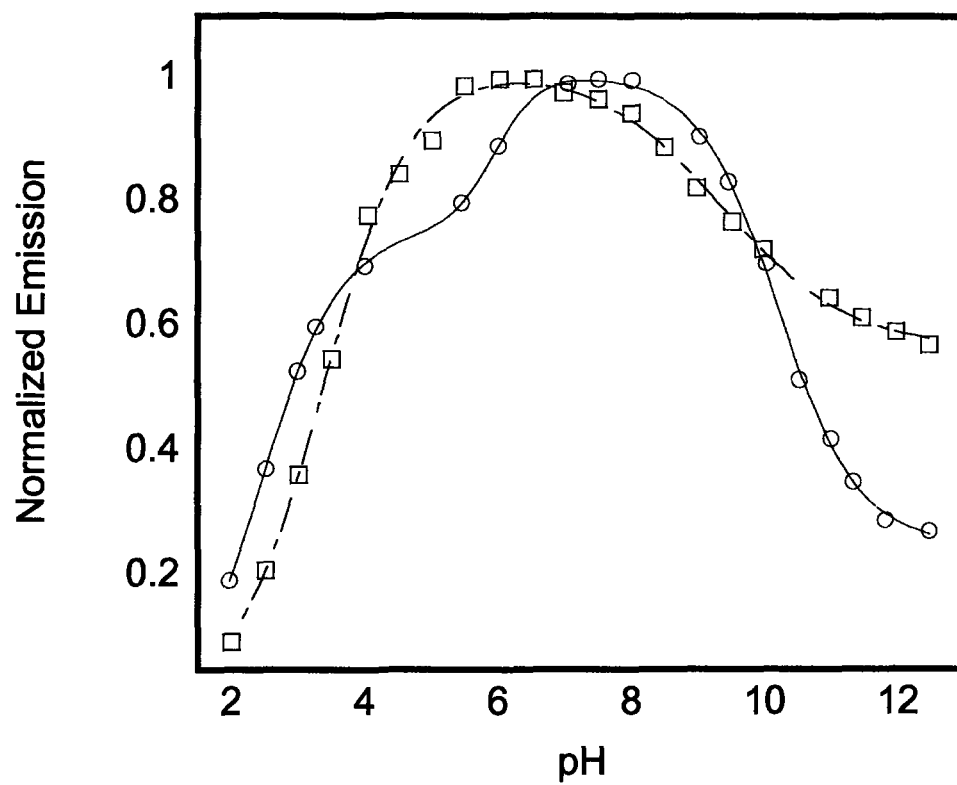


Figure A2.2. pH Dependent fluorescence of 2 (red circles) and 3 (blue squares).

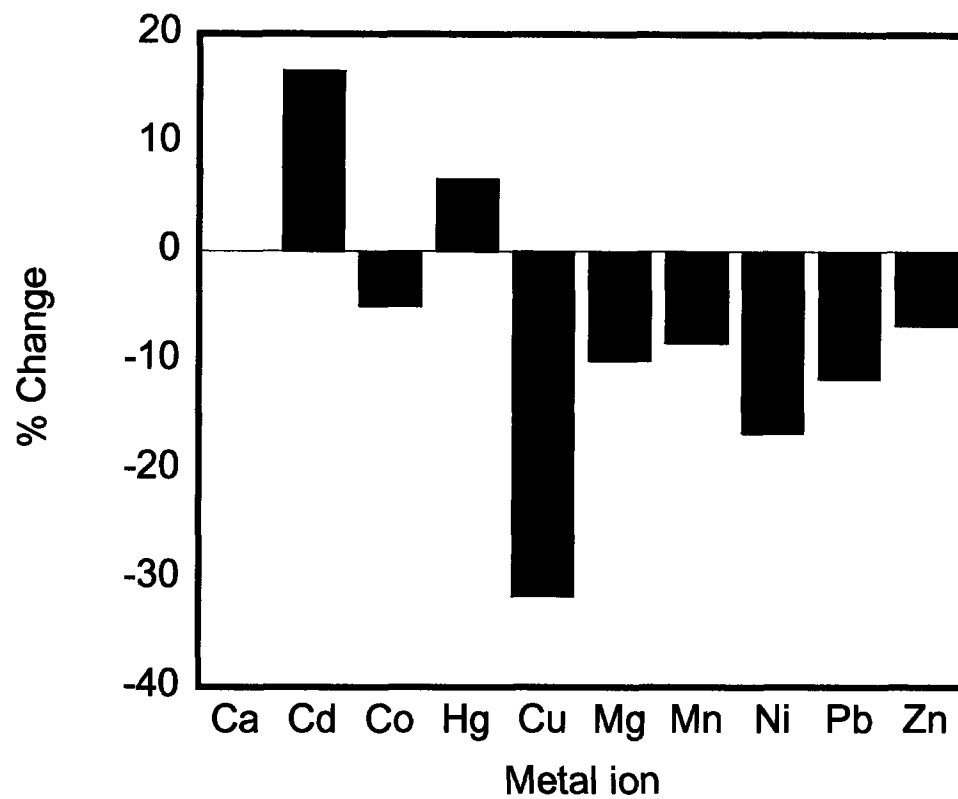
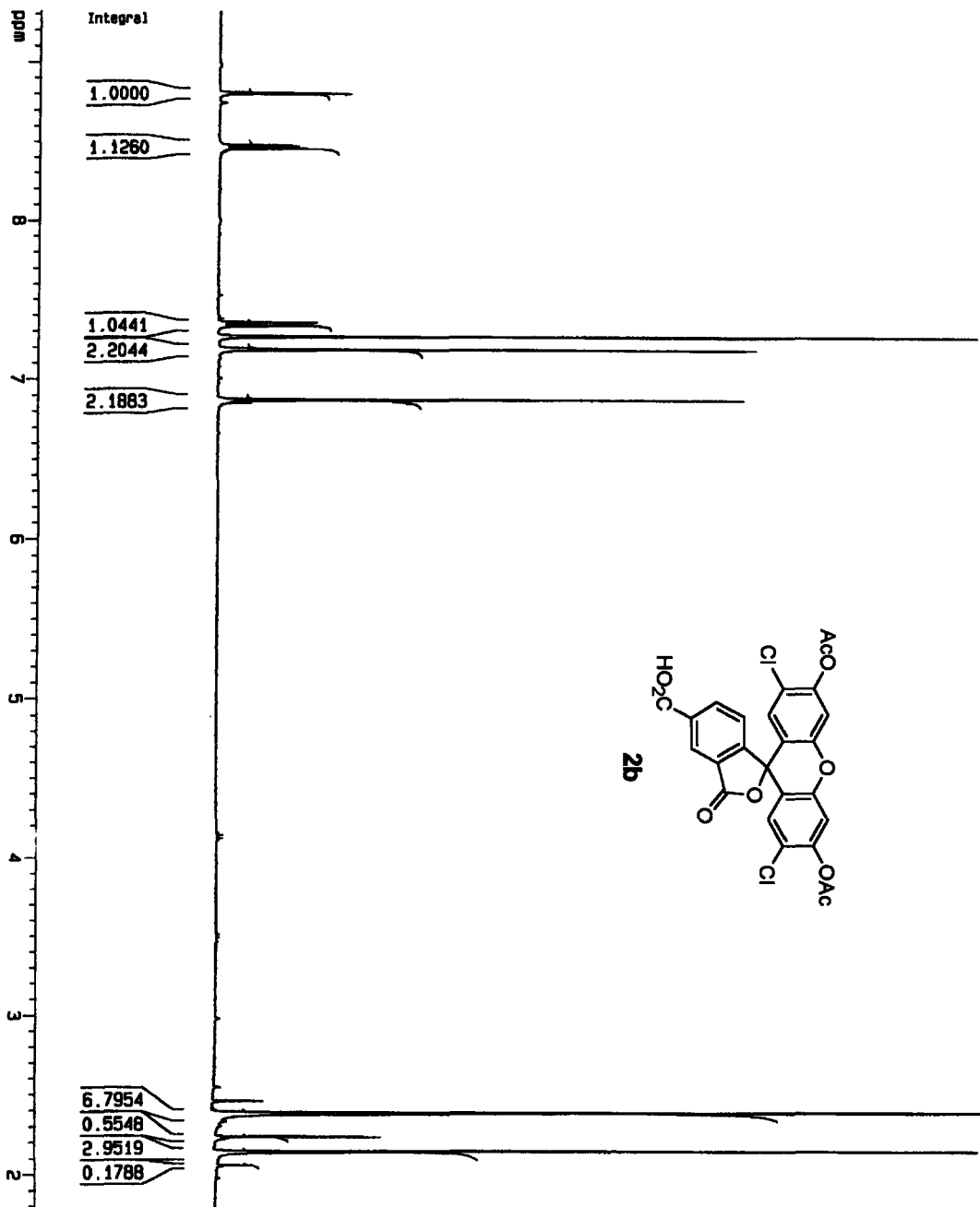


Figure A2.3. Change in fluorescence intensity of **3** (0.5 μM , pH 10.5, KCl 100 mM) in the presence of 10 μM concentrations of various divalent transition metals.

Appendix 3 Selected Spectra



Current Data Parameters
 NAME Jul31-2001
 EXPNO 10
 PROCNO 1

F2 - Acquisition Parameters

Date_ 20010731
 Time 12.02
 INSTRUM spect
 PROBRD 5mm BBO BB-1
 PULPROG zg30
 TD 65536
 SOLVENT CDCl₃
 NS 16
 DS 2
 SWH 8278.146 Hz
 FIDRES 0.126314 Hz
 AQ 3.5294243 sec
 RG 455.1
 DM 50.400 usec
 DE 6.00 usec
 TE 300.0 K
 D1 1.00000000 sec

***** CHANNEL f1 *****

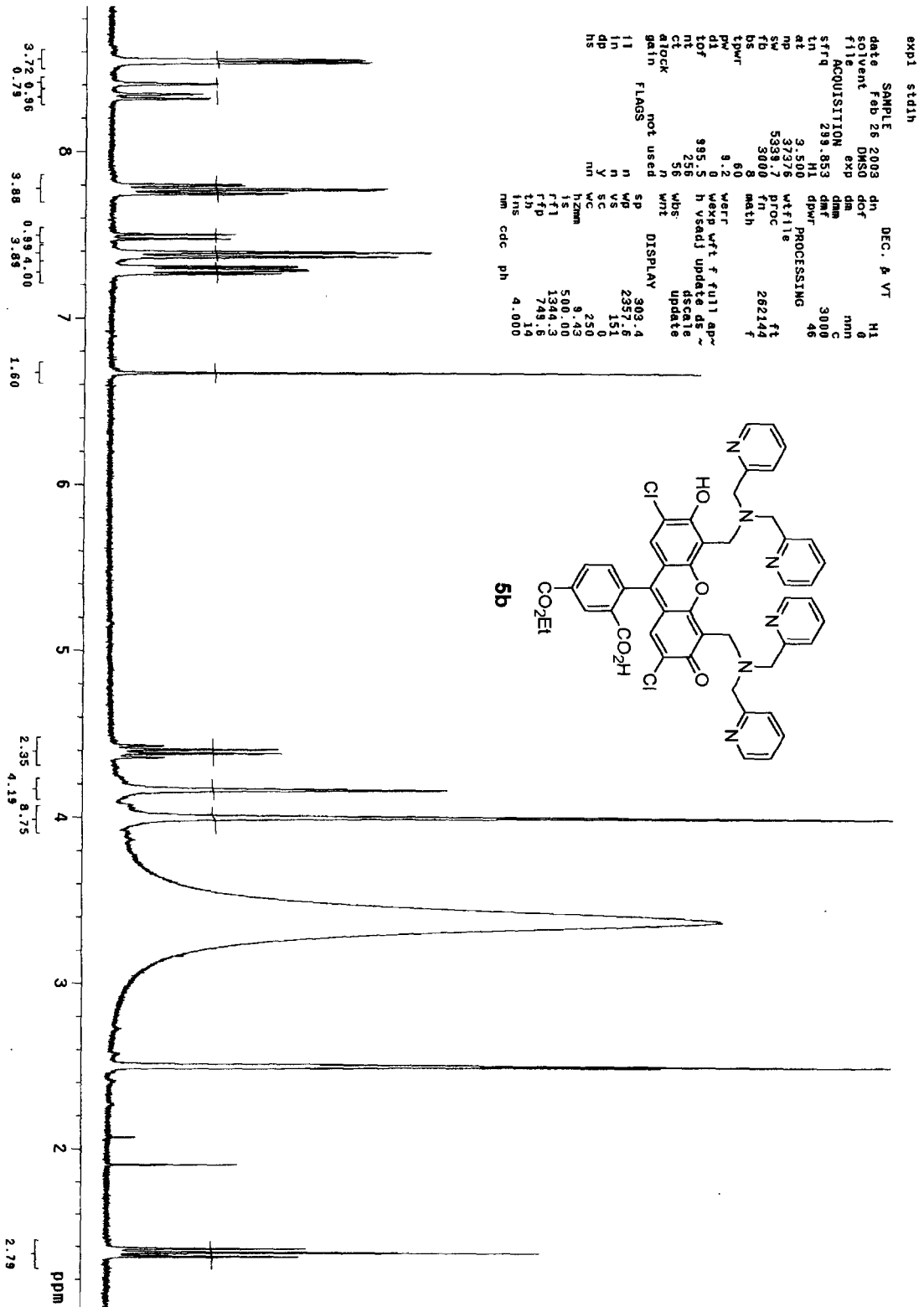
MUCL 1H
 P1 7.90 usec
 PL1 0.00 dB
 SF01 400.1324710 MHz

F2 - Processing parameters

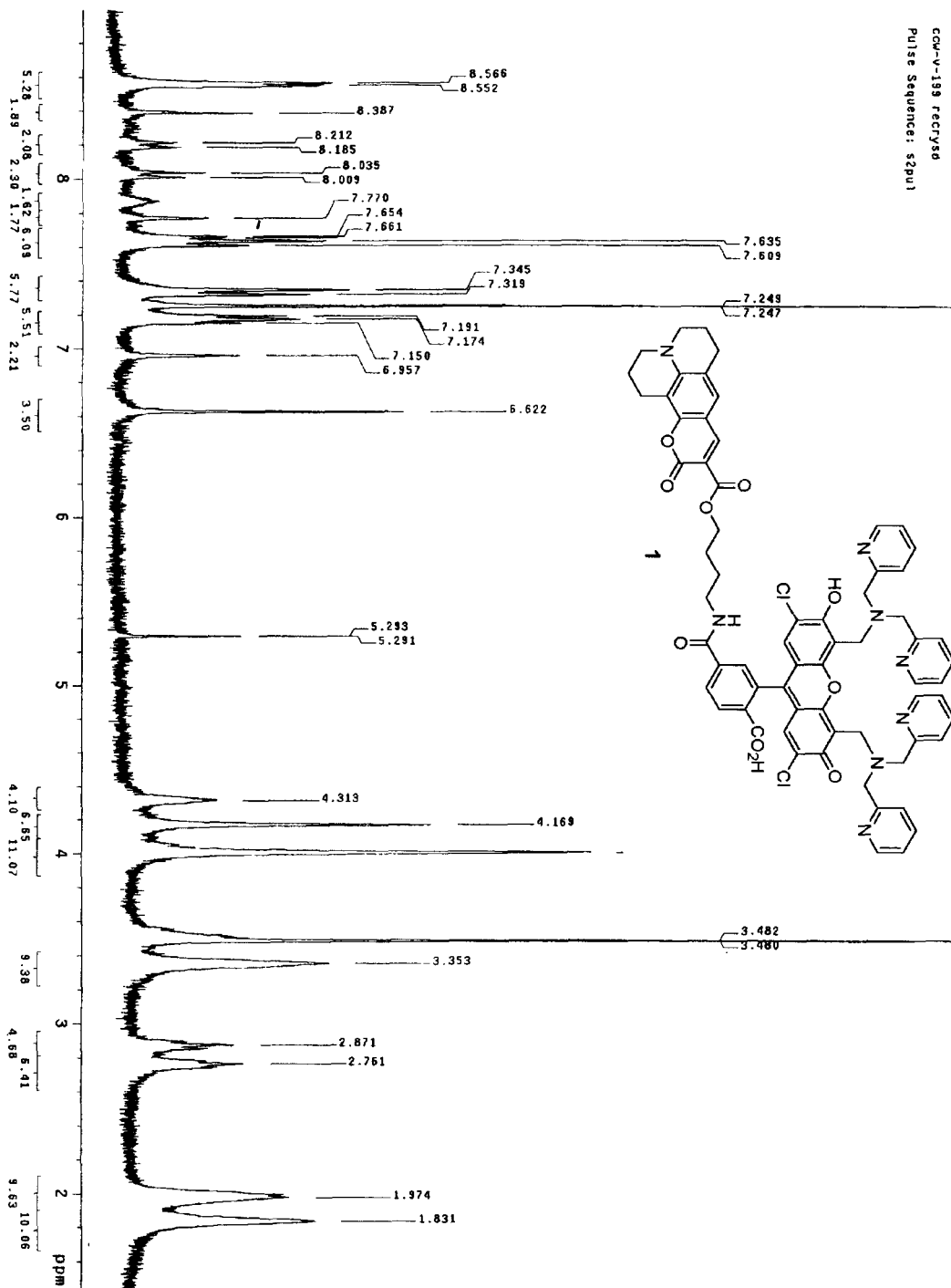
SI 32768
 SF 400.1300049 MHz
 WDW EM
 SSB 0
 LB 0.30 Hz
 GB 0
 PC 1.00

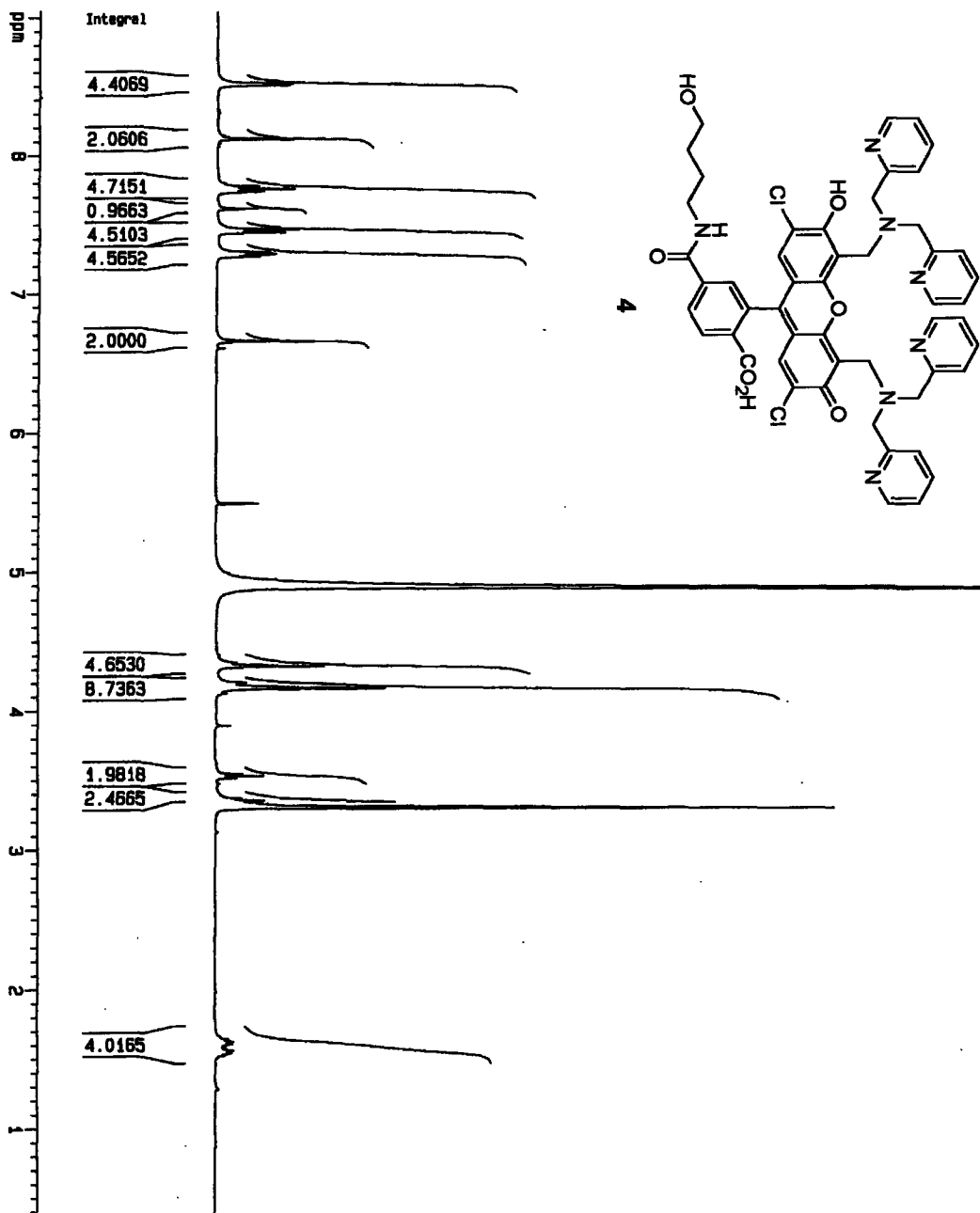
ID NMR plot parameters

CX 20.00 cm
 F1P 9.319 DPM
 F1 3728.75 Hz
 F2P 1.782 DPM
 F2 712.93 Hz
 PPMCM 0.37685 DPM/cm
 HZCM 150.79120 Hz/cm



Chapter 3 Spectra





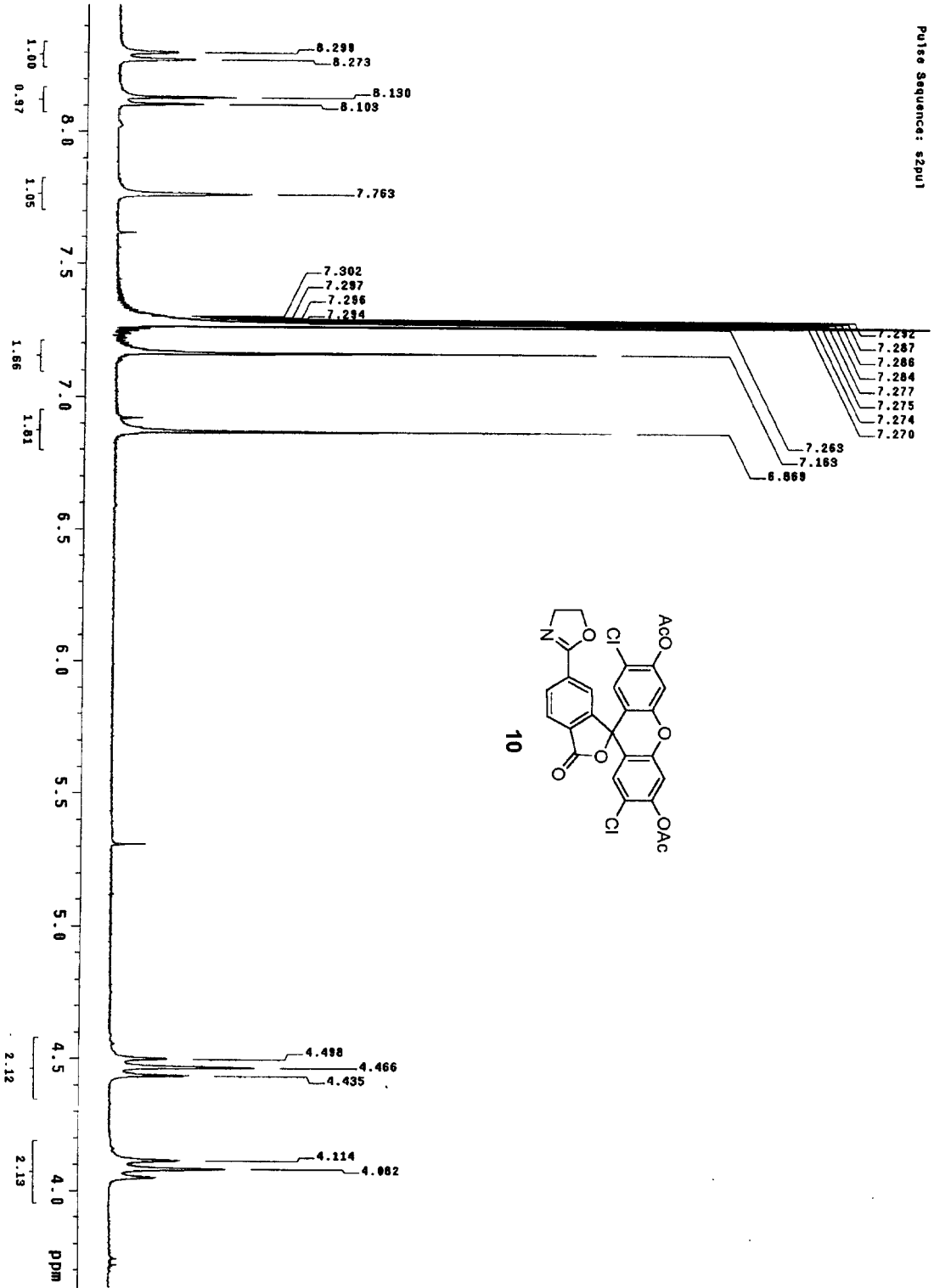
Current Data Parameters
 NAME J121-2003-ACU
 EXPNO 10
 PROCNO 1

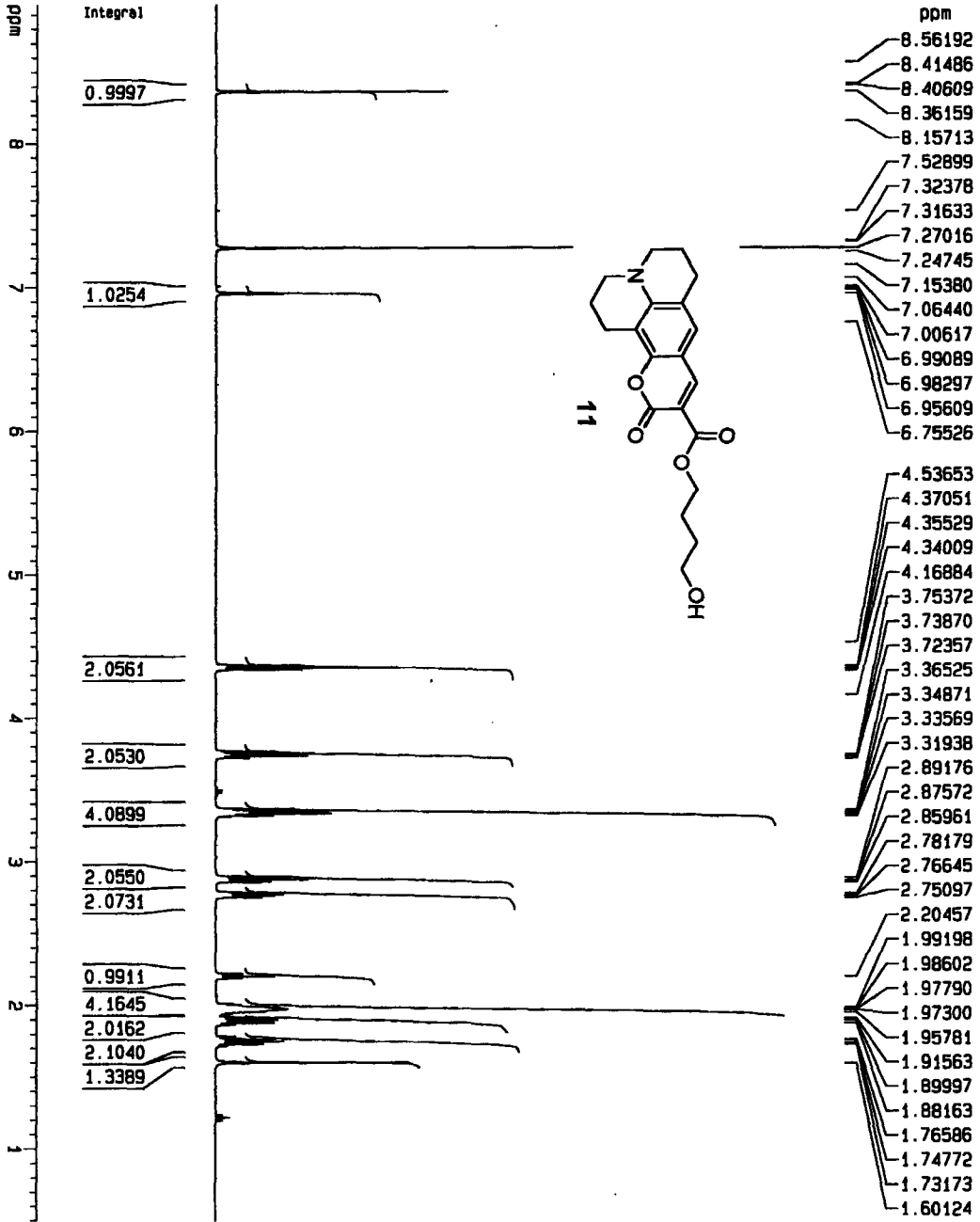
F2 - Acquisition Parameters
 Date_ 20030721
 Time 19.37
 INSTRUM spect
 PROBRD 5mm BBO BB-1
 PULPROG zg30
 TD 65536
 SOLVENT MeOH
 NS 128
 DS 0
 SWH 8278.146 Hz
 FIDRES 0.126314 Hz
 AQ 3.9594243 sec
 RG 406.4
 DW 80.400 usec
 DE 6.00 usec
 TE 300.0 K
 D1 2.00000000 sec

***** CHANNEL f1 *****
 NUC1 1H
 P1 7.50 usec
 PL1 0.00 dB
 SF01 400.1324710 MHz

F2 - Processing parameters
 SI 32768
 SF 400.1300114 MHz
 KW EN
 SSB 0
 LB 0.30 Hz
 GB 0
 PC 1.00

1D NMR plot parameters
 CX 20.00 cm
 F1P 9.047 ppm
 F1 3619.89 Hz
 F2P 0.382 ppm
 F2 156.86 Hz
 PRNCK 0.43273 ppm/cm
 HZCK 173.14689 Hz/cm





Current Data Parameters
 NAME Nov14-2003a
 EXPNO 10
 PROCNO 1

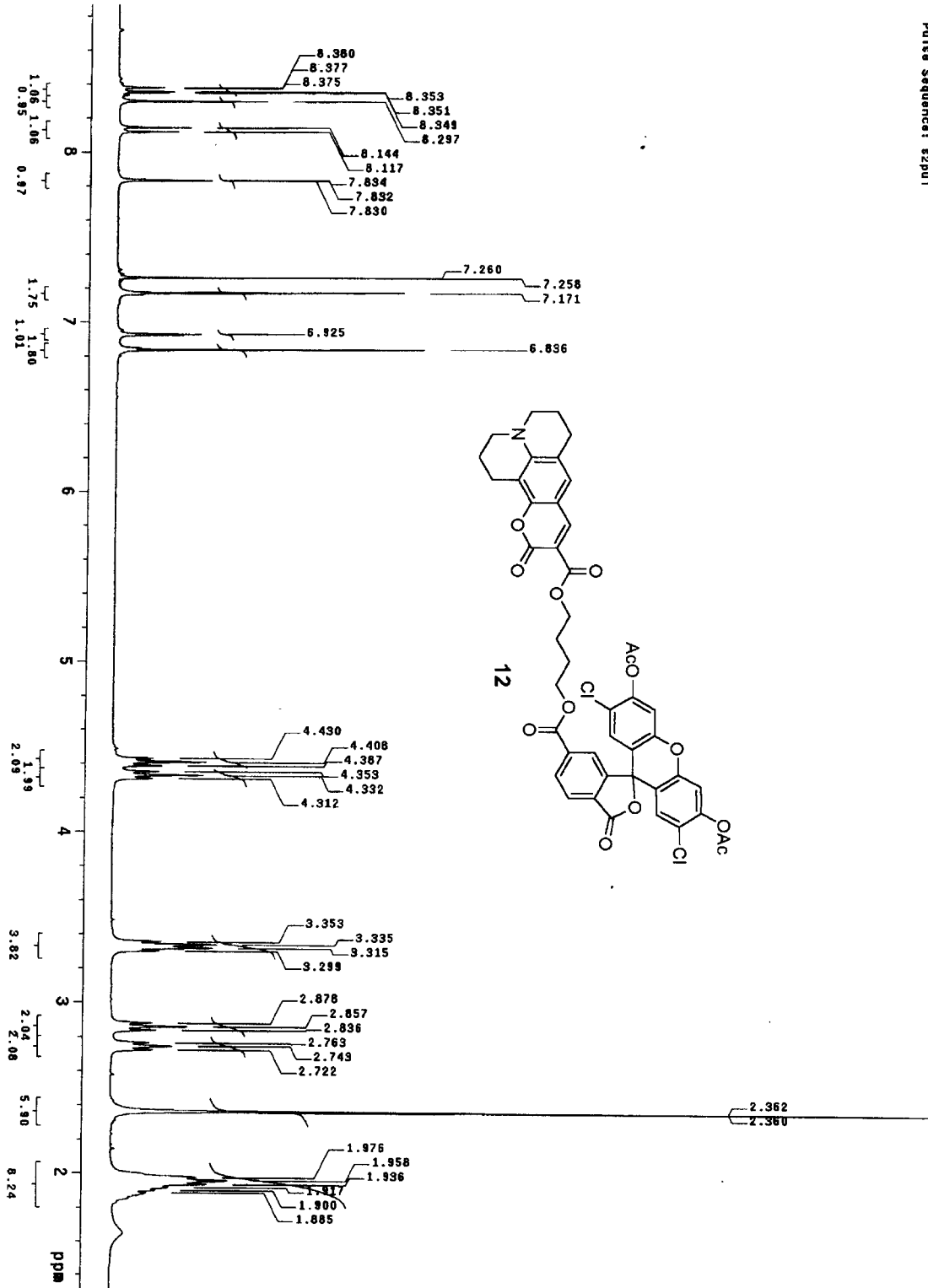
F2 - Acquisition Parameters
 Date_ 20031114
 Time 11.10
 INSTRUM spect
 PROBRD 5mm BBO BB-1
 PULPROG zg30
 TD 65536
 SOLVENT CDCl3
 NS 16
 DS 2
 SMH 8278.146 Hz
 FIDRES 0.126314 Hz
 AQ 3.9584243 sec
 RG 456.1
 DW 60.400 usec
 DE 6.00 usec
 TE 300.0 K
 D1 1.00000000 sec

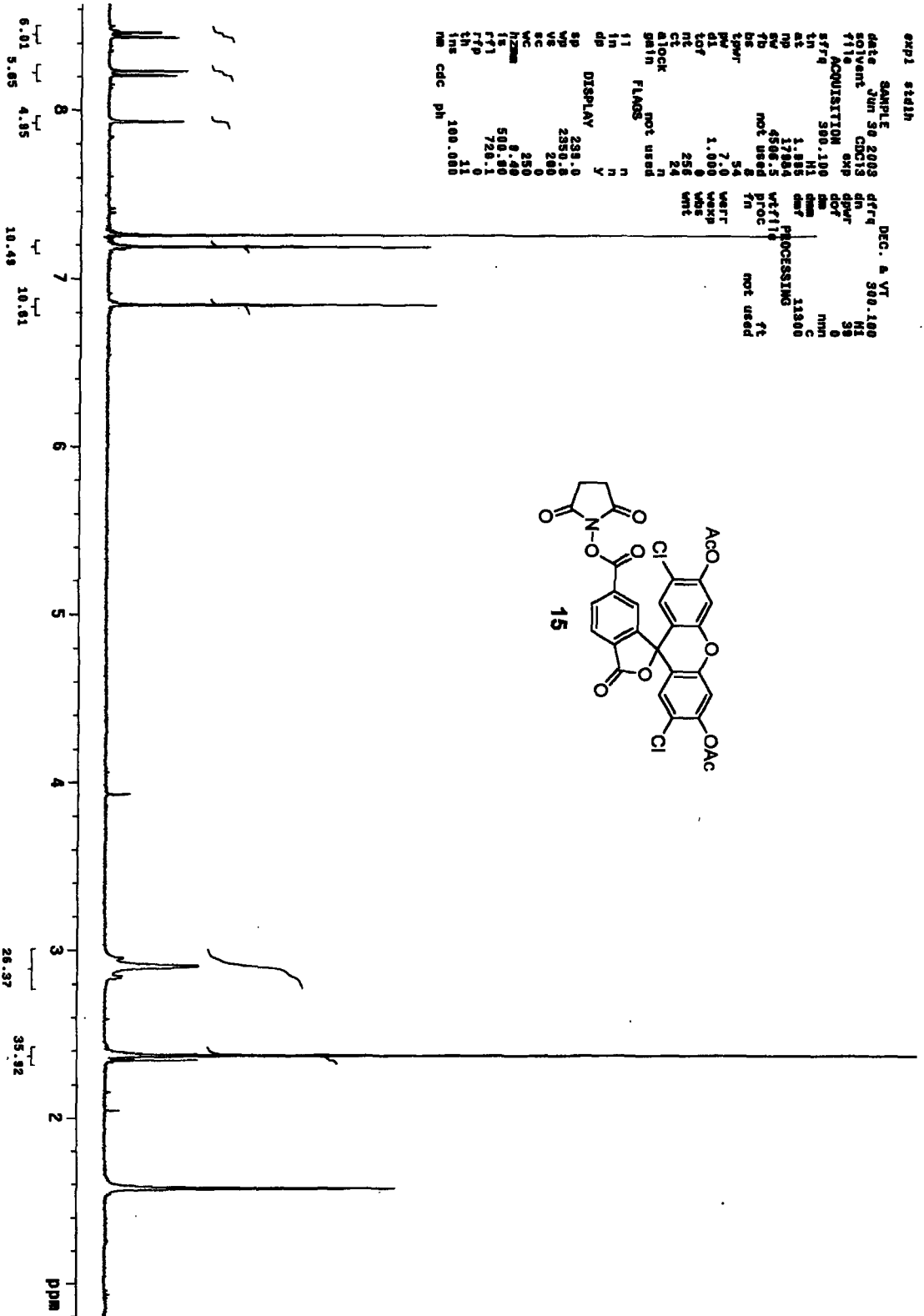
***** CHANNEL f3 *****
 NUC1 1H
 P1 7.50 usec
 PL1 0.00 dB
 SFO1 400.1324710 MHz

F2 - Processing parameters
 SI 32768
 SF 400.1300056 MHz
 KCM EM
 SSB 0
 LB 0.30 Hz
 GB 0
 PC 1.00

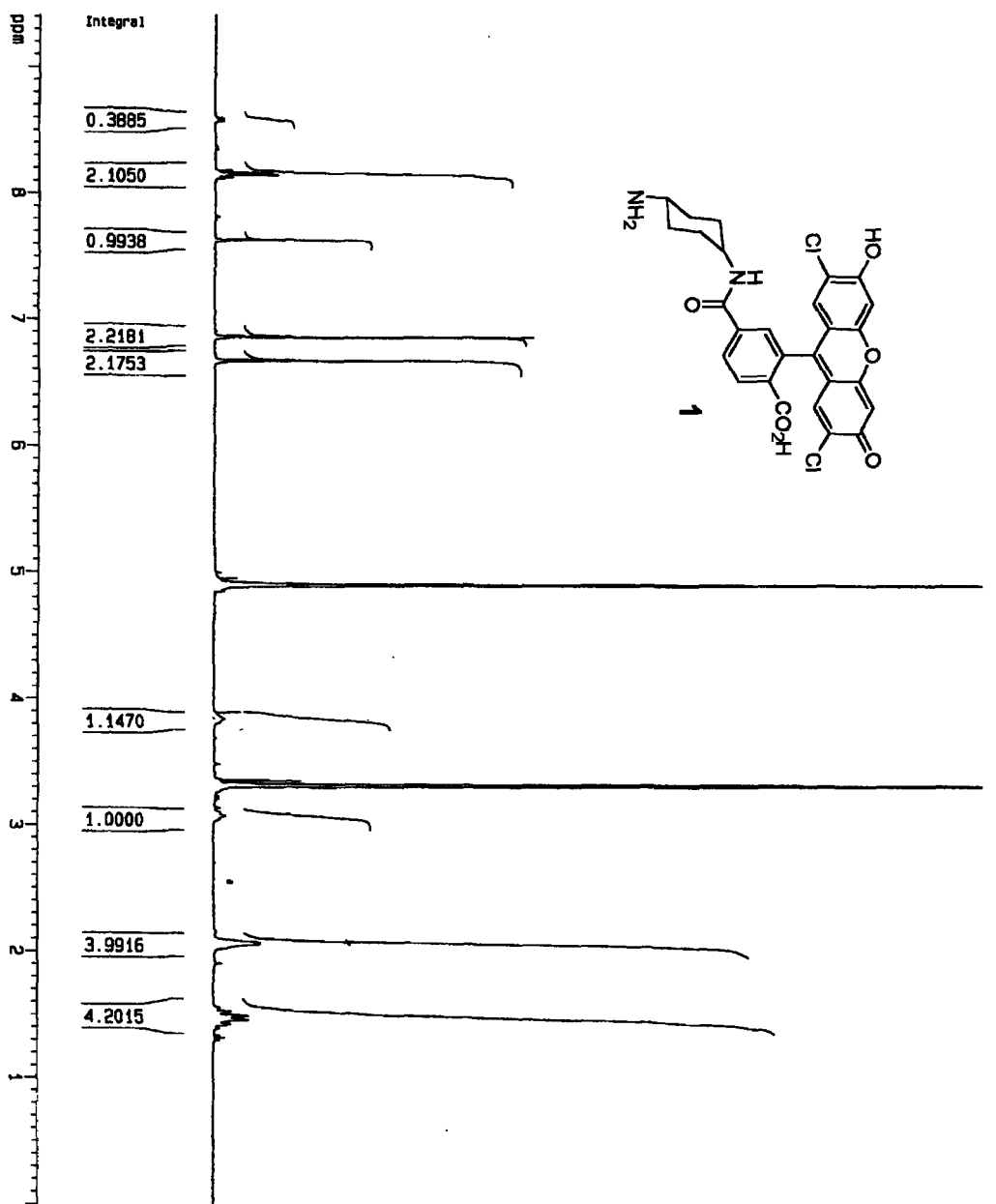
1D NMR plot parameters
 CX 20.00 cm
 F1P 8.970 ppm
 F1 3589.18 Hz
 F2P 0.498 ppm
 F2 199.35 Hz
 PPMCH 0.42359 ppm/cm
 HZCM 169.49184 Hz/cm

Pulse Sequence: szpu1





Chapter 4 Spectra



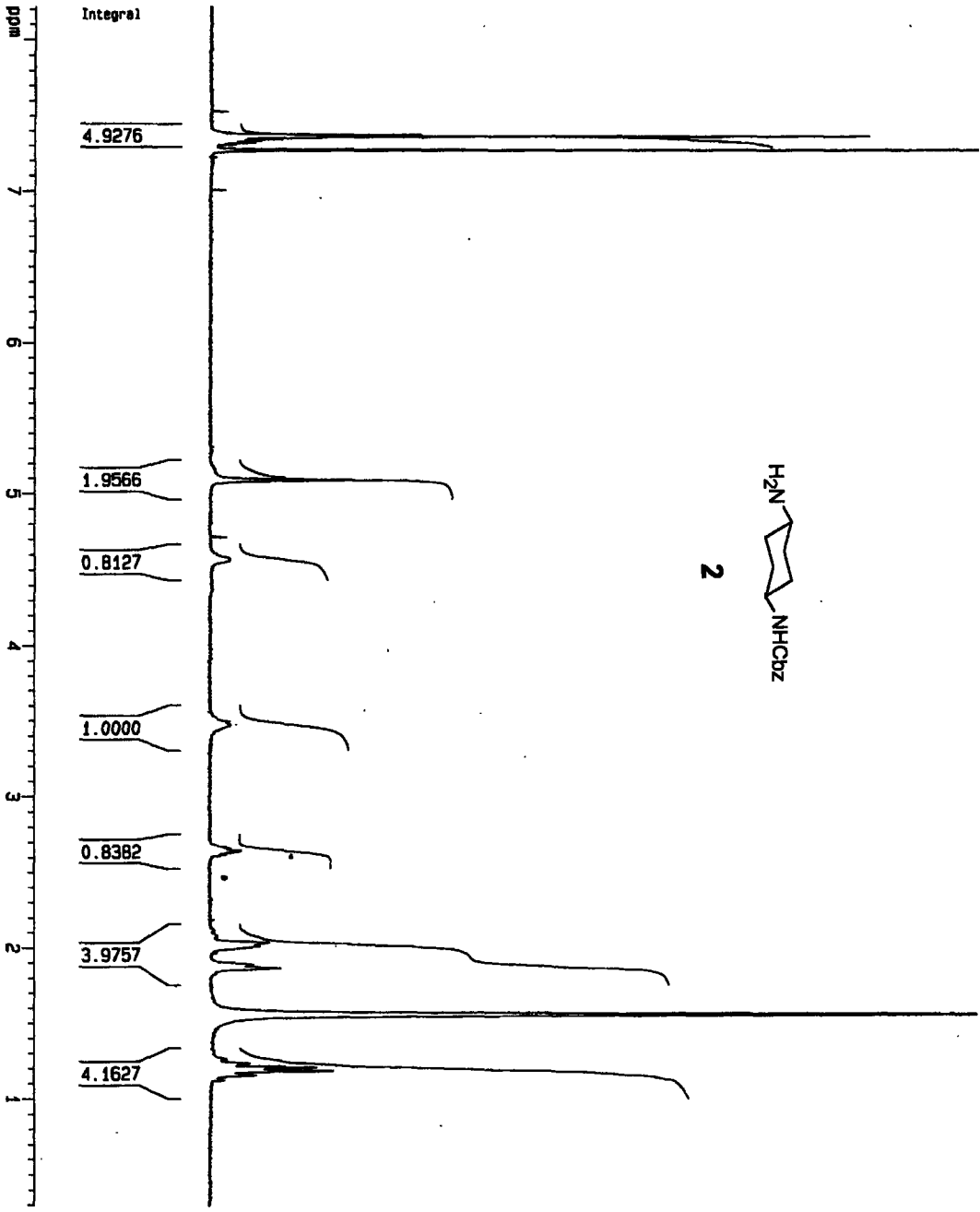
Current Date Parameters
 NAME Aug08-2004-a
 EXPNO 10
 PROCNO 1

F2 - Acquisition Parameters
 Date_ 20040808
 Time 22.21
 INSTRUM spect
 PROBHD 5mm BBO BB-1
 PULPROG zg30
 TD 65536
 SOLVENT H₂O
 NS 128
 DS 0
 SMH 8278.146 Hz
 FIDRES 0.126314 Hz
 AQ 3.5984243 sec
 RG 512
 DW 60.400 usec
 DE 6.00 usec
 TE 300.0 K
 D1 2.00000000 sec

***** CHANNEL f1 *****
 NL1 1H
 P1 7.90 usec
 PL1 0.00 dB
 SFO1 400.1324710 MHz

F2 - Processing parameters
 SI 32768
 SF 400.1300114 MHz
 KW 0
 SSB EM
 LB 0.30 Hz
 GB 0
 PC 1.00

10 NMR plot parameters
 CX 20.00 cm
 FIP 9.412 ppm
 F1 3766.09 Hz
 F2* -0.018 ppm
 F2 -7.50 Hz
 PRNCH 0.47155 ppm/cm
 HZCM 188.67588 Hz/cm



Current Data Parameters
 NAME Aug12-2004
 EXPNO 10
 PROCNO 1

F2 - Acquisition Parameters

Date_ 20040812
 Time 21.50
 INSTRUM spect
 PROCNO 5mm BBO BB-1
 PULPROG zg30
 TD 65535
 SOLVENT CDCl3
 NS 16
 DS 2
 SMH 8278.146 Hz
 FIDRES 0.126314 Hz
 AQ 3.9564243 sec
 RG 512
 DM 60.400 usec
 DE 6.00 usec
 TE 300.0 K
 D1 1.00000000 sec

***** CHANNEL f1 *****

NUC1 1H
 P1 7.90 usec
 PL1 0.00 dB
 SF01 400.1324710 MHz

F2 - Processing parameters

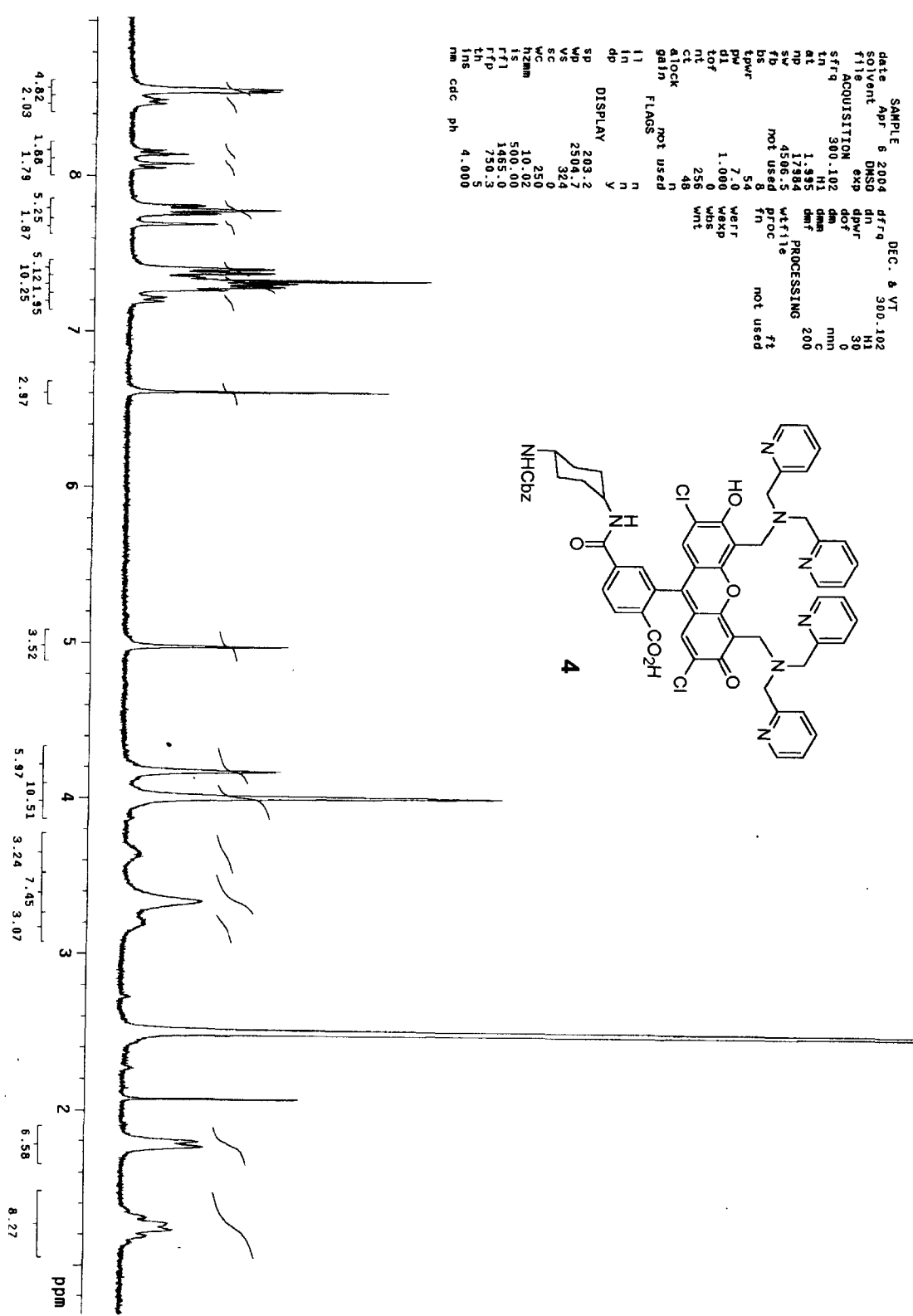
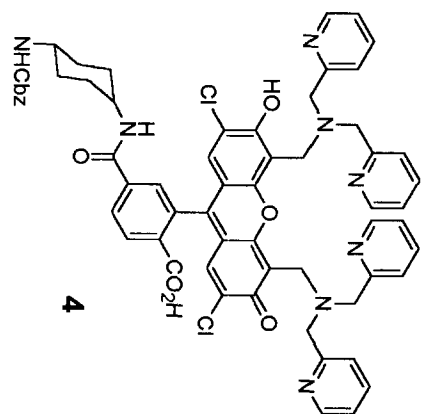
SI 32768
 SF 400.130005 MHz
 WDW EM
 SSB 0
 LB 0.30 Hz
 GB 0
 PC 1.00

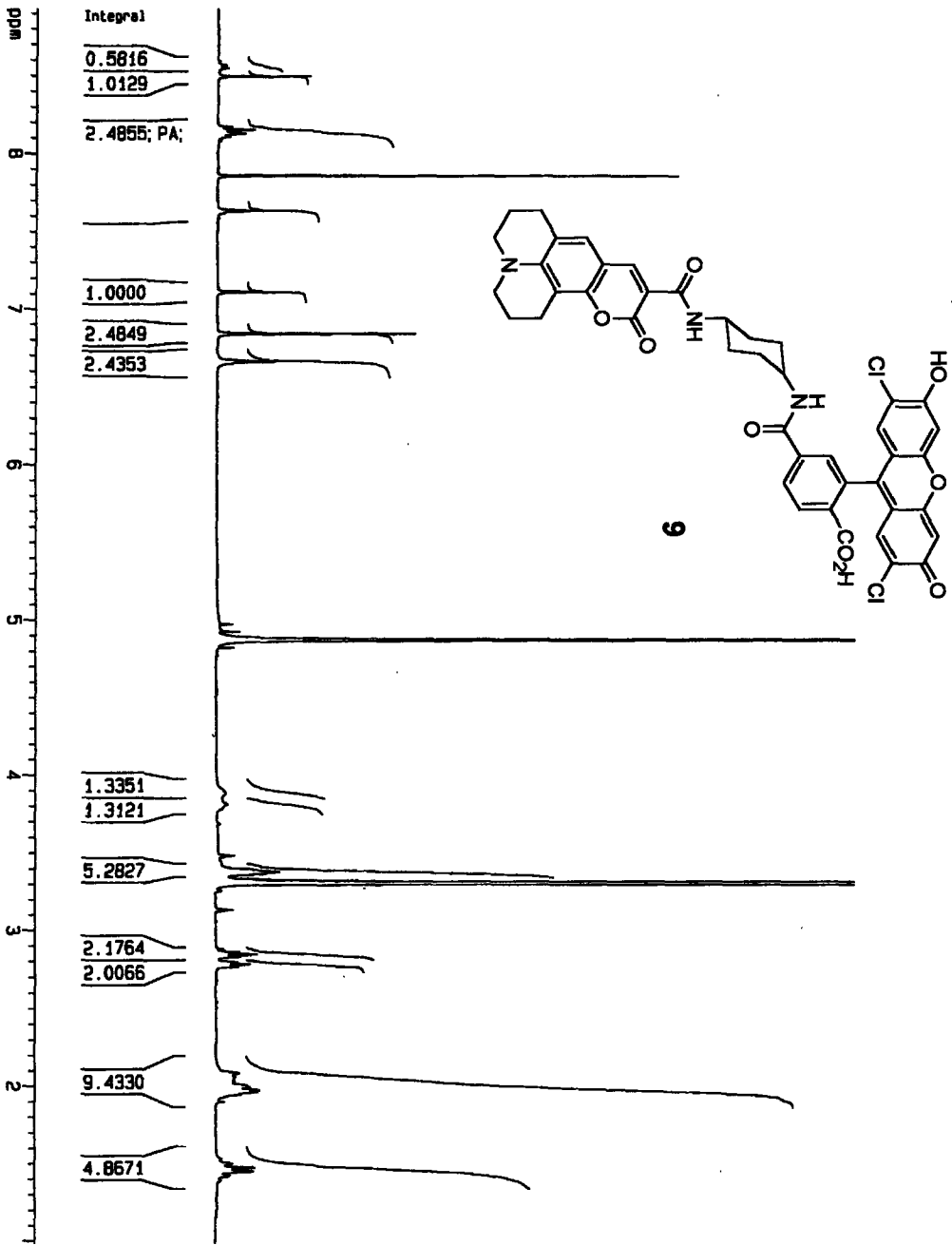
1D NMR plot parameters

CX 20.00 cm
 F1P 8.215 ppm
 F1 3287.66 Hz
 F2P 0.293 ppm
 F2 117.11 Hz
 PWDW 0.39619 ppm/cm
 NZCM 188.52740 Hz/cm

exp2 std1h

date	SAMPLE	6	2004	DEC. 6	VT
solvent	DMSO	dn	30	nm	30
file	exp	dpr	0	nm	0
ACQUISITION	300.102	dm	0	nm	0
frq	300.102	dm	0	nm	0
in	H1	dm	0	nm	0
at	1.985	dm	0	nm	0
np	17984	dm	0	nm	0
z	4306.3	dm	0	nm	0
fb	not used	dm	0	nm	0
bs	not used	dm	0	nm	0
power	54	dm	0	nm	0
pw	7.0	dm	0	nm	0
dl	1.000	dm	0	nm	0
tof	0	dm	0	nm	0
nt	256	dm	0	nm	0
ct	48	dm	0	nm	0
atlock	not used	dm	0	nm	0
gain	not used	dm	0	nm	0
l1	n	dm	0	nm	0
l2	n	dm	0	nm	0
l3	n	dm	0	nm	0
l4	n	dm	0	nm	0
l5	n	dm	0	nm	0
l6	n	dm	0	nm	0
l7	n	dm	0	nm	0
l8	n	dm	0	nm	0
l9	n	dm	0	nm	0
l10	n	dm	0	nm	0
l11	n	dm	0	nm	0
l12	n	dm	0	nm	0
l13	n	dm	0	nm	0
l14	n	dm	0	nm	0
l15	n	dm	0	nm	0
l16	n	dm	0	nm	0
l17	n	dm	0	nm	0
l18	n	dm	0	nm	0
l19	n	dm	0	nm	0
l20	n	dm	0	nm	0
l21	n	dm	0	nm	0
l22	n	dm	0	nm	0
l23	n	dm	0	nm	0
l24	n	dm	0	nm	0
l25	n	dm	0	nm	0
l26	n	dm	0	nm	0
l27	n	dm	0	nm	0
l28	n	dm	0	nm	0
l29	n	dm	0	nm	0
l30	n	dm	0	nm	0
l31	n	dm	0	nm	0
l32	n	dm	0	nm	0
l33	n	dm	0	nm	0
l34	n	dm	0	nm	0
l35	n	dm	0	nm	0
l36	n	dm	0	nm	0
l37	n	dm	0	nm	0
l38	n	dm	0	nm	0
l39	n	dm	0	nm	0
l40	n	dm	0	nm	0
l41	n	dm	0	nm	0
l42	n	dm	0	nm	0
l43	n	dm	0	nm	0
l44	n	dm	0	nm	0
l45	n	dm	0	nm	0
l46	n	dm	0	nm	0
l47	n	dm	0	nm	0
l48	n	dm	0	nm	0
l49	n	dm	0	nm	0
l50	n	dm	0	nm	0
l51	n	dm	0	nm	0
l52	n	dm	0	nm	0
l53	n	dm	0	nm	0
l54	n	dm	0	nm	0
l55	n	dm	0	nm	0
l56	n	dm	0	nm	0
l57	n	dm	0	nm	0
l58	n	dm	0	nm	0
l59	n	dm	0	nm	0
l60	n	dm	0	nm	0
l61	n	dm	0	nm	0
l62	n	dm	0	nm	0
l63	n	dm	0	nm	0
l64	n	dm	0	nm	0
l65	n	dm	0	nm	0
l66	n	dm	0	nm	0
l67	n	dm	0	nm	0
l68	n	dm	0	nm	0
l69	n	dm	0	nm	0
l70	n	dm	0	nm	0
l71	n	dm	0	nm	0
l72	n	dm	0	nm	0
l73	n	dm	0	nm	0
l74	n	dm	0	nm	0
l75	n	dm	0	nm	0
l76	n	dm	0	nm	0
l77	n	dm	0	nm	0
l78	n	dm	0	nm	0
l79	n	dm	0	nm	0
l80	n	dm	0	nm	0
l81	n	dm	0	nm	0
l82	n	dm	0	nm	0
l83	n	dm	0	nm	0
l84	n	dm	0	nm	0
l85	n	dm	0	nm	0
l86	n	dm	0	nm	0
l87	n	dm	0	nm	0
l88	n	dm	0	nm	0
l89	n	dm	0	nm	0
l90	n	dm	0	nm	0
l91	n	dm	0	nm	0
l92	n	dm	0	nm	0
l93	n	dm	0	nm	0
l94	n	dm	0	nm	0
l95	n	dm	0	nm	0
l96	n	dm	0	nm	0
l97	n	dm	0	nm	0
l98	n	dm	0	nm	0
l99	n	dm	0	nm	0
l100	n	dm	0	nm	0





```

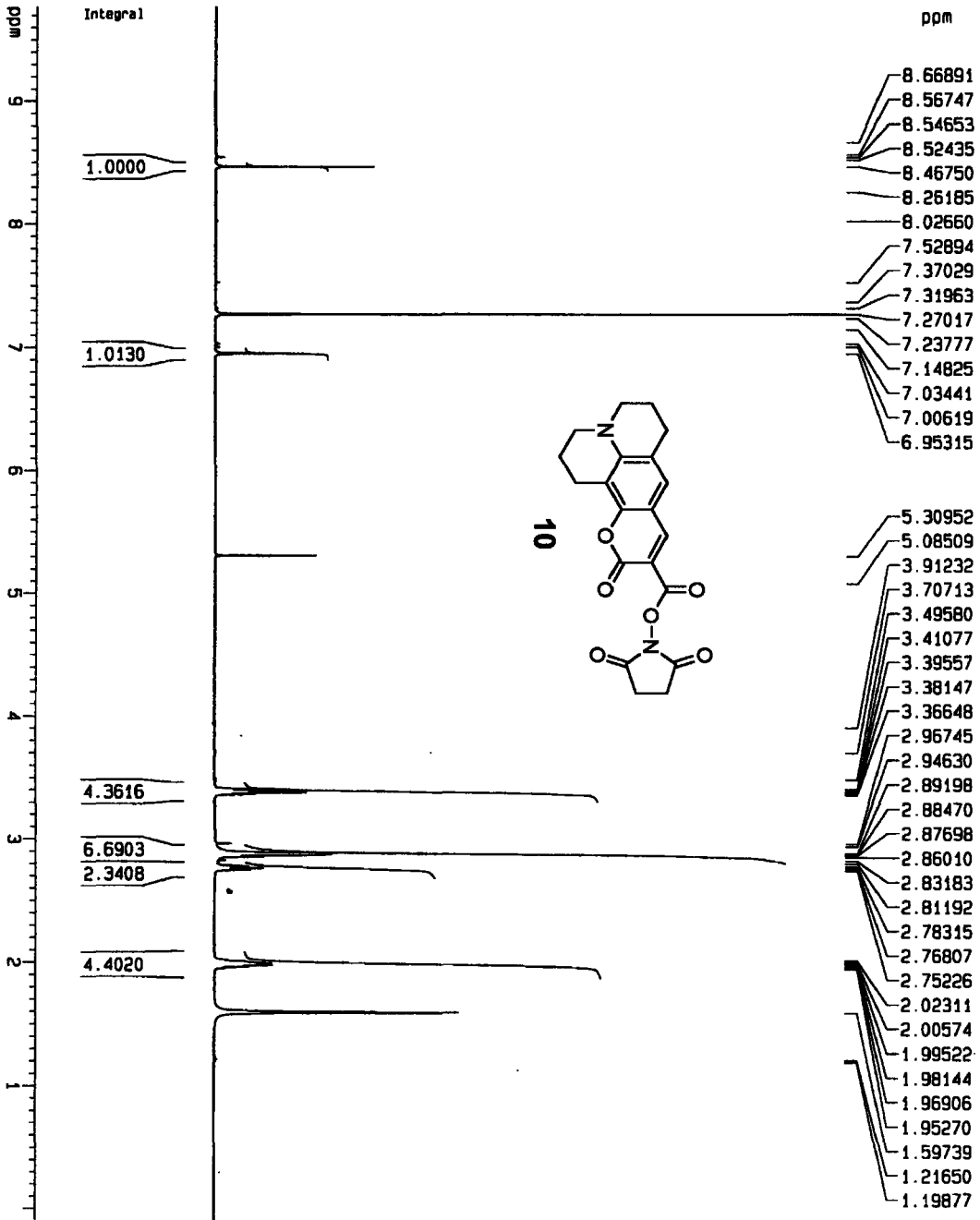
Current Data Parameters
NAME      JUI02-2004
EXPNO    10
PROCNO   1

F2 - Acquisition Parameters
Date_    20040702
Time     18.18
INSTRUM spect
PROBHD   5mm BBO BB-1
PULPROG zg30
TD       65536
SOLVENT MeOH
NS       128
DS       0
SWH      8278.146 Hz
FIDRES  0.126314 Hz
AQ       3.9584243 sec
RG       512
DE       80.400 usec
TE       300.0 K
D1       2.00000000 sec

***** CHANNEL f1 *****
NUC1      1H
P1        7.90 usec
PL1       0.00 dB
SF01     400.1324710 MHz

F2 - Processing parameters
SI        32768
SF        400.1300117 MHz
WDW       EM
SSB       0
LB        0.30 Hz
GB        0
PC        1.00

1D NMR plot parameters
CX        20.00 cm
F1P       8.932 ppm
F1        3873.96 Hz
F2P       0.965 ppm
F2        394.27 Hz
PRN1CM   0.39733 ppm/cm
HZCM     156.59423 Hz/cm
    
```

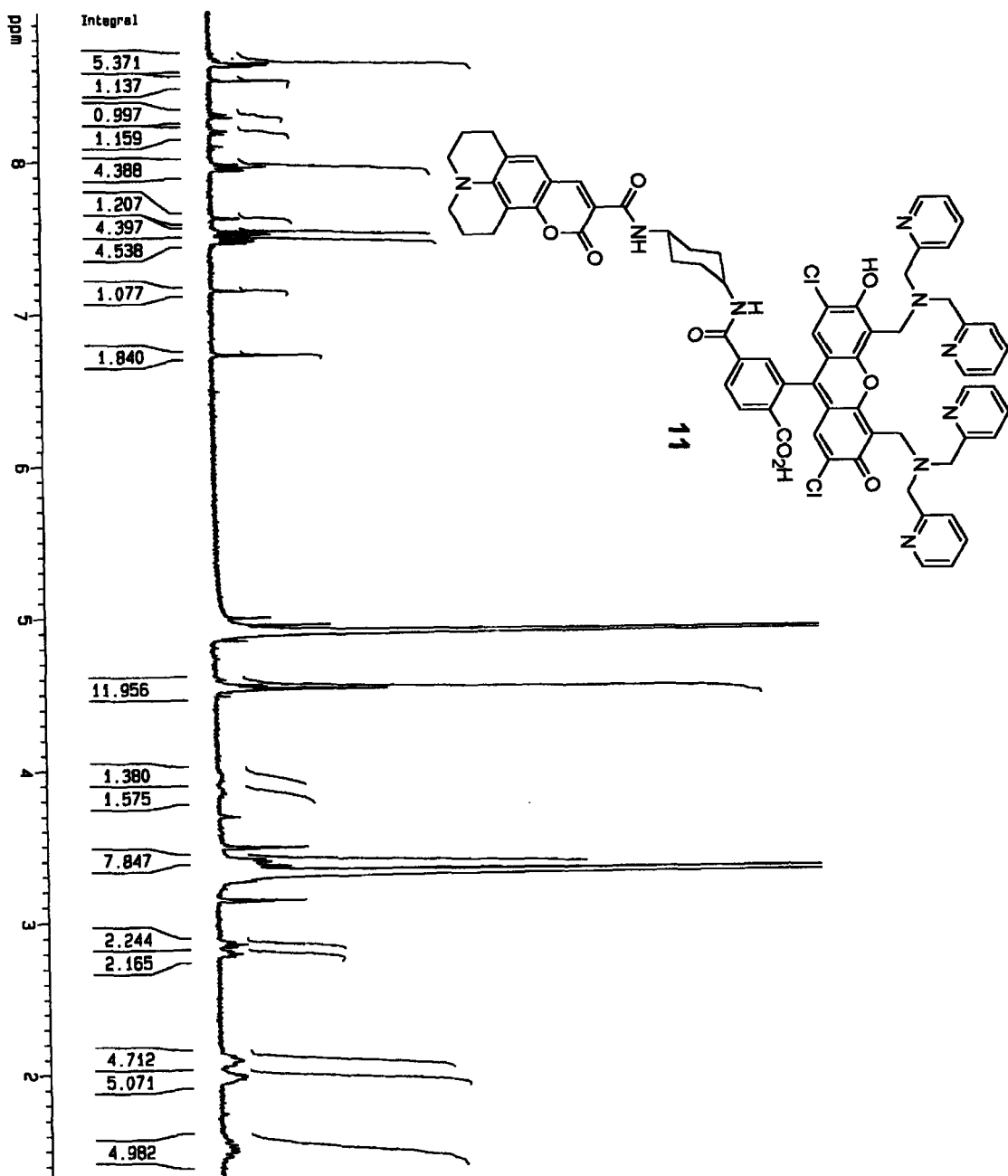
Current Data Parameters
 NAME J1102-2004-ACW
 EXPNO 10
 PROCNO 1

F2 - Acquisition Parameters
 Date_ 20040702
 Time 18.36
 INSTRUM spect
 PROBRD 5mm BBO BB-1
 PULPROG zg30
 TD 65536
 SOLVENT CDCl3
 NS 16
 DS 2
 SMH 8278.146 Hz
 FIDRES 0.126314 Hz
 AQ 3.9584243 sec
 RG 574.7
 DM 50.400 usec
 DE 6.00 usec
 TE 300.0 K
 D1 1.00000000 sec

----- CHANNEL f1 -----
 NUCL1 1H
 P1 7.90 usec
 PL1 0.00 dB
 SF01 400.1324710 MHz

F2 - Processing parameters
 SI 32768
 SF 400.1300056 MHz
 WDW EM
 SSB 0
 LB 0.30 Hz
 GB 0
 PC 1.00

1D NMR plot parameters
 CX 20.00 cm
 F1P 9.769 ppm
 F1 3908.98 Hz
 F2P -0.095 ppm
 F2 -38.22 Hz
 PPMCK 0.49324 ppm/cm
 HZCK 197.35976 Hz/cm



Current Data Parameters
 NAME JUL06-2004
 EXPNO 10
 PROCNO 1

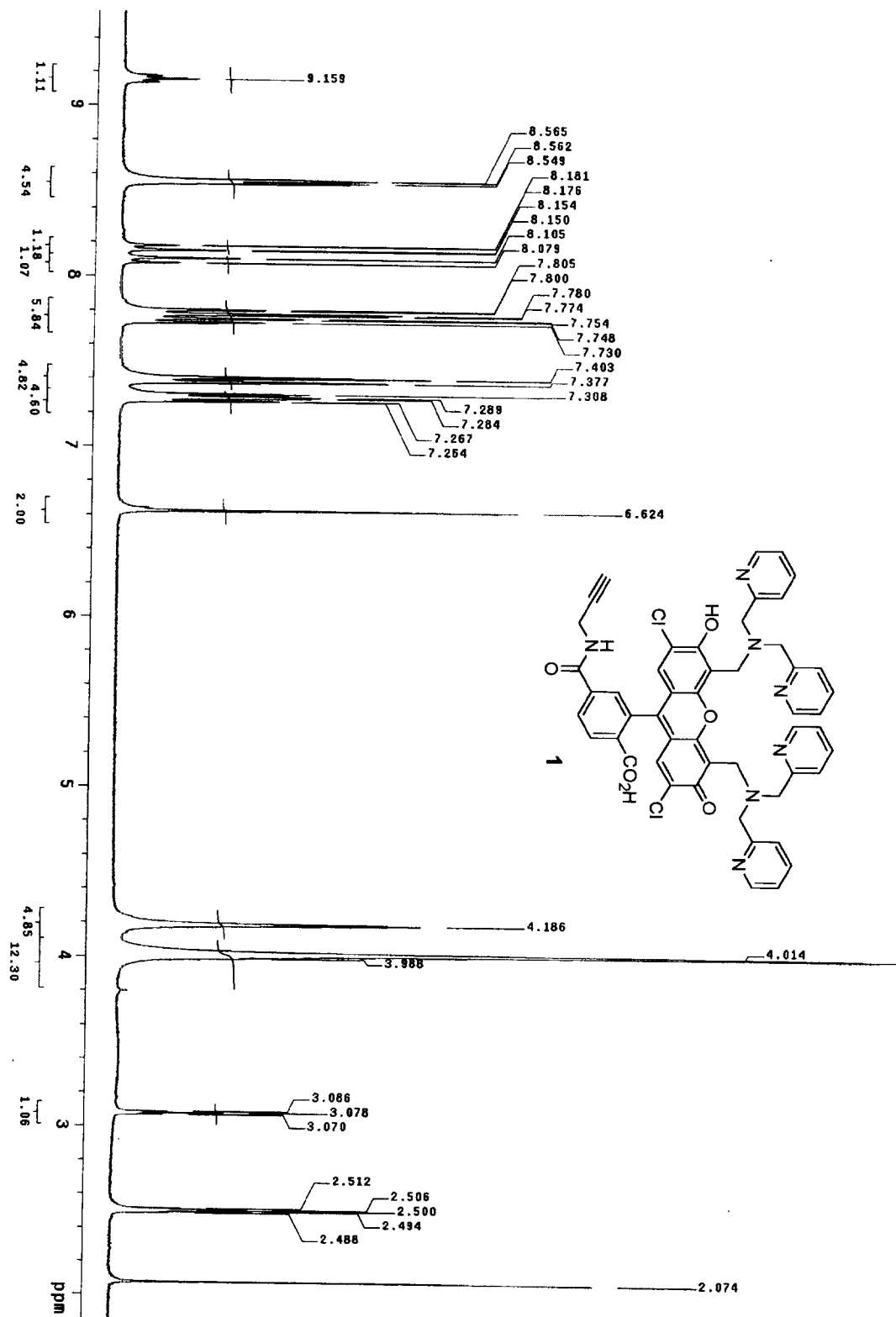
F2 - Acquisition Parameters
 Date_ 20040706
 Time 12.24
 INSTRUM spect
 PROBRD 5mm BBO BB-1
 PULPROG zg30
 TD 65535
 SOLVENT MeOH
 NS 128
 DS 0
 SMH 8278.146 Hz
 FIDRES 0.126314 Hz
 AQ 3.9584243 sec
 RG 574.7
 DW 60.400 usec
 DE 6.00 usec
 TE 300.0 K
 D1 2.00000000 sec

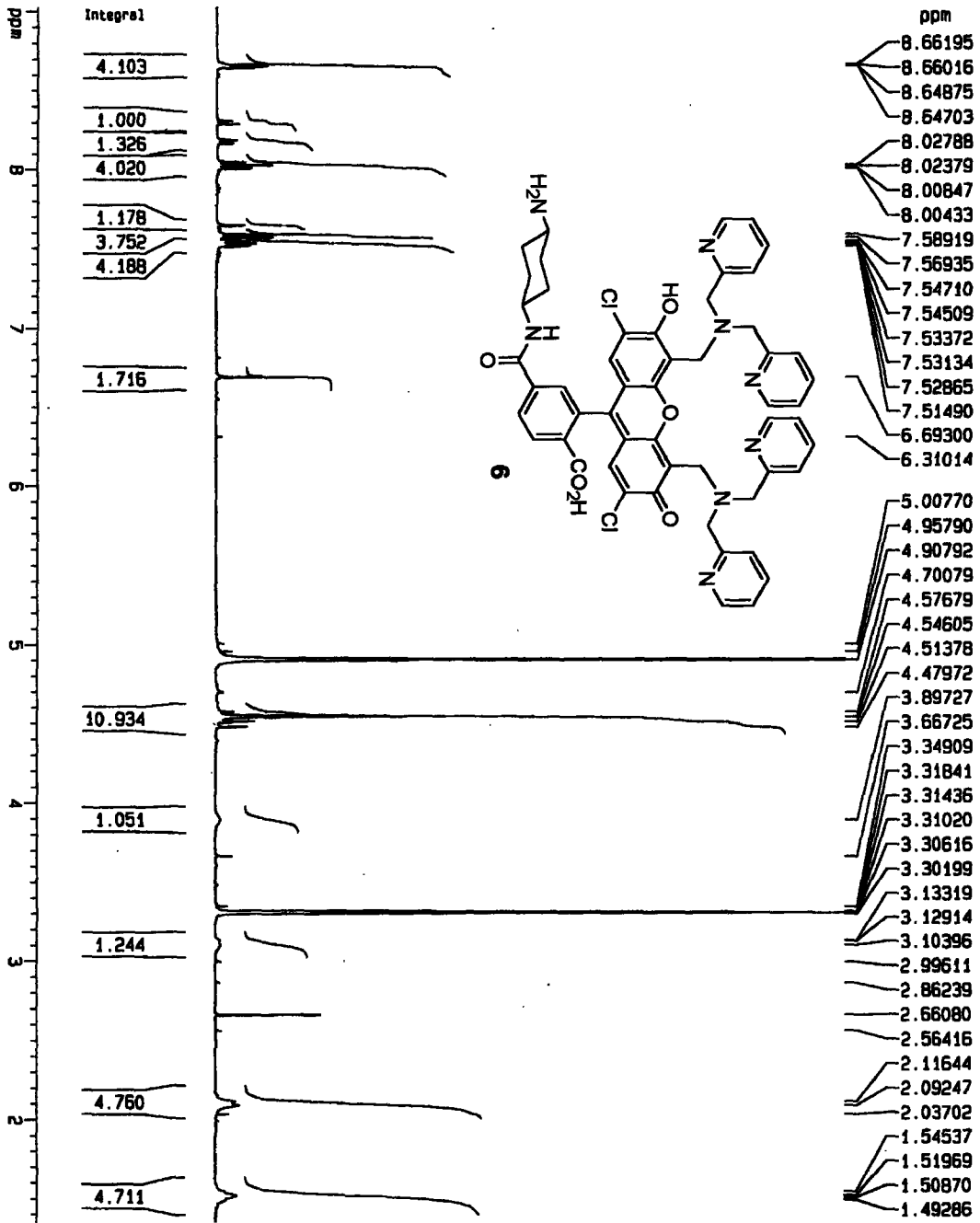
***** CHANNEL f1 *****
 NU1C1 1H
 P1 7.90 usec
 PL1 0.00 dB
 SFO1 400.1324710 MHz

F2 - Processing parameters
 SI 32768
 SF 400.1300114 MHz
 NH 1
 EN 0
 SSB 0
 LB 0.30 Hz
 GB 0
 PC 1.00

1D NMR plot parameters
 CX 20.00 cm
 F1P 8.978 ppm
 F1 3592.48 Hz
 F2P 1.329 ppm
 F2 531.58 Hz
 PPM0M 0.38249 ppm/cm
 N1ZM 153.04520 Hz/cm

Chapter 5 Spectra





Current Data Parameters
 NAME Jun29-2004
 EXPNO 10
 PROCNO 1

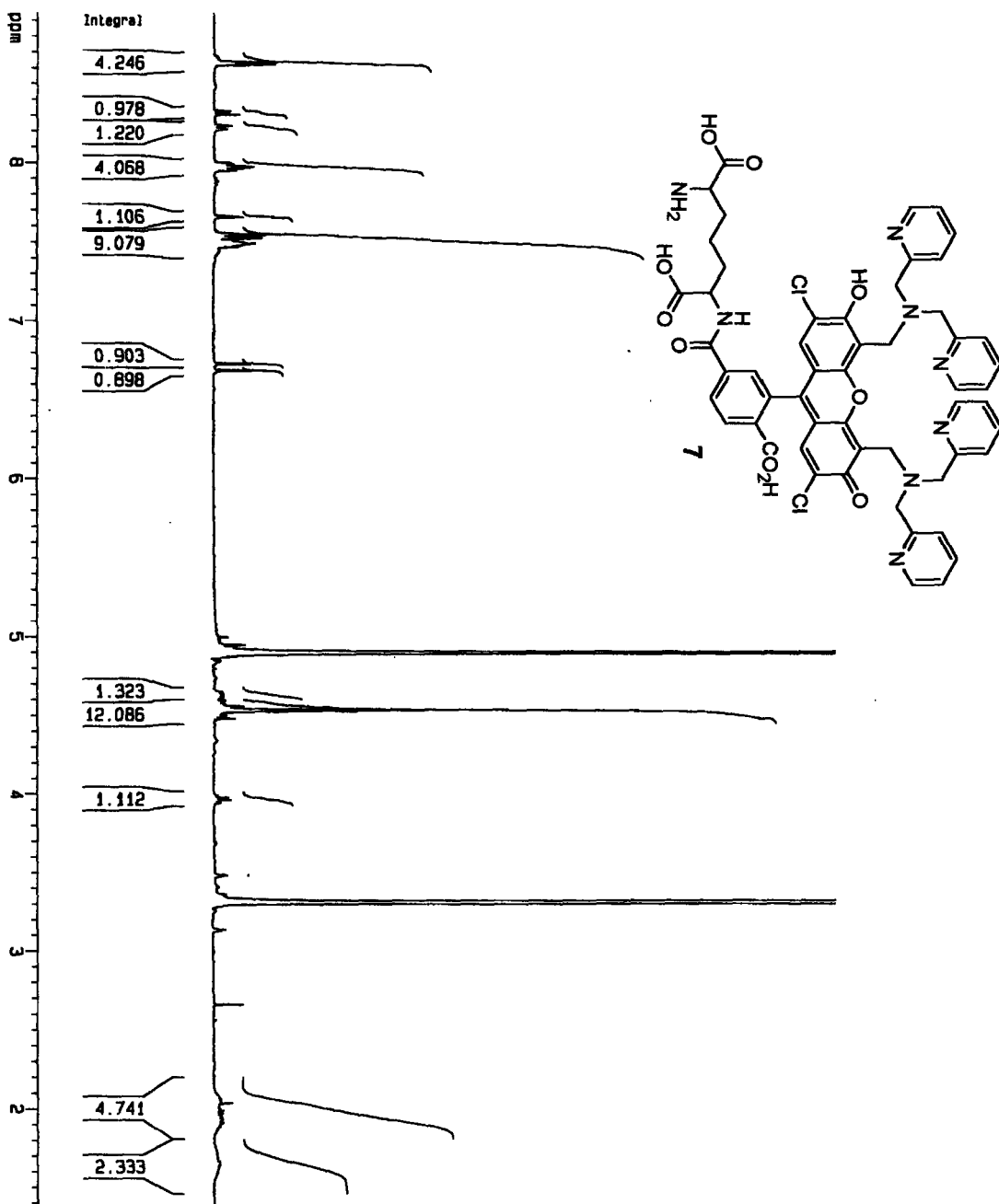
F2 - Acquisition Parameters
 Date_ 20040629
 Time 21.47
 INSTRUM spect
 PROBRD 5mm BBO BB-1
 PULPROG zg30
 TD 65536
 SOLVENT MeOH
 NS 128
 DS 0
 SMI 8278.146 Hz
 FIDRES 0.128314 Hz
 AQ 3.8584243 sec
 RG 456.1
 DM 60.400 usec
 DE 6.00 usec
 TE 300.0 K
 D1 2.00000000 sec

CHANNEL f1

NUC1 1H
 P1 7.90 usec
 PL1 0.00 dB
 SFO1 400.1324710 MHz

F2 - Processing parameters
 SI 32768
 SF 400.1300114 MHz
 KHZ EN
 SSB 0
 LB 0.30 Hz
 BB 0
 PC 1.00

1D NMR plot parameters
 CX 20.00 cm
 F1P 9.024 ppm
 F1 3610.76 Hz
 F2P 1.351 ppm
 F2 540.72 Hz
 PPM2CH 0.36353 ppm/cm
 HZCM 153.50204 Hz/cm



Current Data Parameters
 NAME Jul128-2004
 EXPNO 10
 PROCNO 1

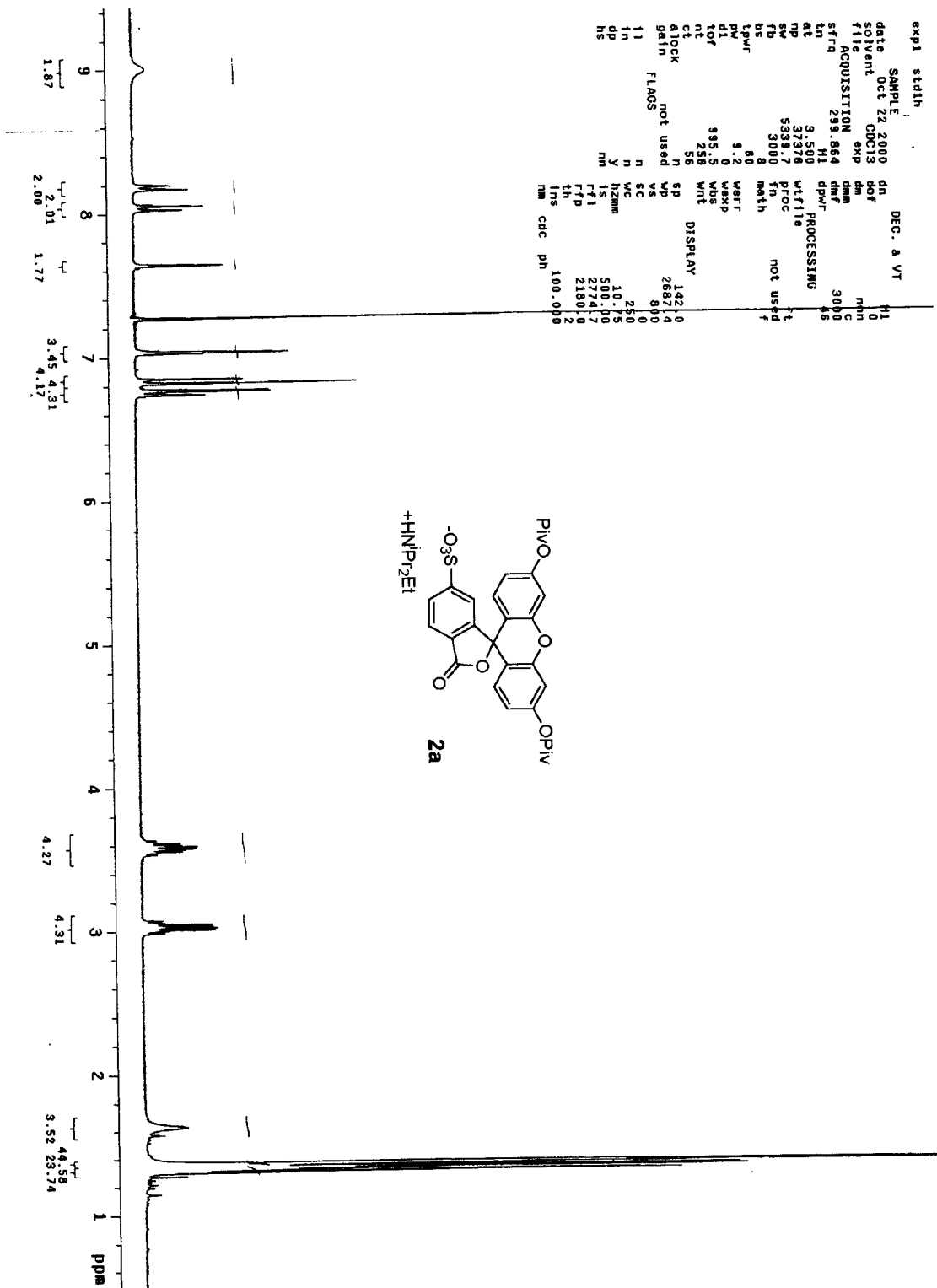
F2 - Acquisition Parameters
 Date_ 20040728
 Time 18:33
 INSTRUM spect
 PROBRD 5mm BBO BB-1
 PULPROG zg30
 TD 65536
 SOLVENT MeOH
 NS 128
 DS 0
 SFO1 8276.146 Hz
 FIDRES 0.126314 Hz
 AQ 3.9584243 sec
 RG 512
 DM 60.400 usec
 DE 5.00 usec
 TE 300.0 K
 D1 2.00000000 sec

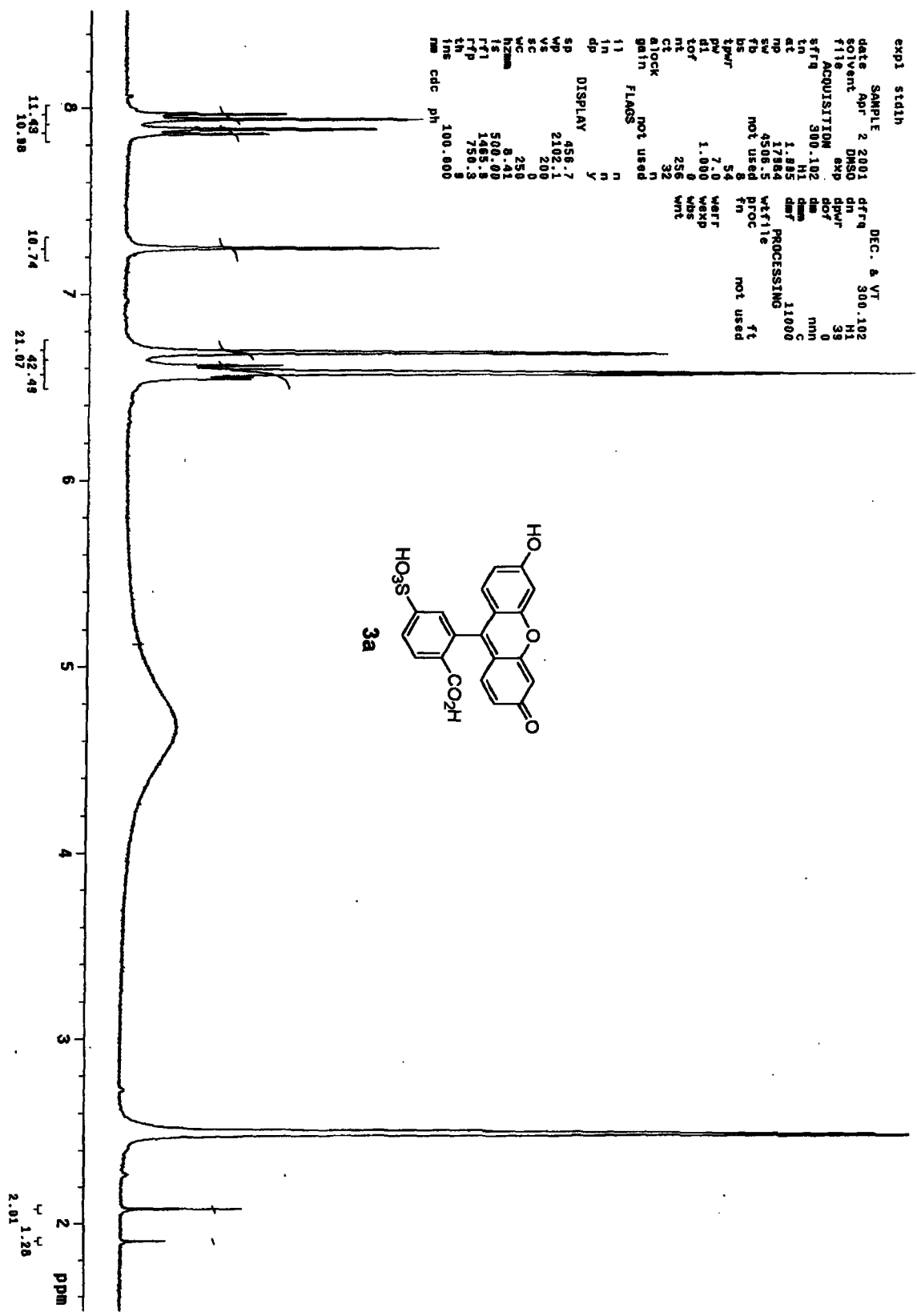
***** CHANNEL f1 *****
 NUC1 1H
 P1 7.90 usec
 PL1 0.00 dB
 SFO1 400.1324710 MHz

F2 - Processing parameters
 SI 32768
 SF 400.1253654 MHz
 MDN EM
 SSB 0
 LB 0.30 Hz
 GB 0
 PC 1.00

1D NMR plot parameters
 CX 20.00 cm
 F1P 8.944 ppm
 F1 3578.90 Hz
 F2P 1.386 ppm
 F2 554.55 Hz
 PPMCN 0.37792 ppm/cm
 HZCN 151.21779 Hz/cm

Appendix 1 Spectra





```

expt stidln
SAMPLE 2 2001 DEC. 8 VT
date Apr 2 2001 dfrq 300.102
solvent DMSO dn HI
f1le ACQUISITION exp dppw 38
sfrq 300.102 dm 0
ln HI dm C
et 1.885 HI dmf 11000
mp 17884 wtfile PROCESsing ft
sw 4508.5 wtfile
fb not used proc not used
bs 8 54
tpwr 7.0 weff
pw 1.000 wexp
dl 0 wds
tof 0 wnt
nt 256
ct 32
atlock not used
gain not used
flags
11 n
12 n
13 n
14 n
15 n
16 n
17 n
18 n
19 n
20 n
21 n
22 n
23 n
24 n
25 n
26 n
27 n
28 n
29 n
30 n
31 n
32 n
33 n
34 n
35 n
36 n
37 n
38 n
39 n
40 n
41 n
42 n
43 n
44 n
45 n
46 n
47 n
48 n
49 n
50 n
51 n
52 n
53 n
54 n
55 n
56 n
57 n
58 n
59 n
60 n
61 n
62 n
63 n
64 n
65 n
66 n
67 n
68 n
69 n
70 n
71 n
72 n
73 n
74 n
75 n
76 n
77 n
78 n
79 n
80 n
81 n
82 n
83 n
84 n
85 n
86 n
87 n
88 n
89 n
90 n
91 n
92 n
93 n
94 n
95 n
96 n
97 n
98 n
99 n
100 n
nm cdc ph
DISPLAY 456.7
SP 2102.1
MP 200
VE 250
WC 250
hzmax 8.41
fs 500.00
rf1 1465.8
rfp 750.3
ins 100.000

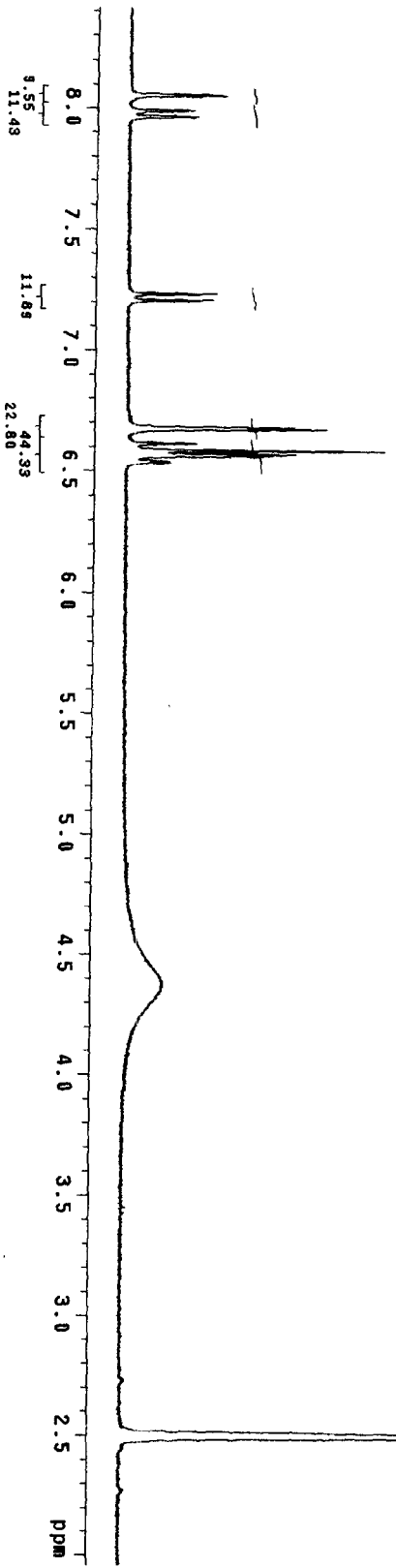
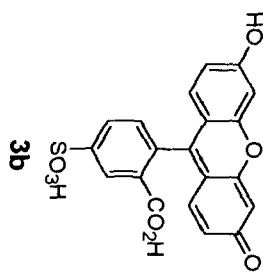
```



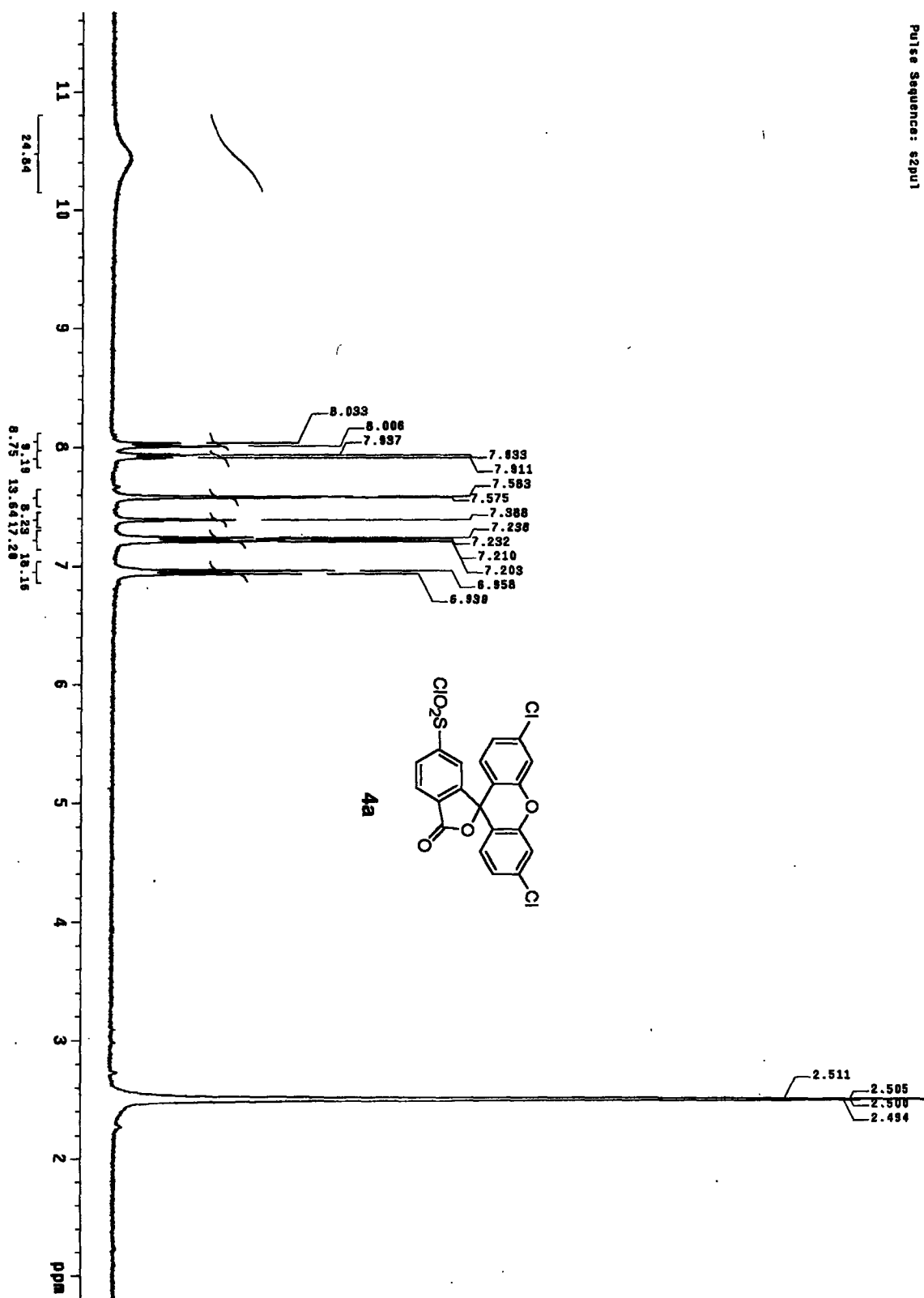
```

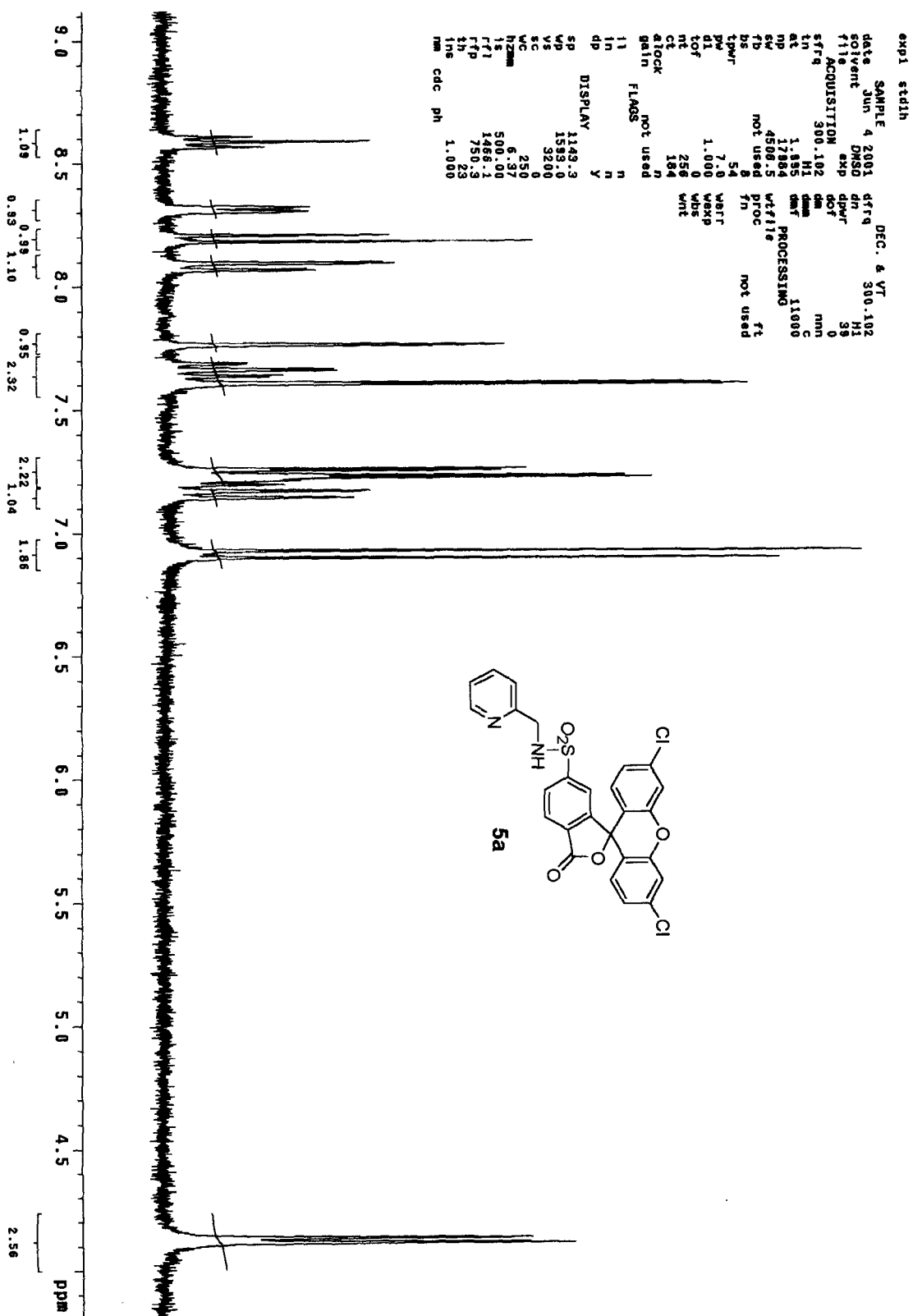
expt statn
SAMPLE 2001
date Jun 10 2001
solvent DMSO
F1 F2 ACQUISITION
SFRq 259.859
IN 3.500
SI 3.579
SP 53007
FB 53008
BS 60
TPWR 9.2
PW 9.6
DI 95.5
TOF 256
CT 48
ALOCK not used
gain n
FLAGS n
11 n
1n n
dp Y
ns Y
DEC. & VT
dn 0
dof 0
dm mm
dmm 3000
dwt C
dpr 46
PROCESsing
WfFlt ft
PRoc not used
Match f
werr 9.2
wexp 9.6
wbs 95.5
wrt 256
DISPLAY
SP 586.0
VP 1836.5
VS 100
SC 0
n WC 7.250
Y hzmm 500.00
1s 1342.3
rF1 749.6
rFP 100.000
tH
tms cdc ph

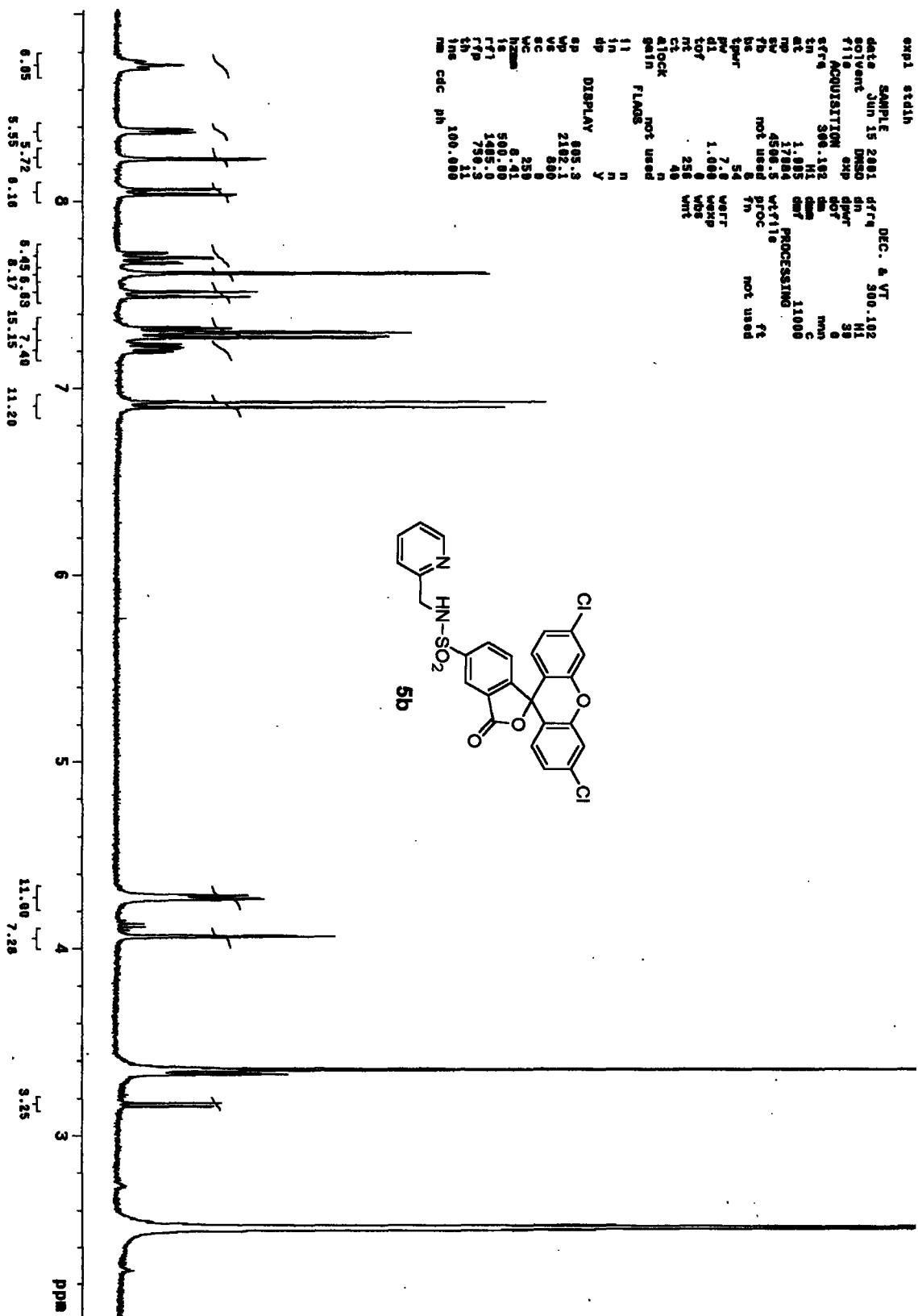
```



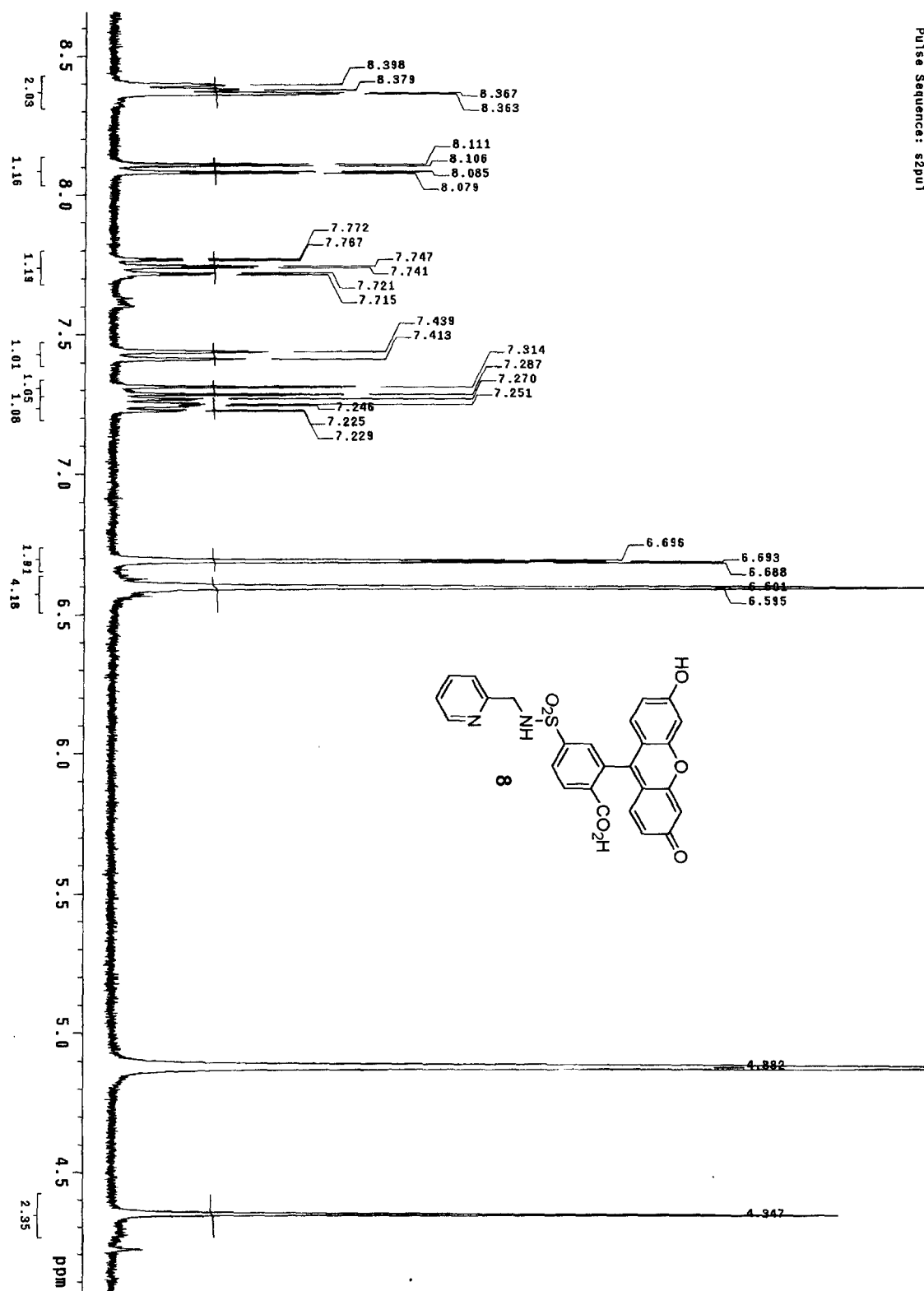
Pulse Sequence: szpu1

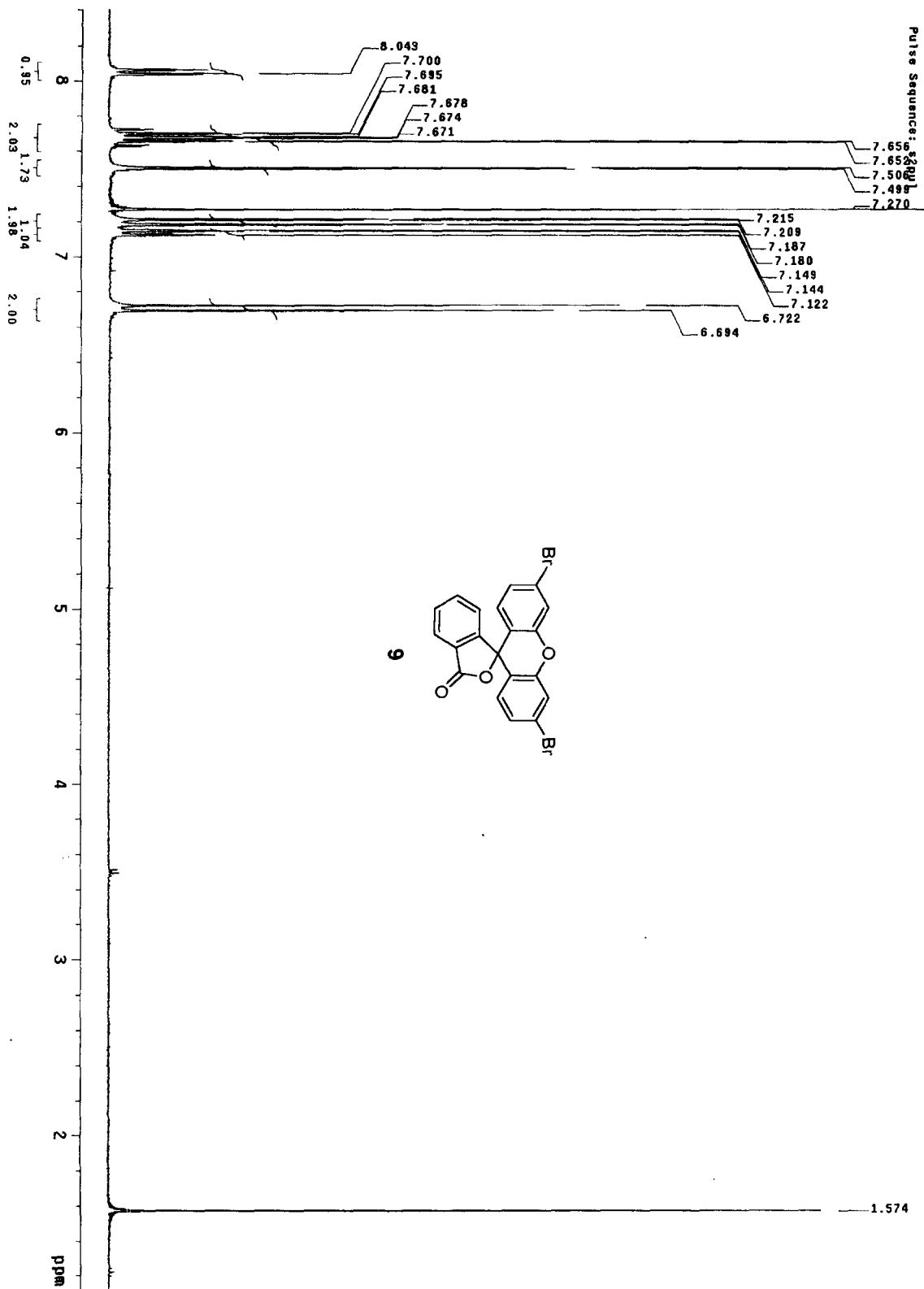


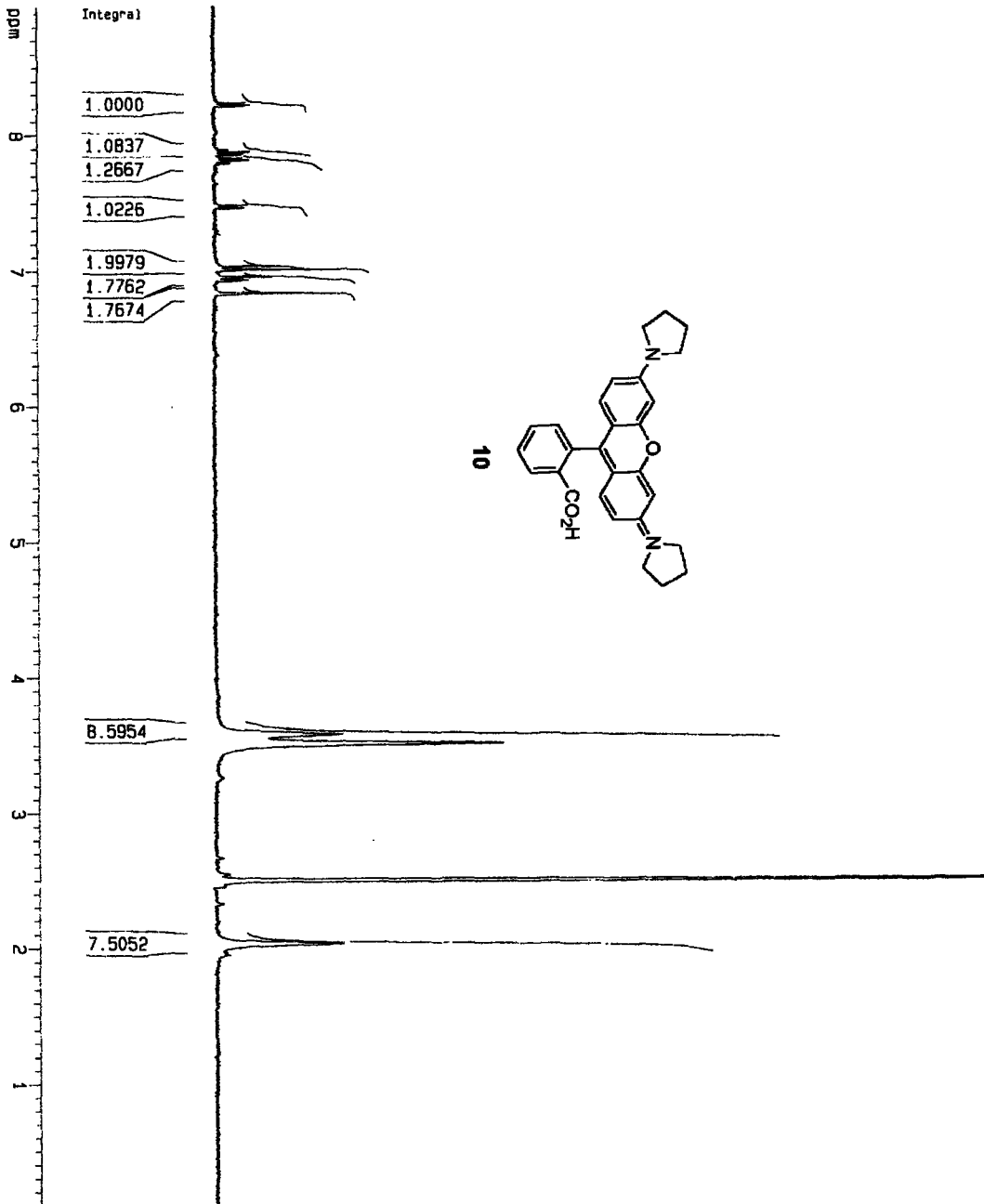




Pulse Sequence: s2pu1







Current Data Parameters
 NAME Aug13-2004
 EXPNO 10
 PROCNO 1

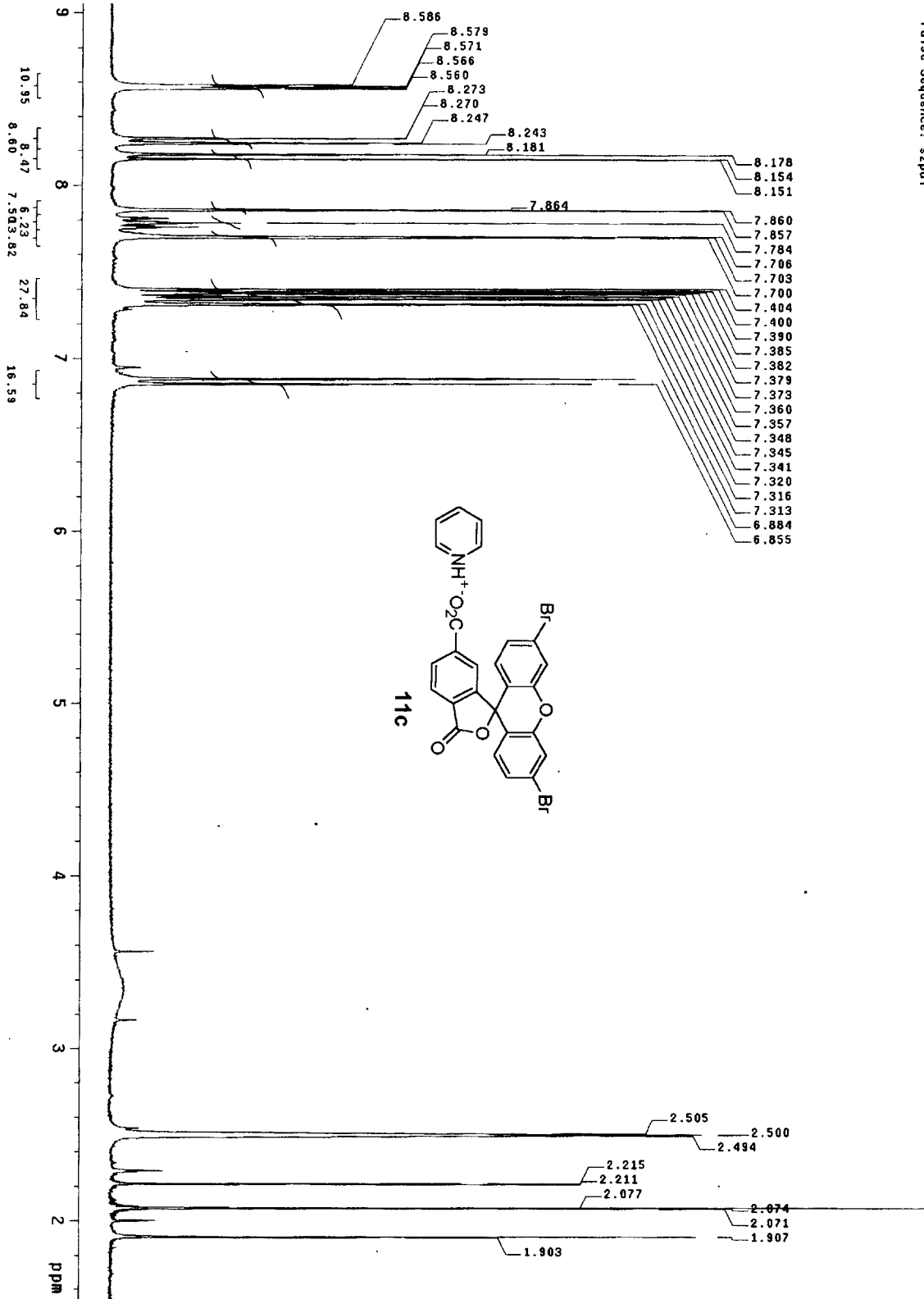
F2 - Acquisition Parameters
 Date_ 20040813
 Time 21.05
 INSTRUM spect
 PROCNO 5mm BBO 99-1
 PULPROG zg30
 TD 65536
 SOLVENT DMSO
 NS 28
 DS 0
 SM 8278.146 Hz
 FIDRES 0.126314 Hz
 AQ 3.9584243 sec
 RG 1024
 DM 60.400 usec
 DE 6.00 usec
 TE 300.0 K
 D1 2.00000000 sec

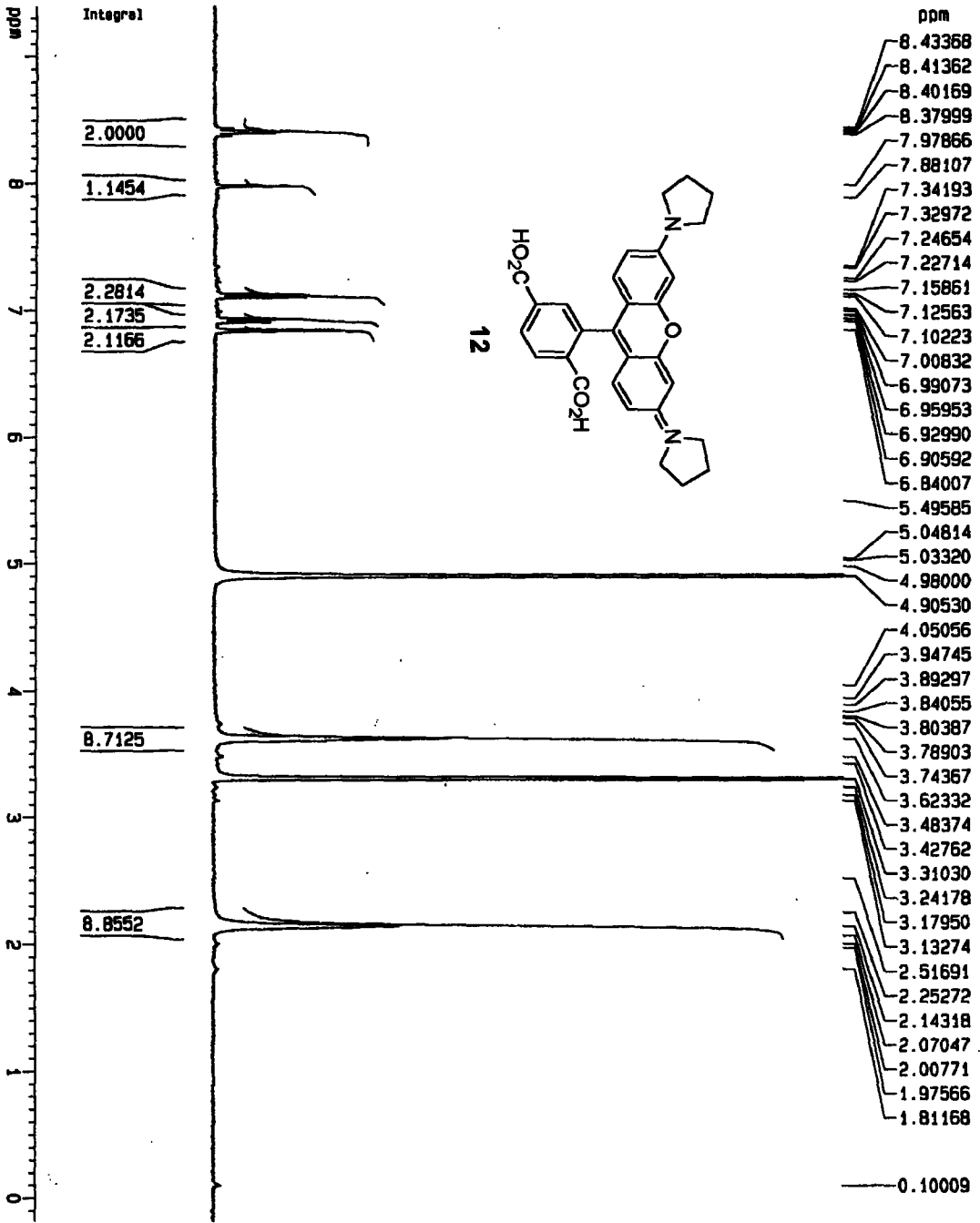
***** CHANNEL f1 *****
 NUC1 1H
 P1 7.50 usec
 PL1 0.00 dB
 SF01 400.1324710 MHz

F2 - Processing parameters
 SI 32768
 SF 400.1300031 MHz
 MDW EM
 SSB 0
 LB 0.30 Hz
 GB 0
 PC 1.00

1D NMR plot parameters
 CX 20.00 cm
 F1P 8.953 ppm
 F1 3582.56 Hz
 F2P 0.116 ppm
 F2 46.53 Hz
 PPMCM 0.44186 ppm/cm
 HZCM 176.80145 Hz/cm

Pulse Sequence: szpu1





Current Data Parameters
 NAME Apr-27-2004
 EXPNO 10
 PROCNO 1

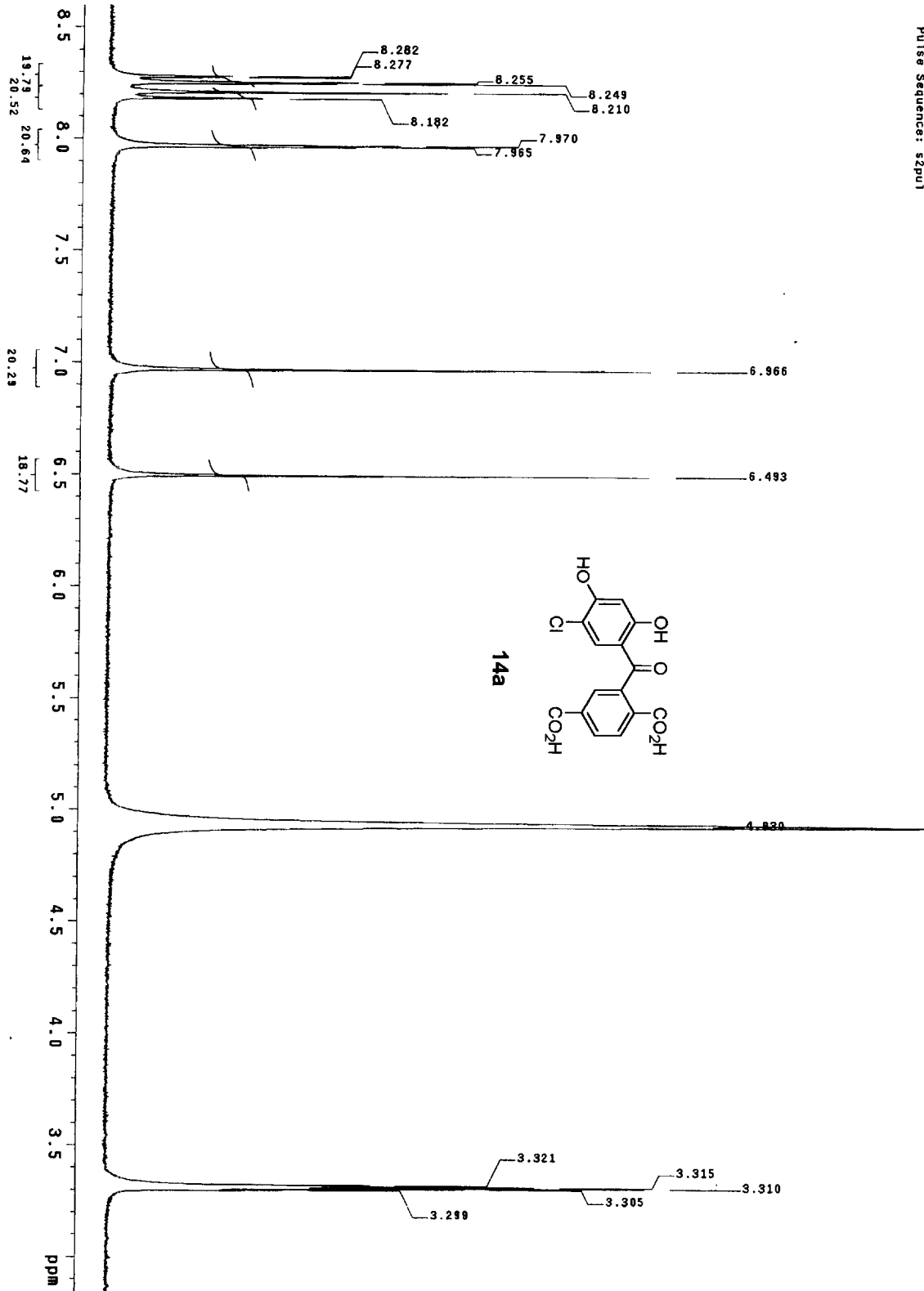
F2 - Acquisition Parameters
 Date_ 20040427
 Time 10.55
 INSTAN spect
 PROBN 5mm BBO BB-1
 PULPROG zg30
 TD 65536
 SOLVENT MeOH
 NS 16
 DS 2
 SFO 8278.146 Hz
 FIDRES 0.126314 Hz
 AQ 3.9584243 sec
 RG 574.7
 DM 60.400 usec
 DE 6.00 usec
 TE 300.0 K
 D1 1.00000000 sec

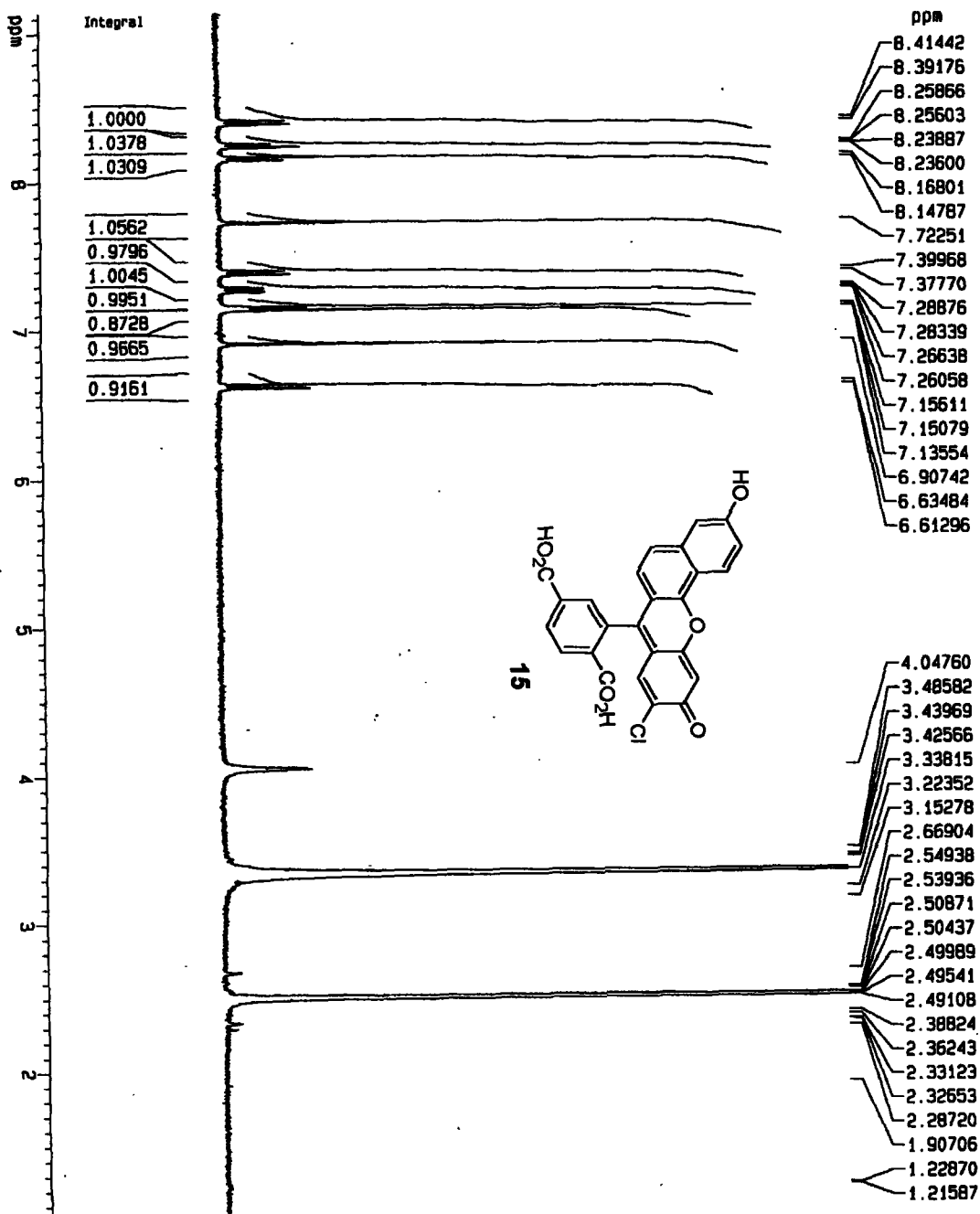
***** CHANNEL f1 *****
 NUC1 1H
 P1 7.90 usec
 PL1 0.00 dB
 SF01 400.1324710 MHz

F2 - Processing parameters
 SI 32768
 SF 400.1300114 MHz
 KW EM
 SSB 0
 LB 0.30 Hz
 GB 0
 PC 1.00

1D NMR plot parameters
 CX 20.00 cm
 F1P 9.389 ppm
 F1 3756.95 Hz
 F2P -0.179 ppm
 F2 -71.46 Hz
 PPMCM 0.47840 ppm/cm
 HZCM 191.42970 Hz/cm

Pulse Sequence: s2pul1





Current Data Parameters
 NAME: AUG03-2004-AW
 EXPNO: 10
 PROCNO: 1

F2 - Acquisition Parameters
 Date_: 20040903
 Time: 20.06
 INSTRUM: spect
 PROCNO: 88-1
 PULPROG: zg30
 TD: 65536
 SOLVENT: DMSO

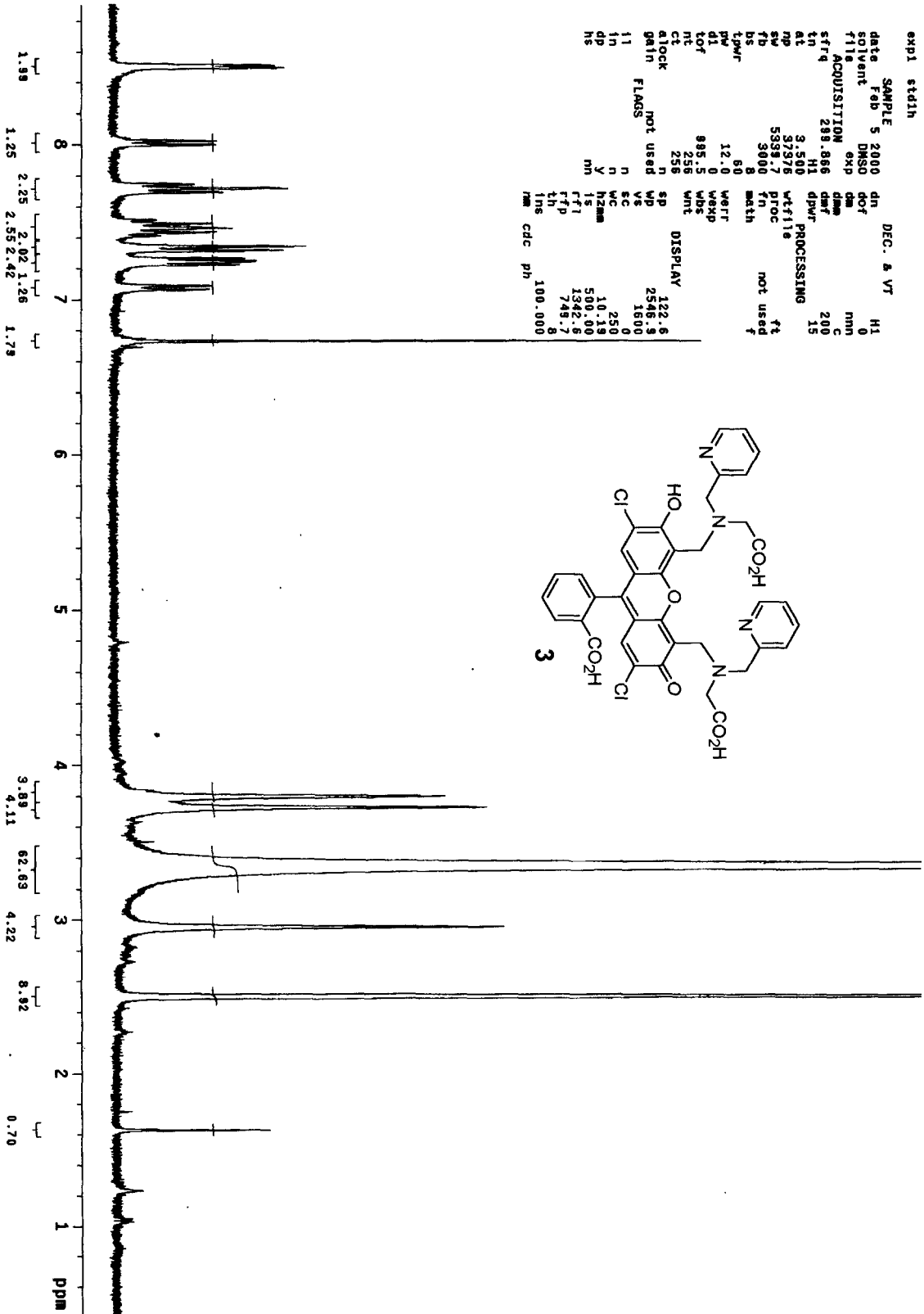
DS: 2
 SMH: 8278.146 Hz
 FIDRES: 0.126314 Hz
 AQ: 3.9584243 sec
 RG: 645.1
 DW: 60.400 usec
 DE: 6.00 usec
 TE: 300.0 K
 D1: 1.00000000 sec

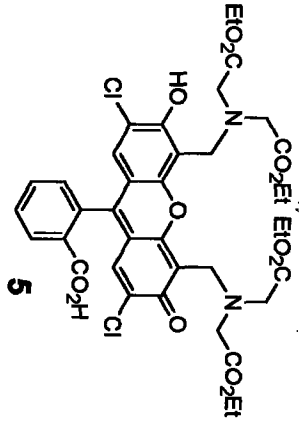
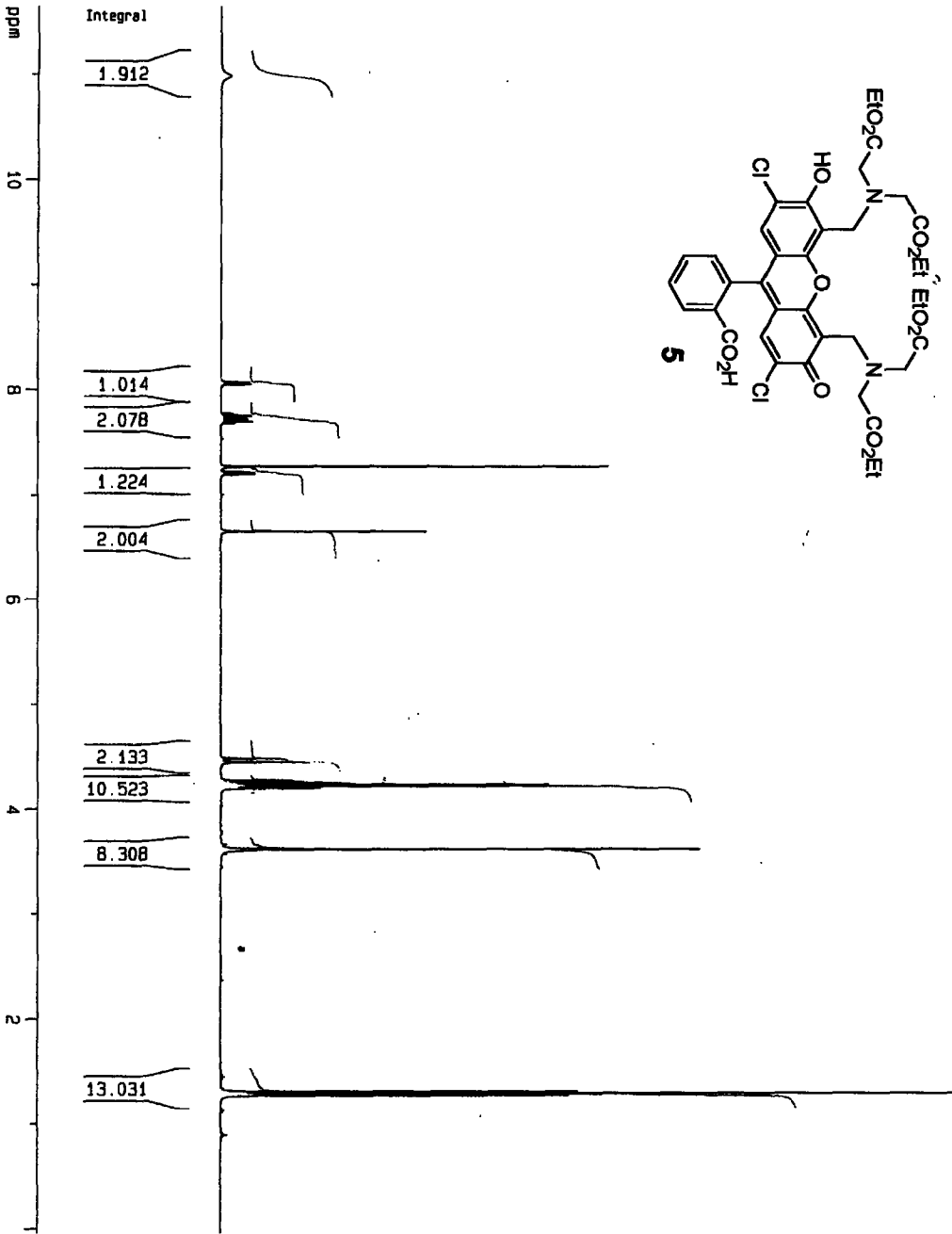
***** CHANNEL f1 *****
 NUC1: 1H
 P1: 7.90 usec
 PL1: 0.00 dB
 SF01: 400.1324710 MHz

F2 - Processing parameters
 SI: 32768
 SF: 400.1300031 MHz
 KW: EN
 SSB: 0
 LB: 0.30 Hz
 GB: 0
 PC: 1.00

10 NMR plot parameters
 CX: 20.00 cm
 F1P: 9.138 ppm
 F1: 3655.86 Hz
 F2P: 1.053 ppm
 F2: 421.15 Hz
 PPMCM: 0.40418 ppm/cm
 HZCM: 161.72537 Hz/cm

Appendix 2 Spectra





Current Data Parameters
 NAME Feb18-2000-ACW
 EXPNO 10
 PROCNO 1

F2 - Acquisition Parameters

Date_ 20000218
 Time 14.43
 INSTRUM spect
 PROBDW 5 mm BBO BB-1
 PULPROG zg30
 TD 65536
 SOLVENT CDCl3
 NS 16
 DS 2
 SWH 8278.146 Hz
 FIDRES 0.126314 Hz
 AQ 3.9584243 sec
 RG 256
 DW 60.400 usec
 DE 6.00 usec
 TE 300.0 K
 D1 1.00000000 sec

CHANNEL f1

M/C1 1H
 P1 8.40 usec
 PL1 0.00 dB
 SF01 400.1324710 MHz

F2 - Processing parameters

SF 400.130054 MHz
 WDM EM
 SSB 0
 LB 0.30 Hz
 GB 0
 PC 1.00

1D NMR Plot Parameters

CX 20.00 cm
 F1P 11.642 ppm
 F1 4658.47 Hz
 F2P -0.049 ppm
 F2 -19.69 Hz
 PPM/CM 0.58458 ppm/cm
 HZ/CM 233.90787 Hz/cm

Biographical Note

The author was born in Cambridge, Massachusetts in 1977 to Michael and Frances Woodroffe. She moved with her family to Ann Arbor, Michigan shortly thereafter, where she was raised with her two brothers. She graduated from Pioneer High School in 1994, and attended Northwestern University, earning a B. A. in chemistry and integrated science in 1998. The academic year 1998-99 was spent in Tübingen, Germany, on an academic fellowship from the Deutsche Akademische Austauschdienst. On graduation, the author plans to begin a postdoctoral fellowship with Professor Brian Stoltz at the California Institute of Technology.

Carolyn C. Woodroffe

- Education**
- Massachusetts Institute of Technology** Cambridge, MA
Ph.D. in Organic Chemistry August 2004
Advisor: Stephen J. Lippard
- Universität Tübingen** Tübingen, Germany
Deutsche Akademische Austauschdienst Fellow 1998-99
Advisor: Heiner Eckstein
- Northwestern University** Evanston, IL
B.A., Chemistry and Integrated Science June 1998.
Advisor: Richard B. Silverman
- Publications**
- “Selective Inhibition of Monoamine Oxidase B by Aminoethyl Substituted Benzyl Ethers.” C.C. Woodroffe, R. Mostashari, X. Lu, R.R. Ramsay, and R.B. Silverman. *Journal of Enzyme Inhibition*, **1999**, *15(1)*, 11-21.
- “Anomalous Schmidt Reaction Products of Phenylacetic Acid and Derivatives.” C.C. Woodroffe, B. Zhong, X. Lu, and R.B. Silverman. *Journal of the Chemical Society, Perkin Transactions 2*, **2000**, *1*, 55-59
- “A Novel Two-Fluorophore Approach to Ratiometric Sensing of Zn²⁺.” C.C. Woodroffe and S.J. Lippard. *Journal of the American Chemical Society*, **2003**, *125(38)*, 11458-11459
- “Membrane-Permeable and Impermeable Sensors of the Zinpyr Family and Their Application to Imaging of Hippocampal Zinc in Vivo.” C.C. Woodroffe, R. Masahla, K. R. Barnes, C. J. Frederickson, and S. J. Lippard. *Chemistry & Biology*, submitted for publication.
- Awards**
- Merck/MIT Fellowship (2001-02), National Science Foundation Predoctoral Fellowship Honorable Mention (2000), MIT Department of Chemistry Teaching Award (1999), Deutsche Akademische Austauschdienst Fellowship (1998), Northwestern University Chemistry Department Scholar (1998).
- Languages**
- German (fluent)
- Activities**
- MIT Women’s Ice Hockey Club Team (team captain 2001-2002).